Design and Construction of Framework Catalysts for Hydrogen Evolution

水素発生反応に向けたフレームワーク触媒の設計と構築

Pondchanok Chinapang

March 2018
Department of Structural Molecular Science
School of Physical Sciences
The Graduate University for Advanced Studies

Contents

General Introduction

Photocatalytic hydrogen evolution

World energy consumption is expected to double by 2050[1], in which huge amount of energy is supplied by fossil fuels. The consumption of fossil fuels correlates to the increase of atmospheric greenhouse gasses level, which results in a profound effect on global climate. One of the most promising solutions to such anticipated crisis in future energy production resides on the combination of two renewable sources: water and sunlight, and converting solar light into a usable form of energy is a very worthy challenge. Taking inspiration from photosynthesis, scientists have early tried to develop artificial photosynthetic system, which is capable of harvesting and converting light and water into chemical fuels in the form of chemical bonds.

One of the most sophisticated energy carriers is molecular hydrogen (H_2). H_2 can produce water in the presence of dioxygen and 285 kJ of energy per 120 MJ kg^{-1} can be obtained. In other words, 1 kg of hydrogen generates three times more energy than 1 kg of gasoline (energy density 44 MJ kg^{-1}).[2] It is thus necessary to develop a sustainable method generating hydrogen from sunlight. One of very attractive ways to produce hydrogen would be to split water into H_2 and O_2 by using sunlight as abundant, sustainable and clean energy. This is symbolized by the well-known and much-desired water splitting reaction (Scheme 1.). Therefore, the development of new systems that are able to convert solar energy into chemical bond in H_2, is of the utmost importance.

The basic components for photochemical proton reduction reactions consists of a chromophore or photosensitizer (PS) to absorb light, a catalyst (Cat) to reduce proton, and a sacrificial electron donor (SD) to supply electrons for the H_2 formation and regenerate the photosensitizer. Typically, these sequential processes are initiated by light absorption by PS, generating its excited state (denote PS*) that can be quenched by electron transfer process through either reductive quenching or oxidative quenching pathway (Scheme 2).

$$2H_2O \longrightarrow 4e^- + 4H^+ + O_2 \qquad E = 1.23\ V - 0.059pH\ V$$

$$4e^- + 4H^+ \longrightarrow 2H_2 \qquad E = 0\ V - 0.059pH\ V$$

$$2H_2O \longrightarrow 2H_2 + O_2$$

Scheme 1. The overall water splitting reaction and two half-equations; water oxidation and proton reduction. Potential are referenced versus the normal hydrogen electrode (NHE).

The reductive quenching of PS* involves an electron transfer from SD to generate a reduced form PS (PS^-), which is able to give an electron to the catalyst and returns to its ground state (PS). The other pathway is the oxidative quenching of PS* by Cat affording the oxidized form of PS (PS^+), which go back to its initial form (PS) after receiving an electron from SD. Since, the reduction of two protons into the molecular hydrogen requires two electron process, the catalyst needs to be reduced twice to promote H_2 formation. It is also possible to obtain Cat^{2-} by the disproportionation of Cat^-.

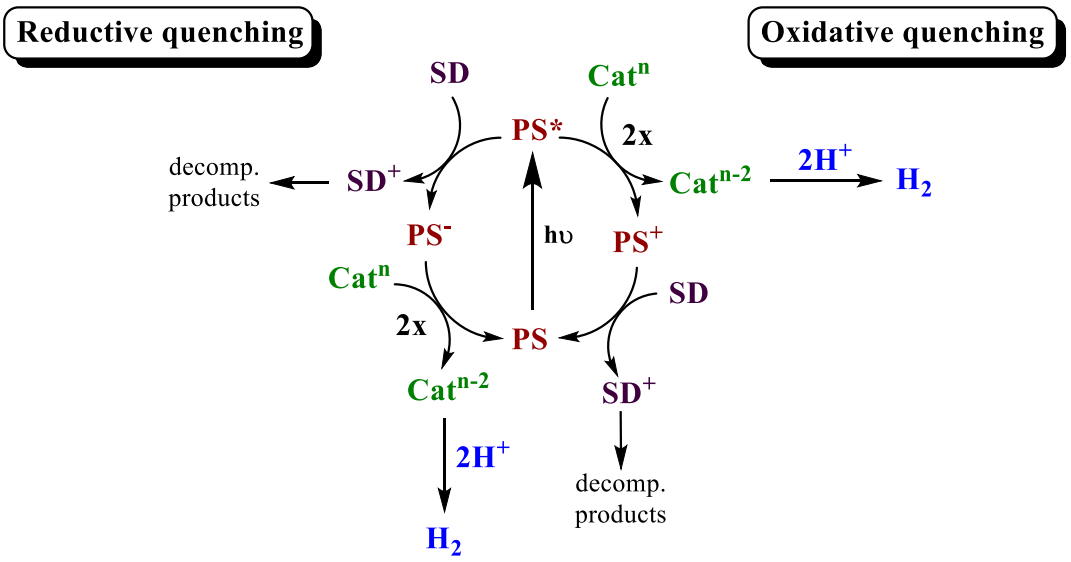

Scheme 2. Illustration of general pathways for photocatalytic H_2 evolution system driven by a reductive quenching pathway (left) and an oxidative quenching pathway (right) that consists of a photosensitizer (PS, red color), a sacrificial electron donor (SD, purple color) and a H_2-evolving catalyst (Cat, green color).

Homogeneous photocatalytic hydrogen evolution systems

As described in the previous section, the development of artificial photosynthesis systems that able to store solar energy in chemical bonds (H_2), and generating energy on demand is extremely important. In this context, molecular complexes have been widely investigated as catalysts for the reduction of water or proton into molecular hydrogen. In general, these molecular catalysts have been developed in "purely-homogeneous", in which all necessary components can be fully dissolved in the reaction medium, or "quasi-homogeneous" system, in which catalytically active species are elucidated as metallic colloids/nanoparticles.[3] A great advantage of such homogenous systems is that we can understand their reaction mechanisms in detail based on well-established spectroscopic techniques.[4,5] The efficient photocatalytic systems for proton reduction to H_2 based on molecular compounds were firstly reported in 1977 by Lehn and Sauvage.[6] Since then, several new molecular-based catalysts for artificial photosynthesis systems have been discovered and subsequently improved.

Generally, there are two approaches for the design of homogeneous photocatalyst for H_2 evolution: i) the utilization of metal complexes as H_2-evolving catalysts in multi-component systems and ii) the linked system involving supramolecular assembles in which catalyst and photosensitizer are covalently assembled into same structures. In the following sections, the several representative examples of molecular-based catalysts for the catalytic reduction of water or proton to H_2 will be introduced.

Homogeneous H_2-evolving catalysts in multi-component systems

Up-to-date, numerous homogeneous multi-component systems for photocatalytic H_2 evolution which consists of a catalyst, photosensitizer, and sacrificial electron donor have been reported. In term of catalyst, transition metal complexes containing abundant first row (Co, Ni, Fe)[7] or rare (Rh, Pt, Pd)[8] . Metals are ideal candidate, arising from their redox-rich properties. Some of these homogeneous systems can operate efficiently in organic or aqueous-organic solvents in combination with required components (a photosensitizer, a sacrificial electron donor and/or electron mediator), so-called multi-component systems. The multi-component photocatalytic systems are very attractive in the sense that each component can be independently optimized, which results in the efficient improvement of the catalytic activity.

The general mechanism for these multi-component systems is shown in Scheme 3, where light is absorbed by photosensitizer leading to an electron transfer (i.e. quenching) process, and sometime subsequent electron transfer reactions by electron mediator (also called electron relay) such as methyl viologen to the catalyst, are required to reduce proton into dihydrogen. In this scheme, an excited photosensitizer that is formed after the photo-induced electron transfer process can be reduced by a sacrificial electron donor through either the reductive quenching or oxidative quenching mechanism, regenerating the ground-state photosensitizer. Though, the electron transfer event in multi-component system is mainly such the intermolecular electron transfer event or diffusional-controlled. It should be also noted that reaction via the reductive quenching process is also possible in the multi-component systems. Examples of molecular-based catalysts and components variation used in the homogeneous multi-component systems for photocatalytic H_2 evolution are depicted in Fig. 1 and 2, respectively.

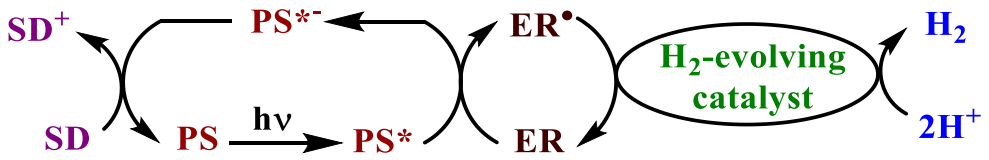

Scheme 3. A schematic illustration of a multi-component system driving photocatalytic H_2 evolution that consists of a sacrificial electron donor (SD, purple color), a photosensitizer (PS, red color), an electron relay (ER, brown color) and a H_2-evolving catalyst (green color).

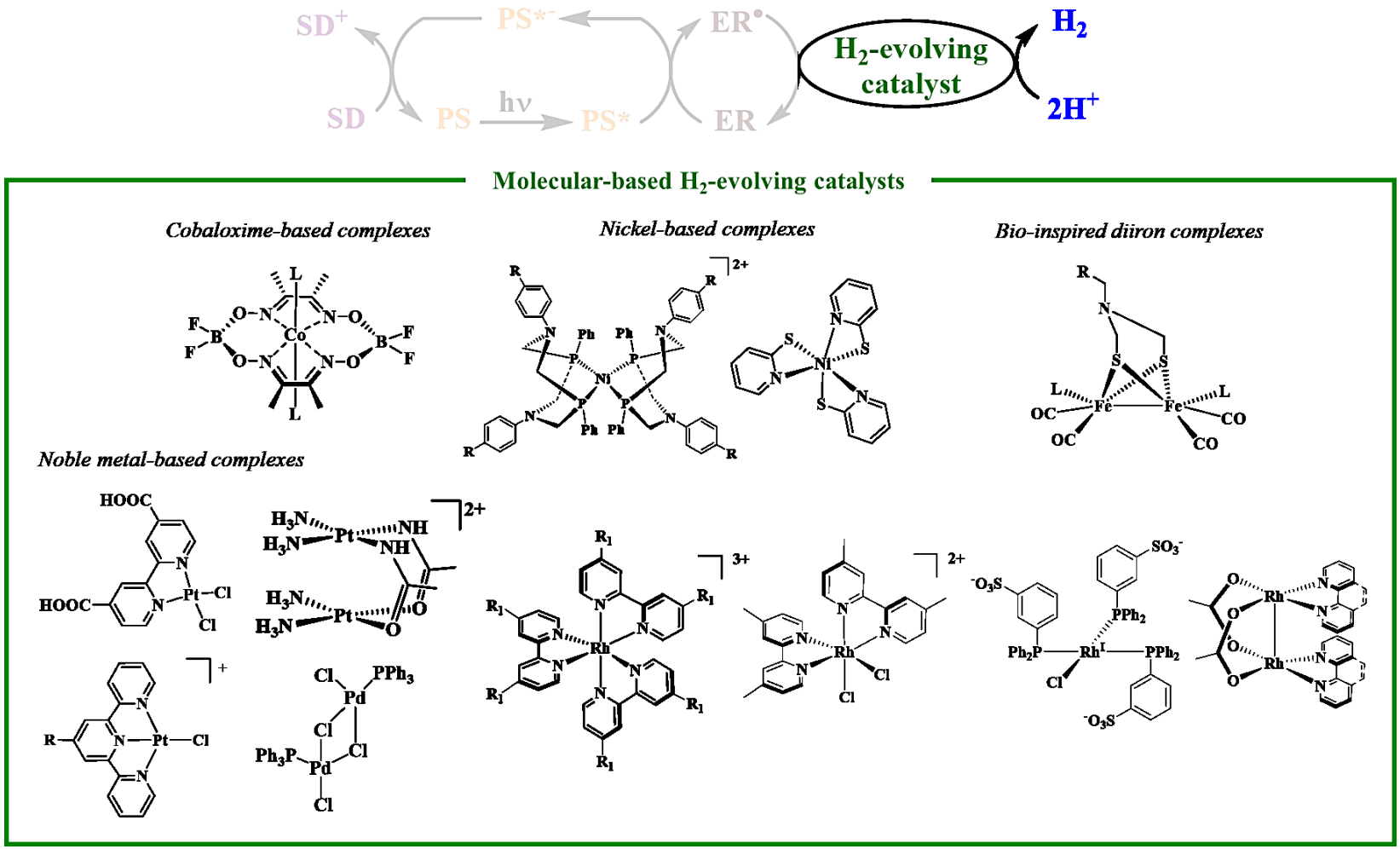

Figure 1. Variation of the molecular-based H_2-evolving catalysts (green block) used in the homogeneous multi-component photocatalytic H_2 evolution, reported by several groups of the investigator.[7,8]

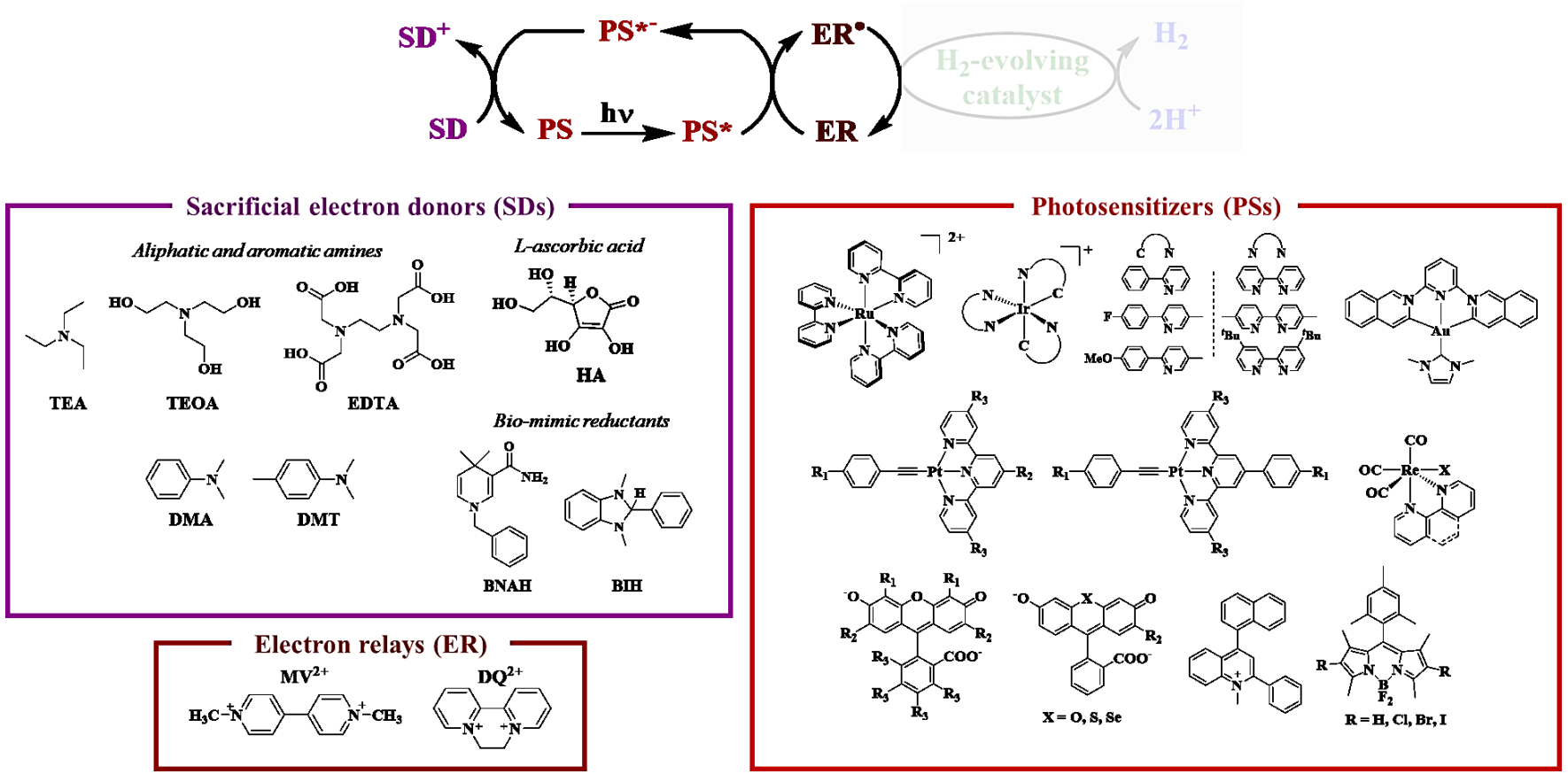

Figure 2. Variation of the sacrificial electron donors (purple block), the photosensitizers (red block) and electron relays (brown block) used for the homogeneous multi-component photocatalytic H_2 evolution, studied by several research groups.[7,8]

Homogeneous H_2-evolving catalysts in linked systems

As mentioned earlier, the efficiency of multi-component system is often limited by the intermolecular electron transfer event between components (a sacrificial donor, a photosensitizer, an electron relay molecule, and a catalyst). However, the electron transfer processes in these systems are commonly limited by the diffusion of species in solutions, which sometimes causes the decrease in their efficiencies. Against this drawback, one of the promising ways to overcome this problem is to link these two components together to form a molecule framework via coordinate or covalent bonding. The anticipated advantage of these assembled structures is to improve the efficiency of catalytic reactions by allowing intramolecular electron transfer between photosensitizer and catalytic center in close distance. Moreover, the additional photosensitizer and/or electron mediator can be diminished in these linked homogeneous photocatalytic H_2 generation systems (Scheme 4). Some of these linked H_2-evolving catalytic systems exhibited superior activity and durability than their corresponded multi-components due to the faster of electron transfer processes.

There have been many reports on linked systems which combine the well-known H_2-evolving catalytic centers, abundant metal-based[9]; Fe and Co or noble metal-based[10]; Rh, Ru, Pd or Pt and inorganic or organic photosensitizer units (Fig. 3). Most of them can operate in aqueous-organic media in the presence of commonly used sacrificial electron donors.

Scheme 4. General schemes of the tethered system containing a sacrificial electron donor (SD, purple color) and supramolecular H_2-evolving catalysts in which photosensitizer(s) (PS, red color) are attached to H_2-evolving catalyst (Cat, green color) in the same molecular framework.

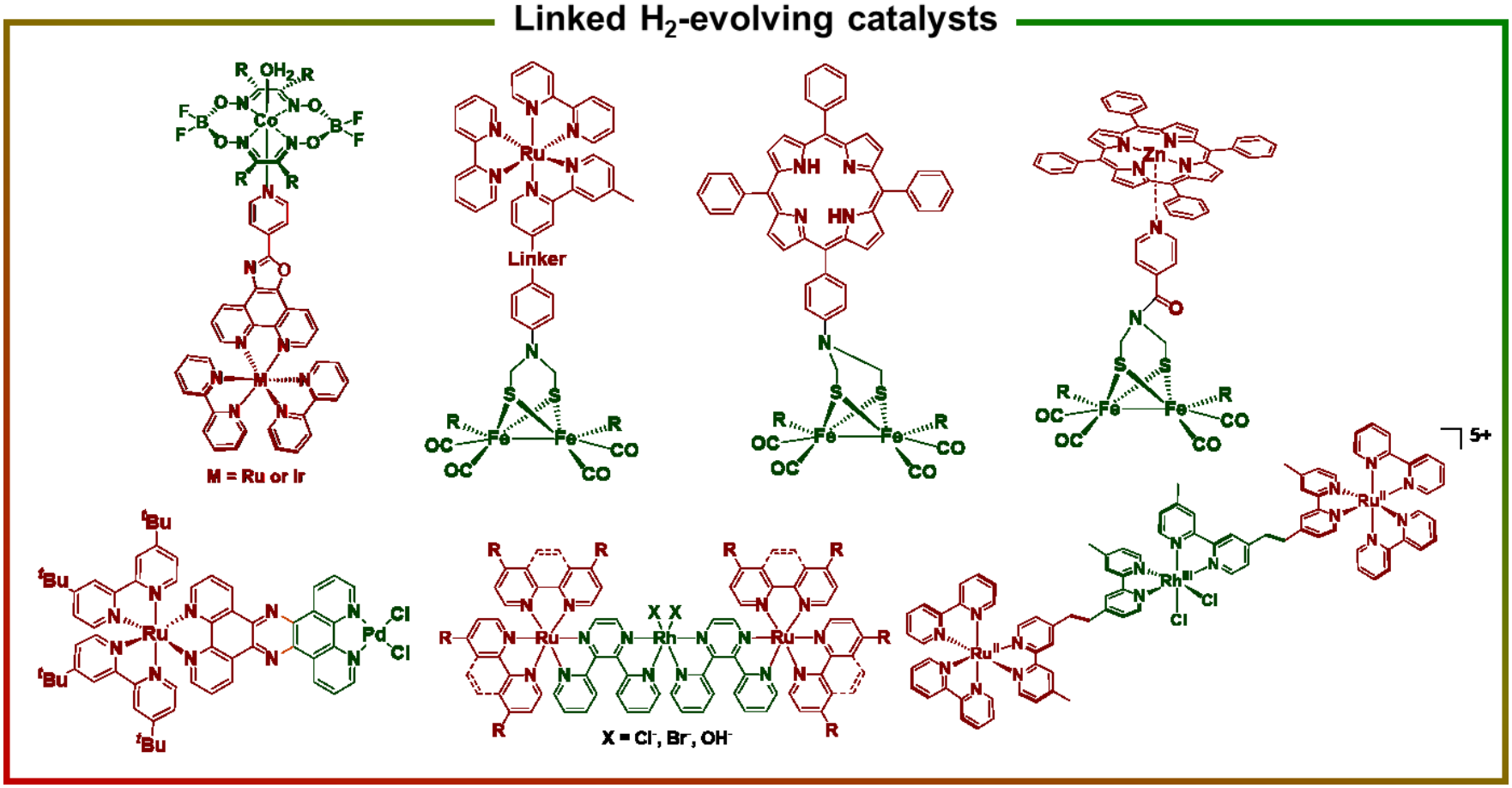

Figure 3. Examples of the reported tethered molecular-based H_2-evolving catalysts, in which the photosensitizer(s) (red color) and the catalytic centers (green color) are covalently or coordinately linked in the same molecular structure.[9,10]

Heterogeneous photocatalytic hydrogen evolution systems

As described in the previous section, a great advantage of homogeneous systems is that their reaction mechanisms can be elucidated in detail based on conventional spectroscopic techniques. The nature of such systems allows us to precisely tune their structures/properties, which results in the improved photocatalytic activities. However, homogeneous systems are considered unsuitable for future practical applications because of their moderate reusability and stability, for which heterogeneous photocatalytic systems are rather advantageous.

Fujishima and Honda firstly demonstrated the potential of TiO_2 semiconductor materials to split water into H_2 and O_2 in 1971.[11] Their work triggered the development of semiconductor-based photocatalysts for a wide range of energy and environment applications and a number of semiconductor-based photocatalysts have been proposed and reported since then.[12] In general, efficient photocatalytic materials contain oxide of either transition-metal cations with d^0 electronic configuration (e.g. Ta^{5+}, Ti^{4+}, Zr^{4+}, Nb^{5+}, W^{6+} and Mo^{6+}) or typical metal cations with d^{10} electronic configuration (e.g. In, Sn, Ga, Ge, and Sb).[13] Also, oxynitrides or nitrides containing d^0 transition-metal cations, such as Ta_3N_5, TaON, and $LaTiO_2N$, have been reported as potential photocatalytic materials to achieve photocatalytic H_2 evolution.[14] These semiconductor-based heterogeneous materials thus become the main collection of the active studies on heterogeneous photocatalytic H_2 evolution. Fig. 4 shows the overview diagram of a water splitting reaction promoted by semiconductor photocatalysts.[15] Even though some of the factors that determine the catalytic activity of semiconductors have been rationalized in semiconductors, many aspects on the structural-function relationship in these photocatalysts are still unclear. In contrast to the detailed mechanisms of homogeneous catalytic systems for H_2 production, it is more difficult to identify the active species on the semiconductor-based photocatalysts in heterogeneous systems. These limitations of semiconductor-based heterogeneous catalysts prompted us to develop the molecular-based catalytic systems, in which the advantageous features of homogeneous and heterogeneous systems are integrated.

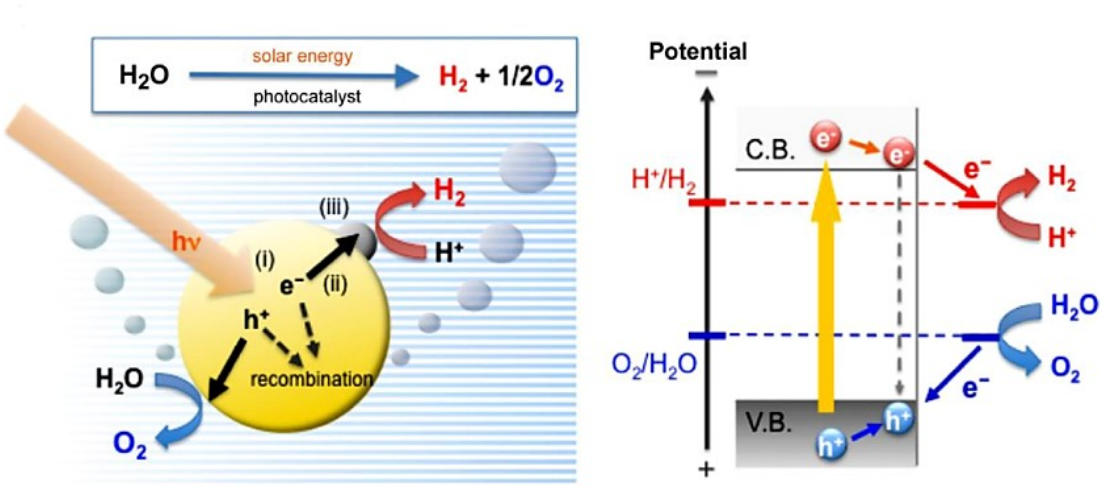

Figure 4. Schematic illustration of the photo-induced water splitting reaction catalyzed by semiconductor photocatalysts in heterogeneous systems (left) and the energy levels of the valence band (V.B.) and conduction band (C.B.).

Molecular-based H_2-evolving catalysts in heterogeneous systems

In this section, some recent examples of the molecular-based heterogeneous photocatalytic H_2 evolution systems, in which a molecular-based catalyst and photosensitizer units are integrated, will be given. There are three prominent ways to heterogenize the molecular-based photocatalytic systems for H_2 evolution. In the first approach, the supramolecular assemblies of organic/metal-organic photosensitizers and molecular catalysts are utilized[16] (Fig. 5a). In the second approach, the dyads of homogeneous H_2-evolving molecular catalysts and organic photosensitizers are immobilized on electrode surfaces[17] (Fig. 5b). The third approach is the simultaneous incorporation of molecular catalysts and/or photosensitizers into the platform of the metal-organic frameworks[18] (Fig. 5c).

In spite of these advanced developments in molecular-based heterogeneous systems, it is still difficult to obtain the completely well-defined structures in these photocatalytic systems because it is hard to obtain highly-ordered or single-crystalline materials. These limits of the existing systems prevent the precise determination of the local environment around the catalytic centers.

One of the solutions for the above-mentioned limitation is the utilization of specific non-covalent bonding such as π–π interactions, hydrogen bonding, van der Waals forces, electrostatic interactions and host-guest interactions.[19] These kinds of non-covalent interactions can provide a promising solution to construct the assembled structure of light-absorbing sites and catalytic centers into an infinite architecture of photocatalyst which would improve the molecular-based catalyzed H_2 evolution in heterogeneous systems. Compared to the conventional coordination or covalent bonding, these interactions are relatively weaker and exhibit fewer directional control but do not deactivate catalytically active sites. Therefore, the self-assembly of functional molecular metal-complexes through non-covalent interactions should afford the conceptual design strategy for the cutting-edge on H_2 production technology.

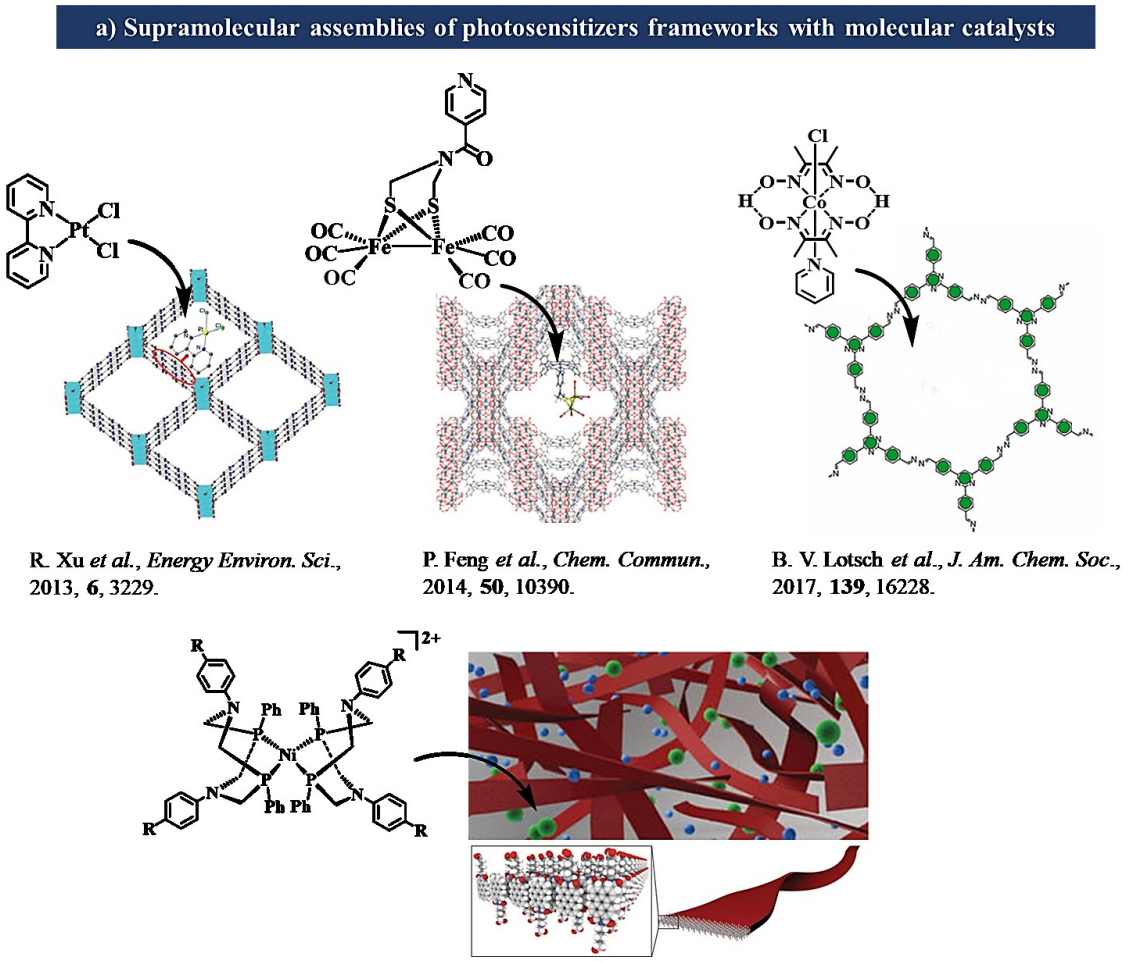

Figure 5. Methods for constructing the heterogenized molecular-based photocatalytic systems for H_2 evolution.

c) Simultaneous incorporation of molecular catalysts and/or photosensitizer into the platforms

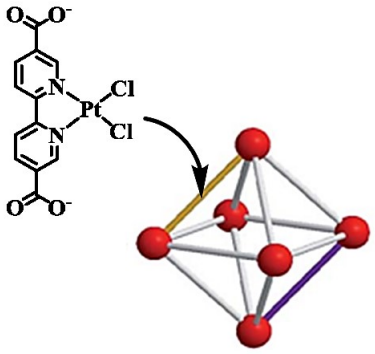

W.-F. Fu *et al.*, *J. Mater. Chem. A*, 2015, **3**, 10386.

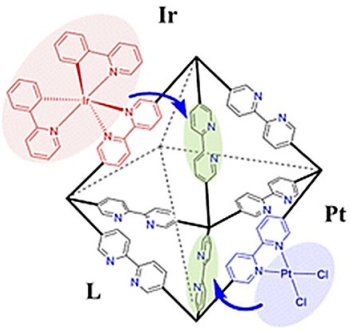

S. Y. Park *et al.*, *J. Am. Chem. Soc.*, 2016, **138**, 8698.

Figure 5. (Continued) Methods for constructing the heterogenized molecular-based photocatalytic for H_2 evolution.

Rh(II) paddle-wheel complexes

A first example of a dinuclear Rh(II) paddle-wheel complex, $Rh_2(CO_2CH_3)_4(H_2O)_2$, was reported by Antsyshikina and co-workers in 1962 (Fig. 6),[20] and the relevant compounds mainly obtained through the ligand exchange reactions of $Rh_2(CO_2CH_3)_4(H_2O)_2$ have been extensively explored since then.[21] This class of complexes exhibits a strong Rh-Rh metal bond between metal centers and possesses four equatorial bridging acetate ligands. As a result, the complexes possess high symmetry (D_{4h}) which contributes to numerous multi-dimensional assembled structures.[22] Additionally, two axial sites of the dirhodium center are coordinatively unsaturated (also called as; *open-metal sites, accessible metal center, exposed metal sites*)[23], which can offer various functional properties induced by various linking ligands or labile axial coordination (Fig. 7a and 7b). Moreover, these open-metal sites of the dirhodium center can serve as catalytically-active sites. They have been known as chiral-control catalysts for a wide range of asymmetric transformation including cycloaddition, C-H activation reactions, which proceeds via Rh(II)-carbenoid/nitrenoid intermediates (Fig. 7c).[24] Especially, in the field of renewable energy technology as mentioned earlier, Rh(II) paddle-wheel complexes are effective homogeneous catalysts for both electrochemical and photochemical proton reduction to produce molecular hydrogen.[8i,8n,25]

Furthermore, dinuclear Rh(II) paddle wheel complexes exhibit intriguing photochemical, electrochemical and magnetic properties, which allow its application in various research fields, such as anti-tumor/DNA active agents,[26] NMR-shifting agents,[27] gas adsorbate[28] and vapor/chemical fluorescence sensors.[29] Representative examples of these applications are given in Fig. 7.

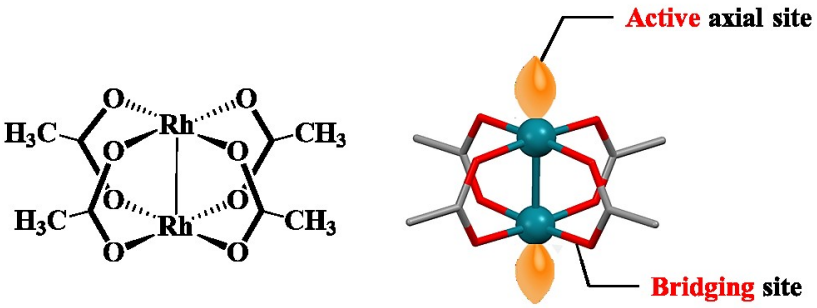

Figure 6. A chemical structure of a Rh(II) paddle-wheel complex (left) and its structural features (right).

Although Rh is in the category of rare noble metals, it is still appealing much attention due to the unique reactivity of their active-axial sites and sufficient stability arising from their metal-carboxylate bonds. In addition, the relative ease of preparation and their stability under air and moisture environment, can also compensate their exclusive price. Therefore, Rh(II) paddle-wheel complexes are considered as attractive candidates for the H_2-evolving catalyst with high durability and recyclability.

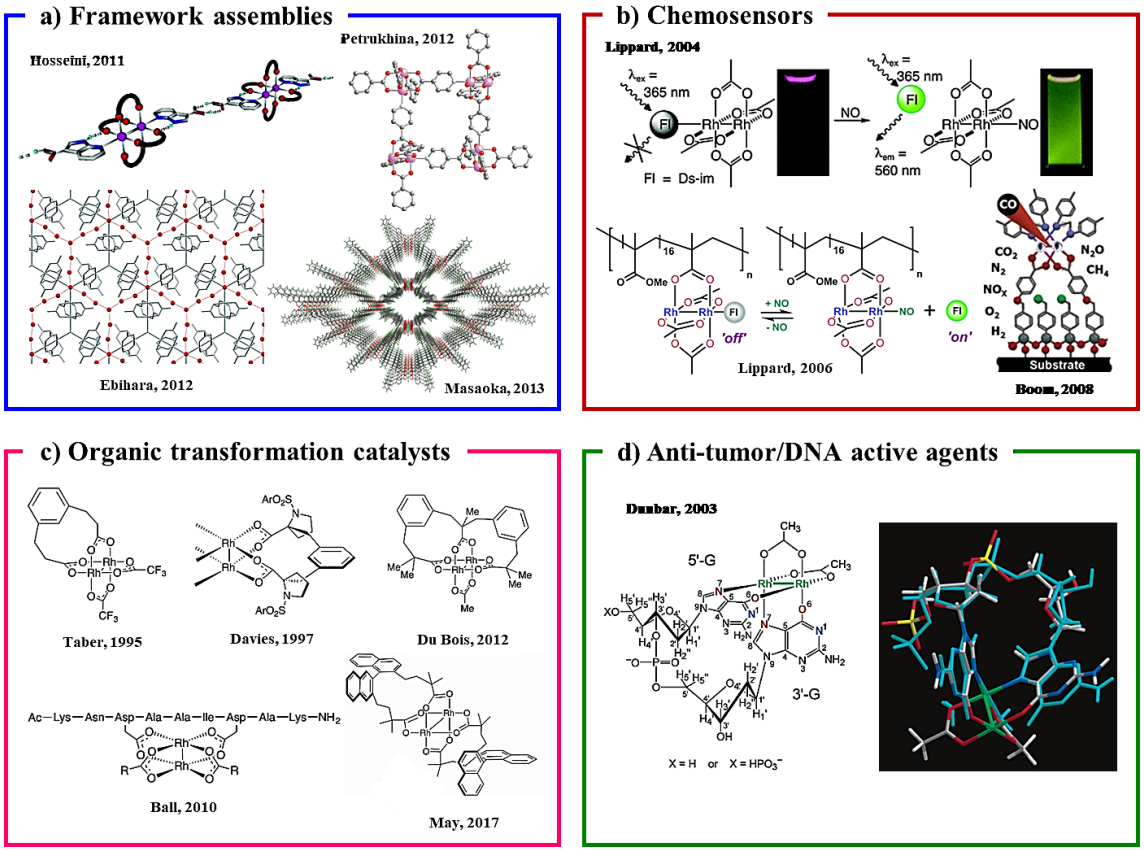

Figure 7. Selected applications of Rh(II) paddle-wheel complexes.

Organic dyes with non-covalent interaction ability

The modern applications of organic materials have been vastly widened our outlook on organic molecules and their functional properties in recent decades. A great success on organic materials can be exampled by the huge impact of functionalized organic material on display and lighting technology as OLEDs (organic light-emitting diodes).[30] In this context, considerable attention has been paid on organic molecules that are able to harvest and emit light at various absorption/emission ranges in recent years. Although the development and utilization of several large and macro-molecules have opened up numerous exceptional research in this field[31], low molecular weight/small molecules can provide distinct advantages. Small molecules offered many applications due to their ease of synthesis and structural fine-tuning[32]

Among low molecular-weight organic dyes, 1,8-naphthalimides derivatives (NIPs) are an attractive class of material because of their great ability for intense absorption and exhibits strong fluorescence.[33] Actually, abundant applications of NIPs have been established in various research areas such as biological imaging, [34] fluorescence recognition,[35] optoelectronic materials,[36] dyes and brightening agents[37] and as DNA-targeting anti-cancer agents[38]. Importantly, NIP derivatives also have tendencies to form the intermolecular π–π stacking interactions between aromatic rings (Fig. 8), which has gained much attention in the past few years. The group of Reger has extensively utilized such features to design NIPs-based supramolecular assemblies and metal-organic frameworks (MOFs) where NIPs act as non-covalent π–π stacking units (Fig. 9).[39] The NIPs-based molecular frameworks draw a vast range of extended packing structure including columns, sheet-layers, orthogonal arrangement, etc.[40] Based on these previous reports, I believe that NIP derivatives can be utilized as a molecular connector to control the assembled framework structures via non-covalent intermolecular interactions at the molecular level.

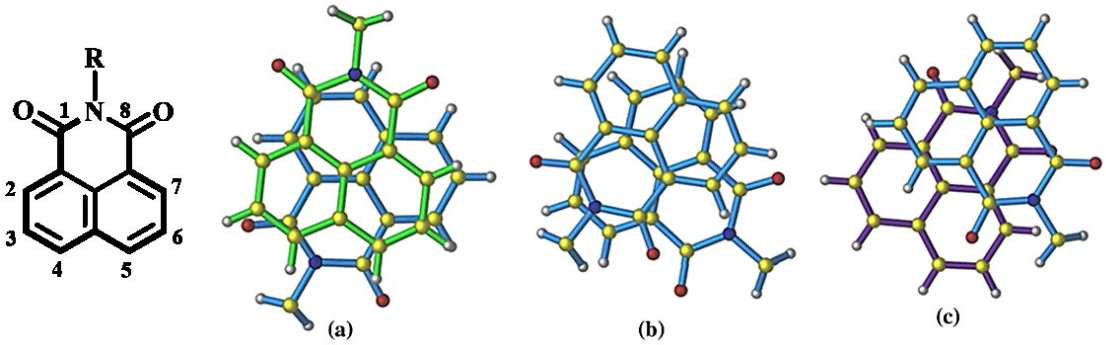

Figure 8. (Left) Chemical structure of 1,8-naphthalimide derivatives. (Right) three types of intermolecular π–π stacking arrangements (a-c) of 1,8-naphthalimide derivatives, reported by Reger and co-workers.[37a]

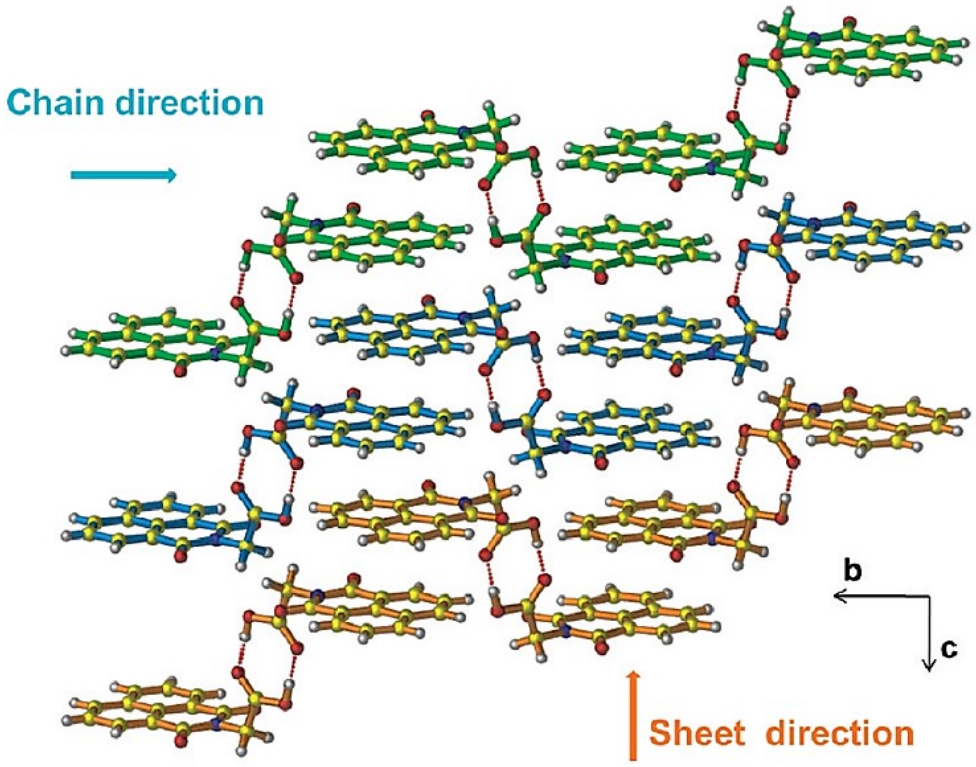

Figure 9. A representative example of the assembled framework constructed by NIPs, reported by Reger and co-workers.[37b] Non-covalent π–π stacking interactions associated with hydrogen-bonding afford high dimensional architecture.

Boron dipyrromethenes (bodipy; BDPs, Fig. 10) dyes are known as small organic molecules that are able to absorb visible light strongly and used in various kinds of applications such as light-harvesting units in either energy or electron transfer systems,[41] photodynamic therapy,[42] fluorescence bio-imaging[43] and in solar cell technology.[44] In addition, their planar structures and $^{-}BF_2$ chelating units can offer additional intermolecular assembled sites via non-covalent interactions (π–π stacking, CH–π interaction and hydrogen interaction (H-F··BF)).[45] Several representative examples of assembled structures based on BDP derivatives are shown in Fig. 11.

Although a large number of bodipy derivatives have been synthesized and explored their applications, the solid-state assembly of bodipy-based metal-complex is less investigated. Therefore, the construction of BDPs-based assembled structures with functionalized properties should be important to develop a new class of assembled materials.

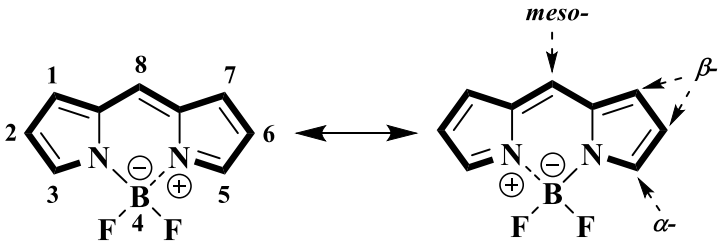

Figure 10. Chemical structure of a boron dipyrromethene (bodipy; BDP) dye.

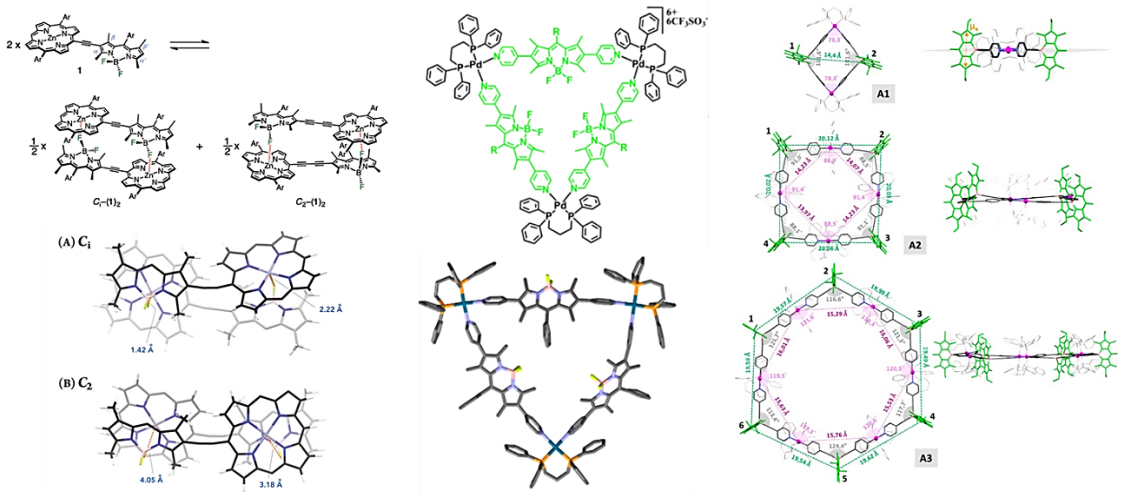

T. Yumura *et al.*, *Chem. Comm.*, 2018, **54**, 144.

C. Y. Lee *et al.*, *Inorg. Chem.*, 2017, **56**, 4615.

G. Pistolis *et al.*, *J. Phys. Chem. C*, 2017, **121**, 5341.

Figure 11. Selected examples of assembled architectures of BDP derivatives.

Aims of this thesis

The catalytic production of energy-rich H_2 from H_2O/H^+ using sunlight would serve an attractive solution to generate clean and renewable fuels. In this study, we aimed to construct an effective approach to heterogenize photocatalytic H_2 evolution system based on the supramolecular assembly of metal-complexes. In this system, a discrete molecular module (Scheme 5, left), which has a metal complex-based catalytic center (catalytic node) and intermolecular interaction sites (molecular connector), can be assembled into an ordered structure via non-covalent interaction to afford a framework catalyst (Scheme 5, right). Unlike assembly that is driven by coordination bonding, known as coordination polymers,[46] we can easily assemble/disassemble catalyst modules by simply changing solvents while maintaining the structure of the active sites.[47] It is also anticipated that the catalytic activities of the system can be fine-tuned and optimized by rationally derivatized the catalytic modules. Therefore, our system can reveal three prominent features; (1) well-defined catalytic sites attributed to the molecular-based modules and (2) reusability and high durability based on the heterogeneous nature or (3) dual homogeneous and heterogeneous photocatalysts for H_2 evolution.

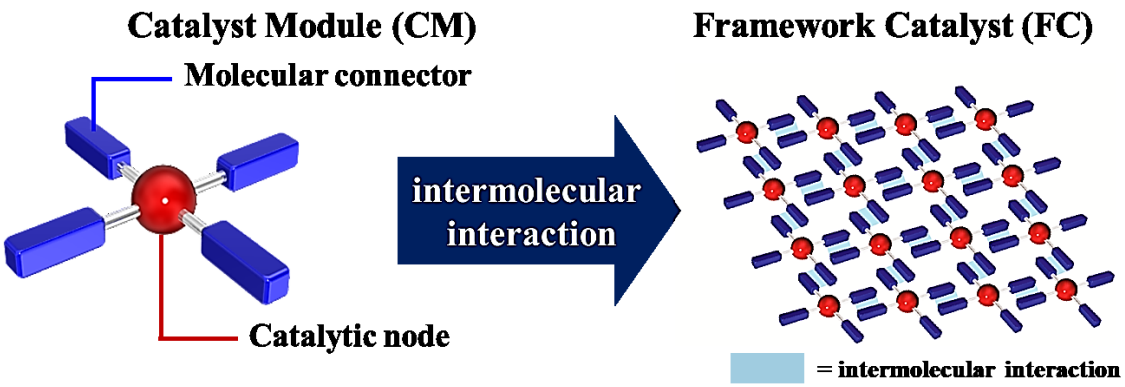

Scheme 5 Schematic illustration of the assembly of catalyst modules via non-covalent intermolecular interactions to afford a framework catalyst.

A schematic illustration of catalytic modules designed in this study is shown in Scheme 6. I newly designed two kinds of Rh(II) dimer complexes with light harvesting units as catalytic modules. In these complexes, a Rh(II) paddle-wheel unit is chosen as a catalytic node because the open-metal sites of these complexes are known to serve as catalytic centers in H_2 formation reactions[8i,8n,27] as mentioned in the previous section. In addition, highly symmetric structures (D_{4h}) of these Rh(II) paddle-wheel complex are expected to construct highly ordered structures. As molecular connectors, I employed 1,8-naphthalimide-derivative (**NIP**) and boron-dipyrromethene-derivative (bodipy; **BDP**) moieties because both of them can exhibit intense light-absorption ability and offer large π plane suitable for the construction of ordered structures.

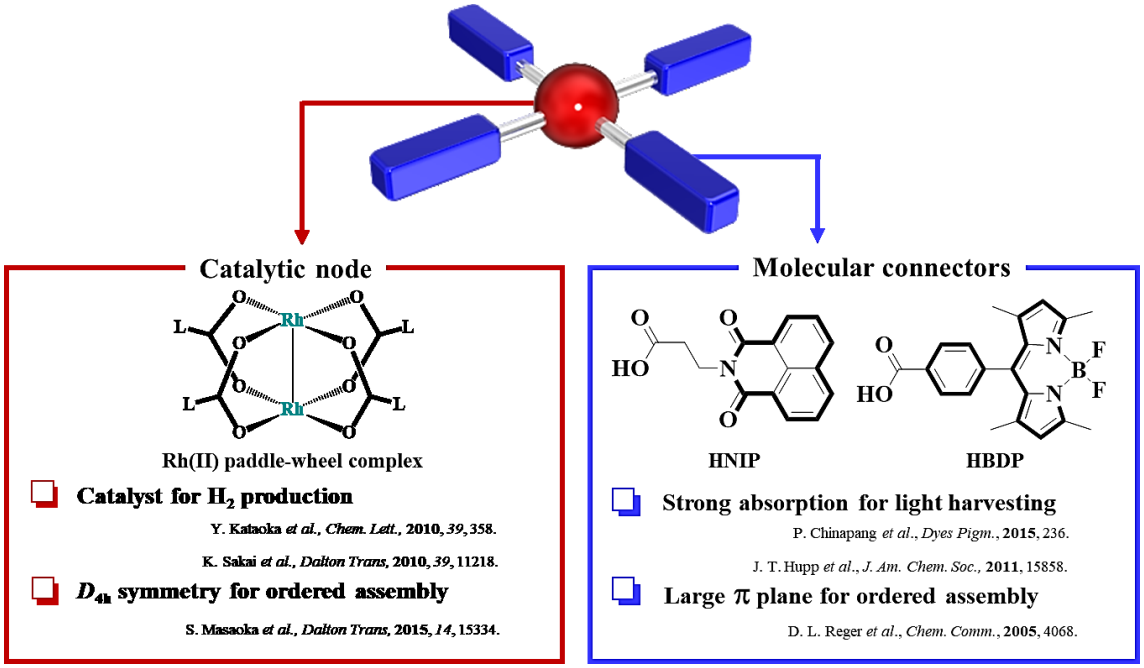

Scheme 6. Specific features of catalytic modules in this study.

Survey of this thesis

Chapter 1 presents the development of a novel heterogeneous photocatalytic system for H_2 evolution. I propose that a heterogeneous photocatalytic system can be constructed by the supramolecular assembly of discrete molecules. In this system, a discrete catalyst module, which contains metal complex-based catalytic center (catalytic node) and intermolecular connection sites (molecular connector), can be assembled into an ordered structure through non-covalent interaction to afford a heterogeneous framework catalyst. Therefore, this system can show two prominent features; (1) well-defined catalytic sites attributed to the molecular-based modules and (2) reusability and high durability based on the heterogeneous nature.

Based on the aforementioned strategy, I employed a Rh(II) dimer complex bearing 1,8-naphthalimide-based ligands, Rh_2(**NIP**)$_4$ (**CM-1**, H**NIP** = 3-(1,8-naphthalimido)-propanoic acid) as a catalyst module. The synthesis and characterization of **CM-1** are described. Subsequently, the self-assembly of **CM-1** to construct a framework catalyst (**FC-1**) was performed and structural analysis of the obtained **FC-1** reveals the formation of framework structure stabilized by the intermolecular via π–π stacking interactions between the aromatic rings of the **NIP** ligands. Electrochemical studies of **CM-1** and **FC-1** exhibited a large irreversible current attributed to the electrocatalytic H_2 evolution in the presence of acetic acid. The photophysical properties investigation of **CM-1** and **FC-1** have shown that the excellent light-harvesting property of 1,8-naphthalimide units is retained after the formation of the metal complex and the construction of the framework. The photocatalytic activity of **FC-1** was consequently examined in an aqueous medium containing a sacrificial electron donor. Upon light irradiation ($\lambda > 320$ nm), the production of H_2 linearly increased with time. Several control experiments demonstrated that integration of the photosensitizer (1,8-naphthalimide moiety) and the catalytic center (Rh(II) paddle-wheel unit) into the same molecule is crucial for photocatalytic H_2 production. Moreover, **FC-1** exhibited long-lived activity and was easily reused without considerable loss of catalytic activity.

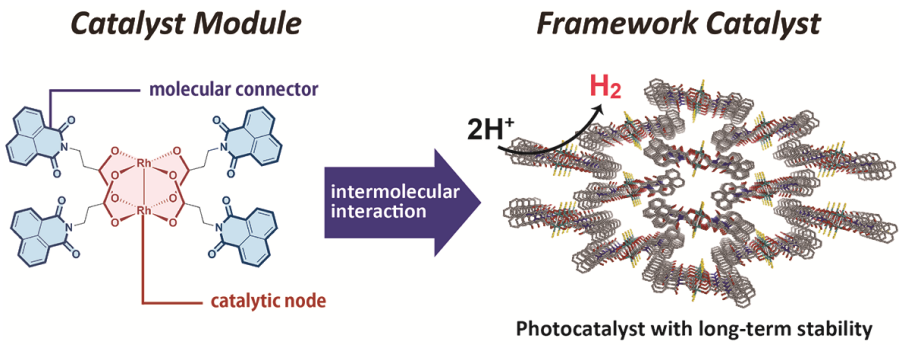

Chapter 1

Chapter 2 describes the development of a photo-active catalyst with visible-light absorbing dye moieties. The new Rh(II) dimer complex bearing bodipy-based ligands, Rh_2(**BDP**)$_4$ (**CM-2**, H**BDP** = 4,4-difluoro-8-[4-(carboxy)phenylic]-1,3,5,7-tetramethyl-4-bora-3a,4a-diaza-4-bora-*s*-indacene acid), was successfully synthesized and characterized. I also succeeded in constructing a framework catalyst (**FC-2**) by the self-assembly of **CM-2** and the structure of **FC-2** was determined by the single-crystal structural analysis. The studies of structural, electrochemical, photophysical properties compared with corresponded H**BDP** fragment, and catalytic activities of both **CM-2** and **FC-2** are also reported.

Electrocatalytic activity of **CM-2** for H_2 evolution was studied by various electrochemical measurements. CVs of **CM-2** in the presence of acetic acid or trifluoroacetic acid (TFA) as a proton source, showed a large irreversible catalytic current attributed to the H_2 formation. The evolution of H_2 was confirmed by controlled potential electrolysis of **CM-2**. Similarly, electrocatalytic activity of **FC-2** as a heterogeneous catalyst was also examined and the quantitative formation of hydrogen was confirmed. This framework catalyst can be reused at least three cycles with gradual increase of its activity and continue to evolve H_2 up to 9 hours. I subsequently investigated the photocatalytic activity of **CM-2** for H_2 evolution under visible light irradiation. Irradiation of visible light ($\lambda_{exc} > 420$ nm) to a solution of **CM-2** in aqueous-organic medium containing a sacrificial electron donor results in the generation of H_2. Several control experiments were also conducted to shed visible-light for further clarify the catalytic activity of **CM-2** in detail.

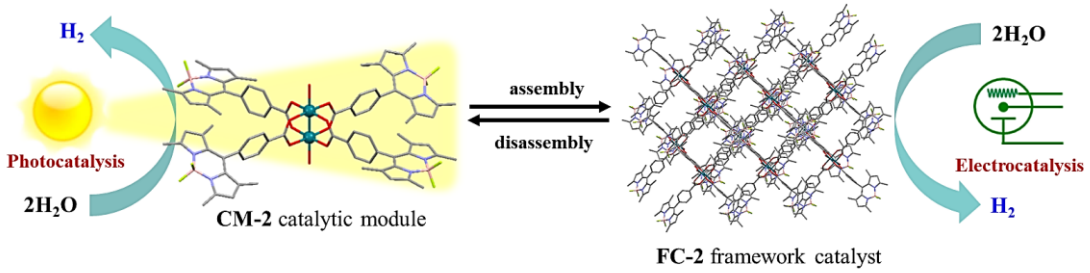

Chapter 2

In Chapter 3, the investigation of a framework catalyst by high energy X-ray measurements (HEXS) and pair distribution analysis (PDF) is reported. X-ray scattering experiments coupled with PDF analysis can reveal the distances between neighboring atoms of overall real space in solid-state. Therefore, quantitative bond distances in the materials can be estimated by comparing the scattering patterns obtained from the experimental and theoretical calculation. In this study, I tried the analysis of **FC-1** by solid-state phase X-ray scattering technique and PDF analysis. The interpretation of results revealed several distances between the **NIP** light-harvesting moiety and the rhodium dimer. I also found the several spectral features reflecting the packing structure of **FC-1**. This outcome study demonstrates the opportunity to resolve the full inner and outer shell ligand structure for coordination complexes in solid-state.

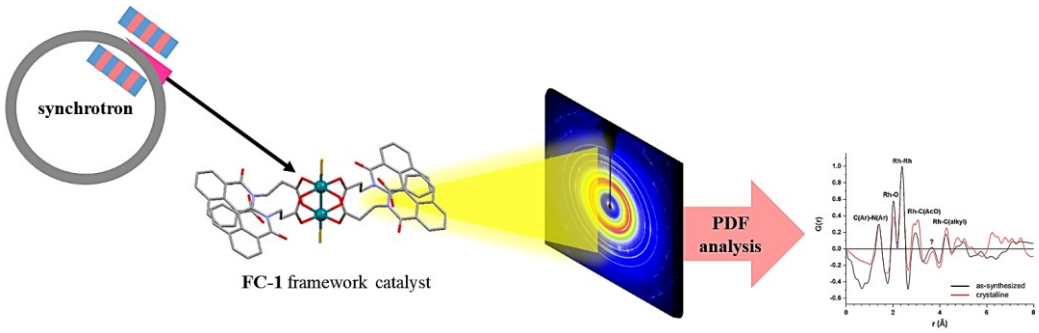

Chapter 3

References

[1] *International Energy Outlook 2017*, U.S. Energy Information Administration, 2017.

[2] (a) J. Ramage, *Energy: A Guidebook*, 1st ed., New York: Oxford University Press, 1983; (b) G. Thomas, *Overview of Storage Development DOE Hydrogen Program*, Sandia National Laboratories, 9 May 2000.

[3] T. Stoll, C. E. Castillo, M. Kanuyama, M. Sandroni, C. Daniel, F. Odobel, J. Fortage and M.-N. Collomb, *Coor. Chem. Rev*., 2015, **304-305**, 20.

[4] (a) E. S. Andreiadis, M. C. Kerlidou, M. Fontecave and V. Artero, *Photochem. Photobiol.*, 2011, **87**, 946; (b) W. T. Eckenhoff and R. Eisenberg, *Dalton Trans*., 2012, **41**, 13004.

[5] (a) M. Wang, Y. Na, M. Gorlov and L. Sun, *Dalton Trans*., 2009, 6458; (b) V. Artero, M. Fontecave and M. Chavarot-Kerlidou, *Angew. Chem. Int. Ed*., 2011, **50**, 7238; (c) F. Wang, W.-G. Wang, H.-Y. Wang, G. Si, C.-H. Tung and L.-Z. Wu, *ACS Catal*., 2012, **2**, 407.

[6] (a) J. M. Lehn and J. P. Sauvage, *Nouv. J. Chim*., 1977, **1**, 449; (b) M. Kirch, J. M. Lehn and J. P. Sauvage, *Helv. Chim. Acta*., **1979**, 1345.

[7] Selected examples on multi-component systems: **abundant metal-based H_2-evolving catalysts:** (a) J. Hawecker, J. M. Lehn and R. Ziessel, *Nouv. J. Chim*., 1983, **7**, 271; (b) P. Du, K. Knowles and R. Eisenberg, *J. Am. Chem. Soc*., 2008, **130**, 12576; (c) P. Du, J. Schneider, G. Luo, W. W. Brennessel and R. Eisenberg, *Inorg. Chem*., 2009, **48**, 4952; (d) X. H. Wang, S. Goeb, Z. Q. Ji, N. A. Pogulaichenko and F. N. Castellano, *Inorg. Chem*., 2011, **50**, 705; (e) A. Fihri, V. Artero, A. Pereira and M. Fontecave, *Dalton Trans*., 2008, 5567; (f) B. Probst, C. Kolano, P. Hamm and R. Alberto, *Inorg. Chem*., 2009, **48**, 1836; (g) B. Probst, A. Rodenberg, M. Guttentag, P. Hamm and R. Alberto, *Inorg. Chem.*, 2010, **49**, 6453; (h) F. Kanoufi, Y. Zu and A. J. Bard, *J. Phys. Chem. B*, 2001, **105**, 210; (i) P. J. DeLaive, T. K. Foreman, C. Giannotti and D. G. Whitten, *J. Am. Chem. Soc*., 1980, **102**, 5627; (j) K. Hashimoto, T. Kawai and T. Sakata, *Nouv. J. Chim.*, 1984, **8**, 693; (k) T. Lazarides, T. McCormick, P. Du, G. Luo, B. Lindley and R. Eisenberg, *J. Am. Chem. Soc.*, 2009, **131**, 9192; (l) P. Zhang, M. Wang, J. Dong, X. Li, F. Wang, L. Wu and L. Sun, *J. Phys. Chem. C*, 2010, **114**, 15868; (m) T. M. McCormick, B. D. Calitree, A. Orchard, N. D. Kraut, F. V. Bright, M. R. Detty and R. Eisenberg, *J. Am. Chem. Soc.*, 2010, **132**, 15480; (n)T. M. McCormick, Z. Han, D. J. Weinberg, W. W. Brennessel, P. L. Holland and R. Eisenberg, *Inorg. Chem*., 2011, **50**, 10660; (o) W. R. McNamara, Z. Han, P. J. Alperin, W. W. Brennessel, P. L. Holland and R. Eisenberg, *J. Am. Chem. Soc*., 2011, **133**, 15368; (p) M. P. McLaughlin, T. M. McCormick, R. Eisenberg and P. L. Holland, *Chem. Commun*., 2011, **47**, 7989; (q) Z. Han, W. R. McNamara, M. E. Eum, P. L. Holland and R. Eisenberg, *Angew. Chem., Int. Ed*., 2012, **51**, 1667; (r) D. Streich, Y. Astuti, M. Orlandi, L. Schwartz, R. Lomoth, L. Hammarström and S. Ott, *Chem.–Eur. J.*, 2010, **16**, 60; (s) 115 F. Wang, W. G. Wang, X. J. Wang, H. Y. Wang, C. H. Tung and L. Z.

Wu, *Angew. Chem. Int. Ed.*, 2011, **50**, 3193; (t) H. Y. Wang, W. G. Wang, G. Si, F. Wang, C. H. Tung and L. Z. Wu, *Langmuir*, 2010, **26**, 9766; (u) H. Kotani, K. Ohkubo, Y. Takai and S. Fukuzumi, *J. Phys. Chem. B*, 2006, **110**, 24047; (v) H. Kotani, T. Ono, K. Ohkubo and S. Fukuzumi, *Phys. Chem. Chem. Phys.,* 2007, **9**, 1487; (w) H. Kotani, K. Ohkubo and S. Fukuzumi, *Faraday Discuss*., 2012, **155**, 89; (x) Y. Yamada, T. Miyahigashi, H. Kotani, K. Ohkubo and S. Fukuzumi, *J. Am. Chem. Soc.*, 2011, **133**, 16136; (y) H. Kotani, R. Hanazaki, K. Ohkubo, Y. Yamada and S. Fukuzumi, *Chem.–Eur. J*., 2011, **17**, 2777; (z) Y. Yamada, T. Miyahigashi, H. Kotani, K. Ohkubo and S. Fukuzumi, *Energy Environ. Sci*., 2012, **5**, 6111; (aa) J. I. Goldsmith, W. R. Hudson, M. S. Lowry, T. H. Anderson and S. Bernhard, *J. Am. Chem. Soc*., 2005, **127**, 7502; (ab) E. D. Cline and S. Bernhard, *Chimia*, 2009, **63**, 709; (ac) E. D. Cline, S. E. Adamson and S. Bernhard, *Inorg. Chem*., 2008, **47**, 10378; (ad) L. L. Tinker, N. D. McDaniel, P. N. Curtin, C. K. Smith, M. J. Ireland and S. Bernhard, *Chem.–Eur. J*., 2007, **13**, 8726; (ae) P. N. Curtin, L. L. Tinker, C. M. Burgess, E. D. Cline and S. Bernhard, *Inorg. Chem*., 2009, **48**, 10498; (af) B. F. DiSalle and S. Bernhard, *J. Am. Chem. Soc.*, 2011, **133**, 11819; (ag) S. Metz and S. Bernhard, *Chem. Commun*., 2010, **46**, 7551; (ah) L. L. Tinker and S. Bernhard, *Inorg. Chem.*, 2009, **48**, 10507; (ai) F. Gärtner, B. Sundararaju, A. E. Surkus, A. Boddien, B. Loges, H. Junge, P. H. Dixneuf and M. Beller, *Angew. Chem., Int. Ed.*, 2009, **48**, 9962; (aj) F. Gärtner, A. Boddien, E. Barsch, K. Fumino, S. Losse, H. Junge, D. Hollmann, A. Bruckner, R. Ludwig and M. Beller, *Chem.–Eur. J*., 2011, **17**, 6425; (ak) F. Gärtner, S. Denurra, S. Losse, A. Neubauer, A. Boddien, A. Gopinathan, A. Spannenberg, H. Junge, S. Lochbrunner, M. Blug, S. Hoch, J. Busse, S. Gladiali and M. Beller, *Chem.–Eur. J.*, 2012, **18**, 3220; (al) F. Gärtner, D. Cozzula, S. Losse, A. Boddien, G. Anilkumar, H. Junge, T. Schulz, N. Marquet, A. Spannenberg, S. Gladiali and M. Beller, *Chem.–Eur. J.*, 2011, **17**, 6998.

[8] Selected examples on multi-component systems: **noble metal-based H_2-evolving catalysts:** (a) G. M. Brown, S. F. Chan and C. Creutz, (b) H. A. Schwarz and N. Sutin, *J. Am. Chem. Soc.*, 1979, **101**, 7638; (c) S. F. Chan, M. Chou, C. Creutz, T. Matsubara and N. Sutin, *J. Am. Chem. Soc.*, 1981, **103**, 369; (d) E. D. Cline, S. E. Adamson and S. Bernhard, *Inorg. Chem*., 2008, **47**, 10378; (e) Z.-T. Yu, Y.-J. Yuan, J.-G. Cai and Z.-G. Zou, *Chem. Eur. J.*, 2013, **19**, 1303; (f) J.-G. Cai, Z.-T. Yu, Y.-J. Yuan, F. Li and Z.-G. Zou, *ACS Catal.*, 2014, **4**, 1953; (g) S. Oishi, *J. Mol. Catal.*, 1987, **39**, 225; (h) R. Bauer and H. A. F. Werner, *Int. J. Hydrog. Energy*, 1994, **19**, 497; S. Fukuzumi, T. Kobayashi and T. Suenobu, *Angew. Chem. Int. Ed.*, 2011, **50** 728; (i) S. Tanaka, S. Masaoka, K. Yamauchi, M. Annaka, K. Sakai, *Dalton Trans.*, 2010, **39**, 11218; (j) T. Stoll, M. Gennari, I. Serrano, J. Fortage, J. Chauvin, F. Odobel, M. Rebarz, O. Poizat, M. Sliwa, A. Deronzier and M.-N. Collomb, *Chem.–Eur. J.*, 2013, **19**, 782; (k) K. Sakai, Y. Kizaki, T. Tsubomura and K. Matsumoto, *J. Mol. Catal*., 1993, **79**, 141; (l) K. Sakai and K. Matsumoto, *J. Mol. Catal*., 1990, **62**, 1; K. Sakai and K. Matsumoto, *J. Coord. Chem*., 1988, **18**, 169; (ay) K. Sakai and H. Ozawa, *Coord. Chem. Rev.*, 2007, **251**, 2753; (m) H. Ozawa and K. Sakai, *Chem. Commun.*, 2011, **47**, 2227; (n) J. Xie,

C. Li, Q. Zhou, W. Wang, Y. Hou, B. Zhang, X. Wang, *Inorg. Chem*., 2012, **51** 6376.

[9] Selected examples on linked systems: **cobaloxime-based catalytic centers**: (a) A. Fihri, V. Artero, A. Pereira and M. Fontecave, *Dalton Trans.*, 2008, 5567; (b) A. Fihri, V. Artero, M. Razavet, C. Baffert, W. Leibl and M. Fontecave, *Angew. Chem. Int. Ed.*, 2008, **47**, 564; (c) T. Lazarides, T. McCormick, P. Du, G. Luo, B. Lindley and R. Eisenberg, *J. Am. Chem. Soc.*, 2009, **131**, 9192; (d) T. M. McCormick, Z. Han, D. J. Weinberg, W. W. Brennessel, P. L. Holland and R. Eisenberg, *Inorg. Chem.*, 2011, **50**, 10660; (e) P. Zhang, M. Wang, C. Li, X. Li, J. Dong and L. Sun, *Chem. Commun*., 2010, **46**, 8806; (f) K. L. Mulfort and D. M. Tiede, *J. Phys. Chem. B*, 2010, **114**, 14572; (g) S. Jasimuddin, T. Yamada, K. Fukuju, J. Otsuki and K. Sakai, *Chem. Commun*., 2010, **46**, 8466. **diiron-based catalytic centers:** (h) C. Tard and C. J. Pickett, *Chem. Rev.*, 2009, **109**, 2245; (i) F. Gloaguen and T. B. Rauchfuss, *Chem. Soc. Rev*., 2009, **38**, 100; (j) W. G. Wang, H. W. Wang, G. Si, C. H. Tung and L. Z. Wu, *Dalton Trans.*, 2009, 2712; (k) G. Si, L. Z. Wu, W. G. Wang, J. Ding, X. F. Shan, Y. P. Zhao, C. H. Tung and M. Xu, *Tetrahedron Lett*., 2007, **48**, 4775; (l) V. Fourmond, S. Canaguier, B. Golly, M. J. Field, M. Fontecave and V. Artero, *Energy Environ. Sci.*, 2011, **4**, 2417; (m) H. Wolpher, M. Borgström, L. Hammarström, J. Bergquist, V. Sundström, S. Styring, L. Sun and B. Åkermark, *Inorg. Chem. Commun.*, 2003, **6**, 989; (n) J. Ekström, M. Abrahamsson, C. Olson, J. Bergquist, F. B. Kaynak, L. Eriksson, L. Sun, H. C. Becker, B. Åkermark, L. Hammarström and S. Ott, *Dalton Trans*., 2006, 4599; (o) S. Ott, M. Borgström, M. Kritikos, R. Lomoth, J. Bergquist, B. Åkermark, L. Hammarström and L. Sun, *Inorg. Chem*., 2004, **43**, 4683; (p) S. Ott, M. Kritikos, B. Åkermark and L. Sun, *Angew. Chem. Int. Ed.*, 2003, **42**, 3285; (q) L. C. Song, M. Y. Tang, S. Z. Mei, J. H. Huang and Q. M. Hu, *Organometallics*, 2007, **26**, 1575; (r) X. Li, M. Wang, S. Zhang, J. Pan, Y. Na, J. Liu, B. Åkermark and L. Sun, *J. Phys. Chem. B*, 2008, **112**, 8198; (s) L. C. Song, L. X. Wang, M. Y. Tang, C. G. Li, H. B. Song and Q. M. Hu, *Organometallics*, 2009, **28**, 3834; (t) L. C. Song, M. Y. Tang, F. H. Su and Q. M. Hu, *Angew. Chem. Int. Ed*., 2006, **45**, 1130; (u) A. P. S. Samuel, D. T. Co, C. L. Stern and M. R. Wasielewski, *J. Am. Chem. Soc*., 2010, **132**, 8813; (v) A. M. Kluwer, R. Kapre, F. Hartl, M. Lutz, A. L. Spek, A. M. Brouwer, P. W. N. M. van Leeuwen and J. N. H. Reek, *Proc. Natl. Acad. Sci. U. S. A.*, 2009, **106**, 10460; (w) W. G. Wang, F. Wang, H. Y. Wang, G. Si, C. H. Tung and L. Z. Wu, *Chem.–Asian J.*, 2010, **5**, 1796, (x) H. Y. Wang, G. Si, W. N. Cao, W. G. Wang, Z. J. Li, F. Wang, C. H. Tung and L. Z. Wu, *Chem. Commun*., 2011, **47**, 8406.

[10] Selected examples on linked systems: **platinum- and palladium-based catalytic centers:** (a) H. Ozawa, M. Haga and K. Sakai, *J. Am. Chem. Soc*., 2006, **128**, 4926; (b) H. Ozawa, Y. Yokoyama, M. Haga and K. Sakai, *Dalton Trans*., 2007, 1197; (c) H. Ozawa and K. Sakai, *Chem. Lett*., 2007, **36**, 920; (d) S. Rau, B. Schäfer, D. Gleich, E. Anders, M. Rudolph, M. Friedrich, H. Görls, W. Henry and J. G. Vos, *Angew. Chem., Int. Ed*., 2006, **45**, 6215; (e) M. Karnahl, C. Kuhnt, F. W. Heinemann, M. Schmitt, S. Rau, J. Popp and B. Dietzek, *Chem. Phys*., 2012, **393**, 65; (f) P. Lei, M. Hedlund, R. Lomoth, H. Rensmo, O. Johansson and L. Hammarström, *J. Am. Chem. Soc*., 2008,

130, 26; (g) P. Du, J. Schneider, F. Li, W. Zhao, U. Patel, F. N. Castellano and R. Eisenberg, *J. Am. Chem. Soc*., 2008, **130**, 5056; (h) K. Yamauchi, S. Masaoka and K. Sakai, *Dalton Trans*., 2011, **40**, 12447; (i) M. Ogawa, G. Ajayakumar, S. Masaoka, H. B. Kraatz and K. Sakai, *Chem.–Eur. J*., 2011, **17**, 1148; (j) M. Hirahara, S. Masaoka and K. Sakai, *Dalton Trans*., 2011, **40**, 3967; (k) G. Ajayakumar, M. Kobayashi, S. Masaoka and K. Sakai, *Dalton Trans*., 2011, **40**, 3955; (l) S. Masaoka, Y. Mukawa and K. Sakai, *Dalton Trans*., 2010, **39**, 5868; (m) R. Okazaki, S. Masaoka and K. Sakai, *Dalton Trans.*, 2009, 6127; (n) M. Kobayashi, S. Masaoka and K. Sakai, *Photochem. Photobiol. Sci.*, 2009, **8**, 196; **rhodium-based catalytic centers**: (o) K. Rangan, S. M. Arachchige, J. R. Brown and K. J. Brewer, *Energy Environ. Sci*., 2009, **2**, 410; (p) T. A. White, S. L. H. Higgins, S. M. Arachchige and K. J. Brewer, *Angew. Chem. Int. Ed. Engl*., 2011, **50**, 12209; (q) J. Wang, T. A. White, S. M. Arachchige and K. J. Brewer, *Chem. Commun.,* 2011, **47**, 4451; (r) S. M. Arachchige, R. Shaw, T. A. White, V. Shenoy, H.-M. Tsui and K. J. Brewer, *ChemSusChem,* 2011, **4**, 514; (s) T. A. White, B. N. Whitaker and K. J. Brewer, *J. Am. Chem. Soc.*, 2011, **133**, 15332; (t) G.F. Manbeck and K. J. Brewer, *Coord. Chem. Rev.*, 2013, **257**, 1660; (u) G. F. Manbeck, E. Fujita and K. J. Brewer, *J. Am. Chem. Soc*., 2017, **139**, 7843; (v) M.-N. Collomb and A. Deronzier, *Eur. J. Inorg. Chem.*, 2009, 2025; (w) T. Stoll, M. Gennari, I. Serrano, J. Fortage, J. Chauvin, F. Odobel, M. Rebarz, O. Poizat, M. Sliwa, A. Deronzier and M.-N. Collomb, *Chem.–Eur. J.*, 2013, **19**, 782; (x) T. Stoll, M. Gennari, J. Fortage, C. E. Castillo, M. Rebarz, M. Sliwa, O. Poizat, F. Odobel, A. Deronzier and M.-N. Collomb, *Angew. Chem. Int. Ed. Engl.*, 2014, **53**, 1654.

[11] (a) A. Fujishima and K. Honda, *Nature*, 1972, **238**, 37; (b) A. Fujishima, K. Honda, *Bull. Chem. Soc. Jpn.*, 1971, **44**, 1148.

[12] Selected reviews: (a) M. Law, L.E. Greene, J.C. Johnson, R. Saykally and P. D. Yang, *Nat. Mater.*, 2005, **4**, 455; (b) X. Chen, S. Shen, L.S. Guo and S. Mao, *Chem. Rev*., 2010, **110**, 6503; (c) Y. Moriya, T. Takata and K. Domen, *Coord. Chem. Rev*., 2013, **257**, 1957; (d) Y. Horiuchi, T. Toyao, M. Takeuchi, M. Matsuoka and M. Anpo, *Phys. Chem. Chem. Phys*., 2013, **15**, 13243; (d) Y. Xu and B. Zhang, *Catal. Sci. Technol*., 2015, **5**, 3084; (e) S. Martha, P. C. Sahoo and K. M. Parida, *RSC Adv*., 2015, **5**, 61535.

[13] Selected examples and reviews: (a) X. Chen, S. Shen, L. Guo, and S. S. Mao, *Chem. Rev*., 2010, **110**, 6503; (b) M.G. Walter, E. L. Warren, J. R. McKone, S. W. Boettcher, Q. Mi, E. A. Santori and N. S. Lewis, *Chem. Rev*., 2010, **110**, 6446; (c) H. Tada, M. Fujishima and H. Kobayashi, *Chem. Soc. Rev.*, 2011, **40**, 4232; (d) K. Shimura, H. Kawai, T. Yoshida and H. Yoshida, *Chem. Commun.*, 2011, **47**, 8958; (e) S. Yan, L. Wan, Z. Li and Z. Zou, *Chem. Commun.*, 2011, **47**, 5632; (f) C. E. Bunker and M. J. Smith, *J. Mater. Chem.***,** 2011, **21**, 12173; (g) K. M. Parida, A. Nashima and S. K. Mahanta, *Dalton Trans.*, 2011, **40**, 12839; (h) H. Liu, J. Yuan, Z. Jiang, W. Shangguan, H. Einagac and Y. Teraoka, *J. Mater. Chem.*, 2011, **21**, 16535; (i) S. Fukuzumi, Y. Yamada, T. Suenobu, K. Ohkuboa and H. Kotani, *Energy Environ. Sci.*, 2011, **4**, 2754; (j) C. X. Kronawitter, L. Vayssieres, S. Shen, L. Guo, D. A. Wheeler, J. Z. Zhang, B. R. Antoun and S. S. Mao, *Energy Environ. Sci.*, 2011, **4**, 3889; (k) B. Chai, T. Peng, P.

Zeng and J. Mao, *J. Mater. Chem.*, 2011, **21**, 14587; (l) T. Grewe and H. Tüysüz, *ACS Appl. Mater. Interfaces*, 2015, **7**, 23153; (m) S. Jin, X. Wang, X. Wang, M. Ju, S. Shen, W. Liang, Y. Zhao, Z. Feng, H. Y. Playford, R. I. Walton and C. Li, *J. Phys. Chem. C*, 2015, **119**, 18221; (n) S. S. Gujral, A. N. Simonov, M. Higashi, X.-Y. Fang, R. Abe and L. Spiccia, *ACS Catal*., 2016, **6**, 3404; (o) H. Du, K. Liang, C.-Z. Yuan, H.-L. Guo, X. Zhou, Y.-F. Jiang and A.-W. Xu, *ACS Appl. Mater. Interfaces*, 2016, **8**, 24550; (p) T. Zheng, W. Sang, Z. He, Q. Wei, B. Chen, H. Li, C. Cao, R. Huang, X. Y., B. Pan, S. Zhou and J. Zeng, *Nano Lett.*, 2017, **17**, 7968; (q) D. Wang, Z.-P. Liu and W.-M. Yang, *ACS Catal*., 2017, **7**, 2744; (r) Z. Lian, W. Wang, G. Li, F. Tian, K. S. Schanze and H. Li, *ACS Appl. Mater. Interfaces*, 2017, **9**, 16959; (s) Y. W. Kim, S. Cha, I. Kwak, I. S. Kwon, K. Park, C. S. Jung, E. H. Cha and J. Park, *ACS Appl. Mater. Interfaces*, 2017, **9**, 36715; (t) X. Cai, M. Zhu, O. A. Elbanna, M. Fujitsuka, S. Kim, L. Mao, J. Zhang and T. Majima, *ACS Catal*., 2018, **8**, 122.

[14] Selected reviews: (a) M. Law, L.E. Greene, J.C. Johnson, R. Saykally and P. D. Yang, *Nat. Mater.*, 2005, **4**, 455; (b) X. Chen, S. Shen, L.S. Guo and S. Mao, *Chem. Rev*., 2010, **110**, 6503; (c) Y. Moriya, T. Takata and K. Domen, *Coord. Chem. Rev*., 2013, **257**, 1957; (d) Y. Horiuchi, T. Toyao, M. Takeuchi, M. Matsuoka and M. Anpo, *Phys. Chem. Chem. Phys*., 2013, **15**, 13243; (d) Y. Xu and B. Zhang, *Catal. Sci. Technol*., 2015, **5**, 3084; (e) S. Martha, P. C. Sahoo and K. M. Parida, *RSC Adv*., 2015, **5**, 61535.

[15] R. Abe, *J. Photochem. Photobiol. C*, 2010, **11**, 179.

[16] (a) T. Zhou, Y. Du, A. Borgna, J. Hong, Y. Wang, J. Han, W. Zhang and R. Xu, *Energy Environ. Sci.*, 2013, **6**, 3229; (b) K. Sasan, Q. Lin, C. Mao and P. Feng, *Chem. Commun*., 2014, **50**, 10390; (c) C.-C. Hou, T.-T. Li, S. Cao, Y. Chen and W.-F. Fu, *J. Mater. Chem. A*, 2015, **3**, 10386; (d) Z. Li, J.-D. Xiao and H.-L. Jiang, *ACS Catal.*, 2016, **6**, 5359; (e) L. Zeng, X. Guo, C. He and C. Duan, *ACS Catal.*, 2016, **6**, 7935; (f) T. Banerjee, F. Haase, G. Savasci, K. Gottschling, C. Ochsenfeld and B. V. Lotsch, *J. Am. Chem. Soc.*, 2017, **139**, 16228; (i) A. S. Weingarten, R. V. Kazantsev, L. C. Palmer, M. McClendon, A. R. Koltonow, A. P. S. Samuel, D. J. Kiebala, M. R. Wasielewski and S. I. Stupp, *Nat. Chem.*, 2014, **6**, 964; (j) A. S. Weingarten, R. V. Kazantsev, L. C. Palmer, D. J. Fairfield, A. R. Koltonow, and S. I. Stupp, *J. Am. Chem. Soc.,* 2015, **137**, 15241.

[17] Selected examples: (a) N. Kaeffer, J. Massin, C. Lebrun, O. Renault, M. Chavarot-Kerlidou, and V. Artero, *J. Am. Chem. Soc*., 2016, **138**, 12308; (b) J. Warnan, J. Willkomm, J. N. Ng, R. Godin, S. Prantl, J. R. Durrant and E. Reisner, *Chem. Sci.*, 2017, **8**, 3070; (c) P. B. Pati, L. Zhang, B. Philippe, R. Fernández-Terán, S. Ahmadi, L. Tian, H. Rensmo, L. Hammarström and H. Tian, *ChemSusChem,* 2017, **10**, 2480.

[18] (a) C.-C. Hou, T.-T. Li, S. Cao, Y. Chen and W.-F. Fu, *J. Mater. Chem. A*, 2015, **3**, 10386; (b) D. Kim, D. R. Whang and S. Y. Park, *J. Am. Chem. Soc*. 2016, **138**, 8698.

[19] M. R. Wasielewski, *Acc. Chem. Res.*, 2009, **42**, 1910.

[20] M. A. Porai-Koshits ans A. S. Antsyshkina, *Dokl. Akad. Sauk. SSSR*, 1962, **146**, 1102.

[21] F. A. Cotton, C. A. Murillo, and R.A Walton, "*Multiple Bonds Between Metal Atoms*", 3rd ed., Springer Science and Business Media, New York, **2005**.

[22] Selected examples: (a) J. F. Berry, F. A. Cotton, P. Huang, C. A. Murillo and X Wang, *Dalton Trans*., 2005, 3713; (b) M. Ebihara, M. Nomura, S. Sakai and T. Kawamura, *Inorg. Chim. Acta*, 2007, **360**, 2345; (c) M. W. Cooke, M.-P. Santoni, G. S. Hanan, F. Loiseau, A. Proust and B. Hasenknopf, *Inorg. Chem.*, 2008, **47**, 6112; (d) D. Pogozhev, S. A. Baudron and M. W. Hosseini, *Dalton Trans*., 2011, **40**, 7403; (e) L. H. Tong, S. Clifford, A. Gomila, S. Duval, L. Guene and A. F. Williams, *Chem. Commun.,* 2012, **48**, 9891; (f) Y. Fuma, O. Miyashita, T. Kawamura and M. Ebihara, *Dalton Trans*., 2012, **41**, 8242; (g) D. K. Kumar, A. S. Filatov, M. Napier, J.Sun, E. V. Dikarev and M. A. Petrukhina, *Inorg. Chem.*, 2012, **51**, 4855; (h) L. H. Tong, S. Clifford, A. Gomila, S. Duval, L. Guene and A. F. Williams, *Chem. Commun*., 2012, **48**, 9891; (i) C. AlvariÇo, D. Simond, P. M. Lorente, C. Besnard and A. F. Williams, *Chem.–Eur. J.*, 2015, **21**, 8851.

[23] B. Chen, M. Eddaoudi, T. M. Reineke, J. W. Kampf, M. O'Keeffe and O. M. Yaghi, *J. Am. Chem. Soc.*, 2000, **122**, 11559.

[24] Selected examples: (a); M. H. Lim and S. J. Lippard, *Acc. Chem. Res.*, 2006, **40**, 41; (b) R. C. Smith, A. G. Tennyson and S. J. Lippard, *Inorg. Chem.,* 2006, **45**, 6222; (c) A. Gulino, T. Gupta, M. Altman, S. Lo Schiavo, P. G. Mineo, I. L. Fragala, G. Evmenenko, P. Dutta and M. E. van der Boom, *Chem. Commun.*, 2008, 2900; ***Oxy*:** (d) M. O. Ratnikov, L. E. Farkas, E. C. McLaughlin, G. Chiou, H. Choi, S. H. El-Khalafy and M. P. Doyle, *J. Org. Chem.,* 2011, **76**, 2585, and references therein; ***Hydrogenation:*** (e) T. Sato, W. Mori, C. N. Kato, T. Ohmura, T. Sato, K. Yokoyama, S. Takamizawa and S. Naito, *Chem. Lett.*, 2003, **32**, 854; (f) S. Naito, T. Tanibe, E. Saito, T. Miyao and W. Mori, *Chem. Lett.*, 2001, **30**, 1178; (g) W. Mori, T. Sato, T. Ohmura, C. N. Kato and T. Takei, *J. Solid State Chem.*, 2005, **178**, 2555; (h) T. Sato, W. Mori, C. Kato, E. Yanaoka, T. Kuribayashi, R. Ohtera, Y. Shiraishi, *J. Catal.*, 2005, **232**, 186; (i) G. Nickerl, U. Stoeck, U. Burkhardt, I. Senkovska and S. Kaskel, *J. Mater. Chem. A*, 2014, **2**, 144. (j) S. Tanaka, S. Masaoka, K. Yamauchi, M. Annaka and K. Sakai, *Dalton Trans.*, 2010, **39**, 11218; Y. Kataoka, K. Sato, Y. Miyazaki, Y. Suzuki, H. Tanaka, Y. Kitagawa, T. Kawakami, M. Okumura and W. Mori, *Chem. Lett.*, 2010, **39,** 358. ***Cycloaddition:*** (k) H. M. L. Davies and C. Venkataramani, *Org. Lett.,* 2003, **5**, 1403; (l) S. Negretti, C. M. Cohen, J. J. Chang, D. M. Guptill and H. M. Davies, *Tetrahedron*, 2015, **71**, 7415; (m) S. Hashimoto, T. Washio, R. Yamaguchi, T. Abe, H. Nambu and M. Anada, *Tetrahedron*, 2007, **63**, 12037; (o) M. P. Doyle, M. Valenzuela and P. L. Huang, *Proc. Natl. Acad. Sci. U. S. A*., 2004, **101**, 5391; (p) M. Anada, T. Washio, N. Shimada, S. Kitagaki, M. Nakajima, M. Shiro and S. Hashimoto, *Angew. Chem., Int. Ed*., 2004, **43**, 2665; (q) R. E. Forslund, J. Cain, J. Colyer and M. P. Doyle, *Adv. Synth. Catal.*, 2005, **347**, 87; (r) M. P. Doyle, R. Duffy, M. Ratnikov, L. Zhou, *Chem. Rev.*, 2010, **110**, 704; H. M. L. Davies and J. R. Manning, *Nature*, 2008, **451**,

417; (s) F. Collet, R. H. Dodd and P. Dauban, *Chem. Commun.*, 2009, 5061; (t) D. A. Colby, R. G. Bergman and J. A. Ellman, *Chem. Rev.*, 2009, **110**, 624; (u) P.-A. Chen, K. Setthakarn and J. A. May, *ACS. Catal.*, 2017, **7**, 6155.

[25] (a) T. A. White, S. E. Witt, Z. Li, K. R. Dunbar and C. Turro, *Inorg. Chem*., 2015, **54**, 10042; (b) G. F. Manbeck, T. Canterbury, R. Zhou, S. King, G. Nam and K. J. Brewer, *Inorg. Chem* , 2015, **54**, 8148; (c) J. Kim, E. Rajkumar, S. Kim, Y. M. Park, Y. Kim, S.-J. Kim and H. J. Lee, *Catalysis Today*, 2017, **295**, 75.

[26] Selected examples: (a) A. Erck, L. Rainen, J. Whileyman, I.-M. Chang, A. P. Kimball and J. Bear, *Exp. Biol. Med.,* 1974, **145,** 1278; (b) H. T. Chifotides and K. R. Dunbar, *Acc. Chem. Res.*, 2005, **38**, 146; (c) A. R. de Souza, E. P. Coelho and S. B. Zyngier, *Eur. J. Med. Chem*., 2006, **41**, 1214.

[27] Selected examples: (a) Z. Rozwadowsk and B. Nowak-Wydra, *Magn. Reson. Chem.*, 2008, **46**, 974. (b) J. T. Mattiza, N. Harada, S. Kuwahara, Z. Hassan and H. Duddeck, *Chirality*, 2009, **21**, 843; (c) H. Duddeck, *Chem. Rec.*, 2005, **5**, 396; (d) Z. Rozwadowski, *Magn. Reson. Chem*., 2007, **45**, 605; (e) H. Duddeck and E. Díaz Gómez, *Chirality*, 2009, **21**, 51.

[28] (a) W. Kosaka, K. Yamagishi, H. Yoshida, R. Matsuda, S. Kitagawa, M. Takata and H. Miyasaka, *Chem. Commun.*, 2013, **49**, 1594; (b) S. Furukawa, N. Horike, M. Kondo, Y. Hijikata, A. Carné-Sánchez, P. Larpent, N. Louvain, S. Diring, H. Sato, R. Matsuda, R. Kawano and S. Kitagawa, *Inorg. Chem*., 2016, **55**, 10843.

[29] Selected examples: (a) S. A. Hilderbrand, M. H. Lim and S. J. Lippard, *J. Am. Chem. Soc.*, 2004, **126**, 4972; (b) M. H. Lim and S. J. Lippard, *Acc. Chem. Res.*, 2006, **40**, 41; (c) R. C. Smith, A. G. Tennyson and S. J. Lippard, *Inorg. Chem.,* 2006, **45**, 6222; (d) A. Gulino, T. Gupta, M. Altman, S. Lo Schiavo, P. G. Mineo, I. L. Fragala, G. Evmenenko, P. Dutta and M. E. van der Boom, *Chem. Commun.*, 2008, 2900.

[30] Selected reviews: (a) C.-T. Chen, *Chem. Mater*., 2004, **16**, 4389; (b) S.-C. Lo and P. L. Burn, *Chem. Rev*., 2007, **107**, 1097; (c) S. Reineke, F. Lindner, G. Schwartz, N. Seidler, K. Walzer, B. Lüssem and K. Leo, *Nature*, 2009, **459**, 234; (d) H. Uoyama, K. Goushi, K. Shizu, H. Nomura and C. Adachi, *Nature*, 2012, **492**, 234; (e) K. S. Yook, J. Y. Lee, *Adv. Mater.*, 2012, **24**, 3169.

[31] Selected reviews and examples: **Reviews:** K. D. Schierbaum, *Sens. Actuator B-Chem*., 1994, **18**, 71; (b) S. I. Stupp and L. C. Palmer, *Chem. Mater*., 2014, **26**, 507; (c) A. Jain, S. J. George, *Mater. Today*, 2015, **18**, 206; **Energy transfer and photon upconversion** (d) C. Fan, W. Wu, J. J. Chruma, J. Zhao, C. Yang, *J. Am. Chem. Soc.*, 2016, **138**, 15405; (e) P. Duan, N. Yanai, H Nagatomi and N.Kimizuka, *J. Am. Chem. Soc*., 2015, **137**, 1887; (f) Z. A. Morseth, T. V. Pho, A. T. Gilligan, R. J. Dillon, K. S. Schanze, J. R. Reynolds and J. M. Papanikolas, *J. Phys. Chem. B*, 2016, **120**, 7937; (g) N. Kimizuka, N. Yanai and M. Morikawa, *Langmuir*, 2016, **32**, 12304; **Photocatalyses:** (h) N. J. Hestand, R. V. Kazantsev, A. S. Weingarten, L. C. Palmer, S. I. Stupp and F. C. Spano, *J. Am. Chem. Soc*., 2016, **138**, 11762; (i) Y.-P. Wu, B.

Yang, J. Tian, S.-B. Yu, H. Wang, D.-W. Zhang, Y. Liu and Z.-T. Li, *Chem. Commun*., 2017, **53**, 13367; (j) M. Xiao, S.-M. Li, Y.-Y. Niu, *J. Chem. Sci*., 2017, **129**, 1521; (k) J. Wang, W.-S. Di, L. Zi, J. Zhang, Y. Zhu, D. Wang, *App. Catal., B: Environ*., 2017, **202**, 289; (l) C. Zhou, C. Lai, D. Huang, G. Zeng, C. Zhang, M. Cheng, L. Hu, J. Wan, W. Xiong, M. Wen, X. Wen and L. Qin, *App. Catal., B: Environ.*, 2018, **220**, 202; **Optoelectronic devices:** (m) G. Chen, I. Mahmud, L. N. Dawe, L. M. Daniels and Y. Zhao, *J. Org. Chem*., 2011, **76**, 2701; (n) D. J. Broer, C. M. W. Bastiaansen, M. G. Debije and A. P. H. J. Schenning, *Angew. Chem. Int. Ed.,* 2012, **51**, 7102; (o) R. Tian, R. Liang, D. Yan, W. Shi, X. Yu, M. Wei, L. S. Li, D. G. Evans and X. Duan, *J. Mater. Chem. C*, 2013, **1**, 5654; (p) L. Li, Y. Zhao, M. Antonietti and M. Shalom, *Small*, 2016, **12**, 6090; (q) Y. Yuan, L. Xu, S. Dai, M. Wang and H. Wang, *J. Mater. Chem. B*, 2017, **5**, 2425.

[32] Selected examples: (a) S. Fujizaki, S. Hamura, H. Eguchi and A. Nishida, *Bull., Chem., Soc. Jpn.*, 1993, 2426; (b) L. Lu and L. Hu, *Dyes Pigm*., 2012, **1026**, 1; (c) S. Rouhani, K. Gharanjig and M. H. Nezhad, *Green Chem. Lett. Rev.*, 2014, **7**, 174.

[33] Selected examples: (a) M. S. Alexiou, V. Tychopoulos, S. Ghorbanian, J. H. P. Tyman, R. G. Brown and P. I. Brittain, *J. Chem. Soc., Perkin Trans. 2*, 1990, **0**, 837; (b) D.-H. Qu, Q.-C. Wang, J. Ren and H. Tian, *Org. Lett.*, 2004, **6**, 2085; (c) B. Liu and H. Tian, *J. Mater. Chem.*, 2005, **15**, 2681; (d) R. M. Duke, E. B. Veale, F. M. Pfeffer, P. E. Kruger and T. Gunnlaugsson, *Chem. Soc. Rev*., 2010, **39**, 3936; (e) S. Banerjee, E. B. Veale, C. M. Phelan, S. A. Murphy, G. M. Tocci, L. J. Gillespie, D. O. Frimannsson, John M. Kelly and T. Gunnlaugsson, *Chem. Soc. Rev*., 2013, **42**, 1601.

[34] Selected examples: (a) J. F. Zhang, S. Kim, J. H. Han, S.-J. Lee, T. Pradhan, Q. Y. Cao, S. J. Lee, C. Kang and J. S. Kim, *Org. Lett*., 2011, **13**, 5294; (b) H.-H. Lin, Y.-C. Chan, J.-W. Chen and C.-C. Chang, *J. Mater. Chem*., 2011, **21**, 3170; (c) R. B. P. Elmes, M. Erby, S. A. Bright, D. C. Williams and T. Gunnlaugsson, *Chem. Commun*., 2012, **48**, 2588; (d) T. Liu, X. Zhang, Q. Qiao, C. Zou, L. Feng, J. Cui and Z. Xu, *Dyes Pigm*., 2013, **99**, 537; (e) L. Zhang, F. Su, X. Kong, F. Lee, S. Sher, K. Day, Y. Tian and D. R. Meldrum, *ChemBioChem* 2016, **17**, 1719; (f) X. Li , J. Hou, C. Peng, L Chen, W. Liu and Y. Liu, *RSC Adv.*, 2017, **7**, 34287; (g) S. Xu, H.-W. Liu, X.-X. Hu, S.-Y. Huan, J. Zhang, Y.-C. Liu, L. Yuan, F.-L. Qu, X.-B. Zhang and W. Tan, *Anal. Chem*., 2017, **89**, 7641.

[35] Selected examples: (a) R. M. Duke, E. B. Veale, F M. Pfeffer, P. E. Kruger and T. Gunnlaugsson, *Chem. Soc. Rev*., 2010, **39**, 3936; (b) T. Gunnlaugsson, H. D. P. Ali and M. Glynn, *J. Fluoresc*., 2005, **15**, 287; (c) R. M. Duke, E. B. Veale, F. M. Pfeffer, P. E. Krugerc and T. Gunnlaugsson, *Chem. Soc. Rev.*, 2010, **39**, 3936; (d) P. Chinapang, V. Ruangpornvisuti, M. Sukwattanasinitt and P. Rashatasakhon, *Dyes Pigm*., 2015, **112**, 236.

[36] Selected examples: a) Y. Zhang, W. Zhu, W. Wang, H. Tian, J. Sua and W. Wang, *J.*

Mater. Chem., 2002, **12**, 1294; (b) D. Kolosov, V. Adamovich, P. Djurovich, M. E. Thompson and C. Adachi, *J. Am. Chem. Soc.*, 2002, **124**, 9945; (c) G. Wang, S. Miao, Q. Zhang, H. Liu, H. Li, N. Li, Q. Xu, J. Lu and L. Wang, *Chem. Commun*., 2013, **49**, 9470.

[37] I. Grabchev and T. Konstantinova, *Dyes Pigm*., 1997, **33**, 197; (b) V. Bojinova and I. Grabchev, *Dyes Pigm*., 2001, **51**, 57; (c) L. G. F. Patrick and A. Whiting, *Dyes Pigm*., 2002, **55**, 123.

[38] (a) I. Ott, Y. Xu, J. Liu, M. Kokoschka, M. Harlos, W. S. Sheldrick and X. Qian, *Bioorg. Med. Chem*., 2008, **16**, 7107; (b) Q. Yang, P. Yang, X. Qian and L. Tong, *Bioorg. Med. Chem. Lett.*, 2008, **18**, 6210; (c) M. Lu and H. Xu, *Curr. Med. Chem*., 2009, **16**, 4797; (d) L. Ingrassia, F. Lefranc, R. Kiss and T. Mijatovic, *Curr. Med. Chem*., 2009, **16**, 1192; (e) Z. Chen, X. Liang, H. Zhang, H. Xie, J. Liu, Y. Xu, W. Zhu, Y. Wang, X. Wang, S. Tan, D. Kuang and X. Qian, *J. Med. Chem*., 2010, **53**, 2589; (f) S. Banerjee, J. A. Kitchen, T. Gunnlaugsson and J. M. Kelly, *Org. Biomol. Chem.*, 2012, **10**, 3033; (g) S. Banerjee, E. B. Veale, C. M. Phelan, S. A. Murphy, G. M. Tocci, L. J. Gillespie, D. O. Frimannsson, J. M. Kelly and T. Gunnlaugsson, *Chem. Soc. Rev*., 2013, **42**, 1601; (h) S. Banerjee, J. A. Kitchen, S. A. Bright, J. E. O'Brien, D. C. Williams, J. M. Kelly and T. Gunnlaugsson, *Chem. Commun*., 2013, **49**, 8522; (i) C. P. Bagowski, Y. You, H. Scheffler, D. H. Vlecken, D. J. Schmitz and I. Ott, *Dalton Trans*., 2009, 10799; (j) K. J. Kilpin, C. M. Clavel, F. Edafe and P. J. Dyson, *Organometallics*, 2012, **31**, 7031.

[39] Selected examples (a) D. L. Reger, A. Debreczeni and M. D. Smith, *Inorg. Chim. Acta.* 2010, **364**, 10; (b) D. L. Reger, A. Debreczeni, J. J. Horger and M. D. Smith, *Crys. Growth. Des.,* 2011, **11**, 4068; (b) D. L. Reger, A. Debreczeni and M. D. Smith, *Inorg. Chem*., 2011, **50**, 11754; (c) D. L. Reger, A. Debreczeni and M. D. Smith, *Inorg. Chem*., 2012, **51**, 1068 and references therein.

[40] S. Mukherjee and P. Thilager, *Phys. Chem. Chem. Phys*., 2014, **16**, 20866.

[41] Selected reviews and examples: (a) A. Loudet and K. Burgess, *Chem. Rev.*, 2007, **107**, 4891; (b) G. Ulrich, R. Ziessel and A. Harriman, *Angew. Chem. Int. Ed*., 2008, **47**, 1184; (c) J. Zhao, K. Xu, W. Yang, Z. Wang and F. Zhong, *Chem. Soc. Rev*., 2015, **44**, 8904.

[42] Selected reviews and recent examples: (a) S. G. Awuah and Y. You, *RSC Adv*., 2012, **2**, 11169; (b) A. Kamkaew, S. H. Lim, H. B. Lee, L. V. Kiew, L. Y. Chung and K. Burgess, *Chem. Soc. Rev.*, 2013, **42**, 77; (c) U. Bhattacharyya, B. Kumar, A. Garai, A. Bhattacharyya, A. Kumar, S. Banerjee, P. Kondaiah and A. R. Chakravarty, *Inorg. Chem*., 2017, **56**, 12457; (d) P. Verwilst, H.-R. Kim, J. Seo, N.-W. Sohn, S.-Y. Cha, Y. Kim, S. Maeng, J.-W. Shin, J. H. Kwak, C. Kang and J. S. Kim, *J. Am. Chem. Soc.*, 2017, **139**, 13393; (e) Y. Zhu, W. Lin, W. Zhang, Y. Feng, Z. Wu, L. Chen and Z. Xie, *Chinese Chem. Lett*., 2017, **28**, 1875; (f) P. Sun, N. Wang, X. Jin and X. Zhu, *ACS Appl. Mater. Interfaces*, 2017, **9**, 36675; (g) A. R. Chakravarty, N. Mukherjee, S. Podder, K. Mitra, S. Majumdar and D. Nandi, *Dalton Trans*., 2017, DOI:

10.1039/C7DT03976J.

[43] Selected reviews and recent examples: (a) T. Kowada, H. Maeda and K. Kikuchi, *Chem. Soc. Rev*., 2015, **44**, 4953; (b) X. Liu, B. Chen, X. Li, L. Zhang, Y. Xu, Z. Liu, Z. Cheng and X. Zhua, *Nanoscale*, 2015, **7**, 16399; (c) Z. Zhou, F. Wang, G. Yang, C. Lu, J. Nie, Z. Chen, J. Ren, Q Sun, C. Zhao and W.-H. Zhu, *Anal. Chem*., 2017, **89**, 11576; (d) Y. Tachapermpon, S. Thavornpradit, A. Charoenpanich, J. Sirirak, K. Burgess and N. Wanichacheva, *Dalton Trans*., 2017, **46**, 16251; (e) L. Zhu, W. Xie, L. Zhao, Y. Zhang and Z. Chen, *RSC Adv*., 2017, **7**, 55839; (f) S. Kolemen and E. U. Akkaya, *Coord. Chem. Rev*., 2018, **354**, 121.

[44] Selected reviews and recent examples: (a) S. P. Singh and T. Gayathri, *Eur. J. Org. Chem*., 2014, 4689; (b) A. Bessette and G. S. Hanan, *Chem. Soc. Rev.*, 2014, **43**, 3342; (c) W. Liu, J. Yao and C. Zhan, *Chin. J. Chem*., 2017, **35**, 1813; (d) M. Ozdemir, S. W. Kim, H. Kim, M.-G. Kim, B. J. Kim, C. Kim and H. Usta, *Adv. Electron. Mater.*, 2017, 3, 1700354; (e) H. Klfout, A. Stewart, M. Elkhalifa and H. He, *ACS Appl. Mater. Interfaces*, 2017, **9**, 39873.

[45] Selected examples: (a) F. Camerel, L. Bonardi, G. Ulrich, L. Charbonnière, B. Donnio, C. Bourgogne, D. Guillon, P. Retailleau and R. Ziessel, *Chem. Mater.*, 2006, **18**, 5009; (b) A. Nagai, J. Miyake, K. Kokado, Y. Nagata and Y. Chujo, *J. Am. Chem. Soc*., 2008, **130**, 15276; (c) A. Kaloudi-Chantzea, N. Karakostas, C. P. Raptopoulou, V. Psycharis, E. Saridakis, J. Griebel, R.Hermann and G. Pistolis, *J. Am. Chem. Soc*., 2010, **132**, 16327; (d) J.-H. Olivier, J. Barberá, E. Bahaidarah, A. Harriman and R. Ziessel, *J. Am. Chem. Soc*., 2012, **134**, 6100; (e) G. Gupta, A. Das, S. Panja, J. Y. Ryu, J. Lee, N. Mandal and C. Y. Lee, *Chem.–Eur. J*. 2017, **23**, 17199; (f) G. Gupta, A. Das, K. C. Park, A. Tron, H. Kim, J. Mun, N. Mandal, K.-W. Chi, C. Y. Lee *Inorg. Chem.*, 2017, **56**, 4615; (g) E. Martinou, K. Seintis, N. Karakostas, A. Bletsou, N. S. Thomaidis, M. Fakis and G. Pistolis, *J. Phys. Chem. C*, 2017, **121**, 5341; (h) G. Gupta, A. Das, S. Panja, J. Y. Ryu, J. Lee, N. Manda and C. Y. Lee, *Chem.–Eur. J*., 2017, **23**, 17199; (i) M. Morisue, S. Nakano, M. Shimizua and T. Yumura, *Chem. Commun*., 2018, DOI: 10.1039/C7CC07049G.

[46] (a) J. L. Wang, C. Wang and W. Lin, *ACS Catal*., 2012, **2**, 2630; (b) T. Zhang and W. Lin, *Chem. Soc. Rev.*, 2014, **43**, 5982; (c) D. Wang, R. Huang, W. Liu, D. Sun and Z. Li, *ACS Catal.*, 2014, **12**, 4254; (d) Y. Fang, Y. Ma, M. Zheng, P. Yang, A. M. Asiri and X. Wang, *Coord. Chem. Rev.*, 2017, DOI: 10.1016/j.ccr.2017.09.013.

[47] (a) T. Itoh, M. Kondo, M. Kanaike and S. Masaoka, *CrystEngComm*, 2013, **15**, 6122; (b) T. Itoh, M. Kondo, H. Sakamoto, K. Wakabayashi, M. Kanaike, K. Itami and S. Masaoka, *Dalton Trans.*, 2015, **44**, 15334.

Chapter 1

Development of a framework catalyst bearing 1,8-naphthalimide moieties for photocatalytic hydrogen evolution

Introduction

The photocatalytic production of H_2 from water is a promising way to provide a sustainable and environmentally friendly chemical fuel.[1] Thus, considerable efforts have been devoted to the development of molecular-based homogeneous photocatalytic systems for hydrogen production by utilizing various combinations of discrete catalysts and photosensitizers.[2] A great advantage of such homogenous systems is that we can understand their reaction mechanisms in detail based on well-established spectroscopic techniques.[3-4] The nature of the systems allows us to precisely tune their structures/properties, which results in improved catalytic activities. However, homogeneous systems are considered unsuitable for future practical applications because of their moderate reusability and stability, for which heterogeneous photocatalytic systems are rather advantageous.[5] While heterogeneous systems can offer additional advantages for practical uses through efficient reusable, ease of separation and robustness enhancement. These limitations of homogeneous catalysts prompted us to develop novel molecular-based catalytic systems, in which the advantageous features of homogeneous and heterogeneous systems are integrated.

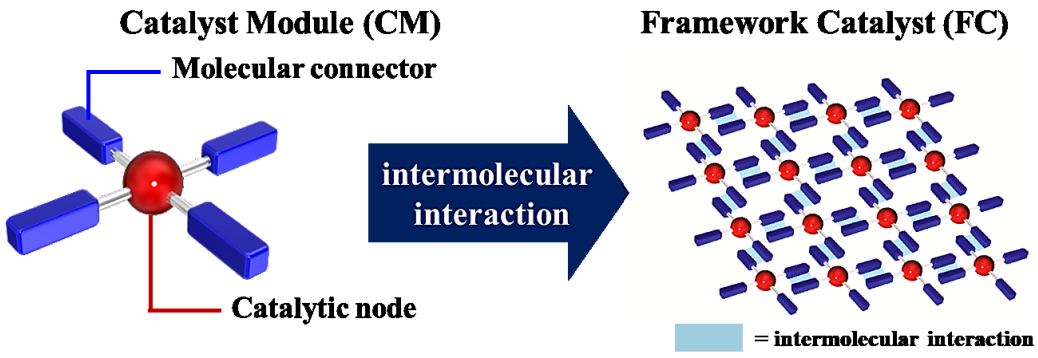

Scheme 1 Schematic illustration of the assembly of catalyst modules via non-covalent intermolecular interactions to afford a framework catalyst.

Here, I propose an effective approach to construct a heterogeneous photocatalytic system based on the supramolecular assembly of molecular catalyst modules. In this system, a discrete catalyst module (Scheme 1, left), which has a metal-complex-based catalytic centre (catalytic node) and intermolecular interaction sites (molecular connector), can be assembled into an ordered structure via non-covalent interactions (Scheme 1, right) to afford a heterogeneous framework catalyst. This self-assembly method, which avoids the strenuous synthesis of bridging ligands and varying the composition of the photosensitizer and catalyst, is thus very promising for the design of molecular photocatalytic water reduction systems. Unlike assembly driven by coordination bonding, known as coordination polymers,[6] I can easily assemble/disassemble catalyst modules simply by changing solvents while maintaining the structure of the active sites.[7] Therefore, our system provides two prominent features: (1) well-defined catalytic sites attributed to the molecular-based modules and (2) reusability and high durability based on the heterogeneous nature.

In this study, I employed a Rh(II) dimer complex bearing 1,8-naphthalimide-based ligands, Rh_2(**NIP**)$_4$ (**CM-1**, H**NIP** = 3-(1,8-naphthalimido)-propanoic acid), as a catalyst module (Fig. 1). **CM-1** is composed of a Rh(II) paddle-wheel unit as a catalytic node and 1,8-naphthalimide moieties as molecular connectors. The Rh(II) paddle-wheel unit is known to catalyse the hydrogen evolution reaction from water[8] and exhibits high (D_{4h}) symmetry suitable for the construction of ordered structures.[7] 1,8-Naphthalimide can serve both as a light-harvesting unit for the photocatalytic reaction and a functional moiety to construct intermolecular π–π stacking interactions.[9] Reported here is the development of a framework catalyst (**FC-1**) via the self-assembly of the catalyst module **CM-1**. The physical properties of **CM-1** and **FC-1** were investigated by spectroscopic techniques and electrochemical measurements. I also examined the activity, durability and reusability of **FC-1** as a heterogeneous photocatalyst for hydrogen evolution.

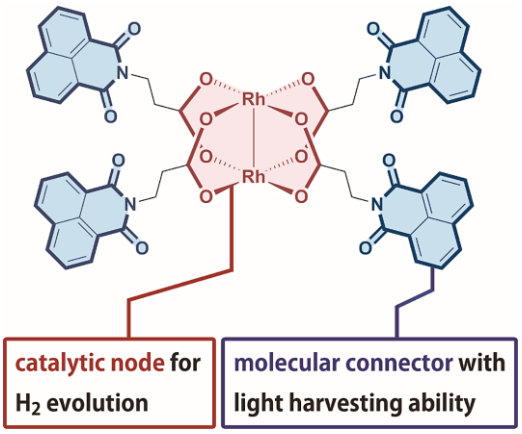

Figure 1. Features of the catalyst module **CM-1** investigated in this chapter.

Results and Discussion

Synthesis of catalytic module 1 (CM-1) and framework catalyst 1 (FC-1)

The catalyst module **CM-1** was successfully synthesized by the ligand exchange reaction between H**NIP** and $Na_4[Rh_2(CO_3)_4]\cdot 3H_2O$, and characterized by several spectroscopic analysis techniques and elemental analysis. The synthesis of **CM-1** was performed as follows. Initially, H**NIP** was synthesized according to a previously reported procedure.[10] Subsequently, 8.0 equivalents of H**NIP** was reacted with $Na_4[Rh_2(CO_3)_4]\cdot 3H_2O$ for 2 hours in water under refluxing conditions (Scheme 5 in the experimental section).[11] The green precipitate formed during the reaction was collected by filtration and washed with methanol, acetone and diethyl ether (for detailed experimental procedures, see the experimental section). The formation of the desired complex, Rh_2(**NIP**)$_4(H_2O)_2$, was confirmed by elemental analysis and ^{1}H NMR spectroscopy and ESI-TOF-MS. **CM-1** was soluble in highly polar solvents, such as dimethylsulfoxide (DMSO) and *N*,*N*-dimethylformamide (DMF)

Subsequently, the self-assembly of **CM-1** to construct a framework catalyst (**FC-1**) was performed by the slow diffusion of $CHCl_3$ into a DMSO solution of **CM-1**. The single-crystal X-ray structure analysis of the obtained crystal reveals the formation of framework structure stabilized by the intermolecular via π–π stacking interactions between the aromatic rings of the **NIP** ligands. The result clearly indicates that the framework catalyst (**FC-1**) can be constructed via the self-assembly of **CM-1**.

X-ray crystallographic structure

The self-assembly of the catalyst module **CM-1** to construct a framework catalyst (**FC-1**) was performed by the slow diffusion of $CHCl_3$ into a DMSO solution of **CM-1**, and single crystals suitable for X-ray structural determination were obtained. As shown in Fig. 2a, the structure of the catalyst module consists of a Rh(II) paddle-wheel unit, and our **NIP** ligands occupy the positions in the equatorial plane of each rhodium atom. Note that DMSO molecules are coordinated to the axial positions of the two rhodium centres. The distance between the two rhodium centres (Rh1-Rh1') was 2.4166(4) Å, which is in the range found for previously reported Rh(II) paddle-wheel dimers (2.316 to 2.486 Å).[7,12] The four naphthalimide rings in the **NIP** ligands are arranged almost parallel to each other within the complex.

The crystal packing structure is shown in Fig. 2b and 2c. An infinite one-dimensional (1-D) columnar structure along the *a* axis was formed via π–π stacking interactions between the aromatic rings of the **NIP** ligands (pale blue lines in Fig. 2b). The mean interplanar separation between two **NIP** moieties in the same column was 3.49 Å (for details, see Fig. 2b). Additionally, these 1-D columns are connected through π–π stacking interactions (pale red lines in Fig. 2c) and framework structure forms (Fig. 3b). The distance of the intercolumn π–π interactions was estimated to be 3.33 Å (Fig. 2b) based on the mean interplanar separation between the **NIP** moieties. Due to such strong intermolecular interactions, the obtained structure exhibited poor solubility in common organic solvents and was not soluble in water, which is an excellent feature for application in heterogeneous systems. These observations confirm the formation of the framework catalyst (**FC-1**) via the self-assembly of the catalyst module **CM-1**.

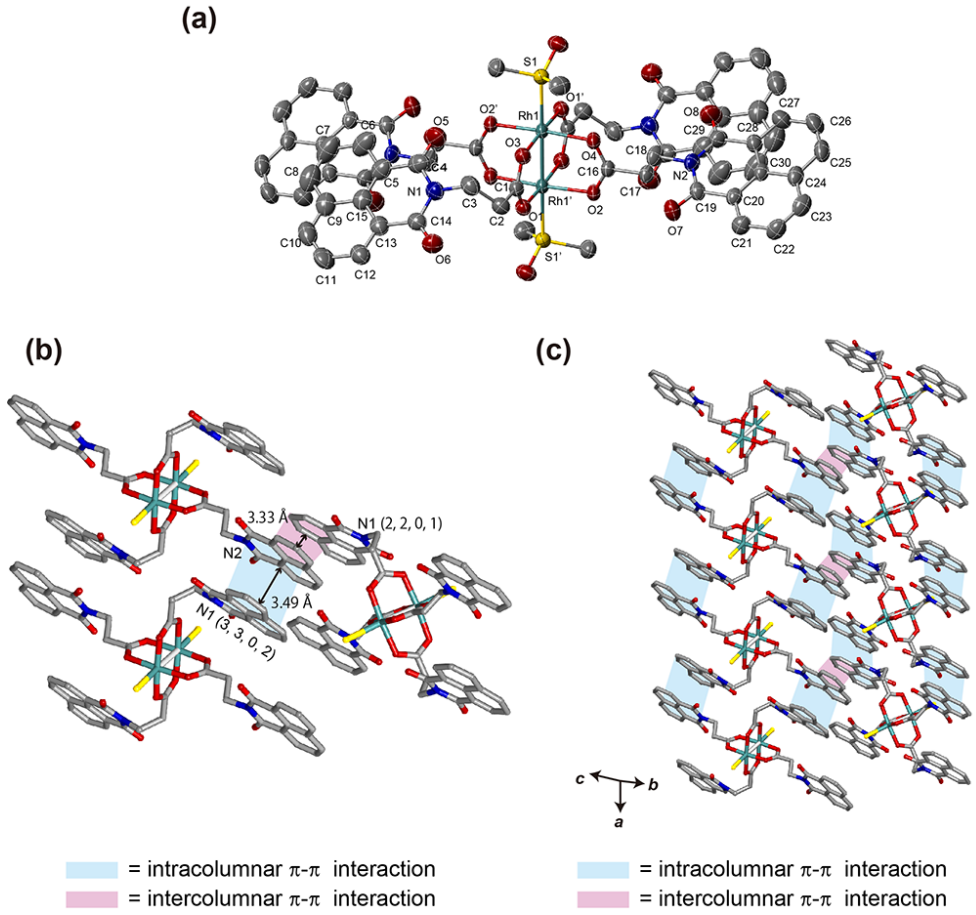

Figure 2. (a) An ORTEP drawing of **FC-1** (50% probability ellipsoids). Hydrogen atoms and crystal solvent molecules are omitted for clarity. (b) Crystal packing of **FC-1** along the *a* axis. Intracolumnar and intercolumnar π–π stacking interactions are shown in pale blue and pale red lines, respectively. Hydrogen atoms, DMSO molecules at the axial positions except for the coordinated sulfur atoms and crystal solvent molecules observed in the channels are omitted for clarity. O = red, C = grey, N = blue, S = yellow, Rh = sea green. (c) Intermolecular interactions observed in **FC-1**. The mean interplanar separation between two **NIP** moieties was calculated as follows. First, the mean plane of the **NIP** moiety containing N2 atom (plane 1: N2 and C19-30) was defined. Next, the distances between plane 1 and atoms constituting the neighboring **NIP** moiety was measured. The average of the obtained distances corresponds to the distance of π-π interactions. Distances of intracolumnar and intercolumnar π-π interactions were estimated using the overlapped **NIP** moieties containing C5-13 and C15 (symmetry operation: 3, 3, 0, 2) and C9-15 (symmetry operation: 2, 2, 0, 1), respectively.

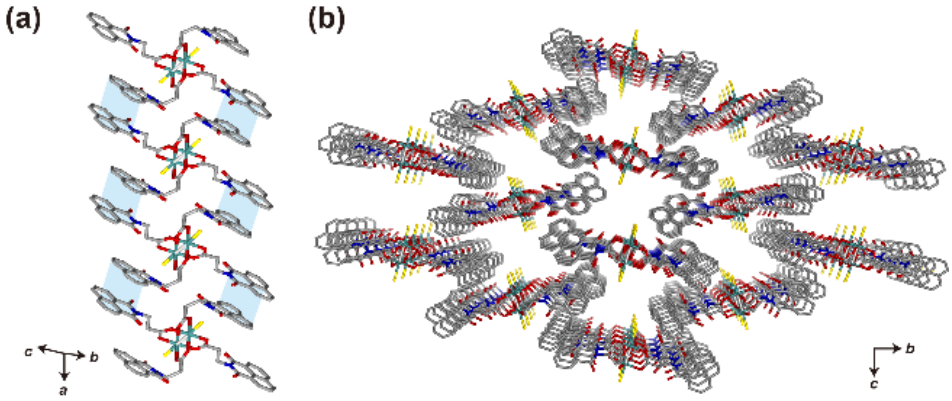

Figure 3. Crystal structure of **FC-1** along (a) the *a* axis and (b) the *c* axis. Hydrogen atoms, DMSO molecules coordinated at the axial positions except for the coordinated sulfur atoms and crystal solvent molecules are omitted for clarity. O = red, C = grey, N = blue, S = yellow, Rh = sea green. Intermolecular π-π interactions within one-dimensional columns are shown in pale blue line.

The photophysical properties

The physical properties of the catalyst module **CM-1** and the framework catalyst **FC-1** were investigated by various techniques. Initially, the photochemical properties of **CM-1** were analysed by UV-vis absorption spectroscopy. The UV-vis spectrum of **CM-1** in DMF exhibited an intense absorption band with an absorption maximum at 334 nm and a band with moderate intensity centred at 585 nm (Fig. 4). The former band corresponds to the π-π* transition of the 1,8-naphthalimide moiety in the ligand, and the latter is attributed to the π* → σ* transition of the dirhodium centre (Scheme 2).[13] I also studied the photochemical properties of **FC-1** by diffuse-reflectance spectroscopy (Fig. 5), and the π-π* transition (λ_{max} = 335 nm) and the π* → σ* transition (λ_{max} = 515 nm) bands of **CM-1** were observed. The existence of the intense band indicates the excellent light-harvesting properties of **FC-1**.

Next, fluorescence spectroscopy of H**NIP**, **CM-1** and **FC-1** was performed. H**NIP** exhibited strong emission both in solution (in DMF, λ_{em} = 393 nm, Fig. 6) and in the solid-state (λ_{em} = 462 nm, Fig. 7), which is typical for 1,8-naphthalimide derivatives.[9a,b] In contrast, **CM-1** and **FC-1** did not show fluorescence at ambient temperature, suggesting that quenching of the excited state of the **NIP** moiety, **NIP***, by the Rh_2 centre occurred. Summary of the solution state UV-Vis absorption and fluorescence emission for **CM-1** and H**NIP** and summary of the UV-Vis diffuse reflectance and solid-state fluorescence emission for **FC-1** and H**NIP** are depicted in Table 1 and 2, respectively.

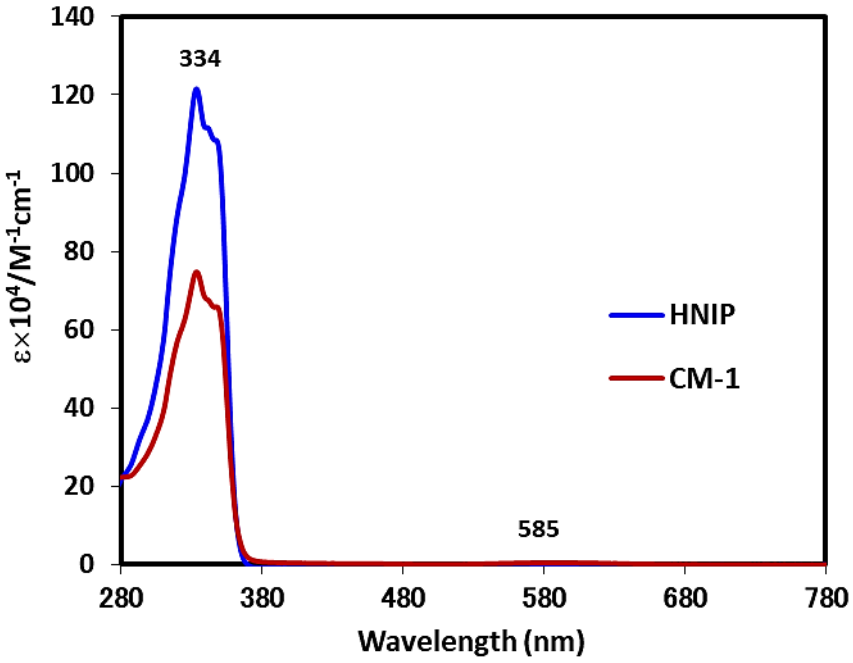

Figure 4. Solution UV-Vis absorption spectra in DMF of free ligand H**NIP** (blue) and **CM-1** (red line). For H**NIP**, the band corresponds to π–π* transition appears at 334 nm. In the case of **CM-1**, the bands correspond to π–π* transition (**NIP** moieties) and π* → σ* transition (Rh_2 centre) were observed at 334 and 585 nm, respectively.

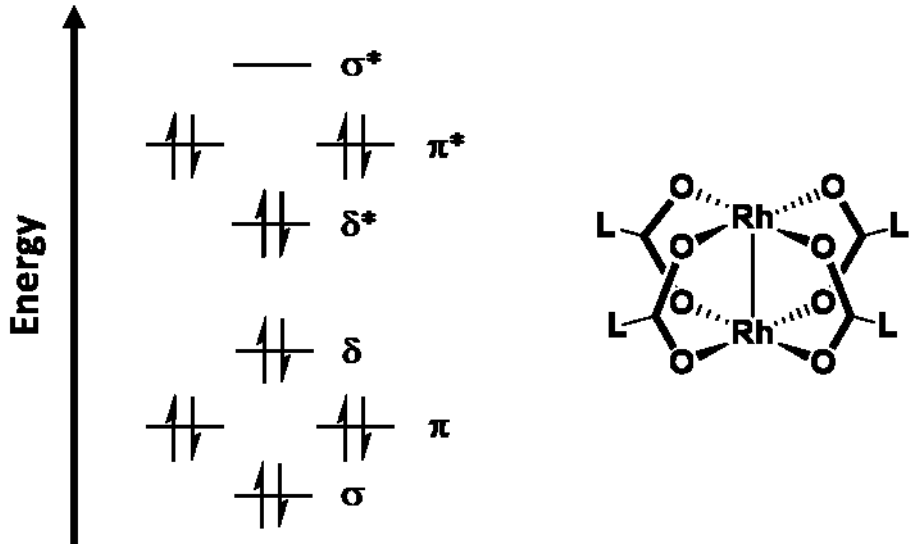

Scheme 2. Schematic illustration of MO diagram of Rh_2 centre having d^7-d^7 configuration.

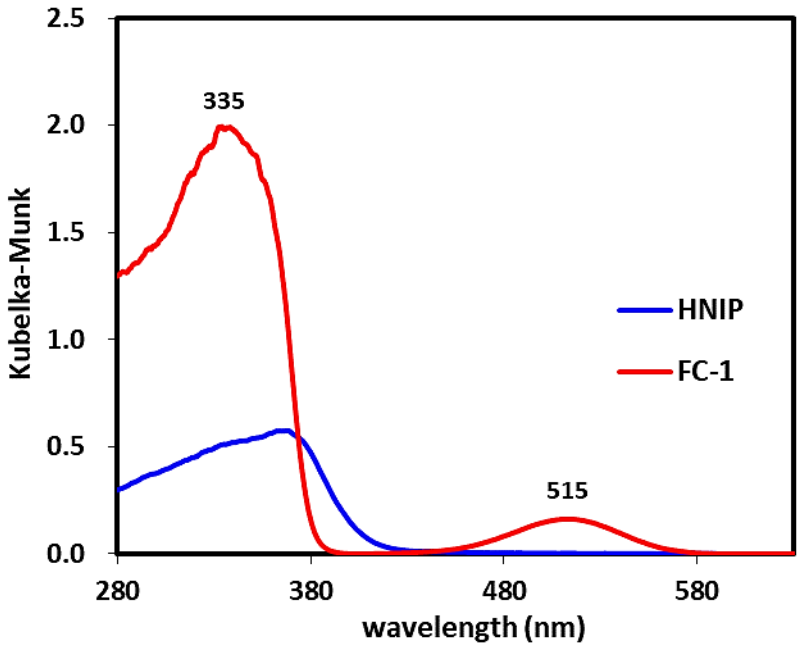

Figure 5. Diffuse reflectance UV-Vis spectra of the solid samples of free ligand H**NIP** (blue line) and **FC-1** (red line). For H**NIP**, the band corresponds to π–π* transition appears at 373 nm. In the case of **FC-1**, the bands correspond to π–π* transition (**NIP** moieties) and π* → σ* transition (Rh(II) centre) were observed at 335 and 515 nm, respectively.

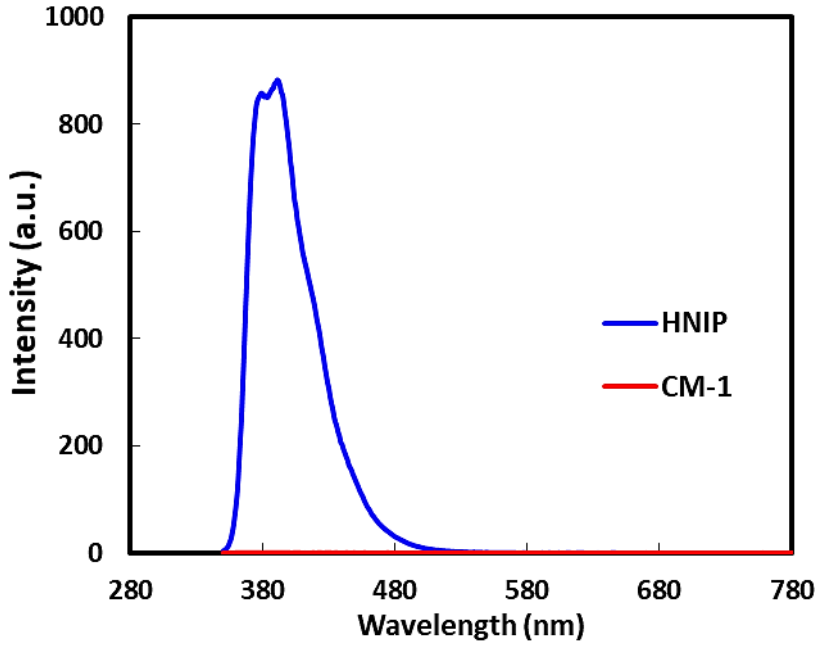

Figure 6. Solution fluorescence emission spectra in DMF solution at 0.04 mM of free ligand H**NIP** (blue) and **CM-1** (red line) at ambient temperature, the excitation wavelength was 334 nm. For H**NIP**, the emission band appears at 393 nm. For **CM-1**, a very weak emission band (less than 1 a.u.) was observed at 379 nm.

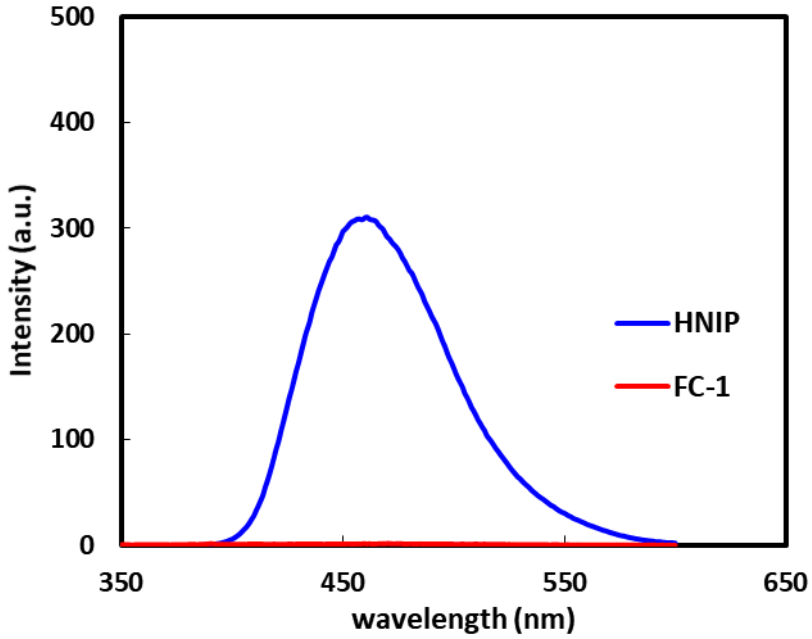

Figure 7. Solid-state fluorescence emission spectra free ligand of H**NIP** (blue) and **FC-1** (red line). The excitation wavelengths were 373 nm and 353 nm for H**NIP** and **FC-1**, respectively. The emission band of H**NIP** appears at 462 nm, while no emission band was not observed in **FC-1**.

Table 1. Summary of the solution state UV-Vis absorption and fluorescence emission for **CM-1** and H**NIP** in dimethylformamide (DMF).

Compound	Solution state (DMF)		
	λ_{abs} /nm ($\varepsilon \times 10^4$ $M^{-1}cm^{-1}$)	λ_{exc}/nm	λ_{ems}/nm (intensity/a.u.)
CM-1	334 (74.13) and 585 (0.53)	334	379 (<1)
HNIP	334 (121.43)	334	393 (872.54)

Table 2. Summary of the UV-Vis diffuse reflectance and solid-state fluorescence emission for **FC-1** and H**NIP**.

Compound	Solid-state		
	λ_{dr} /nm (K.M.)	λ_{exc}/nm	λ_{ems}/nm (intensity/a.u.)
FC-1	335 (1.98) and 515 (0.16)	335	-
HNIP	373 (0.63)	373	462 (308.10)

Electrochemical and spectroelectrochemical studies

The electrochemical properties of **CM-1** were studied by cyclic voltammetry. A cyclic voltammogram of **CM-1** was measured in a DMF solution containing tetra-*n*-butyl ammonium perchlorate (TBAP) as an electrolyte. One reversible oxidation wave and one reversible reduction wave were observed at 1.00 and −1.26 V (vs. NHE), respectively (Fig. 8, red line). The oxidation wave is attributed to the $Rh^{III}Rh^{II}/Rh^{II}Rh^{II}$ redox couple, and the reduction wave is assigned to the reduction of the **NIP** moiety because one reversible reduction wave was observed at a similar potential for the free ligand, H**NIP** (Fig. 8, blue line). The ligand-based reduction of **CM-1** at −1.26 V was also confirmed by spectroelectrochemical measurements of **CM-1** and H**NIP** (Figs. 9 and 10, respectively).

I also investigated the electrochemical properties of **CM-1** upon the addition of acetic acid. As shown in Fig. 11, a large irreversible current was observed at approximately −0.90 V (vs. NHE), indicating catalytic activity of **CM-1** for hydrogen evolution. It should be noted that the electrocatalytic reaction occurs in the potential region in which no redox waves of **CM-1** were observed in the absence of acetic acid (Fig. 12, red line) or in the presence of water (Fig. 12, blue line). These results suggest that the interaction between acetic acid and the Rh_2 centre generates the catalytically active $Rh^{II}Rh^{I}$-H species, and the reduction was observed at the more positive potential region in the electrocatalytic condition as reported in a previous study.[8a,14]

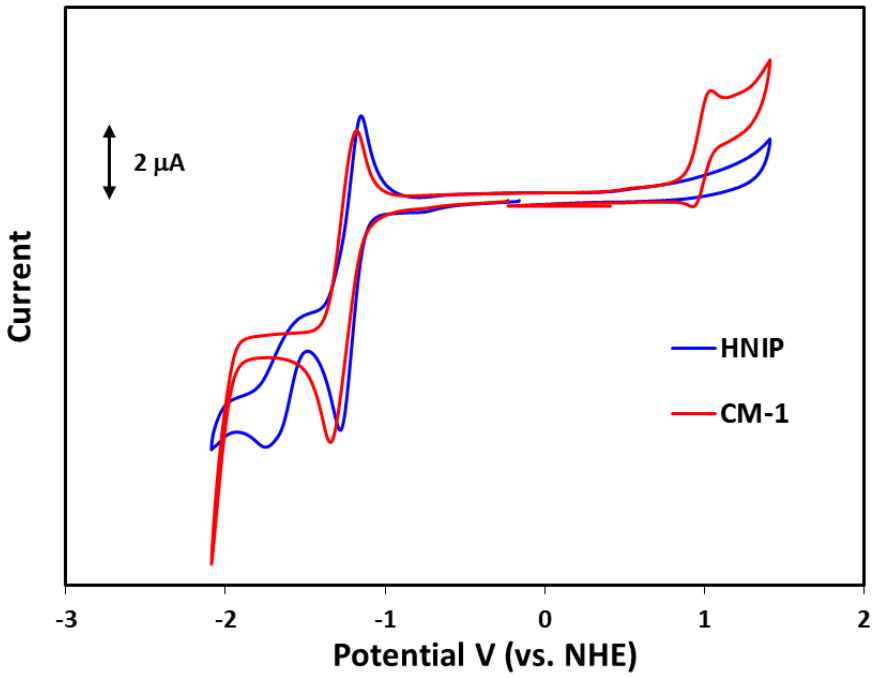

Figure 8. Cyclic voltammograms of 0.5 mM of **CM-1** (red line) and H**NIP** (blue line) in DMF containing 0.1 M TBAP at room temperature under an Ar atmosphere (WE: glassy carbon, AE: Pt wire, RE: Ag/Ag^{+}), at scan rate of 15 mV/s.

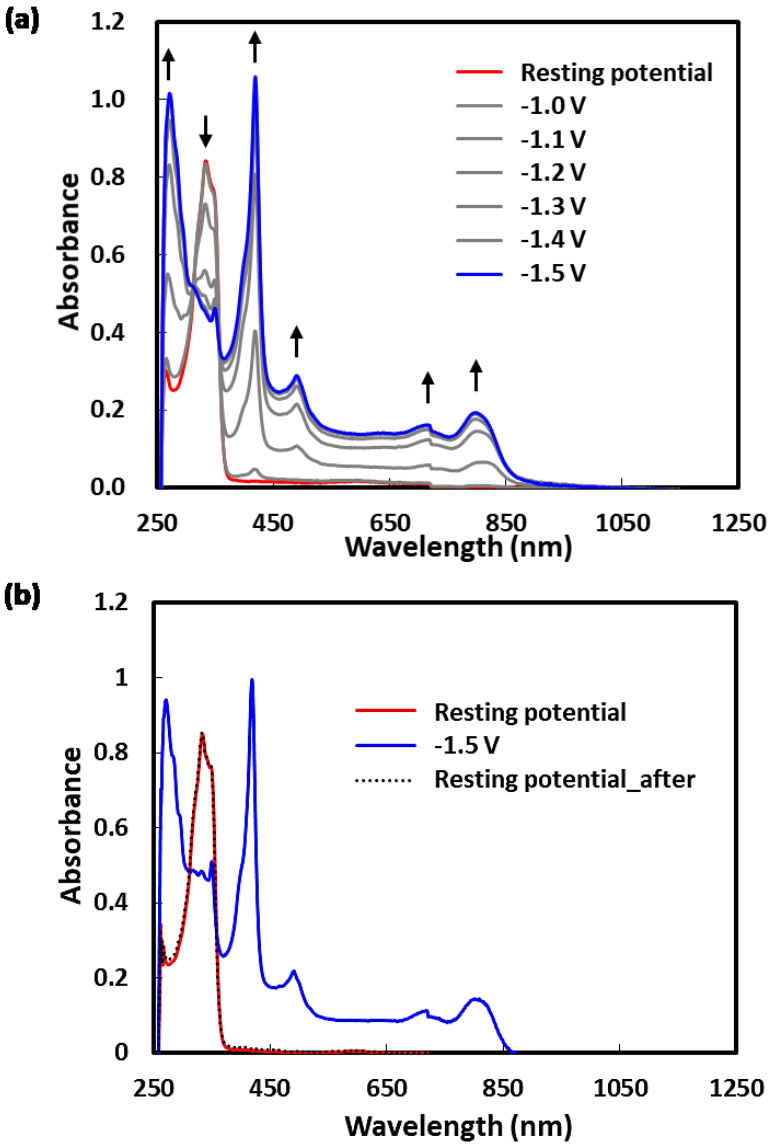

Figure 9. (a) Spectroelectrochemical changes of **CM-1** (0.2 mM) in a DMF solution containing 0.1 M TBAP upon apply potential from the resting potential (0.24 V vs. NHE, red line) to -1.5 V (blue line). (b) UV-vis absorption spectra of **CM-1** at the resting potential (red line), at -1.5 V (blue line), at the resting potential (0.24 V) recorded after the reduction (grey dotted line). All measurements were performed at room temperature under an Ar atmosphere (WE: Pt gauze, AE: Pt wire, RE: Ag/Ag^{+}).

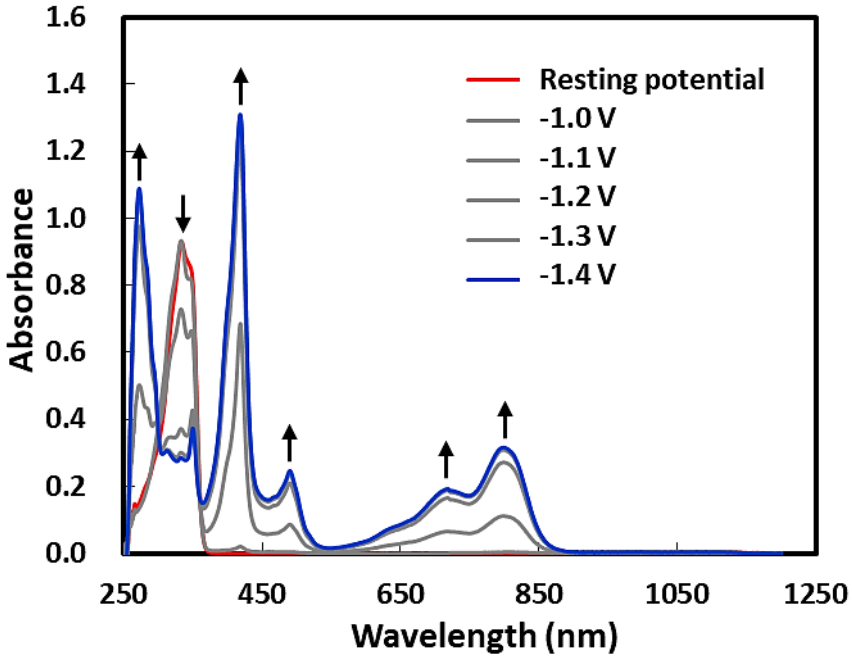

Figure 10. Spectroelectrochemical changes of H**NIP** (0.8 mM) in DMF containing 0.1 M TBAP upon apply potential from the resting potential (0.23 V vs. NHE, red line) to -1.4 V (blue line) at room temperature under an Ar atmosphere (WE: Pt gauze, AE: Pt wire, RE: Ag/Ag^{+}).

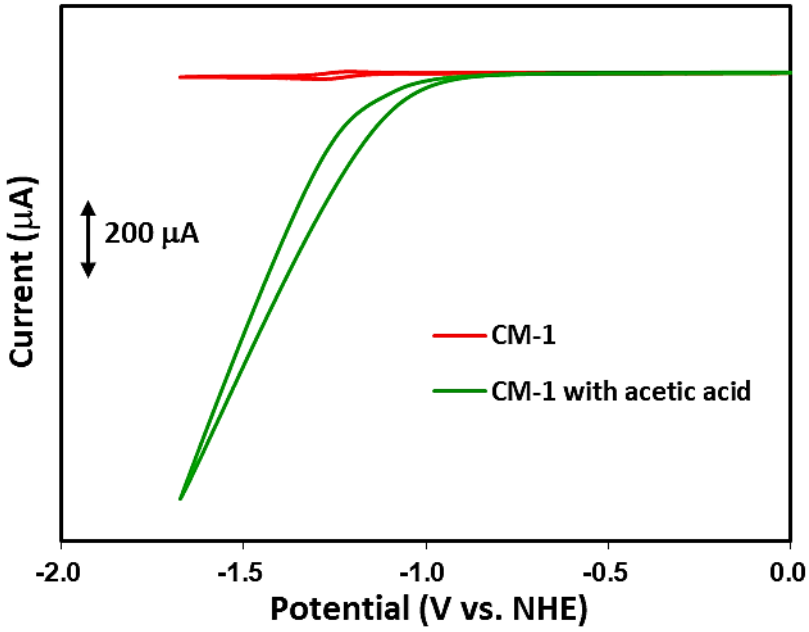

Figure 11. Cyclic voltammogram of **CM-1** (0.5 mM) upon addition of acetic acid (2.90 M) containing 0.1 M TBAP in DMF at room temperature under an Ar atmosphere (WE: glassy carbon, AE: Pt wire, RE: Ag/Ag^{+}), at scan rate of 15 mV/s.

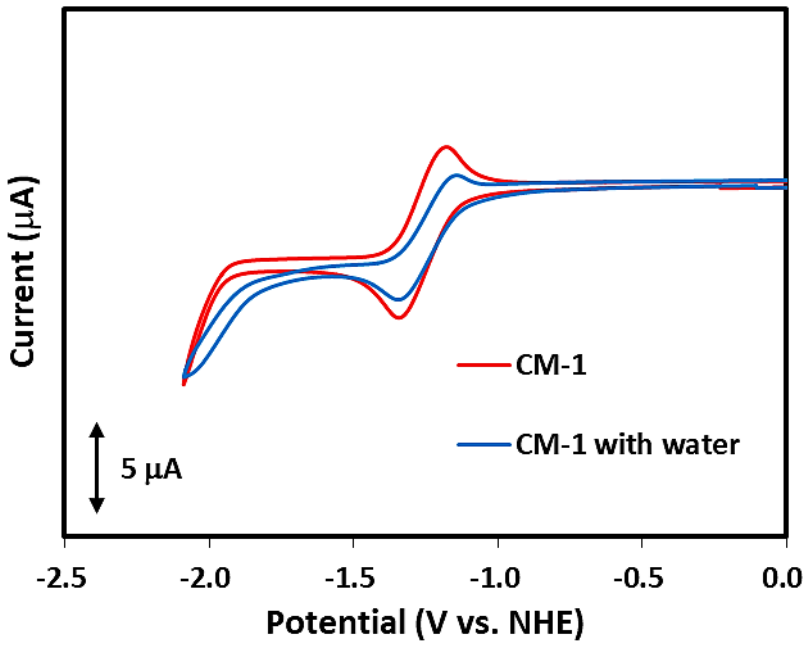

Figure 12. Cyclic voltammogram of **CM-1** (0.5 mM) in the excess amount of water containing 0.1 M TBAP in DMF at room temperature under an Ar atmosphere (WE: glassy carbon, AE: Pt wire, RE: Ag/Ag^{+}), at scan rate of 15 mV/s.

Solid-state cyclic voltammogram measurement

The electrochemical properties of **FC-1** were also investigated by cyclic voltammetry. In this measurement, **FC-1** was deposited on the surface of a glassy carbon working electrode, and the CVs in dichloromethane containing TBAP as an electrolyte and in acetate buffer (pH = 5) were measured (Scheme 3). The CVs of **FC-1** in dichloromethane is shown in Fig. 13. The redox waves attributed to the $Rh^{III}Rh^{II}/Rh^{II}Rh^{II}$ redox couple and the reduction of **NIP** moiety were observed at 1.20 and −0.95 V (vs. NHE), respectively. These potentials were shifted to the positive potential region compared to those of **CM-1**. In the CV in acetate buffer, a large irreversible current similar to **CM-1** was observed (Fig. 14), indicating that **FC-1** can serve as a heterogeneous H_2 production catalyst. The onset potential for H_2 production mediated by **FC-1** was determined to be −0.71 V (vs. NHE). It should be noted that no catalytic current was observed when the measurements were performed in TES and KHP buffer solutions (Fig. 15), which indicates that the interaction between acetic acid and the Rh_2 centre generates the catalytically active Rh_2-H species to promote catalytic hydrogen evolution in the solid-state.

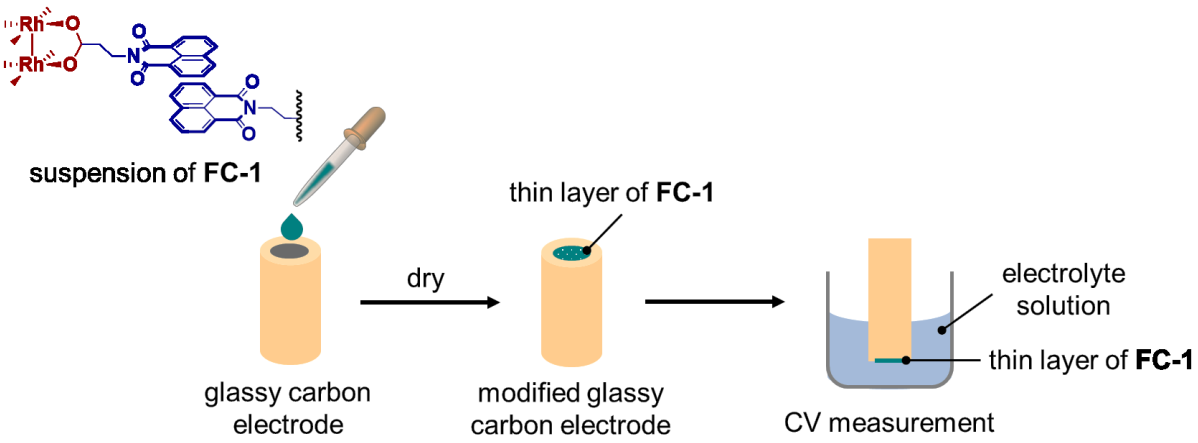

Scheme 3. Schematic illustration of the procedure to modify a glassy carbon electrode with **FC-1**.

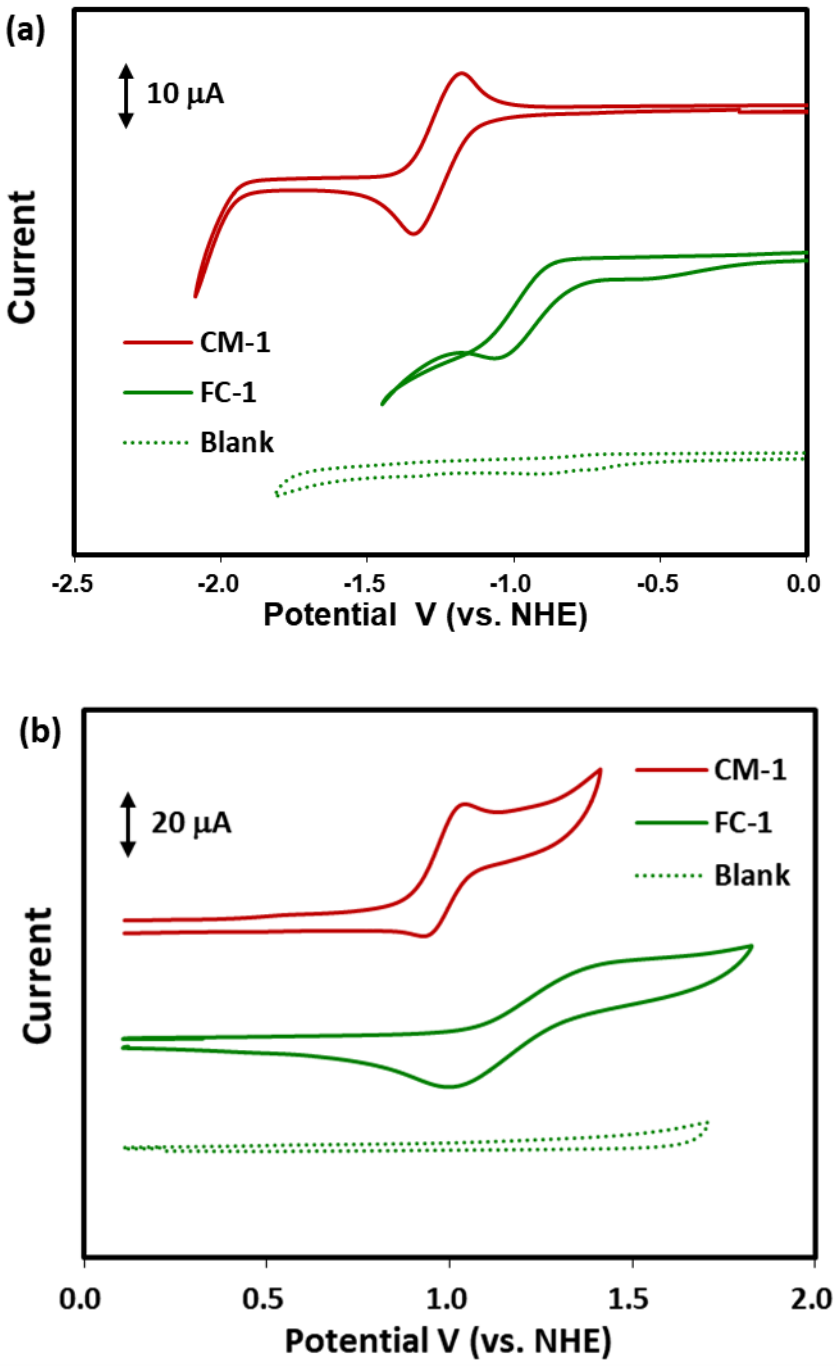

Figure 13. Cyclic voltammograms of **FC-1** deposited on a glassy carbon electrode (green line) and a blank solution (green dots) in dichloromethane containing 0.1 M TBAP and **CM-1** (red line) in a DMF solution containing 0.1 M TBAP. All measurements were performed under an Ar atmosphere (WE: glassy carbon, CE: Pt wire, RE: Ag/Ag^{+}), at scan rate of 100 mV/s.

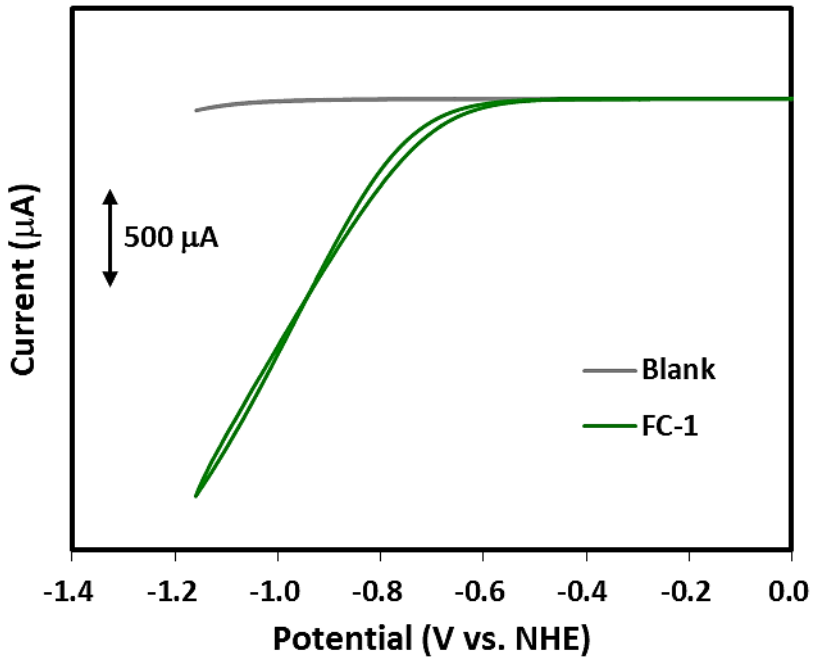

Figure 14. Cyclic voltammograms of **FC-1** deposited on a GC electrode (green line) and a blank solution (grey line) in 1.0 M acetate buffer pH 5 at room temperature under an Ar atmosphere (WE: glassy carbon, CE: Pt wire, RE: SCE), at scan rate of 100 mV/s.

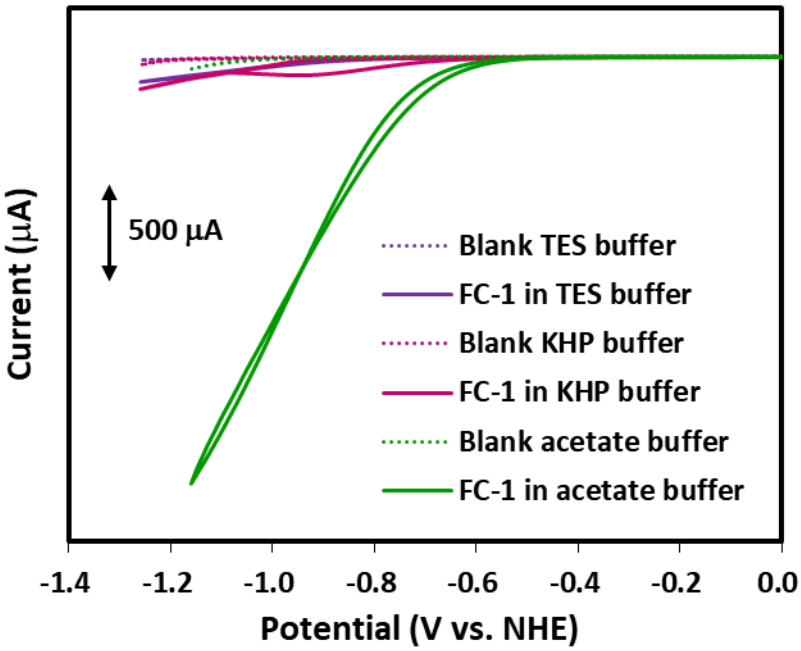

Figure 15. Cyclic voltammograms of **FC-1** deposited on a glassy carbon electrode (solid line) and various buffer blank solution at pH 5 (dash line) under an Ar atmosphere (WE: glassy carbon, CE: Pt wire, RE: SCE), at scan rate of 100 mV/s.

Photocatalytic H_2 production studies

Encouraged by the result of the electrochemical measurement of **FC-1**, the photocatalytic activity of **FC-1** was examined. In a typical experimental setup, **FC-1** (3.5 mg) was suspended in an aqueous acetate buffer solution (4 mL, pH = 5) containing EDTA-2Na (0.2 M) as a sacrificial electron donor (for details of the experimental setup, see the experimental section). The obtained suspension was irradiated by light ($\lambda > 320$ nm), and the product formed in the gas phase was analysed by gas chromatography (GC).

As shown in Fig. 16, the production of H_2 linearly increased with time upon light irradiation. The initial reaction rate (TOF) for 1 h was determined to be 67 $\mu molg^{-1}h^{-1}$ and the turnover number reached to 3.5 after 75 h (for details, see experimental section). Several control experiments in the absence of **FC-1**, EDTA-2Na or light irradiation resulted in no H_2 production (Fig. 17), indicating that **FC-1** serves as a photocatalyst for H_2 production and EDTA-2Na serves as a sacrificial electron donor. I also investigated H_2 production using i) $Rh_2(Bnz)_4$ ($Rh_2(CO_2C_6H_5)_4$), ii) H**NIP**, and iii) a 4:1 mixture of H**NIP** and $Rh_2(Bnz)_4$ as catalysts under identical conditions. However, almost no H_2 production was observed in these experiments (Fig. 16). The results suggest that integrating the photosensitizer (1,8-naphthalimide moiety) and the catalytic centre (Rh(II) paddle-wheel unit) into the same molecule is crucial for photocatalytic H_2 production.

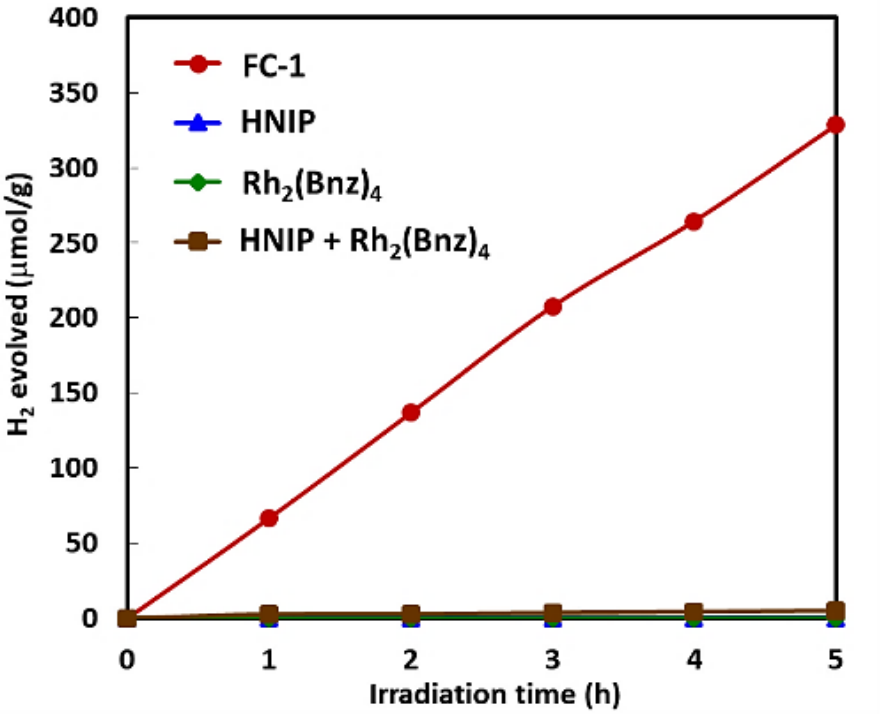

Figure 16. Photocatalytic H_2 production in the presence of **FC-1** (red line), H**NIP** (blue line), **$Rh_2(Bnz)_4$** (green line) and H**NIP** + **$Rh_2(Bnz)_4$** (brown line) in water (3.5 mg of each catalyst was used for each system). Reaction conditions: 0.2 M EDTA-2Na and 4.0 mL of solution (controlled at pH 5 by 1.0 M acetate buffer).

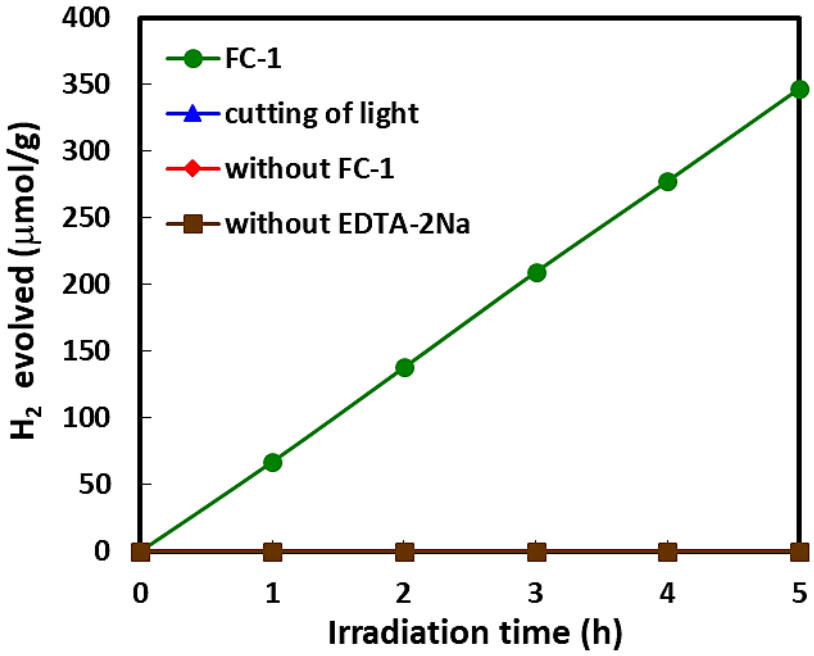

Figure 17. Photocatalytic H_2 production from a reaction mixture containing 3.5 mg of **FC-1** (green line) and 4.0 mL of acetate buffer (1.0 M) with 0.2 M EDTA-2Na at pH 5. Control experiments were carried out in the absence of light (blue line), **FC-1** (red line), and EDTA-2Na (brown line).

Mercury poisoning test of FC-1

The ability of mercury to poison nanoparticle metal catalysts is a widely used investigation to establish reaction mechanism, and the discovery of platinum colloid formation in a supposed homogeneous system using this method was recently reported.[15] The rhodium amalgam is known to form, albeit with more difficulty than the platinum amalgam,[16] and mercury poisoning has been reported for rhodium colloids.[17]

The photocatalytic activity of **FC-1** was examined in the presence of mercury. **FC-1** (3.5 mg) was suspended in 4.0 mL of acetate buffer (1.0 M) containing EDTA-2Na (0.2 M) as a sacrificial electron donor and the pH of the solution was adjusted to 5.0. Prior to the illumination reaction, the suspension was ultra-sonicated for 15 min and then treated with mercury (Fig. 18). If catalytic activity is the result of rhodium colloids forming from degradation of the **FC-1** during the photoreaction, then treated **FC-1** with mercury should affect catalytic activity and should poison the system such that little or no activity is observed. As shown in Fig. 19, the addition of mercury did not affect the photocatalytic activity, which indicates no formation of Rh-based nanoparticles during the catalysis.

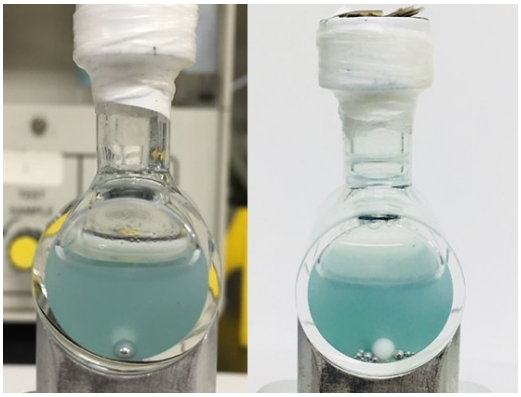

Figure 18. Photocatalytic H_2 production of **FC-1** in the presence (blue line) and absence (red line) of mercury. The reaction mixture contains 3.5 mg of **FC-1** and 4.0 mL of acetate buffer (1.0 M) with 0.2 M EDTA-2Na at pH 5.

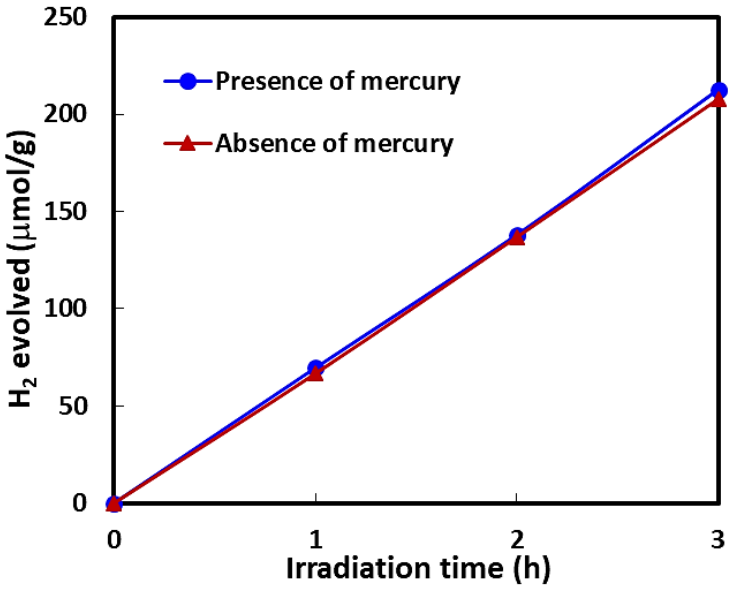

Figure 19. Photographs of the reaction mixture before (left) and after 3 h (right) of photocatalytic reaction.

Dependences of the H_2 evolution efficiency

The photocatalytic activity of **FC-1** can be affected by several factors. First, the catalytic experiments were performed at various pH values (pH = 4.0 – 6.0), and the optimal pH was found to be approximately 5.0 (Fig. 20), which is similar to that observed in the homogeneous Rh-based H_2-production catalytic system.[8a,17] Second, photocatalytic H_2 production by **FC-1** was examined using various kinds of buffer solutions at pH = 5. Similar to the results under electrochemical conditions, H_2 production was not observed in phosphate or TES buffer (Fig. 21). This result indicates that the interaction between acetic acid and the Rh_2 centre in **FC-1** is a key to promote photocatalytic H_2 production. Third, the photocatalytic activity of **FC-1** was investigated in the presence of a strongly coordinating molecule, CH_3CN. As shown in Fig. 22, a considerable decrease in H_2 production was observed under this condition due to the coordination of CH_3CN molecules to the axial positions of the Rh_2 centre (Fig. 23). This observation indicates that the axial sites of the Rh_2 centre are catalytically active for H_2 production.

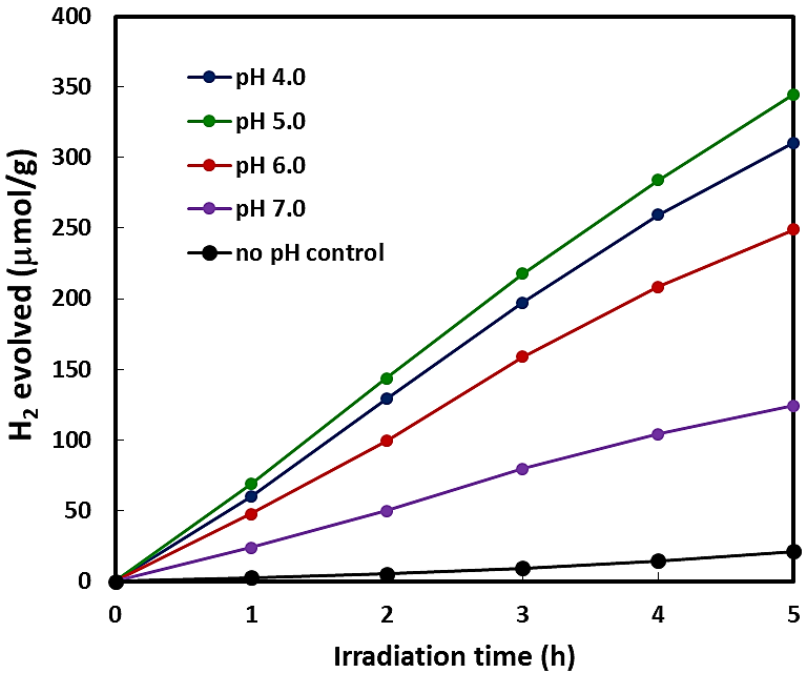

Figure 20. Photocatalytic H_2 production of **FC-1** (3.5 mg) at various pH. The pH values of the reaction media were adjusted by using 1.0 M acetate buffer solution. 0.2 M of EDTA-2Na (4.0 mL) was used as a sacrificial electron donor.

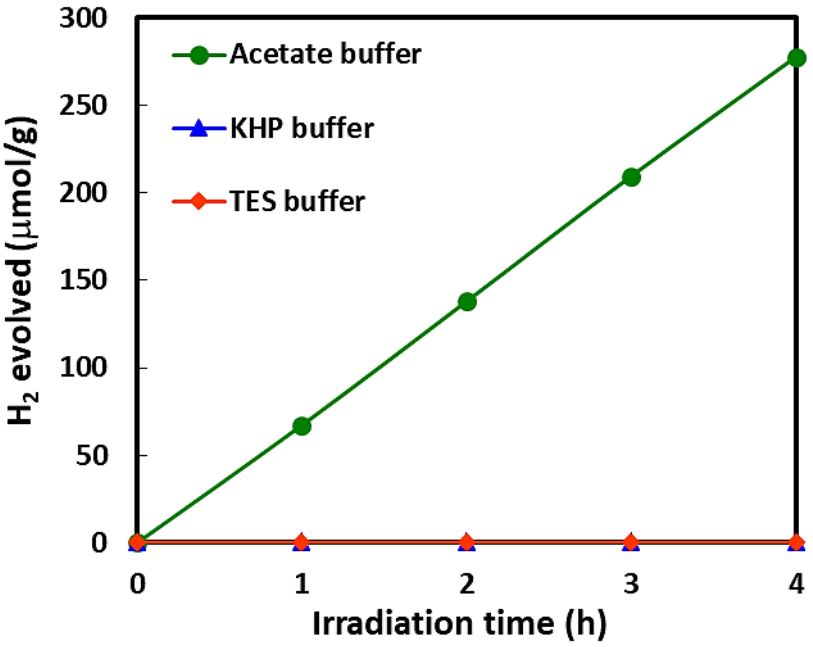

Figure 21. Dependence of buffer solution on photocatalytic H_2 production of **FC-1** (3.5 mg) at pH 5. In all experiments, the concentration of the buffer was 1.0 M. 0.2 M EDTA-2Na (4.0 mL) was used as a sacrificial electron donor.

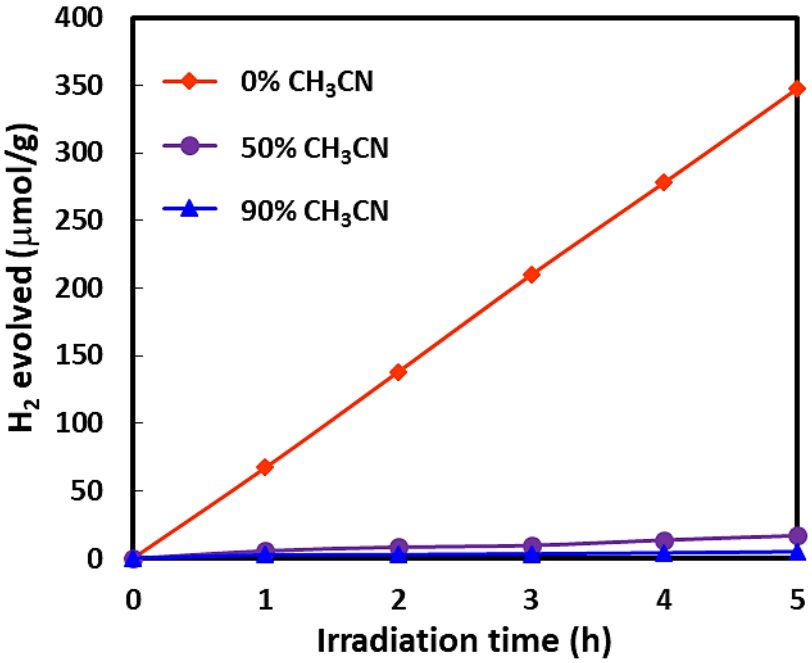

Figure 22. The influence of the capping ligand on photocatalytic H_2 production of **FC-1** (3.5 mg). The reaction was performed in 4.0 mL mixture of CH_3CN/1.0 M buffer solution containing 0.2 M EDTA-2Na as a sacrificial electron donor.

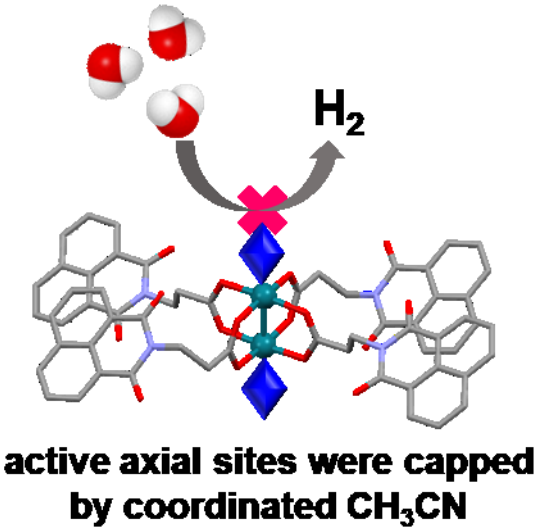

Figure 23. Schematic illustration of influence of the capping ligand of acetonitrile (CH_3CN) on photocatalytic H_2 evolution.

Influence of the particle size on photocatalytic H_2 evolution

The particles of **FC-1** with various were obtained by changing the period of sonication prior to the photocatalytic hydrogen production. The size of **FC-1** particles were determined by using the DLS measurements (Tables 3). As shown in Fig. 24, the catalytic activity of **FC-1** was not affected by the size of the particles.

Table 3. Various particle size of **FC-1** upon sonication period at 5, 10 and 15 min.

Sonication time (min)	Average particle size (μm)
5	80.7
10	62.2
15	41.9

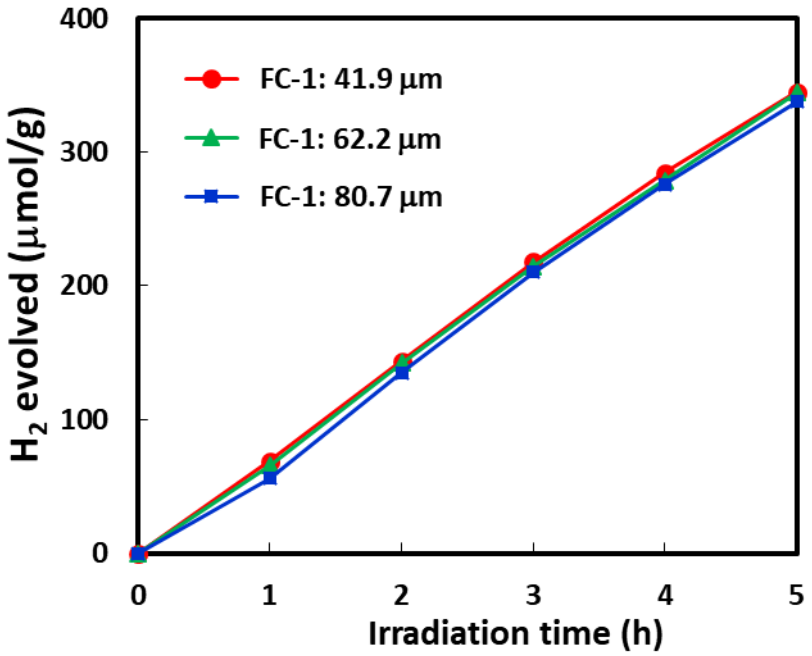

Figure 24. The influence of the average particle size on photocatalytic H_2 production of **FC-1** (3.5 mg). The reaction was performed in 1.0 M acetate buffer solution (pH 5) containing 0.2 M EDTA-2Na as a sacrificial electron donor.

Stability and recyclability of the catalyst

To further explore the properties of **FC-1**, the stability and the reusability were tested. As shown in Fig. 25, an experiment with photoirradiation up to 70 h resulted in almost constant production of H_2, which confirms the robustness of the catalyst. Additionally, the ESI-TOF-MS spectra of the catalyst before and after the photoreaction exhibited similar features (Fig. 26), suggesting almost no degradation of **FC-1** during photocatalysis. The reusability of **FC-1** was examined by the following procedure. **FC-1** after 3 h of the photocatalytic reaction was filtered, washed several times with water and then dried overnight *in vacuo*. The obtained powder was used as the photocatalyst in the next reaction cycle. As shown in Fig.27, hydrogen production without considerable loss of photocatalytic activity was observed for at least three cycles. It seems that the catalytic activity slightly increases upon recycling, although the reason to explain the phenomenon is not clear at this stage.

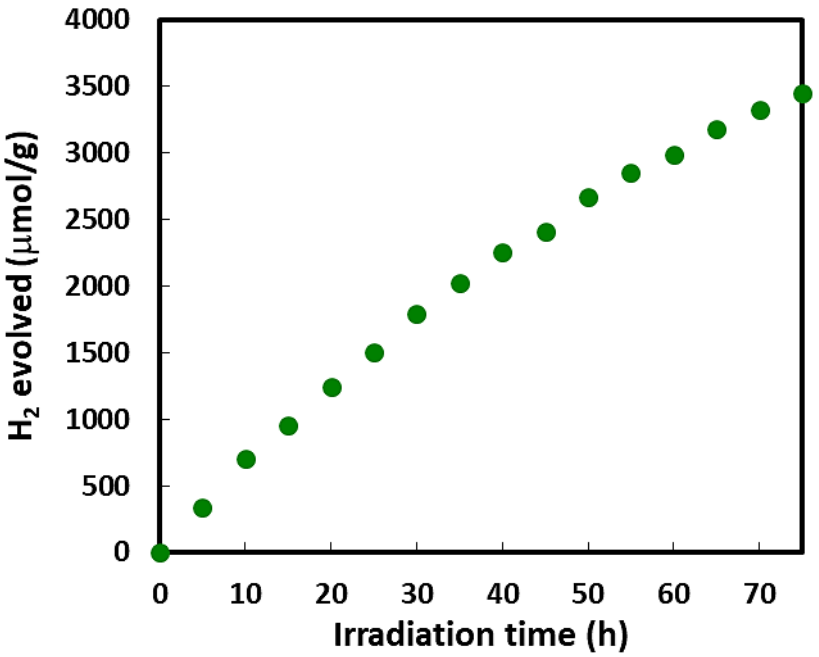

Figure 25. Photocatalytic H_2 production of **FC-1** with prolonged reaction time. Conditions: FC-1 (3.5 mg), 0.2 M EDTA-2Na in 4.0 mL acetate buffer (1.0 M) at pH 5.

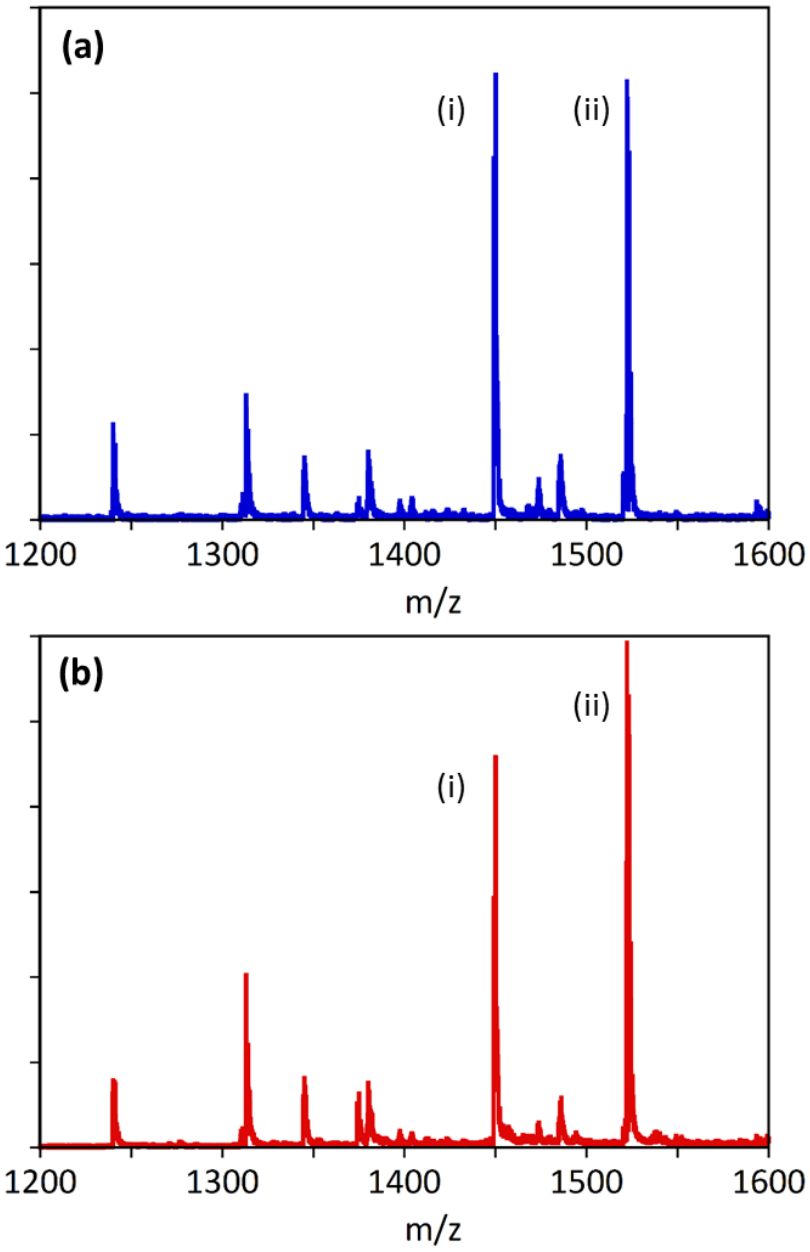

Figure 26. ESI-TOF-MS spectra of **FC-1** (a) before and (b) after photocatalytic reaction 75 h. In this experiment, **FC-1** was dissolved in DMF and 1-methyl-4,4'-bipyridinium, which can coordinate to the axial sites of the Rh_2 centre, was added to the resulting solution to ionize the neutral Rh complex. Major peaks at m/z values of 1450.33 and 1522.41 are assigned to molecular compositions as follows: (i) **FC-1** + 1-methyl-4,4'-bipyridinium − $2H_2O$ and (ii) **FC-1** + 1-methyl-4,4'-bipyridinium + DMF − $2H_2O$**.**

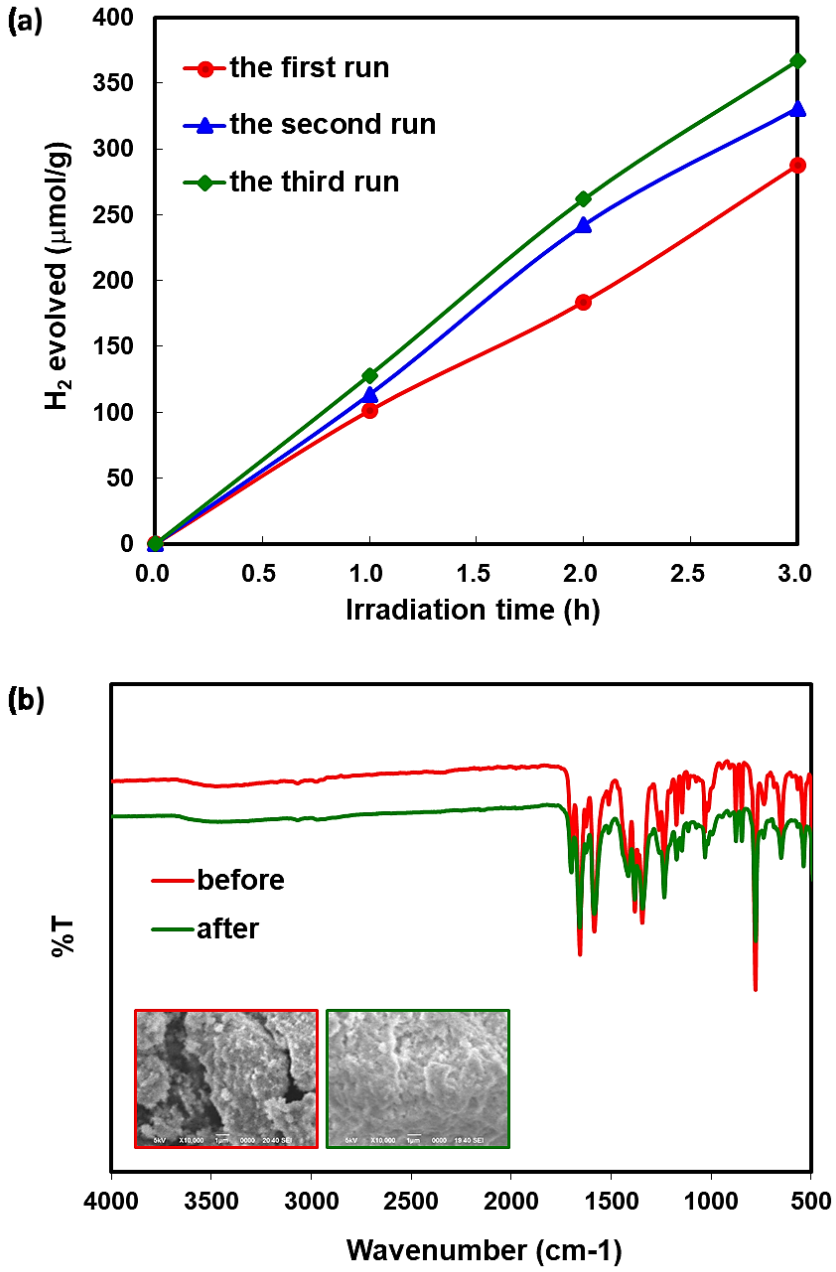

Figure 27 (a) Time course plots of hydrogen evolution of **FC-1** over three consecutive reuse experiments from the system containing 3.5 mg of **FC-1** and 0.2 M EDTA-2Na in 4.0 mL of water at pH 5 (controlled by 1.0 M acetate buffer solution). (b) FT-IR spectra of **FC-1** before and after 75 h of the photoreaction. *Inset*: SEM images of **FC-1** before (left) and after the photoreaction (right).

Mechanistic insight

The mechanism of photoinduced H_2 production mediated by **FC-1** was studied. In hydrogen evolution reactions catalysed by Rh paddle-wheel dimers, the species with a reduced Rh_2 centre, $Rh^{II}Rh^{I}$-H, serve as a catalytically active intermediate. Therefore, the following two pathways are possible in our system: (Path 1) intermolecular reductive quenching of the excited state of the **NIP** moiety, **NIP***, by the sacrificial electron donor, EDTA-2Na, to form **NIP**$^{-}$ and subsequent electron transfer from **NIP**$^{-}$ to the Rh_2 centre to give $Rh^{II}Rh^{I}$-H (Scheme 4a); (Path 2) intramolecular oxidative quenching of **NIP*** by a Rh_2 centre with assistance of acetic acid to generate $Rh^{II}Rh^{I}$-H (Scheme 4b).

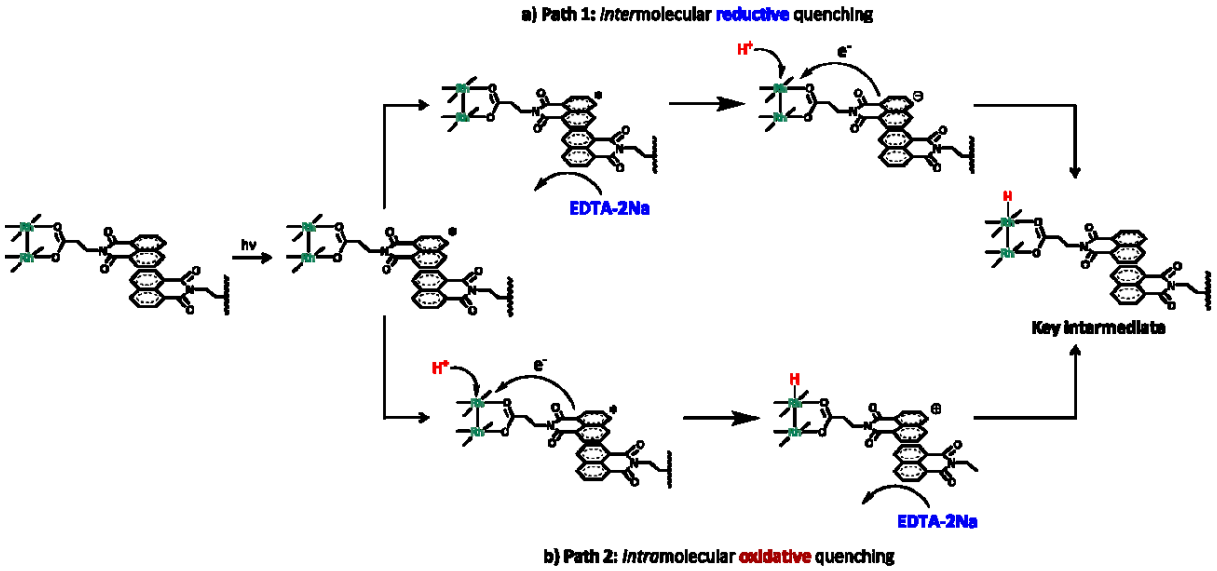

Scheme 4. Two possible pathways to generate a key intermediate, $Rh^{II}Rh^{I}$-H, from **FC-1** in this light-driven H_2 production system. a) Path 1: the intermolecular reductive quenching of **NIP*** by sacrificial electron donor (EDTA-2Na) and b) Path 2: the intramolecular oxidative quenching of **NIP*** by Rh_2 centre.

To clarify the reaction process, fluorescence spectroscopic experiments were conducted. As shown in Fig. 28, the fluorescence of H**NIP** was not quenched by the addition of excess EDTA-2Na (500 eq.). The result suggests that the intermolecular reductive quenching of **NIP*** by EDTA-2Na does not proceed and that **Path 1** is unfavourable. In contrast, consistent results were obtained when assuming that **Path 2** is a plausible pathway. The fluorescence of the NIP moiety was effectively quenched by the introduction of the Rh dimer unit both in **CM-1** and **FC-1**, as evidenced by fluorescence spectroscopy (vide supra). Additionally, the quenching of H**NIP** was also observed upon the addition of 2 eq. of **CM-1** (Fig. 29). It should also be noted that the Gibbs free energy ($\Delta G°$) of Path 2 was calculated to be $\Delta G° > -0.59$ eV using the Rehm-Weller equation, confirming that the process is thermodynamically favourable. These observations strongly indicate that **Path 2** is a preferred process in our system.

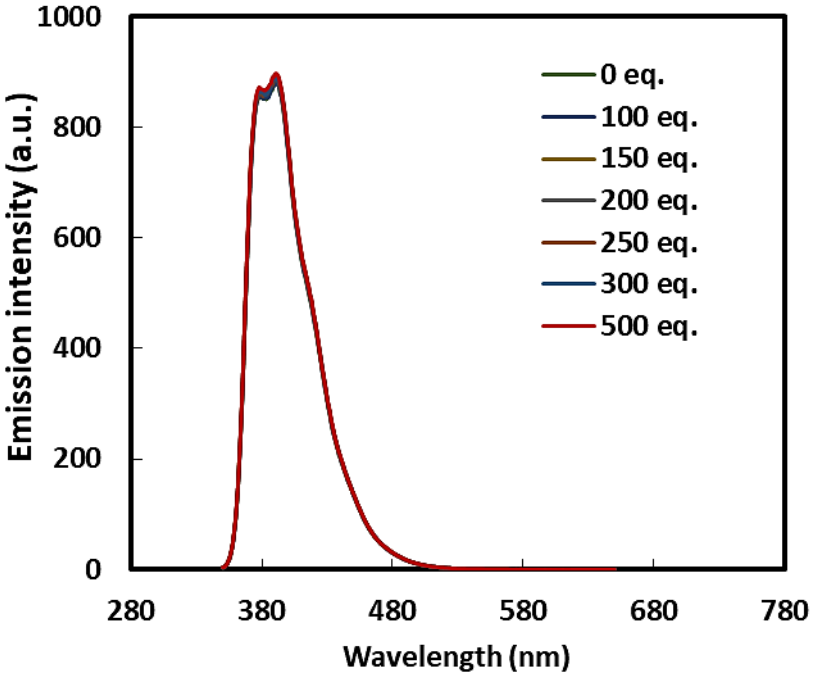

Figure 28. Fluorescence spectra of H**NIP** (40 μM) in EtOH/water (4/6, v/v) in the presence of EDTA-2Na (0 – 500 eq.), excitation wavelength at 342.0 nm.

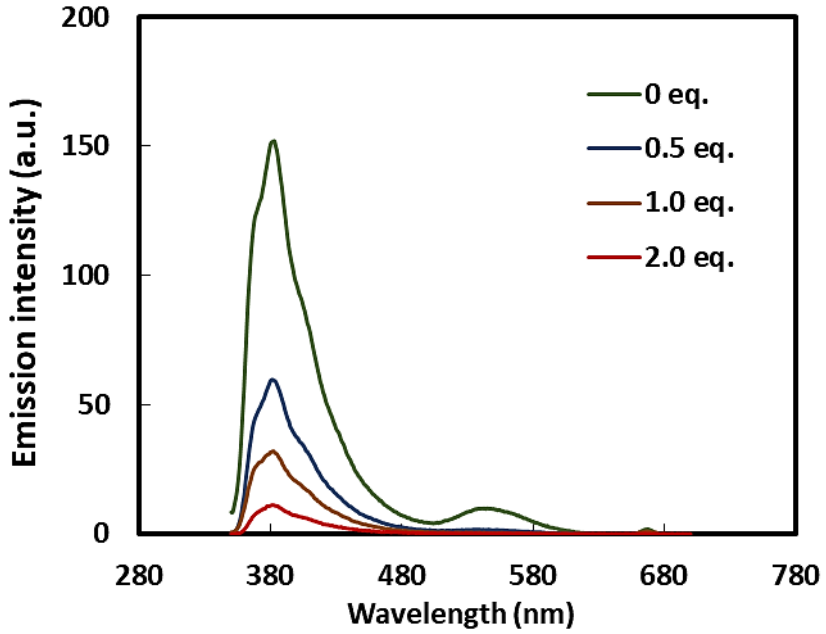

Figure 29. Fluorescence spectra of H**NIP** (50 μM) in DMF in the presence of **CM-1** (0 – 2 eq.), excitation wavelength at 334.0 nm.

The Gibbs free energy estimation

Based on the results of spectroscopic and electrochemical measurements, the Gibbs free energy (ΔG°) of photo induced electron transfer process was estimated by using the Rehm-Weller equation (Eq.1).[18]

$$\Delta G^{\circ} = E_{ox}(D) - E_{red}(A) - E_{00} - C \quad \text{(Eq. 1)}$$

Where E_{00} is the excited-state energy of photosensitizer; $E_{ox}(D)$ and $E_{red}(A)$ represent the oxidation potential of donor and the reduction potential of acceptor, respectively; C is the columbic term. In our system, E_{ox} corresponds to the oxidation potential of the **NIP** moiety (2.14 V vs. NHE in DMF) and E_{red} corresponds to the reduction potential of the Rh centre (–0.71 V vs. NHE in acetate buffer). The lowest excited-state energy of photosensitizer (**NIP***) moiety (E_{00}) was roughly estimated to be 3.44 eV from the cross point of absorption and emission spectra of H**NIP** in DMF at room temperature (Fig. 30). Due to the large dielectric constant of water at 20 ºC (80.103)[19], the columbic term can be negligible[18] and a negative ΔG° of –0.59 eV was obtained. These exergonic value confirm that the photoinduced intramolecular electron transfer process is thermodynamically favorable in our system.

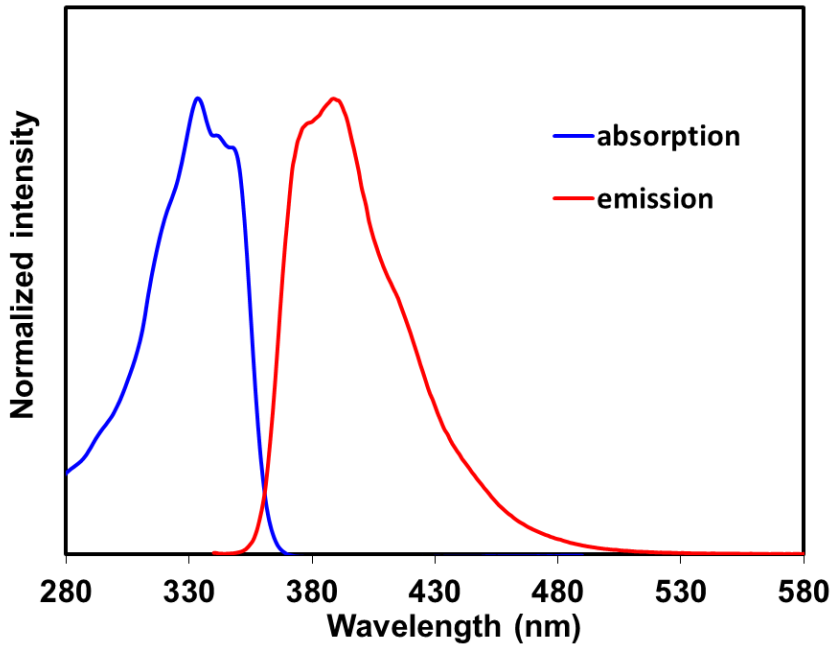

Figure 30. Normalized absorption (blue line) and emission spectra (red line) of H**NIP** in DMF upon excitation wavelength at 320 nm.

Conclusions

In conclusion, I demonstrated a novel approach to develop a framework catalyst (**FC-1**) constructed by the self-assembly of a catalyst module containing a photosensitizer and catalytically active moieties. **FC-1** exhibited a highly ordered structure stabilized by non-covalent π–π interactions between the catalyst modules, and photocatalytic H_2 production without the addition of a co-catalyst or electron mediator was achieved. The catalyst exhibited long-term stability, and its heterogeneous nature afforded the reusability of the photocatalyst without loss of activity. It was also found that the intramolecular oxidative quenching of **NIP*** by the Rh_2 centre was a key step to generate the catalytically active $Rh^{II}Rh^{I}$-H species. Although the catalytic activity of **FC-1** is not high compared to the recently reported excellent heterogeneous systems, in which molecular-based catalyst and photosensitizer units are integrated,[20] our results presented here offer novel strategy constructing molecular-based heterogeneous catalytic systems for small molecular conversions.

Experimental

General Methods

3-Aminopropinoic acid, 1,8-naphthalic anhydride and benzoic acid were purchased from Tokyo Chemical Industry (TCI). Ethylenediaminetetraacetic disodium salt (EDTA-2Na, ≥99.0%) was purchased from Sigma-Aldrich. All solvents and reagents are of the highest quality available and used as received. H**NIP**, $Na_4[Rh_2(CO_3)_4]$, **Rh_2(Bnz)$_4$** and **CM-1** were prepared by the literature methods.[21,22,23,24] All syntheses were performed under an atmosphere of dry nitrogen or dry argon unless otherwise indicated.

Measurement apparatus

^{1}H NMR spectra were acquired on a JEOL JNM-LA400 spectrometer, where chemical shifts in DMF-d_7 or $CDCl_3$ were referenced to internal tetramethylsilane. Elemental analyses were carried out on a J-SCIENCE LAB MICRO CORDER JM10 elemental analyser. UV-Vis absorption spectra and UV-Vis diffuse reflectance spectra were recorded on a Shimadzu UV-3600 UV-Vis-NIR spectrophotometer. A white standard of $BaSO_4$ was used as reference for diffuse reflectance spectroscopic measurement. The photocatalytic studies were performed by using a xenon lamp ($\lambda > 320$ nm, 300 W) equipped CM-2 cold mirror. Gas analysis for H_2 was performed using a Shimadzu GC-2014 gas chromatograph equipped with a thermal conductivity detector (TCD) and fitted with a molecular sieve 5A column (Ar carrier gas), calibrated with standard H_2 (0.5% of H_2 in argon). FT-IR spectroscopy data were collected using a PerkinElmer Spectrum 100 FT-IR spectrometer. ESI-TOF-MS spectra were recorded on a JEOL JMS-T100LP mass spectrometer. Scanning electron microscopy (SEM) images were obtained on JEOL CarryScope JCM-5700. All the ESI-TOF mass spectrometric measurements were recorded in the positive ion mode at a cone voltage of 20 V. Cyclic voltammograms were measured at room temperature on a BAS ALS Model 650DKMP electrochemical analyser in DMF (sample = 0.5 mM; 0.1 M tetra-*n*-butylammonium perchlorate (TBAP)) unless otherwise indicated. A glassy carbon, platinum wire, and Ag/Ag^+ electrode (Ag/0.01 M $AgNO_3$) were used as the working, auxiliary, and reference electrodes, respectively. The redox potentials were calibrated against the redox potential for the ferrocene/ferrocenium (Fc/Fc^+) couple. Dynamic light scattering (DLS) measurements were performed using particle size analyzer (Photal Otsuka Electronic ELSZ-1000).

Synthesis of CM-1

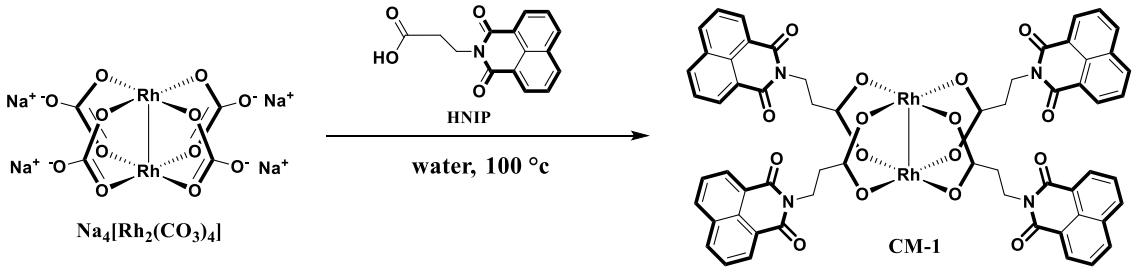

Scheme 5. Synthesis of **CM-1**

3-(1,8-Naphthalimido)propanoic acid (H**NIP**) was synthesized as previously reported.[19] Synthesis of **CM-1** was performed by following a published procedure.[22] A round-bottom Schlenk flask was charged with $Na_4[Rh_2(CO_3)_4]$ (90 mg, 0.15 mmol), H**NIP** (323 mg, 1.20 mmol) and 30 mL of water. The mixture was refluxed for 2 h. The resulting green precipitate was obtained by filtration, washed with water and methanol. The green solid was stirred in the mixture of methanol (150 mL) and acetone (150 mL) to remove the unreacted ligand. The green solid was collected by filtration and washed by diethyl ether. After drying under air, **CM-1** was obtained as green powder. Yield: 76 mg (0.06 mmol), 40%. ^{1}H-NMR (400 MHz, DMF-d_7): 8.54 (d, J = 7.4 Hz, 2H, naphth) 8.39 (d, J = 8.2 Hz, 2H, naphth) 7.87 (t, J = 7.8 Hz, 2H, naphth) 4.18 (t, J = 7.6 Hz, 2H, N-CH_2) 2.48 (t, J = 7.6 Hz, 2H, CH_2-COO) ppm. ESI-TOF MS (DMF): *m/z* 1522.41 [1314.08 + 1-methyl-4,4'-bipyridinium + DMF − $2H_2O$] (Note that 1-methyl-4,4'-bipyridinium iodide was used as an additive for mass spectroscopy measurement). Elemental analysis for **CM-1**·$7.5H_2O$: Found: C, 49.3; H, 4.3; N, 3.7. Calc. for $C_{60}H_{40}N_4O_{16}Rh_2$: C, 49.7; H, 4.1; N, 3.8%. Single crystal X-ray quality crystals of **FC-1** were grown by vapor diffusion technique from DMSO/$CHCl_3$ solution.

X-ray crystallographic data

Crystals of **FC-1** were mounted in a loop. Diffraction data at 123 K were measured on a RAXIS-RAPID Imaging Plate diffractometer equipped with confocal monochromated Mo-Kα radiation and data was processed using RAPID-AUTO (Rigaku). The structure was solved by direct method using *SIR-92*[25] and refined by the full-matrix least squares techniques on F^2 (*SHELXL-97*).[26] All non-hydrogen atoms were refined anisotropically. Crystallographic data have been deposited with Cambridge Crystallographic Data Centre: Deposition number CCDC 1494945 for **FC-1**.

Table 4. Summary of the crystallographic data for FC-1.

Formula	$C_{68}H_{64}N_4O_{20}Rh_2S_4$
Fw	1591.29
crystal color, habit	orange, block
crystal size, mm^3	0.23 × 0.17 × 0.09
crystal system	*monoclinic*
space group	$P\,2_1/n$
a, Å	9.8868(4)
b, Å	27.3918(12)
c, Å	12.3432(5)
β, deg	102.369(7)
V, $Å^3$	3265.2(2)
Z	2
F(000)	1628
d_{calc}, g/cm^3	1.619
μ(MoKα), mm^{-1}	0.714
T, K	123(2)
R_1	0.0611
wR_2	0.1639
GOF	1.135

Electrochemical and spectroelectrochemical studies

All experimental procedures were conducted at ambient temperature, 20 °C, under argon. A standard three-electrode configuration was employed in conjunction with a CH Instruments potentiostat interfaced to a computer with CH Instruments 650 DKMP software. A platinum auxiliary electrode and Ag/Ag^+ reference electrode were used for all measurement in solution. Cyclic voltammetry was performed using a GC disk working electrode (diameter 3 mm, from BAS Inc.). The working electrode was treated between scans by means of polishing with 0.05 μm alumina paste (from BAS Inc.) and washing with purified water. Ferrocene was used as an internal standard, and all potentials reported within this work are referenced to the NHE at 0.551 V.

UV-Vis spectral measurements were recorded using SHIMADZU UV-2550 UV-VIS spectrophotometer with a conventional quartz cuvette (path length, l = 1 cm). Spectroelectrolysis was performed using a BAS Inc. spectroelectrochemical quartz cell (l = 1 mm) containing a Pt gauze (working electrode), Pt wire (auxiliary electrode) and Ag/Ag^+ (reference electrode) in conjunction with the CH Instruments potentiostat.

Solid-state cyclic voltammogram measurement

To investigate redox behavior of **FC-1**, cyclic voltammograms (CVs) of **FC-1** deposited on a glassy carbon (GC) working electrode were measured. The procedure to deposit **FC-1** on the GC electrodes are as follows. First, 5 mg of as synthesized **FC-1** was suspended in methanol. The obtained suspension was further ultra-sonicated for 15 min. Subsequently, 20 μL of the suspension was dropped onto the surface of a freshly polished GC electrode and dried under air for 1 h, yielding a GC electrode modified by thin **FC-1** layer. By utilizing the modified electrode, CVs were measured using a standard three-electrode cell incorporating a GC working electrode, a platinum wire auxiliary electrode and Ag/Ag^+ reference electrode. The measurements were performed at room temperature under Ar atmosphere.

For the investigation of the electrocatalytic H_2 evolution of **FC-1**, the cyclic voltammograms of was measured in in 1.0 M acetate buffer as an electrolyte at pH 5. In this measurement, saturated calomel reference electrode (SCE) was employed as a reference electrode.

Photocatalytic H_2 production studies

All photocatalytic experiments were conducted at 20 °C using a custom-made photoreactor with coolant to control the temperature of sample during photoreaction (Scheme 6). A cylindrical UV cuvette with 4.0 mL of gas head space was used for all experiments. In a typical run, 3.5 mg of catalyst was suspended in 4.0 mL of acetate buffer containing EDTA-2Na as a sacrificial electron donor. Prior the reaction, the suspension was ultra-sonicated for 15 min and then the system was purged by Ar gas bubbling for 30 min. The photocatalytic reactions were executed by using a xenon lamp ($\lambda > 320$ nm, 300 W) equipped CM-2 cold mirror. The evolved H_2 in the gas phase was analyzed by a gas chromatography (GC-2014, molecular sieve 5A column, Ar carrier gas) equipped with a thermal conductivity detector (TCD).

For the study of the influence of particle size on the photocatalytic activity, the particle sizes of **FC-1** were controlled by changing the period of sonication (5, 10 and 15 min) prior to the photoreaction (Ultrasonic cleaner Aiwa AU-16C (28 kHz, 75 W)). The size of **FC-1** particles were determined by dynamic light scattering (DLS) technique.

The reusability experiments of **FC-1** for photocatalytic H_2 production were performed using the system containing 3.5 mg of **FC-1**, and 4.0 mL of acetate buffer (1.0 M) with EDTA-2Na (0.2 M) at pH 5. After 3 h of the photocatalytic reaction, the catalyst was filtered through membrane filter, washed several time with water then dried overnight under vacuum. Resulting powder was further used in the next photocatalytic experiment. Other experimental conditions are same as mentioned above.

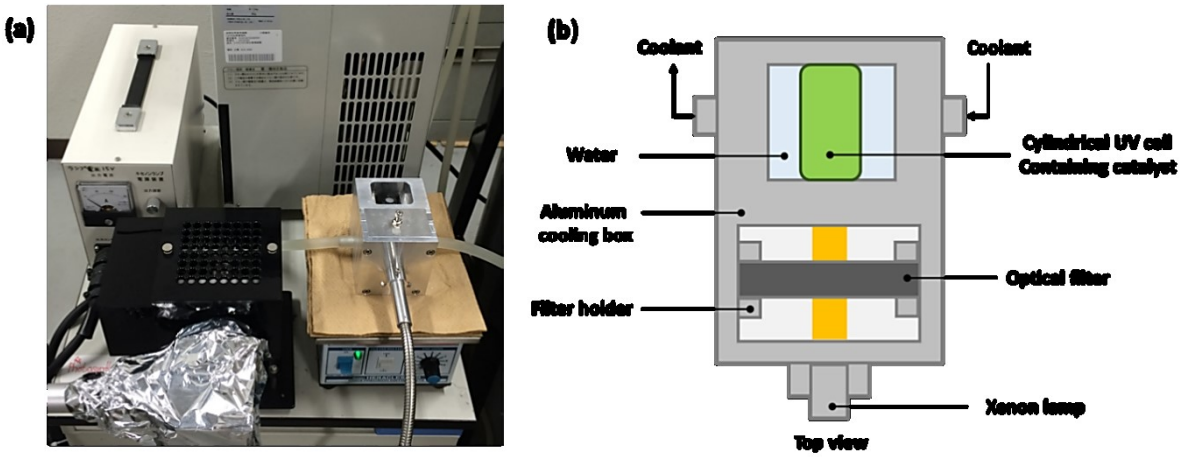

Scheme 6. (a) A photograph of the photocatalytic H_2 production reactor; (b) schematic illustration of the custom-made photoreactor.

Calculation details for H_2 evolution

The number of moles (n_{H_2}) of produced hydrogen was calculated according to the following equation;

$$n_{H_2}(\text{mol}) = \frac{detected\ peak\ area}{calibration\ peak\ area} \times 0.001 \times \frac{Headspace\ volume\ [L]}{24.5\ [Lmol^{-1}]}$$

where 0.001 is the reference percentage of H_2 in Ar base gas (corresponding to 4990 ppm in Ar) which linked to the calibration pick area at 0.1 mL of injection gas volume, 24.5 $Lmol^{-1}$ is the molar volume of ideal gas at a temperature of 298.15 K and pressure of 101325 Pa. The total volume extracted for the measure of evolved H_2 was around 0.2 mL, which 0.1 mL was injected to GC for analysis.

The turnover number related to the catalyst was calculated according to the following equation;

$$\text{TON} = \frac{n_{H_2}}{n_{\boldsymbol{FC-1}}}$$

where n_{H_2} is the number of moles of evolved hydrogen, $n_{\boldsymbol{FC-1}}$ is the number of moles of **FC-1** framework catalyst present in suspension mixture.

References

[1] N. S. Lewis and D. G. Nocera, *Proc. Natl. Acad. Sci.*, 2006, **103**, 15729.

[2] (a) M. Kirch, J.-M. Lehn and J.-P. Sauvage, *Helv. Chim. Acta*., 1979, **62**, 1345; (b) A. J. Esswein and D. G. Nocera, *Chem. Rev.*, 2007, **107**, 4022; (c) M. Wang, Y. Na, M. Gorlov and L. Sun, *Dalton Trans.*, 2009, 6458.

[3] (a) E. S. Andreiadis, M. C. Kerlidou, M. Fontecave and V. Artero, *Photochem. Photobiol.*, 2011, **87**, 946; (b) W. T. Eckenhoff and R. Eisenberg, *Dalton Trans*., 2012, **41**, 13004.

[4] (a) M. Wang, Y. Na, M. Gorlov and L. Sun, *Dalton Trans*., 2009, 6458; (b) V. Artero, M. Fontecave and M. Chavarot-Kerlidou, *Angew. Chem. Int. Ed*., 2011, **50**, 7238; (c) F. Wang, W.-G. Wang, H.-Y. Wang, G. Si, C.-H. Tung and L.-Z. Wu, *ACS Catal*., 2012, **2**, 407.

[5] (a) T. Zhou, Y. Du, A. Borgna, J. Hong, Y. Wang, J. Han, W. Zhang and R. Xu, *Energy Environ. Sci.*, 2013, **6**, 3229; (b) K. Sasan, Q. Lin, C. Mao and P. Feng, *Chem. Commun*., 2014, **50**, 10390; (c) C.-C. Hou, T.-T. Li, S. Cao, Y. Chen and W.-F. Fu, *J. Mater. Chem. A*, 2015, **3**, 10386; (d) Z. Li, J.-D. Xiao and H.-L. Jiang, *ACS Catal.*, 2016, **6**, 5359; (e) L. Zeng, X. Guo, C. He and C. Duan, *ACS Catal.*, 2016, **6**, 7935.

[6] (a) J. L. Wang, C. Wang and W. Lin, *ACS Catal*, 2012, **2**, 2630; (b) T. Zhang and W. Lin, *Chem. Soc. Rev.*, 2014, **43**, 5982; (c) D. Wang, R. Huang, W. Liu, D. Sun, Z. Li, *ACS Catal.*, 2014, **12**, 4254; (d) Y. Fang, Y. Ma, M. Zheng, P. Yang, A. M. Asiri, X. Wang, *Coord. Chem. Rev*., 2017, DOI: 10.1016/j.ccr.2017.09.013.

[7] (a) T. Itoh, M. Kondo, M. Kanaike and S. Masaoka, *CrystEngComm*, 2013, **15**, 6122; (b) T. Itoh, M. Kondo, H. Sakamoto, K. Wakabayashi, M. Kanaike, K. Itami and S. Masaoka, *Dalton Trans.*, 2015, **44**, 15334.

[8] (a) S. Tanaka, S. Masaoka, K. Yamauchi, M. Annaka and K. Sakai, *Dalton Transactions*, 2010, **39**, 11218; (b) Y. Kataoka, K. Sato, Y. Miyazaki, Y. Suzuki, H. Tanaka, Y. Kitagawa, T. Kawakami, M. Okumura, W. Mori, *Chem. Lett.*, 2010, **39**, 358; (c) J. Xie, C. Li, Q. Zhou, W. Wang, Y. Hou, B. Zhang, X. Wang, *Inorg. Chem.*, 2012, 6376.

[9] (a) P. Chinapang, V. Ruangpornvisuti, M. Sukwattanasinitt, P. Rashatasakhon, *Dyes and Pigments*, 2015, **112**, 236; (b) D. L. Reger, A. Debreczeni, J. J. Horger and M. D. Smith, *Crys. Growth. Des.*, 2011, **11**, 4068; (c) D. L. Reger, A. Debreczeni and M. D. Smith, *Inorg. Chem.*, 2011, **50**, 11754; (d) D. L. Reger, A. Debreczeni and M. D. Smith, *Inorg. Chem.*, 2012, **51**, 1068, and references therein.

[10] D. L. Reger, A. Debreczeni, B. Reinecke, V. Rasolov and M. D. Smith, *Inorg. Chem.*, 2009, **48**, 8911.

[11] D. L. Reger, A. Debreczeni and M. D. Smith, *Inorg. Chim. Acta*, 2011, **378**, 42.

[12] (a) T. E. Cassandra, A.-T. Nkongho, K. K. Kenneth, J. Tana and F. Quarshiea, *Acta Cryst. E*, 2012, **69**, m639; (b) M. Ebihara, K. Yamada and T. Kawamura, *Acta Cryst. C,* 2006, **62**, m451; (c) N. N. Sveshnikov, M. H. Dickmana and M. T. Pope, *Acta Cryst.*

C, 2000, **56**, m1193.

[13] P. Atkins, T. Overton, J. Rourke, M. Weller, F. Armstrong and M. Hangerman, *Shriver and Atkins' Inorganic Chemistry Fifth Edition*, Oxford University Press, Great Britain, 2010.

[14] T. Stoll, C. E. Castillo, M. Kayanuma, M. Standroni, C. Daniel, F. Odobel, J. Fortage and M.-N. Collomb, *Coord. Chem. Rev.*, 2015, **304-305**, 20.

[15] Du, P., Schneider, J., Li, F., Zhao, W., Patel, U., Castellano, F. N., and Eisenberg, R. *J. Am. Chem. Soc*. 2008, **130**, 5056.

[16] Guminski, C. *J. Mater. Sci.*, 1989, **24**, 3285.

[17] (a) Weddle, K., Aiken, J., and Finke, R. *J. Am. Chem. Soc.*, 1998, **120**, 5653; (b) Jaska, C. A. and Manners, I., *J. Am. Chem. Soc.*, 2004, **126**, 9776.

[18] S. Yu, F. Wang, J.-J. Wang, H.-Y. Wang, B. Chen, K. Feng, C.-H. Tung and L.-Z. Wu, *Pure Appl. Chem.*, 2013, **85**, 1405.

[19] C. G. Malmberg and A. A. Maryott, *J. Res. Natl. Inst. Stand.*, 1956, **56**, 1.

[20] (a) A. S. Weingarten, R. V. Kazantsev, L. C. Palmer, M. McClendon, A. R. Koltonow, A. P. S. Samuel, D. J. Kiebala, M. R. Wasielewski and S. I. Stupp, *Nat. Chem.*, 2014, **6 (11)**, 964; (b) A. S. Weingarten, R. V. Kazantsev, L. C. Palmer, D. J. Fairfield, A. R. Koltonow, and S. I. Stupp, *J. Am. Chem. Soc.,* 2015, **137**, 15241; (c) N. Kaeffer, J. Massin, C. Lebrun, O. Renault, M. Chavarot-Kerlidou, and V. Artero, *J. Am. Chem. Soc*., 2016, **138**, 12308; (d) D. Kim, D. R. Whang, and S. Y. Park, *J. Am. Chem. Soc*. 2016, **138**, 8698; (e) W. Zhao, Y. Huang, Y. Liu, L. Cao, F. Zhang, Y. Guo and B. Zhang, *Chem. Eur. J.,* 2016, **22**, 15049; (f) J. Warnan, J. Willkomm, J. N. Ng, R. Godin, S. Prantl, J. R. Durrantb and E. Reisner, *Chem. Sci.*, 2017, **8**, 3070; (g) P. B. Pati, L. Zhang, B. Philippe, R. Fernández-Terán, S. Ahmadi, L. Tian, H. Rensmo, L. Hammarström, H. Tian *ChemSusChem,* 2017, **10**, 2480; (h) T. Banerjee, F. Haase, G. Savasci, K. Gottschling, C. Ochsenfeld, and B. V. Lotsch, *J. Am. Chem. Soc.*, in press DOI: 10.1021/jacs.7b07489.

[21] D. L. Reger, A. Debreczeni, B. Reinecke, V. Rasolov and M. D. Smith, *Inorg. Chem.*, 2009, **48**, 8911.

[22] L. Caulder and K. N. Raymond, *Acc. Chem. Res.* 1999, **32**, 975.

[23] W. Mori *et al*., *Chem. Lett*., 1999, 331.

[24] R. Daneil L. *et al*., *Inorg. Chim. Acta*, 2011, **378**, 42 – 48.

[25] A. Altomare, G. Cascarano, C. Giacovazzo, A. Guagliardi. *J. Appl. Crystalogr.*, 1993, **26**, 343.

[26] G. M. Sheldrick, SHELXL-97, *Program for Crystal Structure Refinement*, University of Göttingen, Germany, 1997.

Chapter 2

Development of photo-active catalyst with visible-light absorbing dye moieties

Introduction

The generation of renewable, carbon-neutral fuels is critical for the future of mankind.[1] In particular, the catalytic production of O_2 and H_2 from water using abundant sunlight is one attractive approach to store solar energy in the form of chemical bonds.[2,3,4] Materials that are able to couple the absorption of photons and the transfer of electrons enable the catalytic processes to be easily driven by light.[5] Therefore, the development of highly active and stable molecular systems that composed of photo-harvesting sites and catalytic sites is greatly desired for catalytic reduction of H_2O or H^+ to H_2 by light.

We have successfully demonstrated a novel approach to develop a framework catalyst (**FC-1**) constructed by the self-assembly of the catalytic module (**CM-1**) containing a light-absorbing molecular connector and a catalytically active dinuclear rhodium complex center (Scheme 1). The hydrogen evolution was excellently achieved by light-irradiation to **FC-1** in aqueous media as described in Chapter 1.[6] However, **FC-1** cannot harvest the visible light, which is known as most abundant solar energy source on earth surface (around 1,500 $Wm^{-2}\mu m^{-1}$). Therefore, in this study, I aim to develop new system that can harness the light in the visible region, which represents as a significant goal in the technology of renewable energy research.[7]

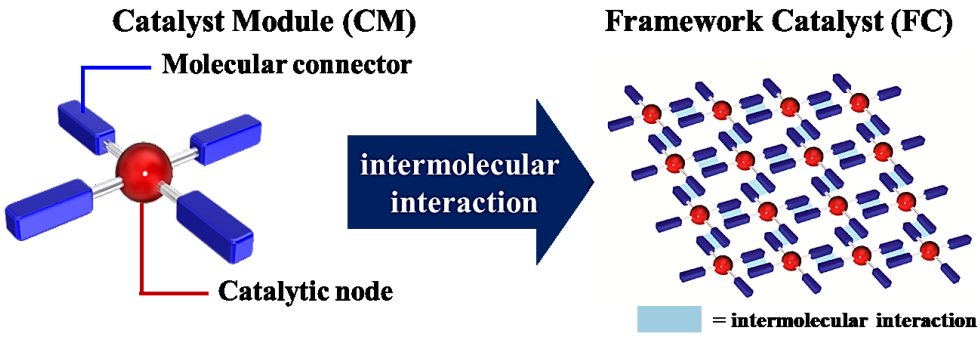

Scheme 1 Schematic illustration of the assembly of catalyst modules via non-covalent intermolecular interactions to afford a framework catalyst.

Chapter 2 describes the utilization of boron dipyrromethene dye (bodipy; BDP), as a visible-light absorbing and framework assembly sites. The bodipy chromophores are known to exhibit narrow and intense absorption bands in yellow-green region, thus have potential to serve as an excellent light-harvesting unit in the photocatalytic hydrogen formation reaction.[8] In addition, these dyes display rich electrochemistry, in which all redox processes of bodipy fragments are clearly resolved. More importantly, bodipy demonstrates efficient either energy or electron transfer to attached molecules.[9] Therefore, the appending of visible-light absorbing bodipy to the redox active dirhodium center would provide conspicuous activities not only for photocatalytic but also for electrocatalytic hydrogen evolution reaction.

It is anticipated that catalytic module (Scheme 2, left), which are designed and optimized for visible light-harvesting and redox catalysis, can be organized into a highly ordered framework catalyst (Scheme 2, right) via non-covalent interactions by using appropriate self-assembly strategies. Unlike assembly driven by coordination bonding, known as coordination polymers,[10] we can easily assemble/disassemble catalyst modules simply by changing solvents while maintaining the structure of the active sites (Scheme 2).[11] Therefore, our system provides two prominent features: (1) well-defined catalytic sites attributed to the molecular-based modules and (2) dual homogeneous and heterogeneous catalyst for electro- and photocatalyzed hydrogen evolution.

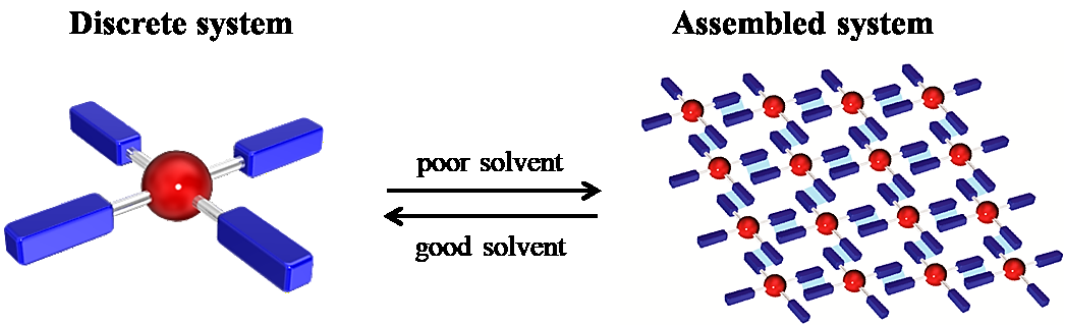

Scheme 2. Schematic illustration of the facile assembly/disassembly between discrete system and assembled system by simplistic changing of solvents

This chapter reports the synthesis and spectroscopic characterization of a new catalytic module (**CM-2**, Fig. 1). **CM-2** is a Rh(II) dimer complex bearing bodipy-based ligands, Rh_2(**BDP**)$_4$ (H**BDP** = 4,4-difluoro-8-[4-(carboxy)phenylic]-1,3,5,7-tetramethyl-4-bora-3a,4a-diaza-4-bora-*s*-indacene acid). **BDP** moiety can serve as both a visible light-harvesting unit for the photocatalytic reaction and a functional moiety to construct intermolecular non-covalent interactions. Incorporation of a highly symmetric structure (D_{4h}) of a Rh(II) paddle-wheel moiety, which has four interaction sites in one molecule, is expected to promote the construction of an ordered structure. I also describe the detailed study of the assembled structures, their electrochemical, photophysical properties in comparison with H**BDP**, and catalytic activities of both **CM-2** and the assembled framework catalyst (**FC-2**) for the hydrogen evolution reaction.

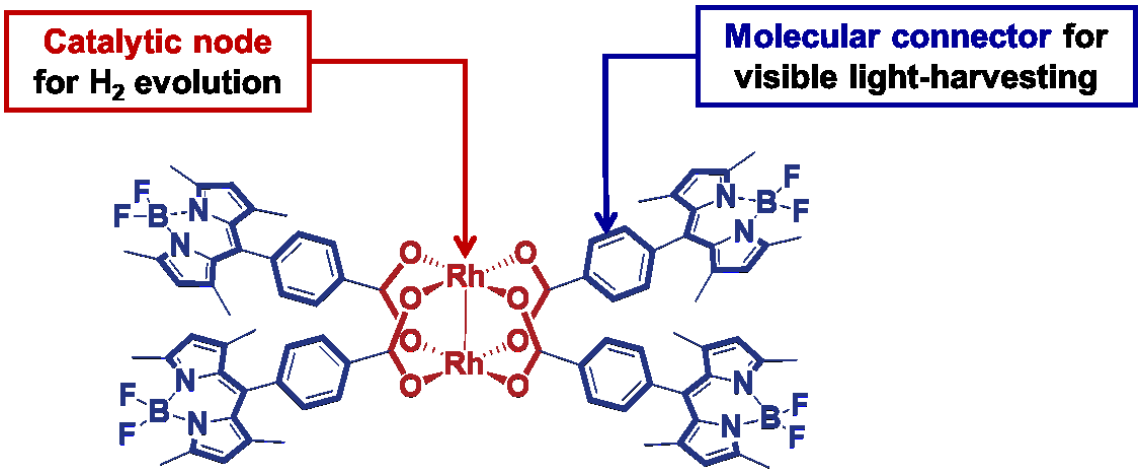

Figure 1. Features of the catalyst module **CM-2** investigated in this chapter.

Results and Discussion

Syntheses of molecular connector (HBDP) and catalytic module (CM-2)

For this study, the bodipy chromophore with phenyl carboxylate connected to *meso* position was employed as a molecular connector unit. The *para*-phenyl carboxylate linkage was anticipated to provide multi-point intermolecular non-covalent interactions suitable for construction of framework structure. A ligand, H**BDP** (H**BDP** = 4,4-difluoro-8-[4-(carboxy)phenylic]-1,3,5,7-tetramethyl-4-bora-*3a*,*4a*-diaza-4-bora-*s*-indacene acid**)**, was synthesized according to the literatures.[12] Synthetic scheme for H**BDP** is shown in Scheme 3. The synthesis of the pre-molecular connector (**2**) was performed via facile 3-step one-pot procedure, which is often used in syntheses of bodipy dyes and allows a straightforward preparation of many hundreds milligram of desired dyes. In the first step, dipyrromethane was prepared by the condensation of methyl-4-formyl benzoate (**1**) and 2,4-dimethylpyrrole in the presence of trifluoroacetic acid (TFA). The obtained dipyrromethane subsequently was oxidized by dichlorodicyanobenzoquinone (DDQ) to the corresponding dipyrrolmethene derivative. Finally, the chelation with BF_2 at the nitrogen atoms of the dipyrrolmethene was accomplished by adding $BF_3{\cdot}OEt_2$ to the reaction mixture in the presence of triethanolamine base. The following purification of the resulting mixture on silica gel auto-column chromatography gave red to purple crystals of **2** in 18 %yield, which is typical range of yield for this type of dyes. Subsequently, the desired molecular connector, H**BDP**, was successfully obtained as dark red crystals by the hydrolysis of compound **2** in methanol containing NaOH in a very good yield (82%). The details of the syntheses and characterization are given in experimental section.

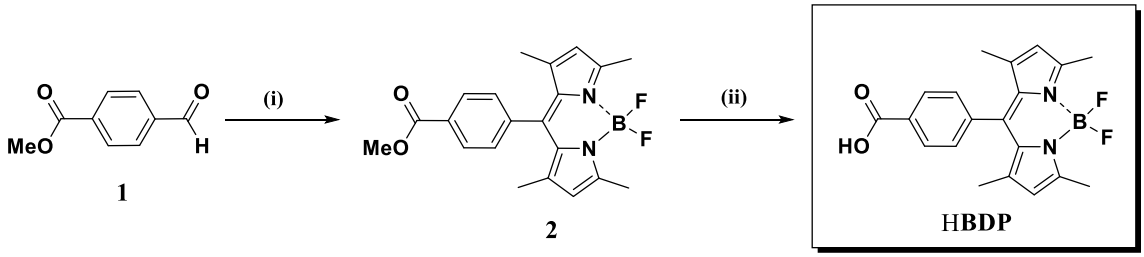

(i) 2,4-dimethylpyrrole, TFA, anhydrous DCM, TFA, rt, 16 h; DDQ, absolute TEA, $BF_3{\cdot}OEt_2$; yield 18%
(ii) MeOH/NaOH, 80°C, 2 h; yield 82%

Scheme 3. Preparation of visible light-absorbing molecular connector, H**BDP**.

With the desired light-absorptive molecular connector (H**BDP**) in hands, the catalytic module **CM-2** was accordingly synthesized through the ligand exchange reaction between excess amount of H**BDP** and $Rh_2(CO_2CH_3)_4$ in *o*-dichlorobenzene/methanol (Scheme 4). After stirring the reaction mixture several hours at high temperature, solvent was removed and the metallic green residue was obtained. The desired *tetra*-substituted product was isolated by conventional silica column chromatography to afford green-metallic red crystal at a moderate yield (21%). The formation of the desired complex, $Rh_2(\mathbf{BDP})_4(H_2O)_2$, was confirmed by ^1H (relatively shielded for phenyl*H* and deshielded for indacence*H*) and ^{19}F NMR spectroscopy, elemental analysis, and ESI-TOF-MS. **CM-2** presented a very high degree of solubility in various organic solvents such as chlorinated solvents and moderate to high polar solvents.

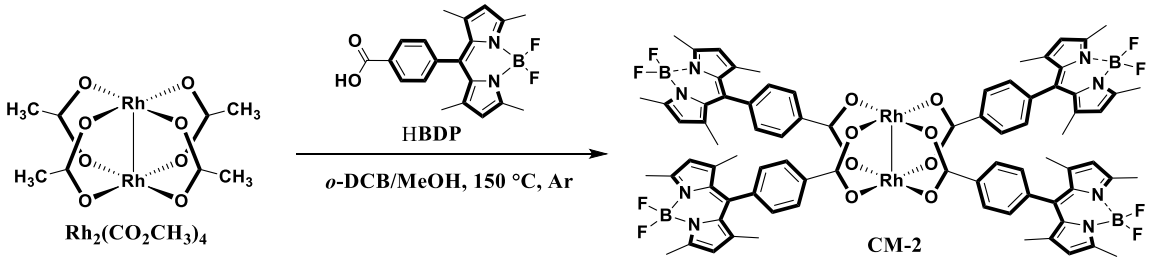

Scheme 4. Synthesis of catalytic module (**CM-2**).

X-ray crystallographic structure analysis of HBDP

Solid-state structure of the visible light-absorbing molecular connector, H**BDP**, was studied by single-crystal X-ray structural analysis. Single crystals of H**BDP** suitable for the measurement were grown from a saturated DMSO solution of the compound. The structural analysis revealed that the compound crystallized in triclinic $P\bar{1}$ space group. Two pyrrole rings of H**BDP** are lied in the same planar with a central six-membered ring containing boron and fluoride atoms (Fig. 2) similar to typical bodipy structures[9a]. The phenyl ring attached to the *meso*-position is likely orthogonal to the indacene skeleton (dihedral angle: 79.7°) due to the steric repulsion between two methyl substituents attached at C-1 and C-7 positions. The plane defined by F-B-F atoms is perpendicular to the indacene skeleton, similar to previous reports[9a]. Further details for X-ray crystallographic structure are provided in the experimental section.

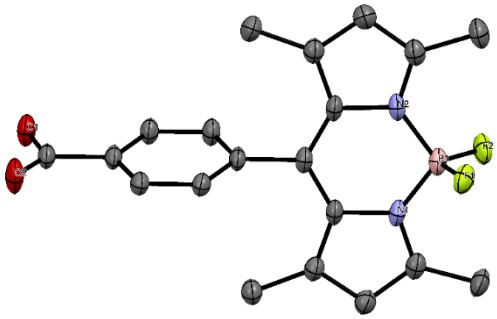

Figure 2. An ORTEP drawing of the molecular connector, H**BDP**, used in this study (50% probability ellipsoids). Hydrogen atoms and crystal solvent molecules are omitted for clarity.

The self-assembly of CM-2

The self-assembly of the catalyst module **CM-2** to construct a framework catalyst (**FC-2**) was performed by the slow diffusion of methanol into a $CHCl_3$ solution of **CM-2**. In addition, the slow diffusion of diethyl ether into $CHCl_3$ solution of **CM-2** also gave the self-assembly structure for **FC-2'** in an analogous manner. A crystallographic analyses of both **FC-2** and **FC-2'** suggest structural arrangement in triclinic $P\bar{1}$ space group with $Z = 2$ (Fig. 3 (top) and 3 (bottom), respectively). The molecular structure of dirhodium **FC-2** and **FC-2'** are found to have an analogous to dirhodium **FC-1** as mentioned in Chapter 1. Four carboxylate bodipy (**BDP**) units are bound to equatorial position of the Rh-Rh metal core, which resulted in paddle-wheel structural arrangement with Rh-O distances of 2.006(1) – 2.029(5) Å (**FC-2**) and 2.012(0) – 2.039(2) Å (**FC-2'**). The Rh1-Rh1' distance of **FC-2** and **FC-2'** are 2.381(6) Å and 2.389(9) Å, respectively, which is typical distance for Rh(II) paddle-wheel dimers (2.316 to 2.486 Å).[11,13] For example, the Rh-Rh bond length of $Rh_2(CO_2CH_3)_4(2H_2O)$ is 2.3855 Å.[14] Also, same as previous reports, the labile axial sites were occupied by solvent molecules (methanol for **FC-2** and diethyl ether for **FC-2'**). Interestingly, the *meso*-phenyl moiety was tilted against the indacene skeletons and the averaged dihedral angles are found to be 82.2° and 87.8° for **FC-2** and **FC-2'**, respectively, which relatively increase to nearly orthogonal compared with H**BDP** (79.7°). Crystallographic details are given in experimental section.

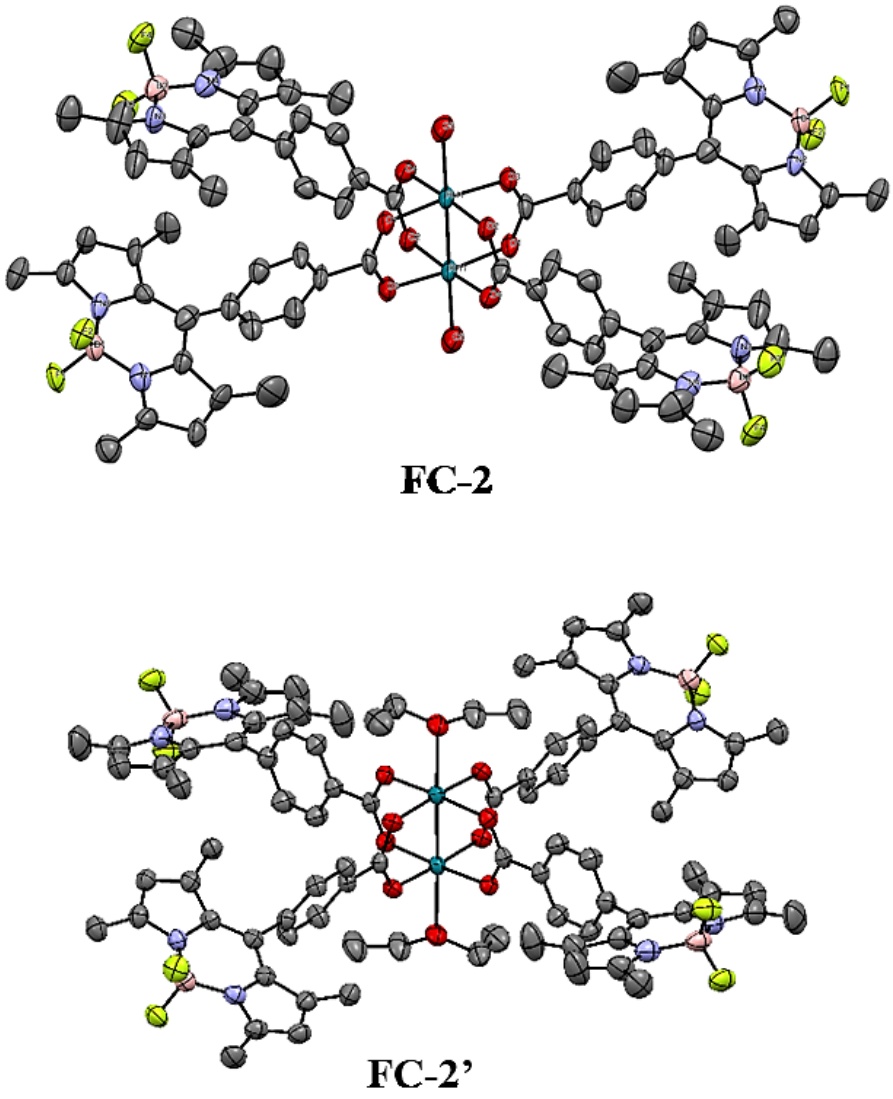

Figure 3. ORTEP drawings of **FC-2** (top) and **FC-2'** (bottom) with methanol and diethyl ether molecules coordinated at labile axial sites, respectively. (50% probability ellipsoids). Hydrogen atoms are omitted for clarity, O = red, C = grey, N = blue, B = pink, F = yellowish green and Rh = sea green.

The most interesting features of the crystal structures are revealed by the analysis of the packing arrangement. Firstly, for **FC-2**, two adjacent molecules pack via C-H(*phenyl*)···π(*pyrrole*) with the average distance of 2.651(5) Å, and B-F···O(*methanol*) interaction of **BDP** moieties to generate 1-D chain structure (Fig. 4 (top)). Second, Fig. 4 (middle) shows the interchain stacking which are stabilized by weak B-F···H(*methyl*) and π···π interactions (distance was estimated to be 3.42 Å) forming 2-D sheets with adjacent Rh-Rh distance approximately 15.244 Å indicated as blue arrow. These two-dimensional sheets are stacked to form a three-dimensional structure (Fig. 4 (bottom)). These observations confirm the formation of the framework catalyst (**FC-2**) via the self-assembly of the catalyst module **CM-2**.

The effect of the solvent coordinated at axials on the packing structure was further surveyed. The crystal packing of **FC-2'**, in which diethyl ether molecules are coordinated at axial positions, as shown in Fig. 5. The packing structure of **FC-2'** exhibits 1-D chains that were built by C-H(*phenyl*)···π(*pyrrole*) interactions similar in **FC-2** with the slightly longer average distance of 2.788(5) Å (Fig. 5 (top)). The stacking of these one-dimensional chains generated a 2-D packing sheet stabilized by weak B-F···H(*methyl*) and π···π interactions between the neighboring molecules, while their adjacent Rh-Rh distance is 18.643 Å (blue arrow in Fig. 5 (middle)). This longer Rh-Rh distance of **FC-2'** can be attributed to the larger size of axial coordinated molecules, and directed the closely linear arrangement of pendent **BDP**s. Interestingly, these 2-D sheet can be stacked and constructed 3-D packing structures with pores, in which $CHCl_3$ molecules are included as guest molecules (Fig. 5 (bottom)). These single-crystal XRD analyses, therefore, revealed that the construction of framework catalysts (**FC-2** and **FC-2'**) was succeed through controlling the self-assembly of **CM-2** by intermolecular non-covalent interaction of **BDP** molecular connector. It should be also noted that the assembled structures can be easily modified by changing of the molecules coordinated at the labile axial coordination sites. Thus, this study can open opportunity for fine-tuning structure arrangement and controlling of the molecular assemblies by modifying the axial sites.

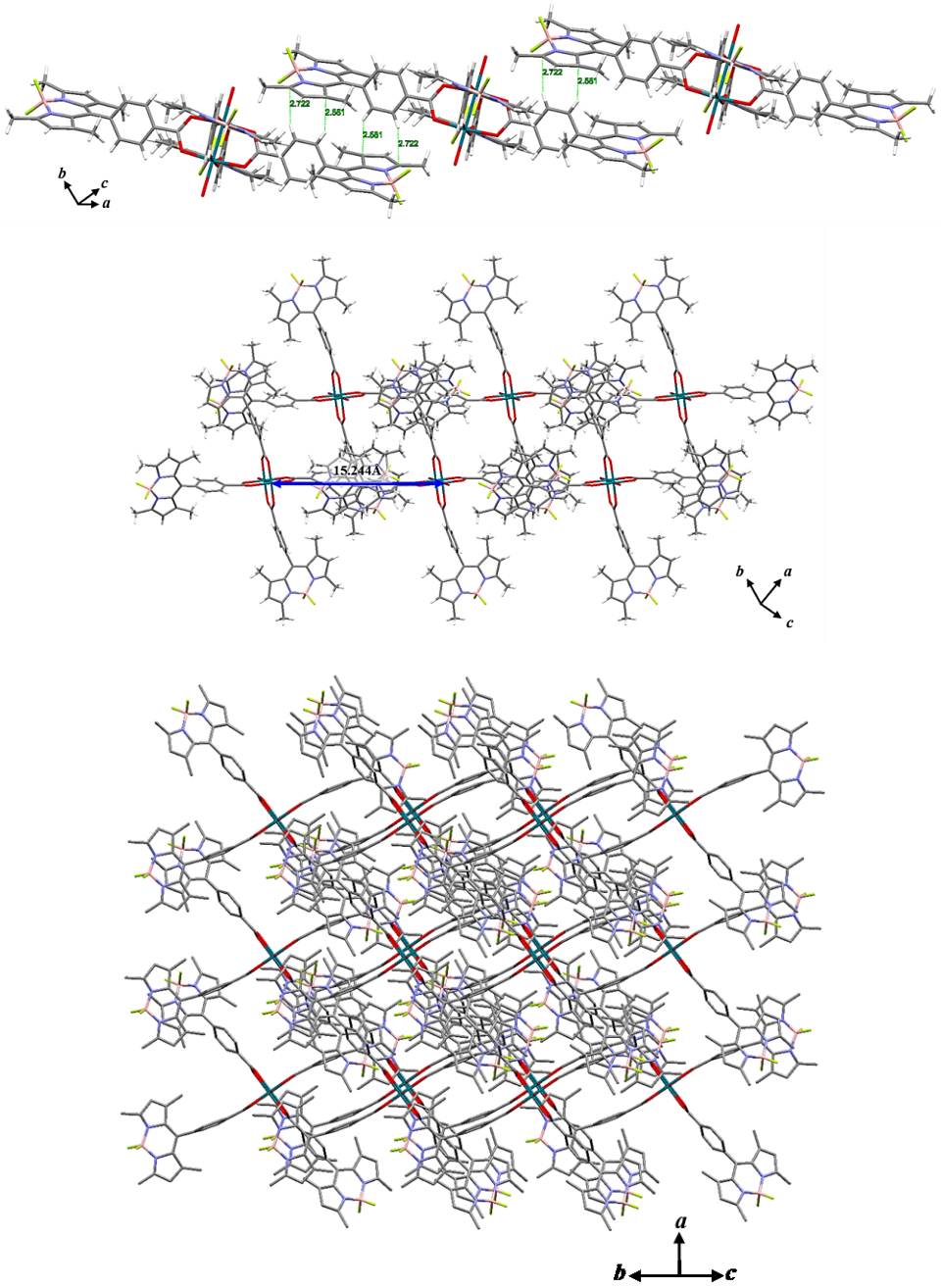

Figure 4. Crystal structure of **FC-2** shown (top) 1-D chain formed by CH-π and B-F···O(*methanol*) interaction, (middle) 2-D sheet formed weak B-F···H(*methyl*) and π···π interaction and (bottom) 3-D packing. Hydrogen atoms, methanol molecules coordinated at the axial positions except for the coordinated oxygen atoms and crystal solvent molecules are omitted for clarity. O = red, C = grey, N = blue, B = pink, F = yellowish green and Rh = sea green.

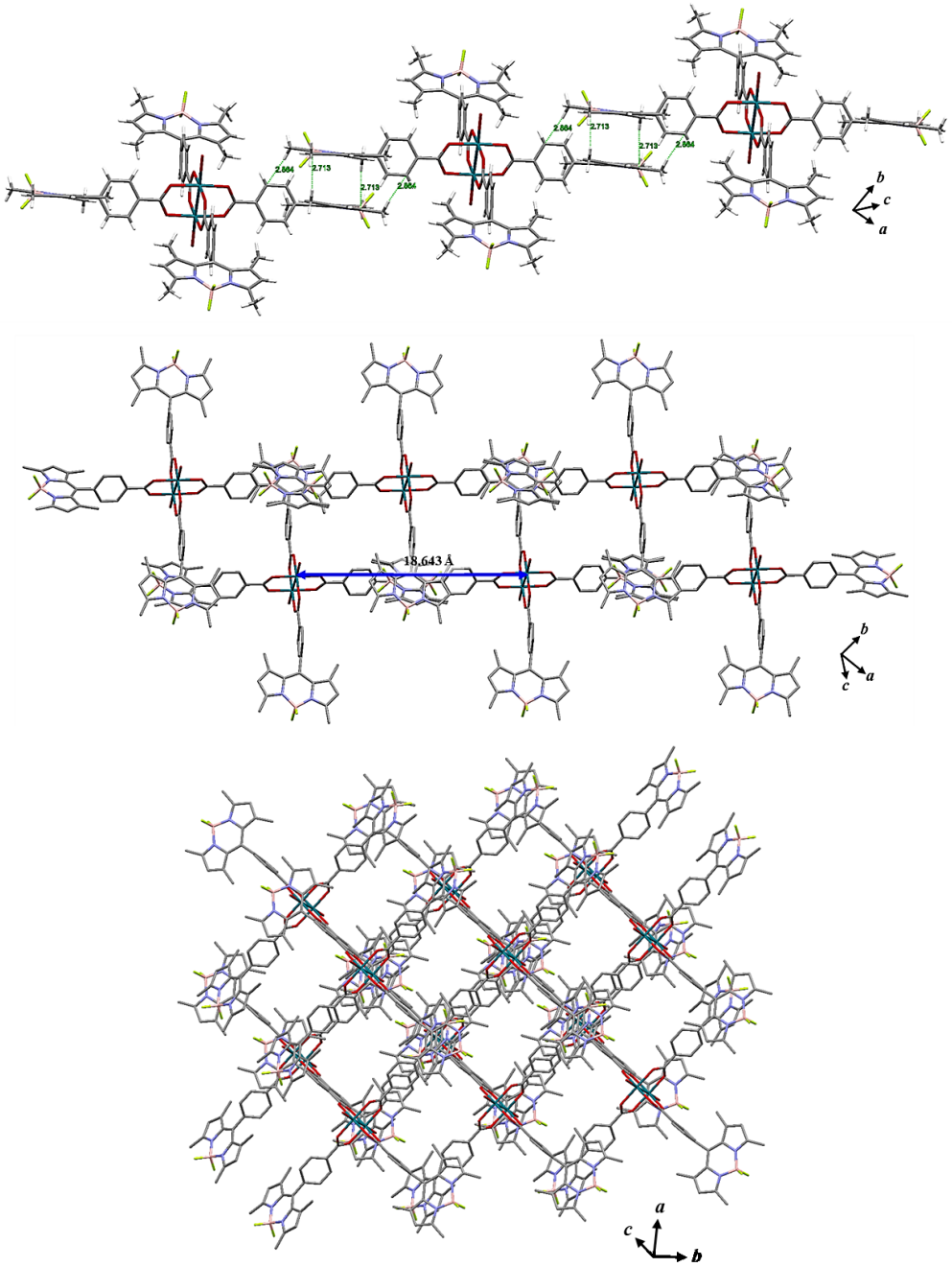

Figure 5. Crystal structure of **FC-2'** shown (top) 1-D chain formed by CH-π and B-F···O(*diethyl ether*) interaction, (middle) 2-D sheet formed weak B-F···H(*methyl*) and π···π interaction and (bottom) 3-D packing. Hydrogen atoms, diethyl ether molecules coordinated at the axial positions except for the coordinated oxygen atoms and crystal solvent molecules are omitted for clarity. O = red, C = grey, N = blue, B = pink, F = yellowish green and Rh = sea green.

Electrochemical properties of CM-2 in DCM

The electrochemical properties of **CM-2** and H**BDP** were studied by cyclic voltammetry. Cyclic voltammetry (CV) measurements conducted in dichloromethane (DCM) containing 0.1 M tetra-*n*-butyl ammonium perchlorate (TBAP) as an electrolyte (Fig. 6). Both compounds exhibited reduction and oxidation peaks at similar positions. The reversible reduction peak attributed to the reduction of **BDP** moiety (–1.08 V (vs. NHE)) for **CM-2**. This reductive peak is appeared at slightly anodic potential than the corresponding redox event of the free ligand H**BDP** (–1.14 V) under same measurement condition. Quasi-reversible oxidation peaks were observed at 1.36 V and 1.63 V (vs. NHE) for **CM-2** which are assigned to the BDP-based oxidation (**BDP**/**BDP**$^{\bullet+}$) and the Rh-based oxidation ($Rh^{III}Rh^{II}/Rh^{II}Rh^{II}$), respectively.

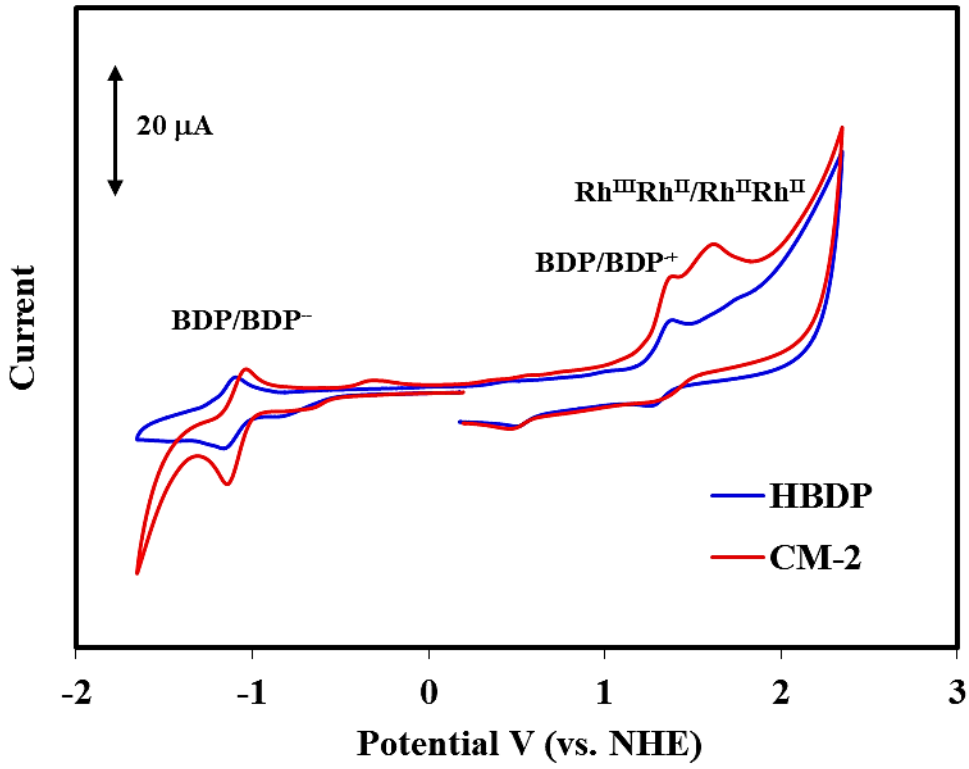

Figure 6. Cyclic voltammograms of 0.5 mM of **CM-2** (red line) and H**BDP** (blue line) in DCM containing 0.1 M TBAP at room temperature under an Ar atmosphere (WE: glassy carbon, AE: Pt wire, RE: Ag/Ag^{+}), at scan rate of 200 mV/s.

Electrocatalytic hydrogen evolution of CM-2

CVs of **CM-2** in γ–butyrolactone containing 0.1 M TBAP in the presence of acetic acid (AcOH) are shown in Fig. 7. A large irreversible catalytic currents probably corresponds to the electrocatalytic H_2 evolution by **CM-2** was observed at approximately –0.87 V (vs. NHE). The current was observed at the more positive onset potential than the reduction of the complex in organic media, indicating that the interaction between acetic acid and the Rh_2 center contributed the catalytically active $Rh^{II}Rh^{I}$-H species similar with observation in the Chapter 1. The ratio between the irreversible current in the presence (i_{cat}) and the absent (i_p) of acetic acid (i_{cat}/i_p) is commonly employed for measure catalytic activity, and in the presence of 1.0 and 2.0 eq. acetic acid for **CM-2**, i_{cat}/i_p is 30.0 and 24.3, respectively. This result is clearly indicates the electrocatalytic reactivity of **CM-2**. Subsequent, the electrocatalytic activity of **CM-2** was examined using 5% and 10% water in γ–butyrolactone acidified with acetic acid. As shown in Fig. 8, upon addition of water into the solution, catalytic currents were gradually amplified (i_{cat}/i_p reached 30.0 and 32.6 when 5% and 10% water added, respectively). The enhanced catalytic current when large amount of water is added showing that water can contributes as a proton source after the formation of hydronium active species ($Rh^{II}Rh^{I}$-H). Importantly, these results suggest that **CM-2** is a highly active electrocatalyst and holds an advantage to tolerate the H_2 formation reaction in acidic aqueous solution. While great strides of the molecular-based electrocatalytic H_2 evolving catalysts have been made in acidic acetonitrile or other non-aqueous media.[15]

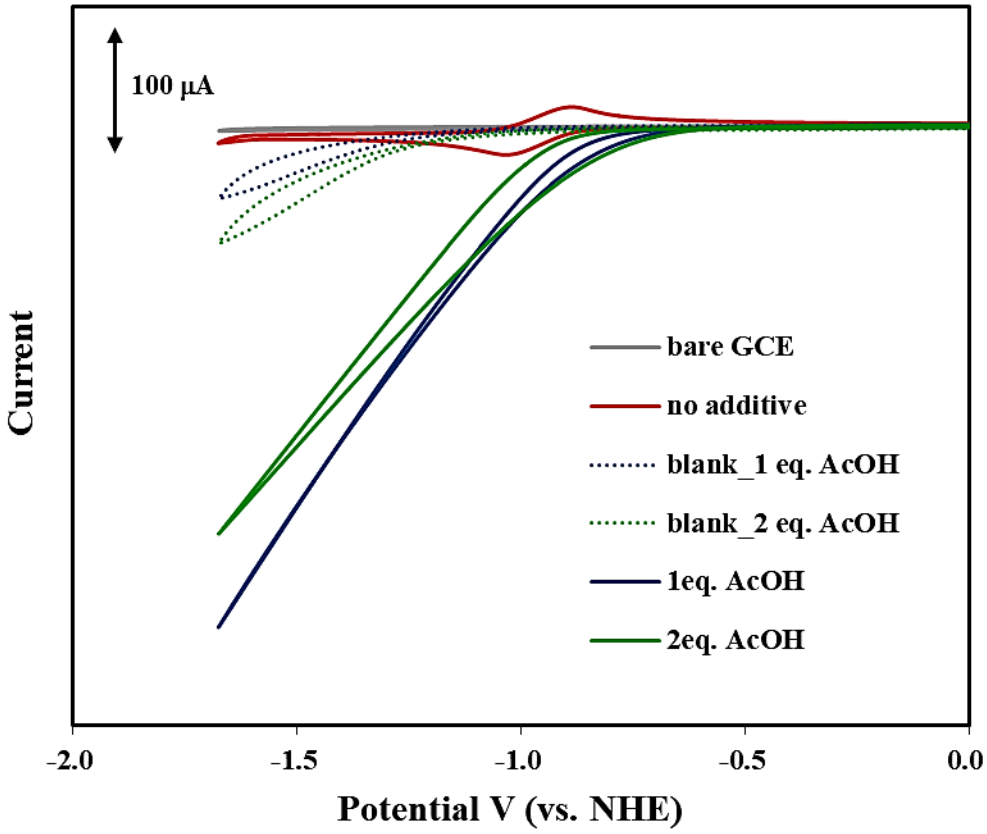

Figure 7. Cyclic voltammograms of **CM-2** (0.5 mM) in the presence of acetic acid (AcOH). Measurements were performed in γ-butyrolactone containing 0.1 M TBAP at room temperature under an Ar atmosphere (WE: glassy carbon, AE: Pt wire, RE: Ag/Ag^{+}) at scan rate of 100 mV/s.

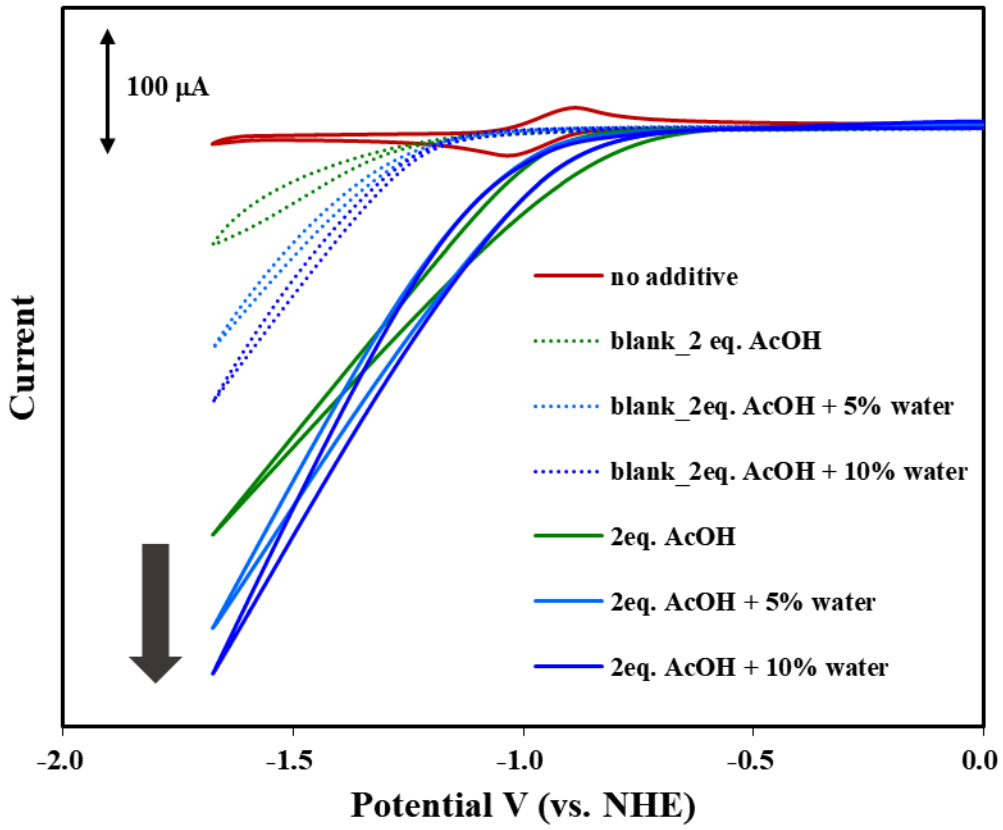

Figure 8. Cyclic voltammograms of **CM-2** (0.5 mM) in the presence of AcOH and water. Measurements were performed in γ-butyrolactone containing 0.1 M TBAP at room temperature under an Ar atmosphere (WE: glassy carbon, AE: Pt wire, RE: Ag/Ag^{+}) at scan rate of 100 mV/s.

Furthermore, CVs of **CM-2** in the presence of trifluoroacetic acid (TFA; pK_a = 0.23[16]) were also studied to examine their reactivity to form H_2 in the presence of stronger acid, compared to a pK_a of 4.75[17] for AcOH (Fig. 9). In these conditions, catalytic currents were trigged at much lower onset potential as –0.70 V (vs. NHE). Overall catalytic activities were improved (i_{cat}/i_p = 38.0 for 1.0 eq. TFA added) compared to the aforementioned conditions in which AcOH used as a proton source. This result suggests proton source with respect to pK_a is a considerable factor which effects to activity of electrocatalytic H_2 generation. A large amount of TFA gradually decreases catalytic activity (i_{cat}/i_p = 31.5 for 5.0 eq. TFA added) compare to smaller amount of TFA added (i_{cat}/i_p = 38.0 and 34.5 for 1.0 and 3.0 eq. TFA added, respectively). However, the onset of the catalytic current was shifted to more positive potential when larger amount of TFA was added. CVs of **CM-2** solution were also measured in the presence of TFA and water. As shown in Fig. 10, vast enlarged catalytic currents can be seen upon increasing the concentration of water (i_{cat}/i_p reached 134 when 25% of water was added). From these preliminary observations of the catalytic module **CM-2** on their electrocatalytic water reduction activity, the catalytic H_2 evolution of the molecular framework **FC-2** in an aqueous medium can be also anticipated.

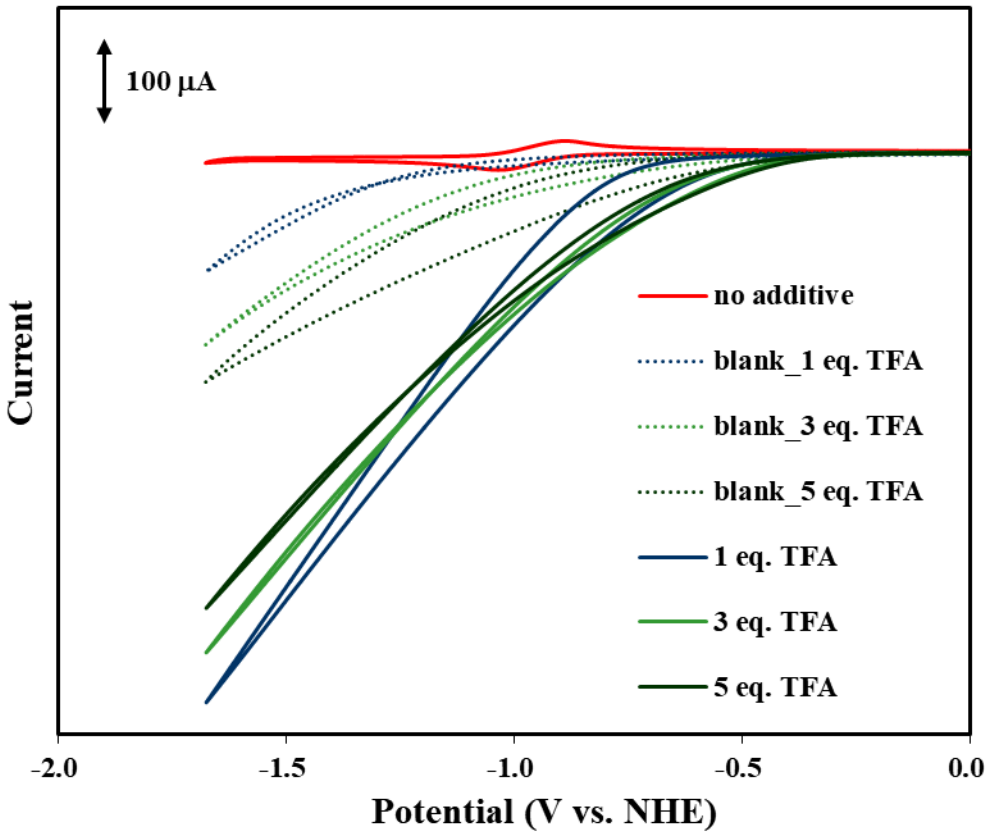

Figure 9. Cyclic voltammograms of **CM-2** (0.5 mM) upon addition of 0–5 eq. of trifluoroacetic acid (TFA). Measurements were performed in γ-butyrolactone containing 0.1 M TBAP at room temperature under an Ar atmosphere (WE: glassy carbon, AE: Pt wire, RE: Ag/Ag^{+}) at scan rate of 100 mV/s.

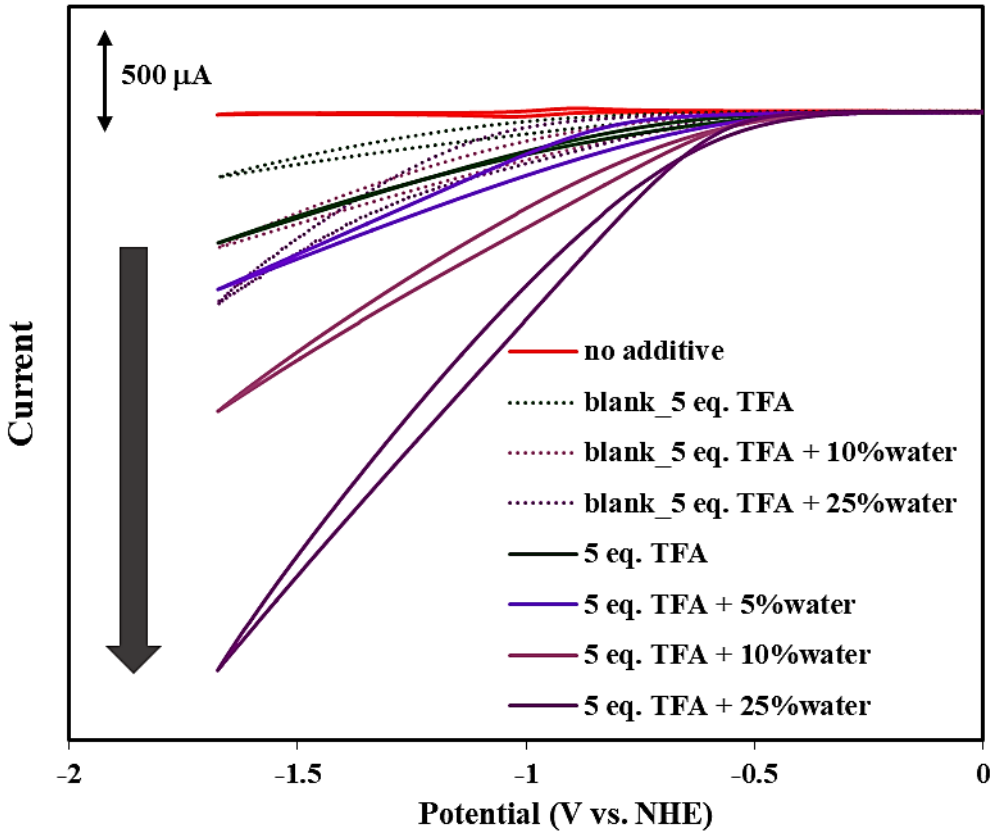

Figure 10. Cyclic voltammograms of **CM-2** (0.5 mM) in the presence of TFA and water. Measurements were performed in γ-butyrolactone containing 0.1 M TBAP at room temperature under an Ar atmosphere (WE: glassy carbon, AE: Pt wire, RE: Ag/Ag^{+}) at scan rate of 100 mV/s.

Controlled potential electrolysis of CM-2

Consequently, the control potential electrolysis (CPE) of **CM-2** was performed in order to confirm and quantify the product of catalytic reaction. The experiments were carried out in a two-compartment cell equipped with a glassy carbon plate as a working electrode (ca. surface area is 2.60 cm^2) under an Ar atmosphere. After an hour of the electrolysis at −1.00 V (vs. NHE) of a solution of **CM-2** (0.2 mM in 0.1 M TBAP/γ-butyrolactone) in the presence of acetic acid (0.05 – 0.10 M) as a proton source, the gas evolved in the headspace of electrochemical cell were analyzed by gas chromatography. As shown in Table 1, investigation of blank (entry 1) and the generation of hydrogen was confirmed, which clearly demonstrates the electrocatalytic activity of **CM-2**. Increased concentration of the proton source (acetic acid) resulted in the enhancement hydrogen production and turnover numbers (TONs) as shown in entries 2 and 3 in Table 1. The CPE experiment in the presence of acetic acid (0.10 M) and 25% water (ca. 16.60 M) was also performed (entry 4 in Table 1). In this condition, overall electrocatalytic ability slightly improved, similar with the observation in CVs measurement. However, the relatively higher concentration of water as proton source (ca. 16.60 M from 25% v/v water added) is required in order to achieve the nearly comparable electrocatalytic efficiency instead of acetic acid (entry 5 in Table 1). These results imply catalytic activity strongly depends on pK_a of proton source similar to the observations in electrochemical properties. Moreover, the effect of TFA, a stronger proton source in the electrocatalysis of **CM-2** was also examined, and an improved faradaic efficiency was obtained (entry 6 in Table 1). The result suggests that pK_a of proton source is one of the importance factors for electrocatalytic hydrogen evolution.

Table 1. Results of CPE experiments. Experiments were conducted for **CM-2** (0.2 mM) in γ-butyrolactone containing 0.1 M TBAP at −1.00 V (vs. NHE) under an Ar atmosphere at room temperature for 1 hour.

Entry	H^+ source (M)	Charge delivered (C)	μMoles H_2 (measurement)[a]	TON[b]	FE[c] (%)
1	blank	0.01	negligible	-	-
2	AcOH (0.05)	1.35	3.75	3.75	53.60
3	AcOH (0.10)	2.09	7.86	7.86	72.58
4	AcOH (0.10) + water (16.60)[d]	3.19	13.70	13.70	82.88
5	water (16.60)[d]	2.78	10.64	10.64	73.84
6	TFA (0.05)	0.32	1.65	1.65	99.52

[a]Experimental amount of produced H_2 was determined from the GC measurements.

[b]Experimental turnover number (TON) was calculated from the experimental amount of produced H_2.

[c]Faradaic efficiency was determined as the ratio of the measured amount of produced hydrogen and the theoretical amount of produced hydrogen according to Faradaic's law.

[d]Concentration of water was estimated from 25% v/v water added.

Electrochemical properties of FC-2

The catalytic proton reduction experiments in organic solvent provide a starting point of analysis. However, purely aqueous medium is an ideal medium for H_2 production because of abundant source. Recently, the efficient electrocatalytic reduction of protons to hydrogen in aqueous medium has been reported.[18] Thus, an electrochemical property of molecular framework **FC-2** in an aqueous medium was also examined. The electrochemical properties of **FC-2** were also investigated by cyclic voltammetry (CV). The CVs of **FC-2** was performed using a glassy carbon working electrode modified by **FC-2** (Scheme 5) in aqueous acetate buffer (pH = 5). A large irreversible reduction wave was observed at –0.65 V (vs. NHE, Fig. 11) and the formation of bubbles, which is probably attributed to H_2, was observed at the surface of glassy carbon electrode (Fig. 12). These observations indicate that **FC-2** can serve as a heterogeneous H_2 production catalyst in aqueous medium. Note that CVs of solid-state **FC-2** in an aprotic electrolyte (e.g. DCM or *o*-DCB) cannot be investigated due to very high solubility of **FC-2** in common organic solvents.

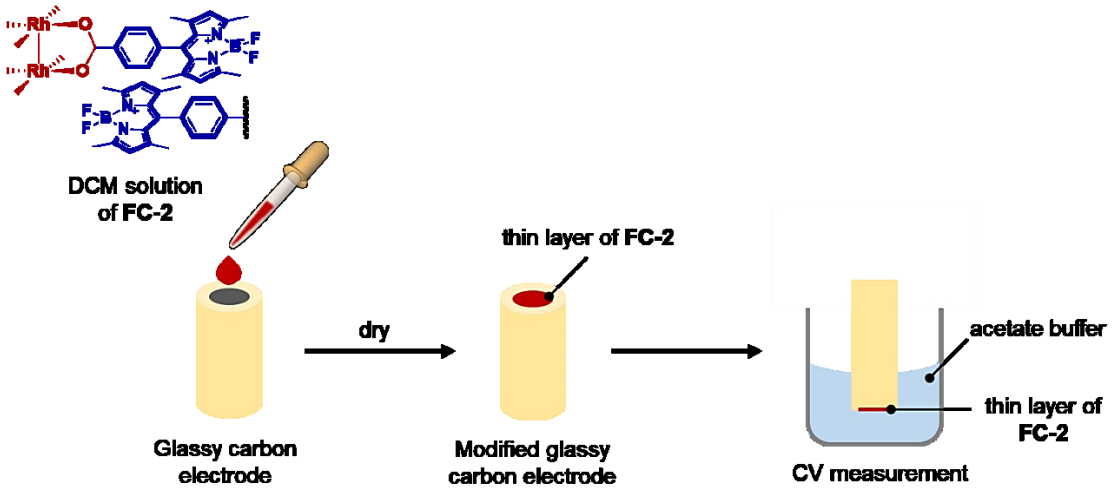

Scheme 5. Schematic illustration of the procedure to modify a glassy carbon electrode with **FC-2**.

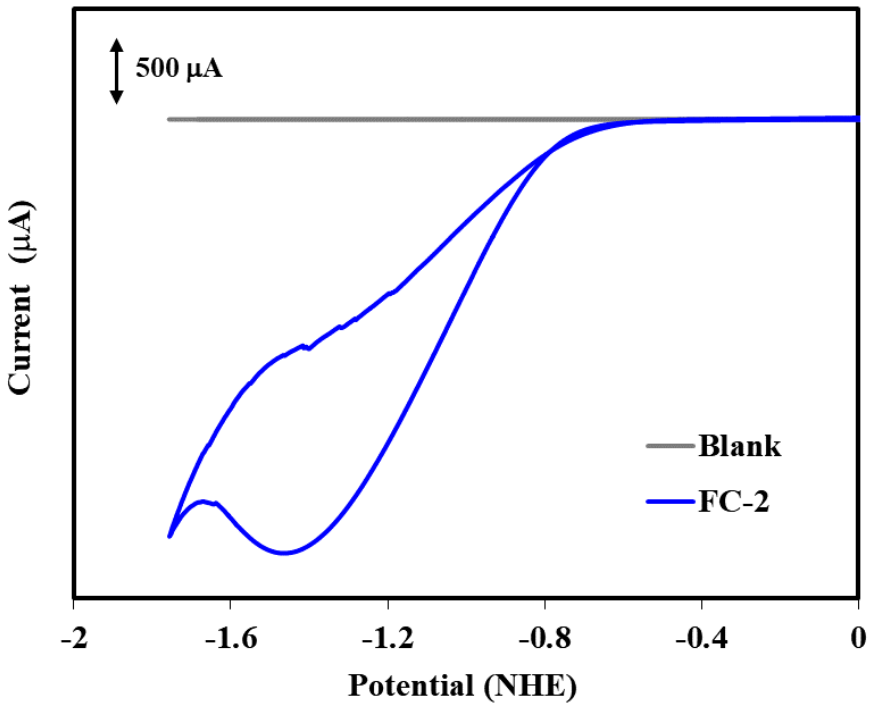

Figure 11. Cyclic voltammograms of **FC-2** deposited on a glassy carbon electrode (blue line) and a blank solution (grey line) in 1.0 M acetate buffer pH 5 at room temperature under an Ar atmosphere (WE: glassy carbon, CE: Pt wire, RE: SCE), at scan rate of 300 mV/s.

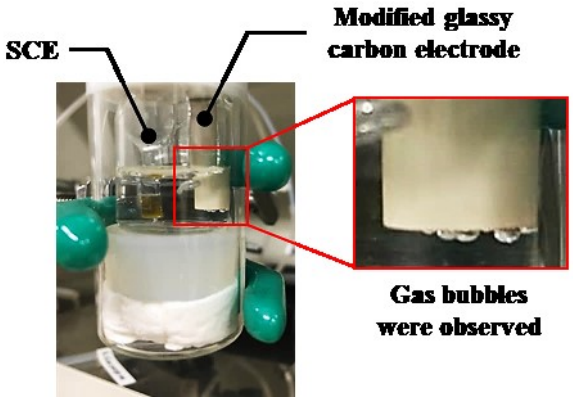

Figure 12. Photograph of electrochemically-generated bubbles by **FC-2** observed during the solid-state cyclic volumetric measurement.

Controlled potential electrolysis of FC-2

In order to unveil the catalytic activity of the framework catalyst, controlled potential electrolysis of **FC-2** was conducted in 1.0 M aqueous acetate buffer at pH = 5 using the two-compartment cell described in the previous section. Similar to the electrochemical studies, **FC-2** was deposited onto a freshly polished glassy carbon working electrode plate (Scheme 6) and the modified electrode was used for the CPE experiments. More details on the preparation of modified working electrodes and experimental details of CPE experiments are given in experimental section.

We initially started by probing the potential required for electrocatalytic production of H_2 by **FC-2**. The results of CPE experiments performed at various applied potentials are summarized in Table 2. After an hour of applied potential at –0.40 V (vs. NHE), H_2 was not detected, which is consistent with the result of electrochemical measurements. By changing the applied potentials to more negative potential region, the amount of evolved H_2 gradually increased (Fig. 13). Electrolysis carried out at –1.00 V results in the H_2 evolution of 116.44 μmol and TON (measurement) of 78,430.

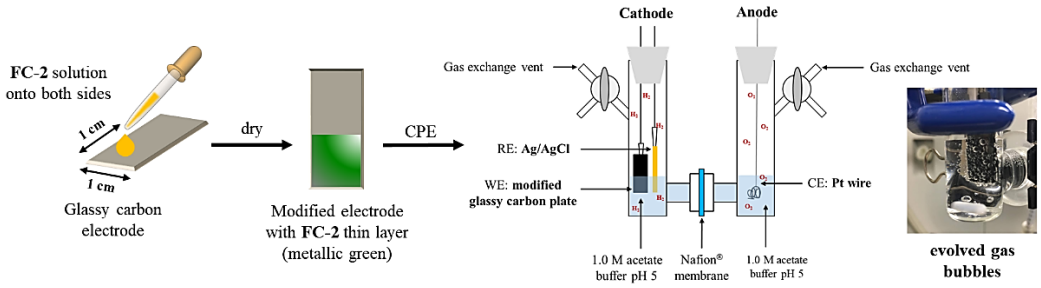

Scheme 6. Schematic illustration of the procedure to perform heterogeneous control potential electrolysis of **FC-2**. An inset photograph shows H_2 gas bubbles evolved during an hour of electrolysis.

Table 2. Results of CPE experiments. Experiments were conducted in 1.0 M acetate buffer (pH = 5) at various applied potential under an Ar atmosphere at room temperature for 1 hour. Thin layers were prepared by drop casting an 80 μM DCM solution of **FC-2** (20 μL) onto freshly polished glassy carbon electrode for 1 layer.

Entry	Applied potential (V vs NHE)	Charge delivered (C)	μMoles H_2 (measurement)[a]	TON[b] ($\times 10^3$)	FE[c] (%)
1	–0.40	0.42	-	-	-
2	–0.70	12.50	32.91	20.57	50.81
3	–0.80	13.40	66.24	28.75	66.24
4	–0.90	20.00	96.78	48.39	93.37
5	–1.00	30.27	116.44	78.43	74.22

[a]Experimental amount of produced H_2 was determined from the GC measurements.

[b]Turnover number (TON) was calculated from the experimental amount of produced H_2.

[c]Faradaic efficiency was determined as the ratio of the measured amount of produced hydrogen and the theoretical amount of produced hydrogen according to Faradaic's law.

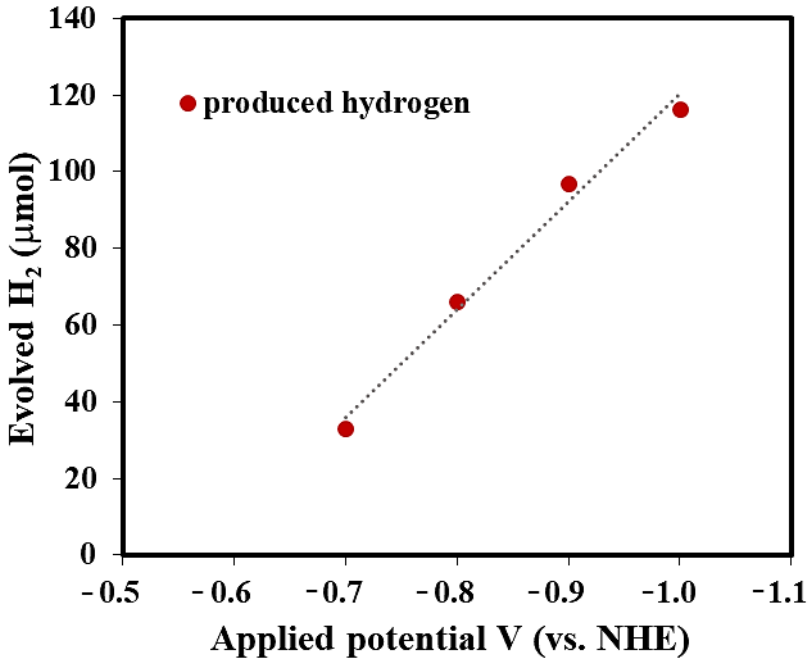

Figure 13. The electrocatalytic H_2 production by **FC-2** at various applied potentials. Data retrieved from Table 2.

To optimize the conditions for the CPE experiments, I subsequently increased number of layers of **FC-2** on a glassy carbon electrode because a single layer of **FC-2** was found to be hard to cover the whole surface of the glassy carbon plate (Fig. 14). Details of the preparation of a glassy carbon electrode modified by multi-layers of **FC-2** are given in the experimental part.

The CPE experiment with the applied potential at −1.0 V (vs. NHE) was performed using the glassy carbon electrode modified with the multi-layered **FC-2** in stirred 1.0 M acetate buffer (pH = 5). A plot of the charge passed over the time during electrolysis is shown in Fig. 15 and the results are summarized in Table 3. A multi-layered **FC-2** passes relatively fewer charge during an hour of controlled potential electrolysis compared to a single-layered **FC-2**. However, the multi-layered **FC-2** can evolve H_2 with almost quantitative faradaic efficiency. The electrolysis under same condition using a bare glassy carbon plate evidences negligible charge consumption by environments. These results indicate that the multi-layered **FC-2** is more preferable for the electrocatalytic H_2 production.

Next, I examined the effect of the amount of the catalyst on the catalytic activity. The volume of **FC-2** (240 μM) used in the deposition was changed from 20 to 30 μL. As shown in Fig. 16 and Table 4, the electrode modified with a larger amount of **FC-2** (30 μL) affords the faster rate of accumulated charge than the electrode with a fewer catalyst amount (20 μL) during the electrolysis. However, the faradaic efficiencies of these modified electrodes were similar.

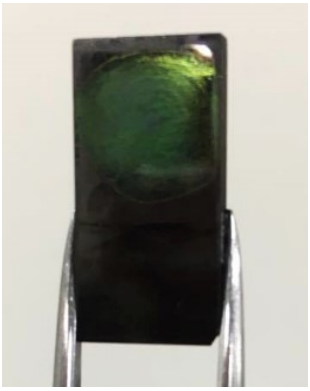

Figure 14. A photograph of a glassy carbon plate modified with single-layer of **FC-2** (metallic green). The surface of the electrode is partially covered by **FC-2**.

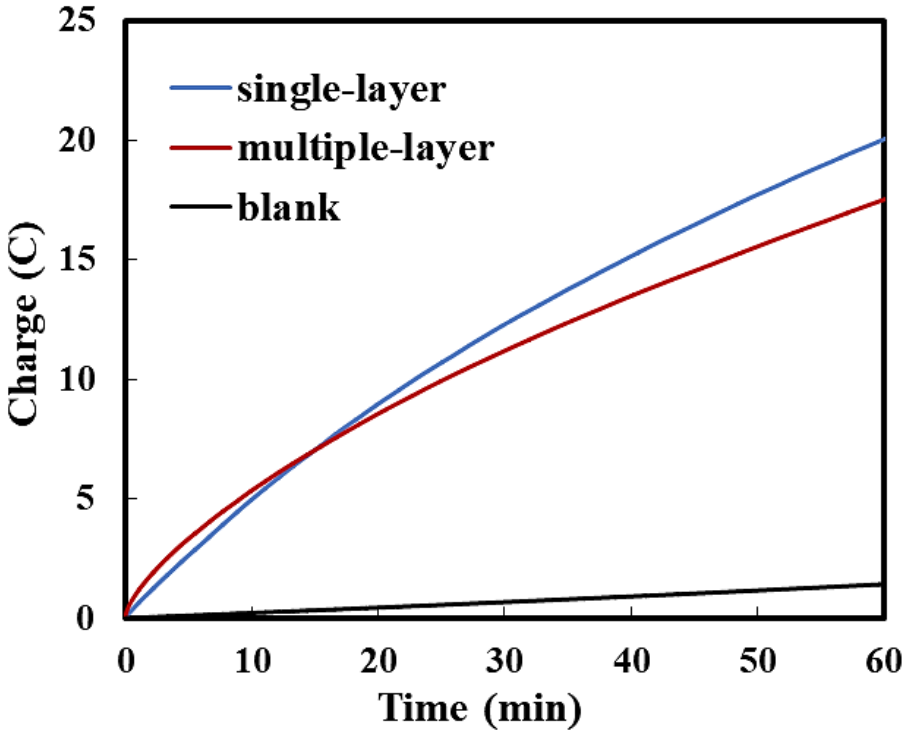

Figure 15. The results of controlled potential electrolysis of a single-layer (light-blue line) and multiple-layers (red line) of **FC-2**. Experiments were performed in 1.0 M acetate buffer (pH = 5) with an applied potential at −1.00 V (vs. NHE) under Ar at room temperature. The result of electrolysis of a bare glassy carbon working electrode under same condition is shown for comparison (black line).

Table 3. Results of CPE of **FC-2**. Experiments were performed in 1.0 M acetate buffer (pH = 5) at −1.00 V (vs. NHE) under an Ar atmosphere at room temperature for 1 hour.

Entry	FC-2	Charge delivered (C)	Current (mA)	μMoles H_2 (measurement)[a]	FE[b] (%)
1	Single-layer[c]	30.27	7.03	116.44	74.22
2	Multiple-layer[d]	17.60	1.55	190.33	quantitative
3	none	1.60	0.45	-	-

[a]Experimental amount of produced H_2 was determined from the GC measurements.

[b]Faradaic efficiency was determined as the ratio of the measured amount of produced hydrogen and the theoretical amount of produced hydrogen according to Faradaic's law.

[c]Data retrieved from Table 2.

[d]Pre-activated **FC-2** prior the electrolysis for an hour.

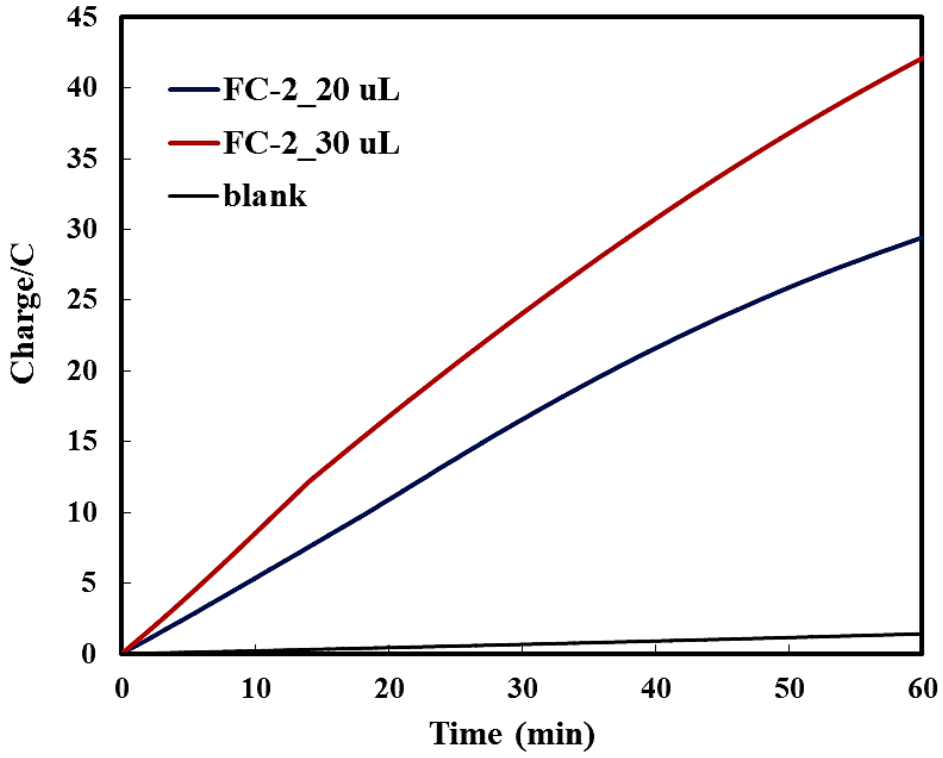

Figure 16. The results of controlled potential electrolysis **FC-2** (red line) in 1.0 M acetate buffer (pH = 5) of at −1.00 V (vs. NHE) under an Ar at room temperature. A single-layer modified electrodes were prepared by drop casting of a DCM solution (240 μM) of **FC-2** onto a freshly polished glassy carbon electrode. The result of electrolysis of a bare glassy carbon working electrode is shown for comparison (black line).

Table 4. Results of CPE experiments of **FC-2**. Experiments were performed in 1.0 M acetate buffer (pH = 5) at −1.00 V (vs. NHE) under an Ar atmosphere at room temperature for 1 hour.

Entry	Volume of FC-2 (μL)	Charge delivered (C)	Current (mA)	μMoles H_2 (measurement)[a]	FE[b] (%)
1	20	29.40	5.61	124.53	81.74
2	30	42.20	8.23	187.05	85.53
3	none	1.60	0.45	-	-

[a]Experimental amount of produced H_2 was determined from the GC measurements.

[b]Faradaic efficiency was determined as the ratio of the measured amount of produced hydrogen and the theoretical amount of produced hydrogen according to Faradaic's law.

Subsequently, the recyclability of **FC-2** was investigated. The glassy carbon electrode modified with **FC-2** which was used in the first CPE experiment was rinsed with water, and the additional electrolysis was performed using in fresh 1.0 M acetate buffer (pH = 5) under identical experimental condition as the first run. Interestingly, the electrocatalytic activity of the modified electrode was retained at least 3 for cycles with quantitative faradaic efficiencies (Fig. 17). The gradual increase of accumulated charge in later cycles may be due to the gradually activated **FC-2** species at the surface of working electrode.

The stability of **FC-2** activity after long-catalysis period was also examined. The CPE was executed at same condition for 9 hours. Over 9 hours of the electrolysis, charge almost linearly as time (Fig. 18), and the faradaic efficiency of the hydrogen evolution was determined to be quantitative (Table 5). Most importantly, this framework catalyst **FC-2** maintained activity hydrogen formation reaction for long term, which is rare in available reports. These reactivity, recyclability and durability of **FC-2** framework catalyst may be attributed to the highly organized and porous framework structure, which provides a rigid support for each catalytic modules, and allowing constant diffusion of substrate to the active sites for continuous catalytic reaction.

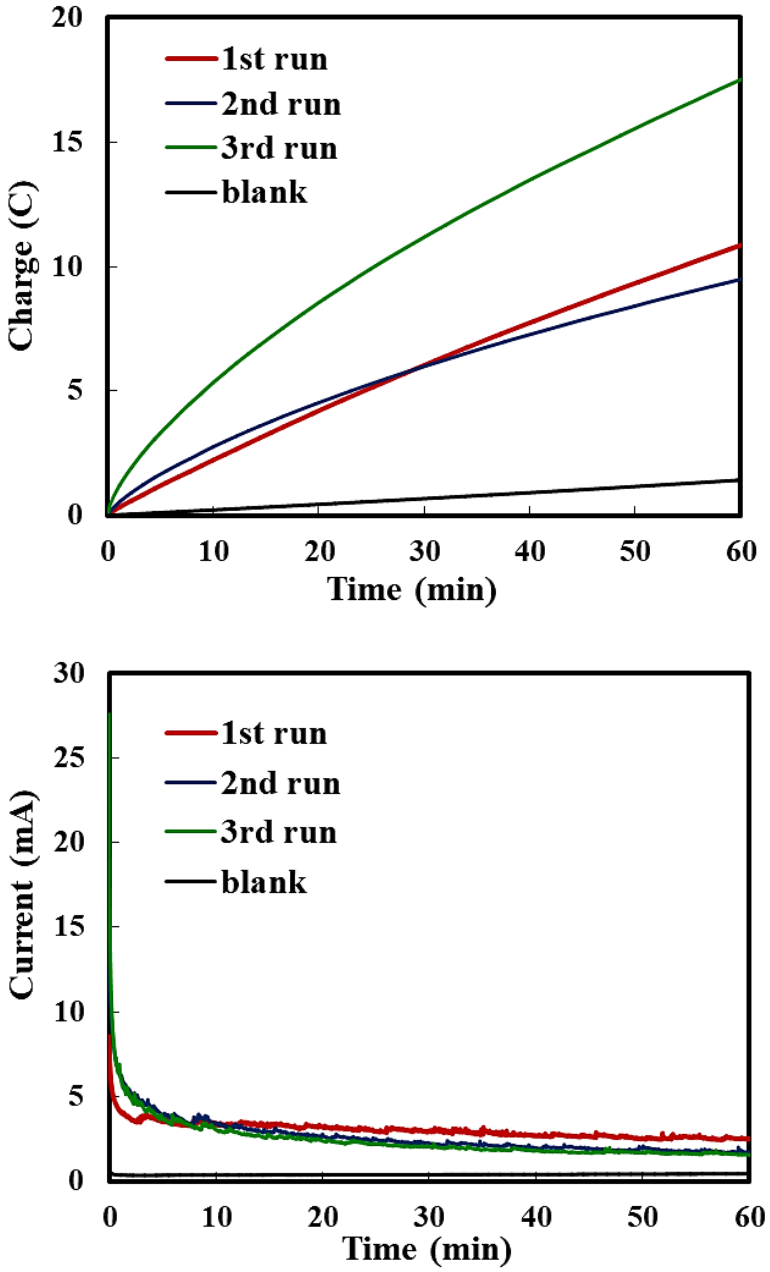

Figure 17. Controlled potential electrolysis of **FC-2** in 1.0 M acetate buffer (pH = 5) at −1.00 V (vs. NHE) under Ar at room temperature. After each run of electrolysis, the modified glassy working plate was rinsed with water, dried over air 30 min and used in the subsequent CPE experiment in a fresh electrolyte solution under the identical experimental condition as the first run. The result of electrolysis of a bare glassy carbon working electrode is shown for comparison (black line).

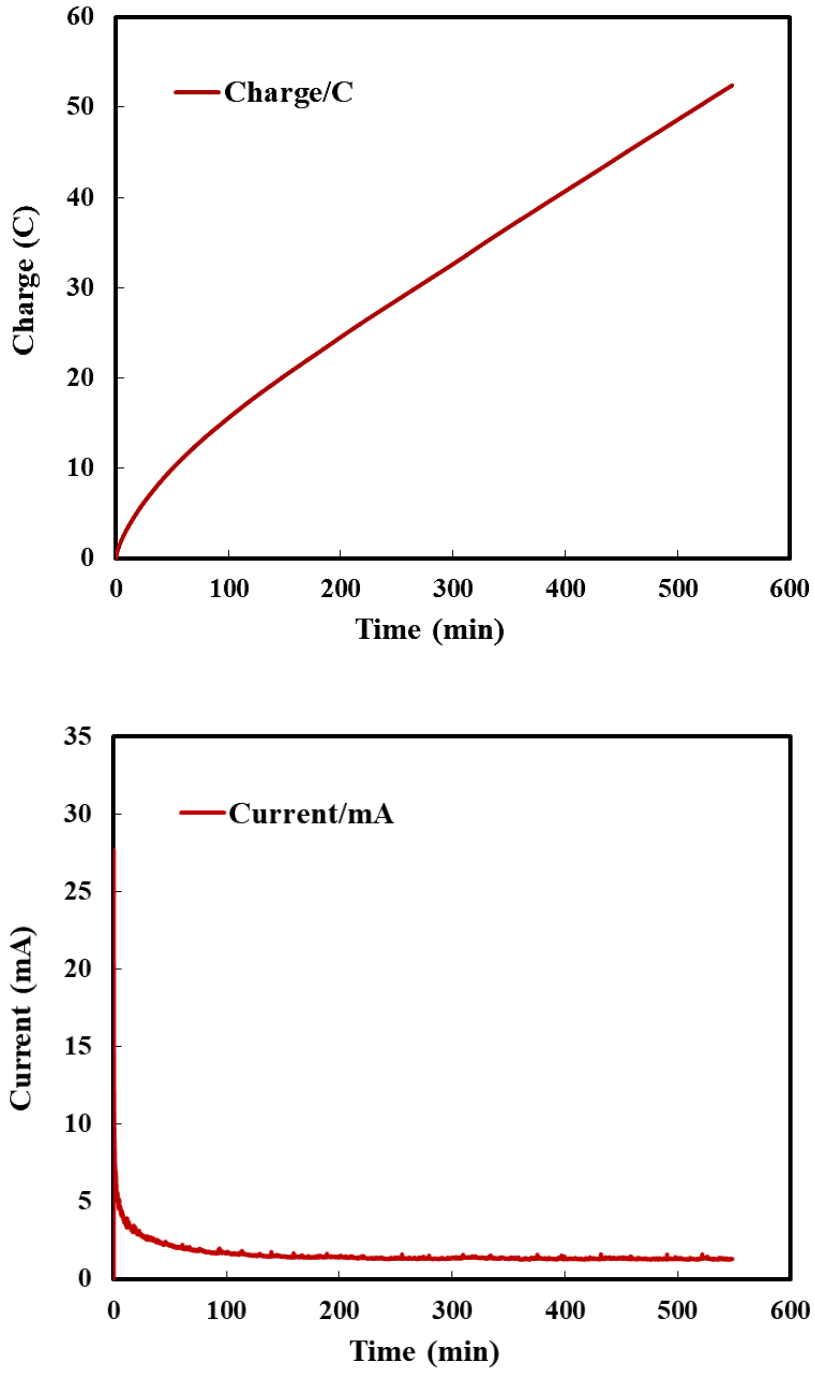

Figure 18. The result controlled potential electrolysis of **FC-2** in 1.0 M acetate buffer (pH = 5) with an applied potential at −1.00 V (vs. NHE) under Ar at room temperature showing (top) accumulative charge and (bottom) current involves over 9 hours.

Table 5. Results of CPE experiments of **FC-2** over 9 hours. Experiments were performed using multi-layer **FC-2** deposited on a glassy carbon working plate in 1.0 M acetate buffer (pH = 5) at –1.00 V (vs. NHE) under an Ar atmosphere at room temperature for 1 hour.

Entry	Reaction time (min)	Charge delivered (C)	Current (mA)	μMoles H_2 (measurement)[a]	FE[b] (%)
1	60[c]	17.60	1.55	190.33	quantitative
2	550	52.40	1.30	1413.66	quantitative

[a]Experimental amount of produced H_2 was determined from the GC measurements.

[b]Faradaic efficiency was determined as the ratio of the measured amount of produced hydrogen and the theoretical amount of produced hydrogen according to Faradaic's law.

[c]Data retrieved from Table 3 (entry 2; multiple-layer of **FC-2** on a modified glassy carbon plate).

The photophysical properties of CM-2 and FC-2

The dirhodium bearing light-absorbing ligands have been shown to be an excellent photocatalyst for hydrogen evolution as demonstrated in Chapter 1. However, a major limitation of the complex is a lack of absorption bands in the visible light region. The inability to harvest visible light (420 – 650 nm) can be a major drawback to utilize solar light efficiently. Since bodipy derivatives are known to strongly absorb light in the visible region, I hypothesized that the **CM-2** catalyst module (**$Rh_2(BDP)_4$**, H**BDP** = 4,4-difluoro-8-[4-(carboxy)phenylic]-1,3,5,7-tetramethyl-4-bora-3a,4a-diaza-4-bora-*s*-indacene acid) and **FC-2** might exhibit an improved photophysical properties and photocatalytic activities for hydrogen evolution driven by visible light. Therefore, the photophysical properties of **CM-2**, **FC-2** and their corresponded molecular connector (H**BDP**) were subsequently investigated by various techniques.

Firstly, the UV-Visible absorption spectroscopic studies were conducted. The UV-vis absorption spectrum **CM-2** in dichloromethane revealed a sharp and strong absorption band with an absorption maxima located at 499 nm and a small shoulder approximately at 471 nm (Fig. 19, red line). The former intense absorption band is attributed to the π–π* ($S_0 \rightarrow S_1$) transition of the bodipy, while the latter band is assigned to the intramolecular vibronic coupling of the **BDP** unit.[19] In addition, a broad and weak absorption band is also observed at approximately 370 nm, corresponding to the $S_0 \rightarrow S_2$ transition of the **BDP** unit.[8c] These absorption profile of **CM-1** is found to be similar to the corresponding bodipy precursor, H**BDP** (Fig. 19, blue line), which suggests the preservation of this bodipy excited state in **CM-1**. In addition, **CM-1** exhibited a band with moderate intensity at 699 nm, which is assigned to the π* → σ* transition of the dirhodium center (Scheme 7).

The photochemical properties of **FC-2** were also studied by diffuse-reflectance spectroscopy (Fig. 20), and the π–π* transition (λ_{max} = 510 nm) of the **BDP** moieties and the π* → σ* transition (λ_{max} = 653 nm) band of dirhodium center were observed. Condensed structure in the solid-state may causes slight bathochromic shift of the bands in **FC-2**. These results indicate that integration of **BDP** successfully tuned up the light-harvesting features of the catalytic module and the framework catalyst to the visible-light region.

Next, the emission properties of **CM-2** and **FC-2** were investigated in solution and solid phase, respectively. The emission properties of the free H**BDP** ligand was also studied for comparison. The H**BDP** exhibited strong yellowish-green emission both in solution (in dichloromethane, λ_{em} = 515 nm, Fig. 21) and in the solid state (λ_{em} = 511 nm, Fig. 22), which is typical for BDP derivatives.[9a] The intense fluorescence of H**BDP** (Φ_{FL} = 0.57 in dichloromethane) is originated from the electronic "push-pull" and the steric effect of the methyl substituents on pyrrole rings (**BDP** moieties).[20] In contrast, the installation of **BDP** into dirhodium center cause the quenching of the emission; approximately 97% of emission is quenched in **CM-2** (Fig. 21) and **FC-2** did not show detectable emission (Fig. 22). These results suggest that the quenching of the excited state of the **BDP** moiety (**BDP***) by the Rh_2 center efficiently occurred either by energy or electron transfer mechanism. The summary of the photophysical properties of **CM-2** and **FC-2** are depicted in Tables 5 and 6, respectively.

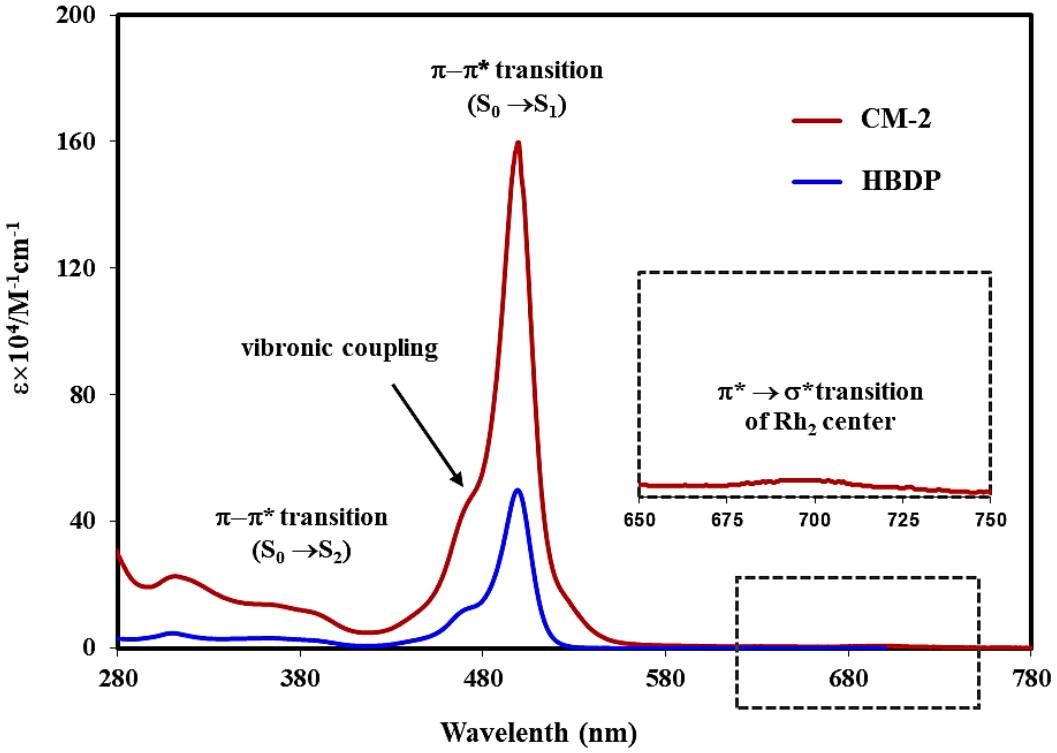

Figure 19. UV-Vis absorption spectra of free ligand H**BDP** (blue line) and **CM-2** (red line) in dichloromethane. In the case of H**BDP,** the band corresponds to π–π* ($S_0 \rightarrow S_1$) transition appeared at 499 nm with vibronic coupling shoulder at 471 nm. A weak broad band centered approximately at 370 nm is attributed to the $S_0 \rightarrow S_2$ transition. In the case of **CM-2**, the band correspond to π–π* transition (**BDP** moieties) and π* → σ* transition (Rh(II) center) were observed at 499 and 699 nm, respectively.

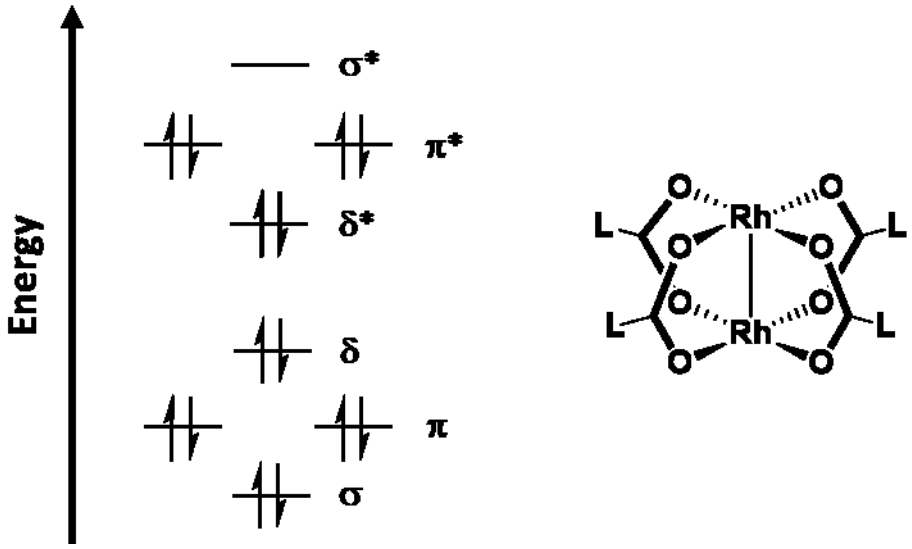

Scheme 7. Schematic illustration of MO diagram of a Rh_2 centre having d^7-d^7 configuration.

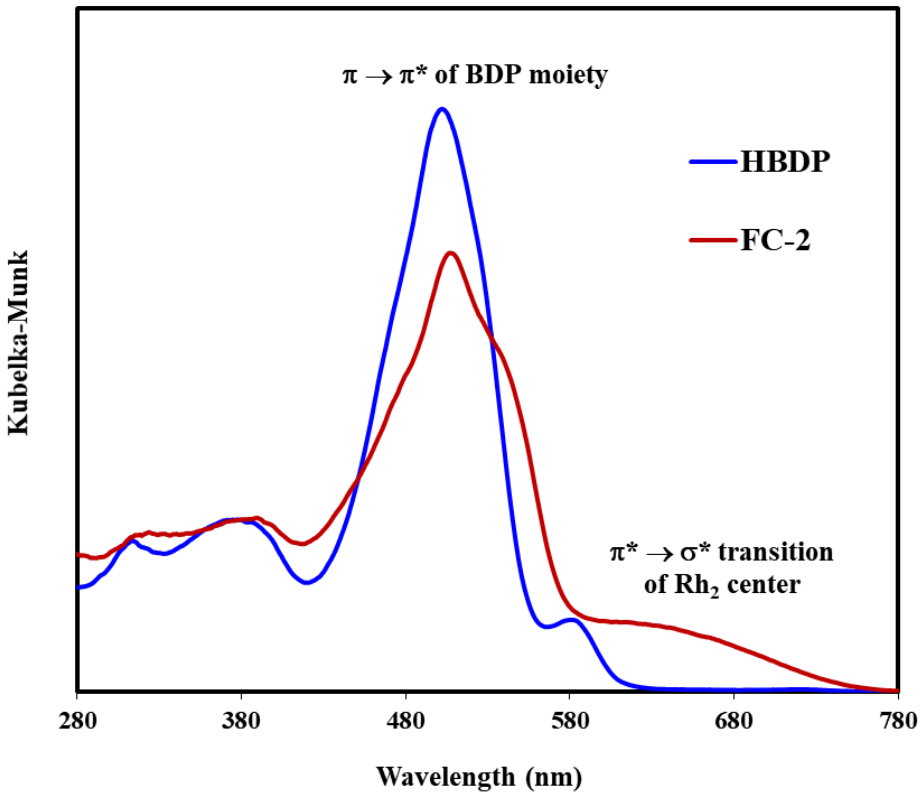

Figure 20. Diffuse reflectance UV-Vis spectra of the solid samples of free ligand H**BDP** (blue line) and **FC-2** (red line). For H**BDP**, the band corresponds to π–π* transition appears at 505 nm. In the case of **FC-2**, the bands correspond to π–π* transition (**BDP** moieties) and π* → σ* transition (Rh(II) centre) were observed at 510 and 653 nm, respectively.

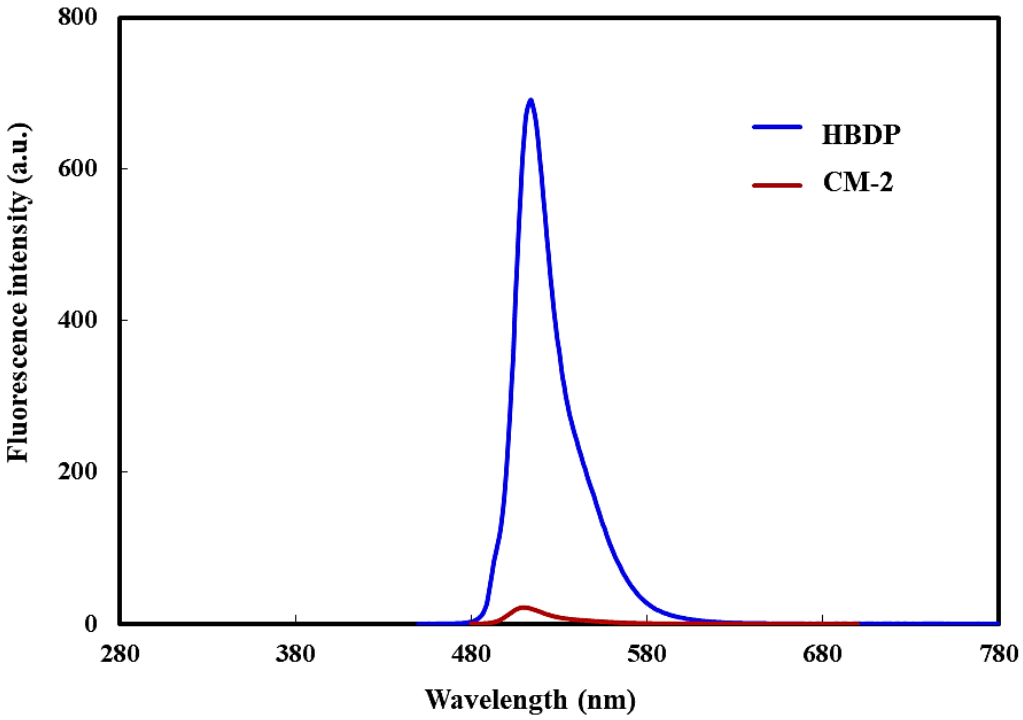

Figure 21. Fluorescence emission spectra of free ligand H**BDP** (0.02 mM, blue line) and **CM-2** (0.02 mM, red line) in dichloromethane under Ar at ambient temperature. The excitation wavelength was 499 nm. For H**BDP**, the emission band appears at 515 nm. For **CM-2**, a very weak emission band (less than 20 a.u.) was observed at 511 nm.

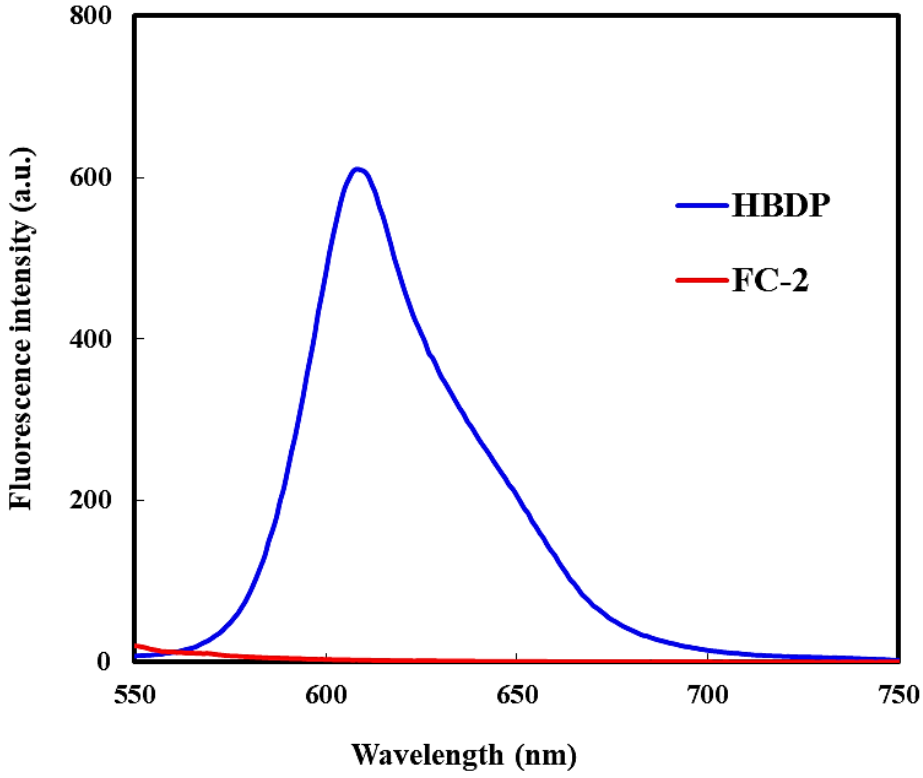

Figure 22. Solid-state fluorescence emission spectra of free ligand H**BDP** (blue line) and **FC-2** (red line). The excitation wavelengths were 505 nm and 510 nm for H**BDP** and **FC-2**, respectively. The emission band of H**BDP** appears at 609 nm, while no emission band was observed in **FC-2**.

Table 6. Summary of the photophysical properties of **CM-2** and H**BDP** in dichloromethane (DCM).

Compound	**Solution-state (DCM)**		
	λ_{abs} /nm ($\varepsilon\times10^4$ $M^{-1}cm^{-1}$)	**λ_{exc}/nm**	**λ_{ems}/nm (intensity/a.u.)**
CM-2	499 (159.75), 699 (0.75)	499	515 (686.89)
H**BDP**	499 (50)	499	511 (21.23)

Table 7. Summary of the photophysical properties of **FC-2** and H**BDP** in the solid state.

Compound	**Solid state**		
	λ_{dr} /nm (K.M.)	**λ_{exc}/nm**	**λ_{ems}/nm (intensity/a.u.)**
FC-2	510 (19.00), 653 (2.59)	510	-
H**BDP**	505 (25.56)	505	609 (607.63)

Photocatalytic H_2 production studies

Since the fundamental photophysical characters of the newly synthesized catalytic module **CM-2** were investigated, I subsequently explored the photocatalytic H_2 evolution activity of **CM-2** driven by visible light. In a typical experiment, a solution of **CM-2** (0.05 mM) in aqueous-organic medium (2 mL) containing a sacrificial electron donor was irradiated by light in visible region ($\lambda_{irr} > 420$ nm) and the gas evolved at headspace of the cell was analyzed by gas chromatography.

I initially started from the examination of the effect of sacrificial electron donors, which is necessary component in the photocatalytic cycle in order to generate reduced species of photosensitizer, on the catalytic reaction. Four kinds of sacrificial electron donor species were employed for the photocatalytic hydrogen evolution of **CM-2**; BIH (1,3-dimethyl-2-phenyl-2,3-dihydro-1*H*-benzimidazole), HA (ascorbic acid), TEOA (triethanolamine) and EDTA (ethylenediaminetetraacetic acid) (Fig. 23). As shown in Fig. 24, irradiation of visible light to a solution of **CM-2** (0.05 mM) in THF/water (9:1, v/v) containing BIH as sacrificial electron donor produced a moderate amount of H_2 over time as judged by gas chromatography, while there was negligible amount of H_2 produced by using other sacrificial electron donors. Therefore, BIH is applied as a sacrificial electron donor for further photocatalytic investigation. Several control experiments were also carefully examined in the absence of **CM-2**, BIH or light irradiation. As shown in Fig.25, no H_2 evolved from the conditions in the absence of each component, indicating that **CM-2** serves as a photocatalyst for H_2 production and BIH serves as a sacrificial electron donor in this system.

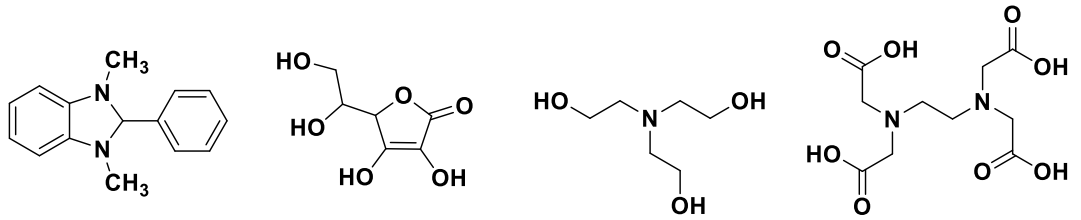

BIH **HA** **TEOA** **EDTA**

Figure 23. Chemical structures of the sacrificial electron donors employed in photocatalytic hydrogen evolution studies of **CM-2**.

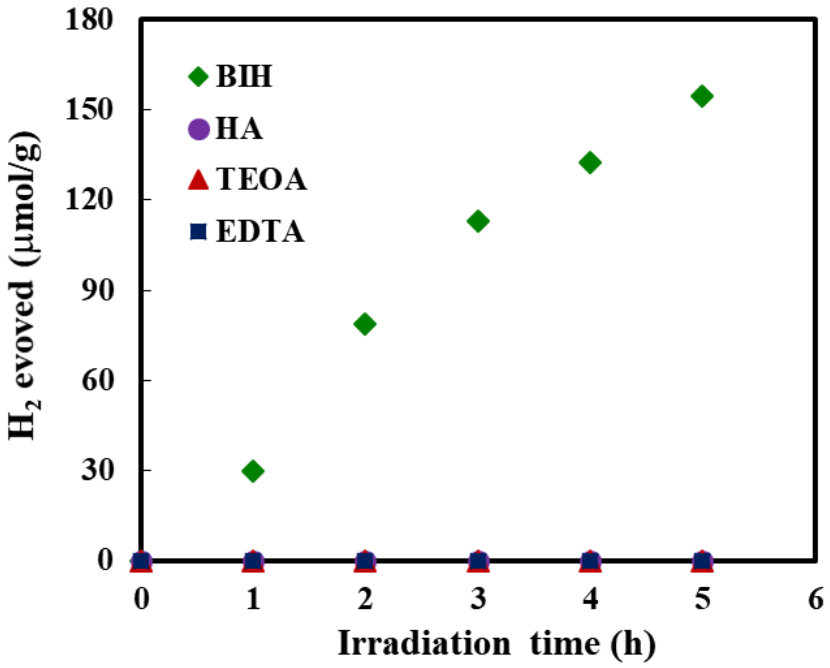

Figure 24. Photocatalytic H_2 production by **CM-2** (0.05 mM) in THF/water (9:1, v/v; total volume 2.0 mL) containing 0.1 M of BIH (green diamond), HA (purple dot), TEOA (red triangle) and EDTA (blue square) as sacrificial electron donors.

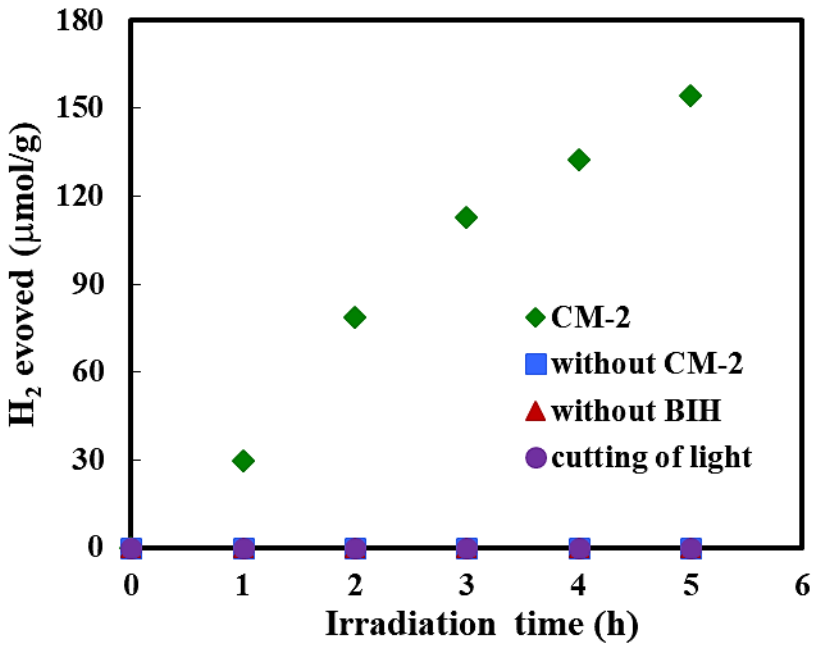

Figure 25. Photocatalytic H_2 production from a solution containing 0.05 mM of **CM-2** and 0.1 M of BIH (green diamond) in THF/water (9:1, v/v; total volume 2.0 mL). Control experiments were carried out in the absence of **CM-2** (blue square), BIH (red triangle) and light (purple dot).

Next, photocatalytic activities of **CM-2** were investigated under various experimental conditions to clarify the factors that can affect the activity. First, photolysis reactions using various concentration of **CM-2** (0 – 0.2 mM) were inspected. As shown in Fig. 26, upon visible-light irradiation to a solution of 0.025 mM of **CM-2** in mixed THF/water (9/1, v/v), the amount of evolved H_2 linearly increased after 3 h and induction period was observed in first two hours. This may correspond to the too low concentration of catalytic active species in the system. In contrast, the catalysis using 0.05 and 0.10 mM of **CM-2** resulted in the linear increase of evolved H_2 without induction period. Rates of the hydrogen production were not largely different for first hour between 0.05 and 0.10 mM of **CM-2**. However, the photolysis of **CM-2** at 0.10 mM showed fewer amount of H_2 after 5 h compared to that at 0.05 mM. Similar trend was also observed in the experiment using higher concentration of **CM-2** (0.20 mM), which resulted in the poorer amount of H_2 after the 5 h of reaction. This result indicates that competition between the photocatalyst to absorb photon and quenching by BIH, which resulted in non-productive event. From these investigations, it was found that the constant generation of hydrogen can be achieved when the concentration of **CM-2** is 0.05 mM and the amount of the generated hydrogen after 5 h reached to the maxima at this concentration (Fig. 27). Therefore, **CM-2** at 0.05 mM is the most appropriate concentration for this photocatalytic system.

Second, the influence of solvent mediums was studied and the results are presented in Fig. 28. The photocatalytic activity of **CM-2** was investigated in the presence of acetonitrile (CH_3CN), which is known as a relatively strong coordinating solvent. The H_2 production was reduced significantly under this condition due to the coordination of CH_3CN molecules to the axial positions of the Rh_2 center. This observation indicates that the axial sites of the Rh_2 center are catalytically active for H_2 production and the choices of reaction medium is an important factor for the light-driven hydrogen production. Additionally, this result is consistent with the results reported in Chapter 1.

Third, photocatalytic reaction of **CM-2** was examined in the absence of water. It was found that the amount of evolved H_2 was decreased in pure THF (Fig. 29), which indicates the importance of water as a potential proton source for the photocatalytic hydrogen evolution by **CM-2**. Though, it also have possibility that protons can be supplied from BIH, which known as two-electron and a proton (hydride) donor,[21] because the H_2 evolution in the absence of water was observed.

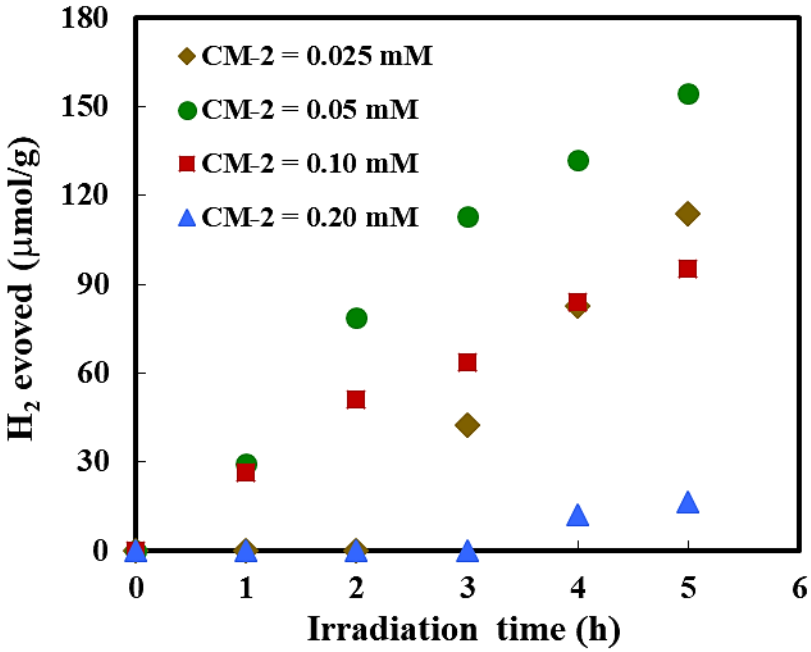

Figure 26. Photocatalytic H_2 production from a solution containing 0.025 mM (brown diamond), 0.05 mM (green dot), 0.10 mM (red square) and 0.20 mM (light blue triangle) of **CM-2** and 0.1 M of BIH in THF/water (9:1, v/v; total volume 2.0 mL). All experiments were performed at same condition system mentioned above.

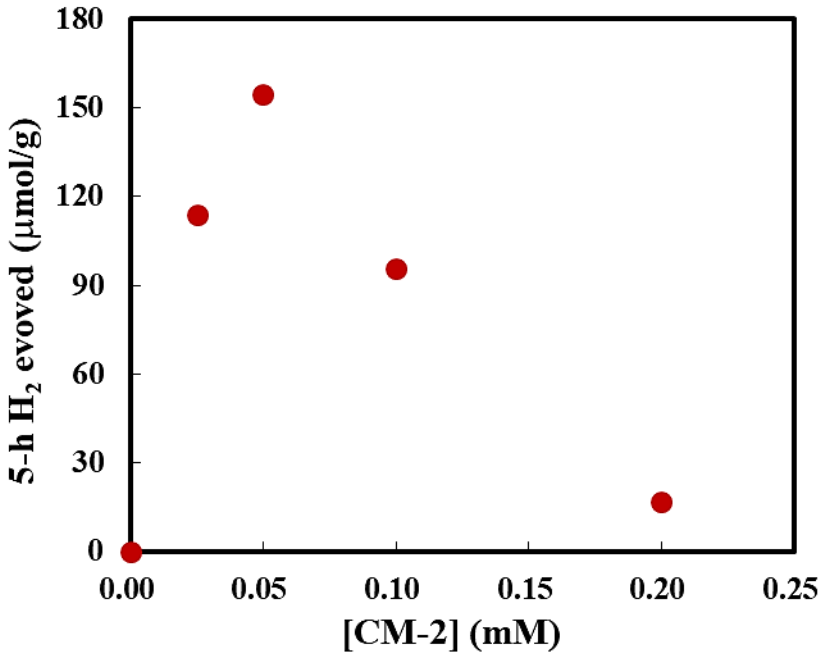

Figure 27. Plot of evolved H_2 after 5 hours of photocatalytic reaction at various concentration of **CM-2**. All data were attained from Fig. 26.

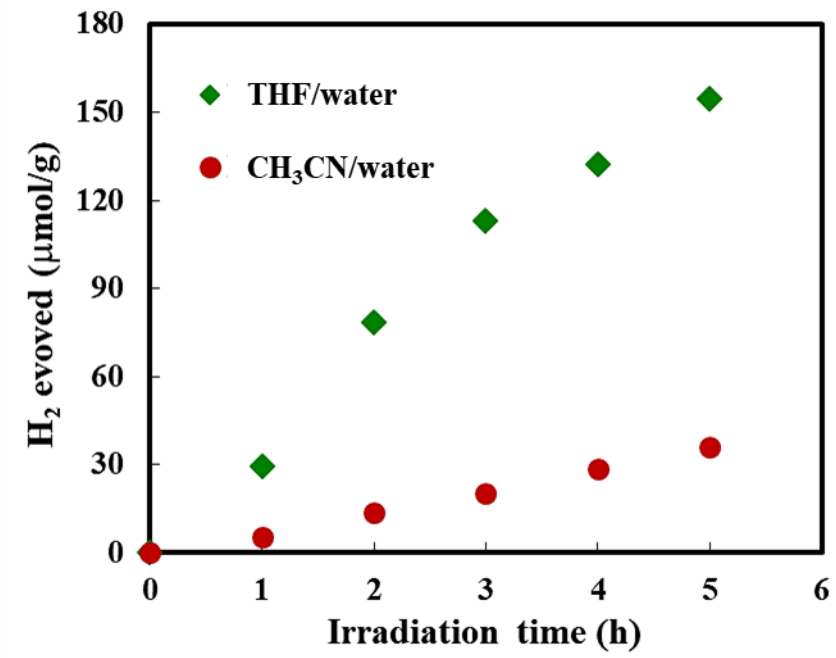

Figure 28. Photocatalytic H_2 production from a solution (total volume 2.0 mL) containing **CM-2** (0.05 mM) and 0.1 M of BIH in THF/water (green diamond) and CH_3CN/water (red dot) at ratio of 9:1, v/v.

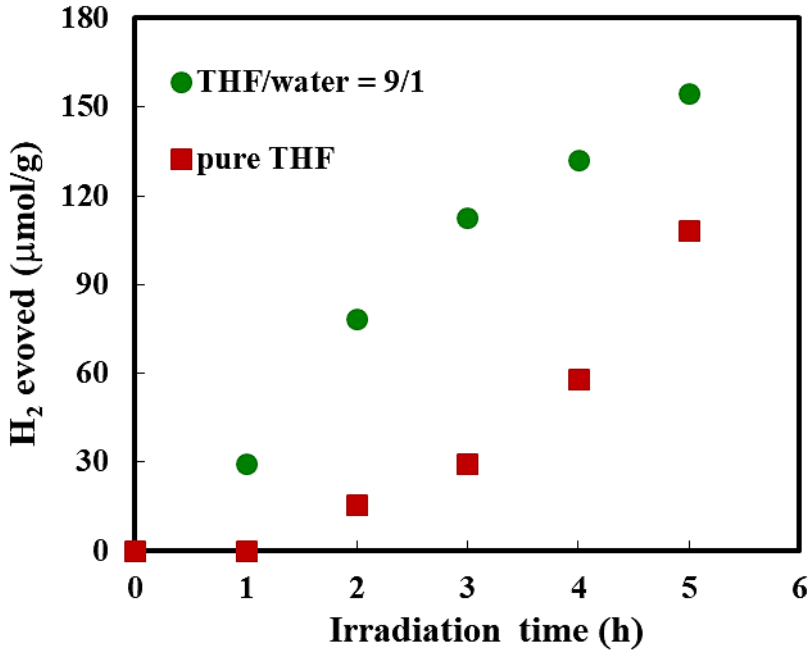

Figure 29. Photocatalytic H_2 production from a solution (total volume 2.0 mL) containing 0.05 mM of **CM-2** and 0.1 M of BIH in THF/water at ratio 9:1, v/v (green dot) and THF only (red square).

Conclusions

The utilization of bodipy derivative as a visible-light harvesting molecular connector for the construction of framework catalyst was successfully demonstrated. A novel catalytic module, **CM-2** was synthesized through the ligand exchange reaction of $Rh_2(CO_2CH_3)_4$ precursor and characterized. **CM-2** shows high solubility in a wide range of organic solvents, which afforded the ease of investigations by using conventional spectroscopic measurements. **CM-2** can be assembled via non-covalent interactions into infinite structures as framework catalyst, **FC-2**, with the well-defined catalytic sites as confirmed by single-crystal structure analysis. The change of coordinated solvent binding at the axial sites of Rh_2 centers led the variation in framework architecture, which indicated the fine-tuning of the molecular assemblies by easily changing of the molecules at the axial sites. Electrocatalytic hydrogen evolution of **CM-2** was investigated, showing excellent catalytic activity with high turnover number and faradaic efficiency. Electrocatalytic activity of **FC-2** was also investigated in heterogeneous system, exhibiting considerable catalytic activity, recyclability, and durability were demonstrated. Photophysical characterization of both **CM-2** and **FC-2** indicated that the integration of **BDP** moieties successfully tuned up the light-harvesting features to visible region. The photocatalytic hydrogen evolution of **CM-2** was achieved in mixed aqueous/organic medium without additional photosensitizer, co-catalyst or an electron relay. Several factors were systematically examined in order to access the best hydrogen evolution condition. Our results presented that the bodipy appended rhodium paddle-wheel complex is a promising electrocatalyst and photocatalyst for proton reduction in both homogeneous and heterogeneous system.

Experimental

General Methods

4-Formylbenzoic acid, 2,3-dichloro-5,6-dicyano-1,4-benzoquinone (DDQ), boron trifluoride-ethyl ether complex and glacial acetic acid were purchased from Tokyo Chemical Industry (TCI). 2,4-Dimethylpyrrole was acquired from either Tokyo Chemical Industry (TCI) or Sigma-Aldrich Company. Triethylamine was obtained from Wako and was dried by reflux over CaH_2, distilled under argon and kept avoid of light over KOH pellets. Trifluoroacetic acid (TFA) and *o*-dichlorobenzene were also purchased from Wako. $Rh_2(CO_2CH_3)_4$ were prepared by literature method[22]. Nafion® perfluorinated membrane (117, thickness 0.007 in) was purchased from Sigma-Aldrich USA. A.ll syntheses were performed under an atmosphere of dry nitrogen or dry argon unless otherwise indicated.

Measurement apparatus

Syntheses of the framework connector H**BDP** were purified on Biotage (Isolera One) auto-column chromatography equipped with SNAP Ultra (ultra-high performance silica column 25 μm particle size). ^{1}H spectra were acquired on a JEOL JNM-LA400 spectrometer, where chemical shifts in MeOD-d_4 or $CDCl_3$ were referenced to internal tetramethylsilane. ^{19}F NMR spectra were acquired on a JEOL JNM-LA400 spectrometer, where chemical shifts in MeOD-d_4 or $CDCl_3$ were referenced to external standard trifluorotoluence. Elemental analyses were carried out on a J-SCIENCE LAB MICRO CORDER JM10 elemental analyzer. UV-Vis absorption spectra and UV-Vis diffuse reflectance spectra were recorded on a Shimadzu UV-3600 UV-Vis-NIR spectrophotometer. A white standard of $BaSO_4$ was used as reference for diffuse reflectance spectroscopic measurement. The photocatalytic studies were performed by using a xenon lamp ($\lambda > 420$ nm, 300 W) equipped CM-1 cold mirror. Gas analysis for H_2 was performed using a Shimadzu GC-2014 gas chromatograph equipped with a thermal conductivity detector (TCD) and fitted with a molecular sieve 5A column (Ar carrier gas), calibrated with standard H_2 (4990 ppm of H_2 in argon). ESI-TOF-MS spectra were recorded on a JEOL JMS-T100LP mass spectrometer. All the ESI-TOF mass spectrometric measurements were recorded in the positive ion mode at a cone voltage of 20 V. Cyclic voltammograms were measured at room temperature on a BAS ALS Model 650DKMP electrochemical analyzer in *o*-dichlorobenzene (sample = 0.5 mM; 0.1 M tetra-*n*-butylammonium perchlorate (TBAP)). A glassy carbon disk and the glassy carbon plate, platinum wire, and Ag/Ag^+ electrode (Ag/0.01 M $AgNO_3$) were used as the working, auxiliary, and reference electrodes, respectively. The redox potentials were calibrated against the redox potential for the ferrocene/ferrocenium (Fc/Fc^+) couple.

Synthesis of 4,4-difluoro-8-[4-(carboxy)phenylic]-1,3,5,7-tetramethyl-4-bora-*3a*,*4a*-diaza-4-bora-*s*-indacene acid, HBDP.

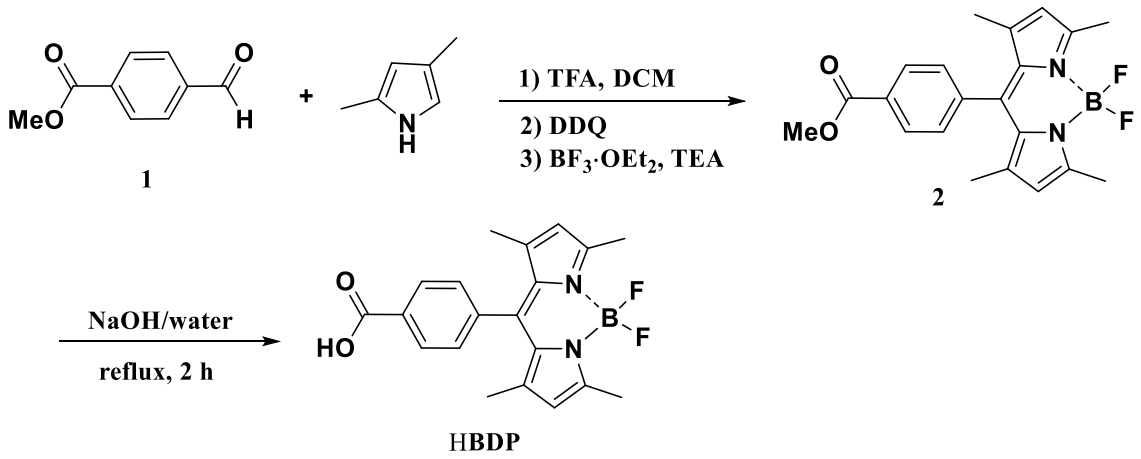

Scheme 8. Preparation of framework connector H**BDP**.

Preparation of methyl 4-formylbenzoate (1)[23] (Scheme 4).

To 4-formyl benzoic acid (1.00 g, 7.24 mmol) in superdehydrated methanol (200 mL), thionyl chloride (6.00 mL, 7.24 mmol) was added dropwise at 0 °C until all compound dissolved. The reaction was slowly brought to room temperature and then stirred for another 2 h. The reaction was monitored by TLC (eluent: hexane/ethyl acetate: 60/40). After all starting compound was consumed, the solvent was then removed in vacuo by co-evaporation with dichloromethane (3×50 mL) to remove an excess thionyl chloride and the residue was then purified on a silica gel over auto-column chromatography using hexane/ethyl acetate (60/40) as eluent to afford a white solid of compound **1** (91% yield). ^{1}H-NMR (400 MHz, $CDCl_3$): δ 10.02 (s, 1H, ArC*H*O) 8.10 (d, *J* = 8 Hz, 2H, Ar*H*) 7.87 (d, *J* = 8 Hz, 2H, Ar*H*) 3.88 (s, 3H, ArCOOC*H*$_3$) ppm.

Preparation of 4,4-difluoro-8-[4-(methoxycarbonyl)phenyl]-1,3,5,7-tetramethyl-4-bora-*3a*,*4a*-diaza-4-bora-*s*-indacene (2)[12] (scheme 4).

468 mg (2.86 mmol) of 4-formylbenzoate (**1**) was added to a 200 mL flame-dried three-necked flask. The compound was degassed for 30 min before substituted with argon gas. Then anhydrous dichloromethane (50 mL) was added into flask, following by dropwise of 2,4-dimethyl pyrrole (546 mg, 5.74 mmol). Then two drops of trifluoroacetic acid (TFA) was added and the mixture was stirred under Ar for 18 h at room temperature. After amount of **1** was totally consumed, monitored by TLC (eluent: dichloromethane), 648 mg of 2,3-dichloro-5,6-dicyano-1,4-benzoquinone (DDQ) was added to the reaction mixture, stirring was continued for 30 min. The reaction mixture was brought to 0 °C before absolute TEA 3.5 mL was added dropwise. After continue stirring for another 15 min, 3.50 mL of boron trifluoride-ethyl ether complex ($BF_3{\cdot}OEt_3$) was added. The reaction mixture was continued for the next 2 h with gradually increase of green emission under UV light irradiation. Then the mixture was run through silica flash column chromatography using dichloromethane as eluent to remove undesired solid. The organic phase with strong green emissive was collected and evaporated by rota-evaporator. The crude residue was purified on silica gel over auto-column chromatography using dichloromethane as eluent to afford compound **2** as a red crystal (19% yield). ^{1}H-NMR of (400 MHz, $CDCl_3$): δ 8.19 (d, *J* = 8 Hz, 2H, Ar*H*), 7.42 (d, *J* = 8 Hz, 2H, Ar*H*), 6.00 (s, 2H, pyrrole*H*), 2.57 (s, 6H, pyrroleCH_3), 1.37 (s, 6H, pyrroleCH_3). ^{19}F-NMR (400 MHz, $CDCl_3$): δ -146.08 (*d*, *J* = 34.7 Hz) and -146.26 (*d*, *J* = 28.9 Hz).

Preparation of 4,4-difluoro-8-[4-(carboxy)phenylic]-1,3,5,7-tetramethyl-4-bora-3a,4a-diaza-4-bora-s-indacene acid (HBDP) (scheme 4).

The synthesis of H**BDP** was modified according to literature.[24] Compound **2** (650 mg, 1.70 mmol) was dissolved in methanol (150 mL), then 10 mL of 0.2 N of NaOH was added dropwise. The mixture was refluxed at 80 °C for 4 h. The reaction completion was monitored by TLC (eluent: ethyl acetate/hexane = 80/20). Then the reaction mixture was evaporated and acidified by 2 N HCl. The aqueous solution was extracted with ethyl acetate until green emission was diminished. The organic layers were combined, dried over anhydrous Na_2SO_4, filtered and evaporated. The crude was purified by silica gel auto-column chromatography using chloroform/methanol (95/5) as eluent to afford the framework connector H**BDP** as a red to purple crystal (82% yield). ^{1}H-NMR of (400 MHz, MeOD-d_4): δ 8.20(d, J = 8 Hz, 2H, Ar*H*), 7.48 (d, J = 8 Hz, 2H, Ar*H*), 6.09 (s, 2H, pyrrole*H*), 2.50 (s, 6H, pyrroleCH_3), 1.41 (s, 6H, pyrroleCH_3). ^{19}F-NMR (400 MHz, MeOD-d_4): δ -146.98 (*d*, J = 32.2 Hz) and -147.16 (*d*, J = 33.3 Hz). Elemental analysis for H**BDP**: Found: C, 64.18; H, 5.21; N, 7.38. Calc. for $C_{20}H_{19}N_2O_2BF_2$: C, 64.09; H, 5.51; N, 7.29%. Single crystal X-ray quality crystals of H**BDP** were grown from DMSO solution.

Synthesis of the catalytic module CM-2

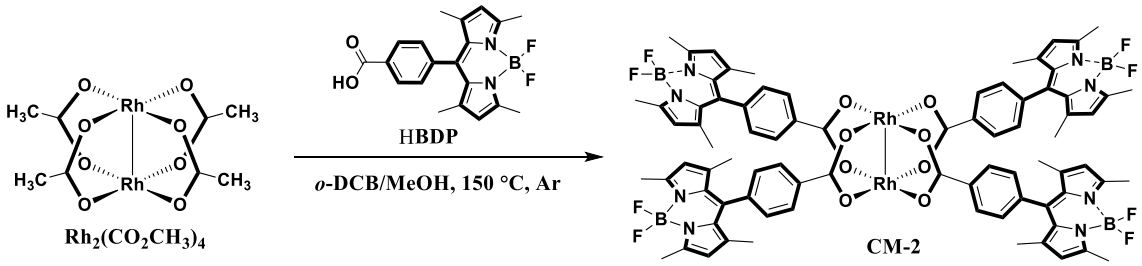

Scheme 9. Synthesis of **CM-2.**

A round bottom Schlenk's flask was charged with $Rh_2(CO_2CH_3)_4$ (30 mg, 67.9 μmol), H**BDP** (200 mg, 0.54 mmol) and degassed for 30 min. Then 15 mL of *o*-dichlorobenzene (*o*-DCB) and 1 mL of methanol was added. The reaction mixture was heated to 150 °C and keep stirring for 5 h. The solvent was then removed in vacuo by co-evaporation with dichloromethane (2×30 mL). After removal of solvent, the green-metallic residue was purified by column chromatography using chloroform/diethyl ether (99/1) as eluent to afford the desired product as a green metallic red crystal (21% yield). ^{1}H-NMR of **CM-2** (400 MHz, $CDCl_3$): δ 8.13 (2H, Ar*H*), 7.72 (1H, Ar*H*), 7.30 (1H, Ar*H*), 5.96 (2H, pyrrole*H*), 2.55 (*s*, 6H, pyrroleC*H*$_3$), 1.63 (*s*, 6H, pyrroleC*H*$_3$) ppm. ESI-TOF MS (DMF): m/z 1919.89 [1674.54 + 1-methyl-4,4'-bipyridinium + DMF + H^+]. Elemental analysis for **CM-2**: Found: C, 56.34; H, 4.92; N, 5.95. Calc. for $C_{80}H_{72}N_8O_8B_4F_8Rh_2$: C, 64.09; H, 5.51; N, 7.29%. Single crystal X-ray quality crystals of **FC-2** were grown by vapor diffusion technique from $CHCl_3$/MeOH solution.

X-ray crystallographic data

Crystal of samples were mounted in a loop. Diffraction data at 123 K were measured on a RAXIS-RAPID Imaging Plate diffractometer equipped with confocal monochromated Mo-Kα radiation and data was processed using RAPID-AUTO (Rigaku). The structure was solved by direct method using *SIR-92*[25] and refined by the full-matrix least squares techniques on F^2 (*SHELXL-97*).[26] All non-hydrogen atoms were refined anisotropically.

Table 8. Summary of the crystallographic data for H**BDP.**

Formula	$C_{20}H_{19}N_2O_2BF_2$
Fw	368.18
crystal color, habit	orange, block
crystal size, mm^3	0.51 × 0.15 × 0.08
crystal system	*triclinic*
space group	$P\bar{1}$
a, Å	8.574(4)
b, Å	9.789(4)
c, Å	14.699(7)
α, deg	95.814(5)
β, deg	103.023(15)
γ, deg	114.667(5)
V, $Å^3$	1065.4(9)
Z	2
F(000)	384
d_{calc}, g/cm^3	31.148
μ(MoKα), mm^{-1}	0.714
T, K	123(2)
R_1	0.0801
wR_2	0.2997
GOF	1.302

Table 9. Summary of the crystallographic data for **FC-2.**

Formula	$C_{80}H_{72}N_8O_8B_4F_8Rh_2$
Fw	1674.52
crystal color, habit	red, needle
crystal size, mm^3	0.78 × 0.09 × 0.05
crystal system	*triclinic*
space group	$P\bar{1}$
a, Å	11.7410(6)
b, Å	14.0835(7)
c, Å	14.1286(8)
α, deg	99.028(7)
β, deg	104.793(7)
γ, deg	99.455(5)
V, $Å^3$	2179.1(14)
Z	2
F(000)	1708
d_{calc}, g/cm^3	2.552
μ(MoKα), mm^{-1}	0.714
T, K	123(2)
R_1	0.0738
wR_2	0.2318
GOF	1.104

Table 10. Summary of the crystallographic data for **FC-2'.**

Formula	$C_{88}H_{92}B_4F_8O_{10}N_8Rh_2$
Fw	1826.82
crystal color, habit	red, needle
crystal size, mm^3	0.34 × 0.05 × 0.04
crystal system	*triclinic*
space group	$P\bar{1}$
a, Å	13.1294（3）
b, Å	13.8532(3)
c, Å	14.4797(4)
α, deg	80.175(5)
β, deg	82.179(6)
γ, deg	89.470(6)
V, $Å^3$	2574.54(16)
Z	2
F(000)	1708
d_{calc}, g/cm^3	2.552
μ(MoKα), mm^{-1}	0.714
T, K	123(2)
R_1	0.0519
wR_2	0.1593
GOF	1.061

Electrochemical measurements

All experimental procedures were conducted at ambient temperature, under argon. A standard three-electrode configuration was employed in conjunction with a CH Instruments potentiostat interfaced to a computer with CH Instruments 650 DKMP software. A platinum auxiliary electrode and Ag/Ag^+ reference electrode were used for all measurement in solution. Cyclic voltammetry was performed using a glassy carbon working electrode (diameter 3 mm, from BAS Inc.). The working electrode was treated between scans by means of polishing with 0.05 μm alumina paste (from BAS Inc.) and washing with purified water. Ferrocene was used as an internal standard, and all potentials reported within this work are referenced to the NHE at 0.551 V.

To investigate the redox behavior of **FC-2** framework catalyst, cyclic voltammograms (CVs) of **FC-2** deposited on a glassy carbon working electrode were measured. The procedure to deposit **FC-2** on the glassy carbon electrodes are as follows. First, **FC-2** was dissolved in dichloromethane. The obtained suspension was further ultra-sonicated for 10 min. Subsequently, 20 μL of the suspension was dropped cast onto the surface of a freshly polished glassy carbon electrode and dried over air for 1.5 h, yielding a modified glassy carbon electrode with a thin **FC-2** layer. By utilizing the modified electrode, CVs were measured in 1.0 M acetate buffer at pH 5 as an electrolyte, and using a standard three-electrode cell incorporating a glassy carbon working electrode, a platinum wire auxiliary electrode, and saturated calomel reference electrode (SCE) was employed as a reference electrode.

Controlled-electrolysis measurements

Controlled-potential electrolysis measurements were conducted in a sealed two-compartment H-cell where the first chamber held a glassy carbon plate as working electrode and Ag/Ag^+ reference electrode in 5.0 mL of γ-butyrolactone solution of **CM-2** (0.2 mM) containing TBAP as an electrolyte, and the second chamber held an auxiliary electrode in 5.0 mL of γ-butyrolactone solution containing TBAP as an electrolyte (Scheme 10). The two compartment were separated by a pre-treated Nafion® membrane. Glassy carbon plates (12 mm × 25 mm × 0.3 mm; BAS Inc., Japan) were used as working electrode and submerged such as ca. 2.6 cm^2 of the plate into an electrolyte solution. The cell were purged with Ar for ca. 30 min and then sealed under an atmosphere of Ar before beginning of each electrolysis experiment. For 1-hour measurements, the amount of H_2 evolved was quantified from an analysis of the gas headspace of both compartments with GC-2014 gas chromatography using the thermal conductivity detector. Faradaic efficiencies were determined by dividing the measured H_2 produced by the amount of H_2 expected on the basis of charge passed during the controlled-potential electrolysis measurement.

For the investigation of the electrocatalytic H_2 evolution of **FC-2**, similar procedures were performed using a modified glassy carbon plate with thin layer of **FC-2** as a working electrode and submerged such as ca. 2.0 cm^2 of the plate into 1.0 M acetate buffer (pH = 5) as electrolyte solution (5 mL). All measurements were performed at room temperature under an Ar atmosphere.

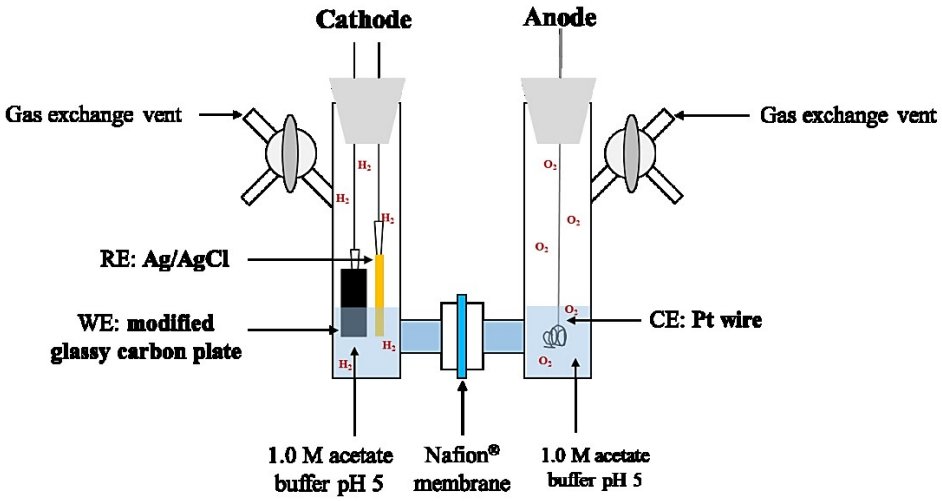

Scheme 10. A schematic illustration of the setup of controlled-potential electrolysis measurements

Photocatalytic H_2 production studies

All photocatalytic experiments were conducted at 20 °C using a custom-made photoreactor with coolant to control the temperature of sample during photoreaction (Scheme 6). A cylindrical cuvette with 6.0 mL of gas headspace was used for all experiments. In a typical run, 0.05 mM of **CM-2** in 2.0 mL of THF/water (9:1, v/v) containing BIH as a sacrificial electron donor unless other conditions are mentioned. Prior the reaction, the **CM-2** mixture was purged by Ar gas bubbling for 15 min. The photocatalytic reactions were executed by using a xenon lamp (λ > 420 nm, 300 W) equipped CM-1 cold mirror. The evolved H_2 in the gas phase was analyzed by a gas chromatography (GC-2014, molecular sieve 5A column, Ar carrier gas) equipped with a thermal conductivity detector (TCD).

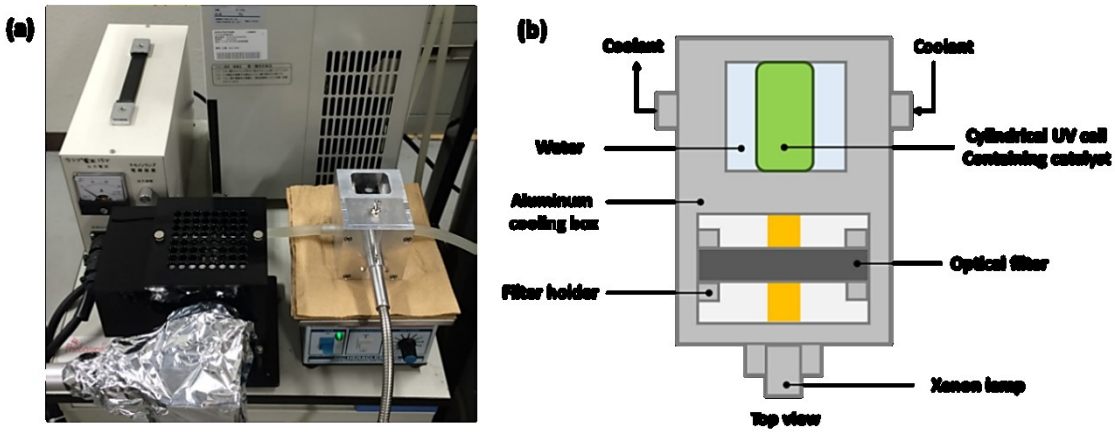

Scheme 11. (a) A photograph of the photocatalytic H_2 production reactor; (b) schematic illustration of the custom-made photoreactor.

Calculation details for H_2 evolution

Electrochemical calculation of number of moles of H_2 evolved:

After an hour of bulk electrolysis, the current charge (I_t) over the duration of experiment can be measured. According to Faradaic's law of electrolysis:

$$n_{H_2}(\text{mol}) = \left(\frac{I_t}{F}\right) \times \left(\frac{1}{Z}\right)$$

n = number of moles of H_2

F = Faradaic's constant (96,485 $Cmol^{-1}$)

z = electron transferred per ion

Photochemical calculation of number of moles of H_2 evolved:

The number of moles (n_{H_2}) of produced hydrogen was calculated according to the following equation;

$$n_{H_2}(\text{mol}) = \frac{detected\ peak\ area}{calibration\ peak\ area} \times 0.001 \times \frac{Headspace\ volume\ [L]}{24.5\ [Lmol^{-1}]}$$

where 0.001 is the reference percentage of H_2 in Ar base gas (corresponding to 4990 ppm in Ar) which linked to the calibration pick area at 0.1 mL of injection gas volume, 24.5 $Lmol^{-1}$ is the molar volume of ideal gas at a temperature of 298.15 K and pressure of 101325 Pa. The total volume extracted for the measure of evolved H_2 was around 0.2 mL, which 0.1 mL was injected to GC for analysis.

The turnover number related to the catalyst was calculated according to the following equation;

$$\text{TON} = \frac{n_{H_2}}{n_{\boldsymbol{FC-1}}}$$

where n_{H_2} is the number of moles of evolved hydrogen from electrolysis or photolysis, $n_{\boldsymbol{FC-1}}$ is the number of moles of **FC-1** framework catalyst present in suspension mixture.

References

[1] (a) N. S. Lewis and D. G. Nocera, *Proc. Natl. Acad. Sci*., 2006, **103**, 15729; (b) B. Vincenzo, C. Alberto and V. Margherita, *ChemSusChem*, 2008, **1**, 26; (c) D. Gust, T. A. Moore and A. L. Moore, *Acc. Chem. Res.*, 2009, **42**, 1890; (d) W. Song, Z. Chen, M. K. Brennaman, J. J. Concepcion, A. O. T. Patrocinio, N. Y. Murakami Iha and T. J. Meyer, *Pure Appl. Chem*., 2011, **83**, 749; (e) D. Kim, K. K. Sakimoto, D. Hong and P. Yang, *Angew. Chem., Int. Ed.*, 2015, **54**, 3259; (f) K. Takanabe, *ACS Catal.*, 2017, **7**, 8006.

[2] (a) M. Yagi and M. Kaneko, *Chem. Rev*., 2001, **101**, 21; (b) E. S. Adreeiadis, M. Chavarot-Kerlidou, M. Fontecave and V. Artero, *Photochem. Photobiol*., 2011, **87**, 946; (c) Y. Tachibana, L. Vayssieres and J. R. Durrant, *Nature Photonics*, 2012, **6**, 511; (d) S. Fukuzumi and K Ohkubo, *J. Mater. Chem*., 2012, **22**, 4575; (e) S. Berardi, S. Drouet, L. Francàs, C. Gimbert-Suriñach, M. Guttentag, C. Richmond, T. Stoll and A. Llobet, *Chem. Soc. Rev*., 2014, **43**, 7501; (f) M. D. Kärkäs, O. Verho, E. V. Johnston and B. Åkermark, *Chem. Rev.*, 2014, **114**, 11863; (g) X. Sala, S. Maji, R. Bofill, J. García-Antón, L. Escriche and A.Llobet, *Acc. Chem. Res.*, 2014, **47**, 504.

[3] (a) K. Akihiko, K. Hideki and T. Issei, *Chem. Lett.*, 2004, **33**, 1534; (b) K. Maeda, K. Teramura, D. Lu, T. Takata, N. Saito, Y. Inoue and K. Domen, *Nature*, 2006, **440**, 295; (c) R. Abe, *J. Photochem. Photobiol. C*., 2010, **12**, 179; (d) X. Chen, S. Shen, L. Guo and S. S. Muo, *Chem. Rev*., 2010, **110**, 6503; (e) K. Maeda, *J. Photochem. Photobiol. C*., 2011, **12**, 237; (f) Y. Ma, X. Wang, Y. Jia, X. Chen, H. Han and C. Li, *Chem. Rev.*, 2014, **114**, 9987; (g) W.-J. Ong, L.-L. Tan, Y. H. Ng, S.-T. Yong and S.-P. Chai, *Chem. Rev.*, 2016, **116**, 7159.

[4] (a) K. Kalyanasundaram and M. Graetzel, *Curr. Opin. Biotechnol*., 2010, **21**, 298; (b) R. Croce and H. van Amerongen, *Nat. Chem. Biol.*, 2014, **10**, 492; (c) L.-Z. Wu, B.Chen, Z.-J. Li and C.-H. Tung, *Acc. Chem. Res*., 2014, **47**, 2177.

[5] (a) A. Fujishima and K. Honda, *Nature*, 1972, **238**, 37; (b) M. G. Walter, E. L. Warren, J. R. McKone, S. W. Boettcher, Q. Mi, E. A. Santori and N. S. Lewis, *Chem. Rev.*, 2010, **110**, 6446; (c) W. R. McNamara, Z. Han, P. J. Alperin, W. W. Brennessel, P. L. Holland and R. Eisenberg, *J. Am. Chem. Soc*., 2011, **133**, 15368; (d) D. G. Nocera, *Acc. Chem. Res.*, 2012, **45**, 767; (e) J. Yang, D. Wang, H. Han and C. Li, *Acc. Chem. Res*., 2013, **46**, 1900; (f) A. Das, Z. Han, W. W. Brennessel, P. L. Holland and R. Eisenberg, *ACS Catal.*, 2015, **5**, 1397; (g) L. Chen, G. Chen, C.-F. Leung, S.-M. Yiu, C.-C. Ko, E. Anxolabéhère-Mallart, M. Robert and T.-C. Lau, *ACS Catal*., 2015, **5**, 356; (h) M. Aydemira, D. Akyüzb, B. Agopcanc, M. K. Şenerd, F. K. Albayraka, C.

Sarıoğluc and A. Koca, *Int. J. Hydrog. Energy*, 2016, **41**, 8209.

[6] P. Chinapang, M. Okamura, T. Itoh, M. Kondo and S. Masaoka, *Chem. Comm*., 2018 DOI: 10.1039/C7CC08013A.

[7] (a) L. L. Tinker, N. D. McDaniel and S. Bernhard, *J. Mater. Chem.*, 2009, **19**, 3328; (b) M. Wang, Y. Naa, M. Gorlovb and L. Sun, *Dalton Trans.*, 2009, 6458; (c) W. T. Eckenhoff and R. Eisenber, *Dalton Trans.*, 2012, **41**, 13004; (d) Y. Gao, X. Ding, J. Liu, L. Wang, Z. Lu, L. Li and L. Sun, *J. Am. Chem. Soc.*, 2013, **135**, 4219.

[8] (a) R. P. Sabatini, T. M. McCormick, T. Lazarides, K. C. Wilson, R. Eisenberg and D. W. McCamant, *J. Phys. Chem. Lett*., 2011, **2**, 223; (b) J. Bartelmess, A. J. Francis, K. A. El Roz, F. N. Castellano and W. W. Weare, *Inorg. Chem*., 2014, **53**, 4527; (c) J. C. Manton, C. Long, J. G. Vos and M. T. Pryce, *Phys. Chem. Chem. Phys*., 2014, **16**, 5229; (d) G.-G. Luo, K. Fang, J.-H. Wu, J.-C. Dai and Q.-H. Zhao, *Phys. Chem. Chem. Phys.*, 2014, **16**, 23884; (e) G.-G. Luo, H. Lu, X.-L., Zhang, J.-C. Dai, J.-H. Wu and J.-J. Wu, *Phys. Chem. Chem. Phys.*, 2015, **17**, 9716; (f) R. P. Sabatini, B. Lindley, T. M. McCormick, T. Lazarides, W. W. Brennessel, D. W. McCamant and R. Eisenberg, *J. Phys. Chem. B*, 2016, **120**, 527; (g) L. Dura, J. Ahrens, M.-M. Pohl, S. Hofler, M. Broring and T. Beweries, *Chem. Eur. J*., 2015, **21**, 13549; (h) J. Zhao, K. Xu , W. Yang , Z. Wang and F. Zhong, *Chem. Soc. Rev.*, 2015, **44**, 8904.

[9] (a) A. Loudet and K. Burgess, *Chem. Rev.*, 2007, **107**,4891; (b) G. Ulrich, R. Ziessel and A. Harriman, *Angew. Chem. Int. Ed*., 2008, **47**, 1184; (c) J. Zhao, K. Xu, W. Yang, Z. Wang and F. Zhong, *Chem. Soc. Rev*., 2015, **44**, 8904.

[10] (a) J. L. Wang, C. Wang and W. Lin, *ACS Catal*, 2012, **2**, 2630; (b) T. Zhang and W. Lin, *Chem. Soc. Rev.*, 2014, **43**, 5982; (c) D. Wang, R. Huang, W. Liu, D. Sun and Z. Li, *ACS Catal.*, 2014, **12**, 4254; (d) Y. Fang, Y. Ma, M. Zheng, P. Yang, A. M. Asiri and X. Wang, *Coord. Chem. Rev*., 2017, DOI: 10.1016/j.ccr.2017.09.013.

[11] (a) T. Itoh, M. Kondo, M. Kanaike and S. Masaoka, *CrystEngComm*, 2013, **15**, 6122; (b) T. Itoh, M. Kondo, H. Sakamoto, K. Wakabayashi, M. Kanaike, K. Itami and S. Masaoka, *Dalton Trans.*, 2015, **44**, 15334.

[12] W. Qin, M. Buruah, W. M. De Borggraeve and N. Boens, *J. Photochem. Photobiol. A*, 2006, **183**, 190.

[13] (a) T. E. Cassandra, A.-T. Nkongho, K. K. Kenneth, J. Tana and F. Quarshiea, *Acta Cryst. E*, 2012, **69**, m639; (b) M. Ebihara, K. Yamada and T. Kawamura, *Acta Cryst. C,* 2006, **62**, m451; (c) N. N. Sveshnikov, M. H. Dickmana and M. T. Pope, *Acta Cryst. C,* 2000, **56**, m1193.

[14] V. M. Miskowski, W. P. Schaefer, B. Sadeghi, B. D. Santarsiero and H. B. Gray, *Inorg. Chem.* 1984, **23**, 1154.

[15] Selected examples: (a) M. Razavet, V. Artero and M. Fontecave, *Inorg. Chem*., 2005, **44**, 4786; (b) P.-A. Jacques, V. Artero, J. Pécaut and M. Fontecave, *Proc. Natl. Acad. Sci. U. S. A.*, 2009, **106**, 20627; (c) S. Wiese, U. J. Kilgore, D. L. DuBois and R. M. Bullock, *ACS Catal*., 2012, **2**, 720; (d) M. P. Stewart, M.-H. Ho, S. Wiese, M. L. Lindstrom, C. E. Thogerson, S. Raugei, R. M. Bullock and M. L. Helm, *J. Am. Chem. Soc*., 2013, **135**, 6033; (e) J. R. McKone, S. C. Marinescu, B. S. Brunschwig, J. R. Winkler and H. B. Gray, *Chem. Sci.*, 2014, **5**, 865; (f) J. L. Dempsey, A. J. Esswein, D. R. Manke, J. Rosenthal, J. D. Soper and D. G. Nocera, *Inorg. Chem*., 2005, **44**, 6879; (g) S. Kal, A. S. Filatov and P. H. Dinolfo, *Inorg. Chem*., 2014, **53**, 7137; (h) N. Kaeffer, M. Chavarot-Kerlidou and V. Artero, *Acc. Chem. Res*., 2015, **48**, 1286; (i) E. S. Rountree and J. L. Dempsey, *Inorg. Chem*., 2016, **5**, 5079; (j) N. Elgrishi, B. D. McCarthy, E. S. Rountree and J. L. Dempsey, *ACS Catal*., 2016, **6**, 3644; (k) K. J. Lee, N. Elgrishi, B. Kandemir and J. L. Dempse, *Nature Rev. Chem*., 2017, **1**, doi:10.1038/s41570-017-0039.

[16] J. B. Milne, T. J. Parker, *J. Solution Chem*., 1981, **10**, 479.

[17] Department of Chemistry, Michigan State University (28 December 2017), *Ionization constants of heteroatom organic acids*. Data retrieved from URL: http://www2.chemistry.msu.edu/faculty/reusch/OrgPage/tables.htm. The pK_a values given are extrapolated for water at 25 °C.

[18] (a) G. F. Manbeck, T. Canterbury, R. Zhou, S. King, G. Nam, and K. J. Brewer, *Inorg. Chem.*, 2015, **54**, 8148; (b) B. D. Stubbert, J. C. Peters and H. B. Gray, *J. Am. Chem. Soc.*, 2011, **133**, 18070; (c) J. P. Bigi, T. E. Hanna, W. H. Harman, A. Chang and C. J. Chang, *Chem. Commun.*, 2010, **46**, 958; (d) C. C. L. McCrory, C. Uyeda and J. C. Peters, *J. Am. Chem. Soc.*, 2012, **134**, 3164; (e) W. M. Singh, T. Baine, S. Kudo, S. L. Tian, X. A. N. Ma, H. Y. Zhou, N. J. DeYonker, T. C. Pham, J. C. Bollinger, D. L. Baker, B. Yan, C. E. Webster and X. Zhao, *Angew. Chem., Int. Ed.*, 2012, **51**, 5941; (f) P. Zhang, M. Wang, F. Gloaguen, L. Chen, F. Quentel and L. Sun, *Chem. Commun*., 2013, **49**, 9455; (g) H. I. Karunadasa, C. J. Chang and J. R. Long, *Nature*, 2010, **464**, 1329; (h) S. Dey, A. Rana, S. G. Dey and A. Dey, *ACS Catal.*, 2013, **3**, 429.

[19] P. Atkins, T. Overton, J. Rourke, M. Weller, F. Armstrong and M. Hangerman, *Shriver and Atkins' Inorganic Chemistry Fifth Edition*, Oxford University Press, Great Britain, 2010.

[20] K. Krumova and G. Cosa, *J. Am. Chem. Soc.*, 2010, **132**, 17560.

[21] Y. Pellegrin and F. Odeobel, *C. R. Chimie*, 2017, **20**, 283.

[22] G. A. Rempel, P. Legzdins, H. Smith and G. Wilkinson, *Inorg. Syn*., 1972, **13**, 90.

[23] S. K. Sharma, M. Tandon and J. W. Lown, *Eur.–J. Org. Chem.*, 2000, 2095.

[24] M. Kondo, S. Furukawa K. Hirai and S. Kitakawa, *Angew. Chem., Int. Ed*., 2010, **49**, 5327.

[25] A. Altomare, G. Cascarano, C. Giacovazzo and A. Guagliardi. *J. Appl. Crystalogr.*, 1993, **26**, 343.

[26] G. M. Sheldrick, SHELXL-97, *Program for Crystal Structure Refinement*, University of Göttingen, Germany, 1997.

Chapter 3

Investigation of a framework catalyst by high energy X-ray measurements and pair distribution analysis

Introduction

One of the current challenges in artificial photosynthesis is to create an efficient and simplest photocatalyst systems for hydrogen production consists of a catalytic module linked to a photosensitizer. Numerous research groups illustrated innovative efforts on the linked supramolecular assemblies systems which aimed to overcome inherent limitations of conventional multi-component photocatalytic systems (for example, diffusional timescale, and strong solvent dependent and uncontrolled back electron transfer).[1] Advanced in synchrotron light sources have been developed and now present an opportunity of powerful X-ray techniques to effectively investigate both static and dynamic structure of even amorphous materials at supramolecular,[2] nano-particles/crystals[3] or biohybrids systems[4] at atomic levels. In addition, the evidences through synchrotron-based X-ray can significantly complement to information attained from traditional spectroscopic techniques.

The knowledge of the local atomic arrangement of materials is important for understanding their chemical/physical properties. In case of crystalline materials, their structure can be basically explained by giving unit cell, space group symmetry, and atomic distance parameter.[5] However, not all compounds exist as single-crystals or well-crystalline powders. Thus, it is necessary to gain information on the structural arrangement of materials in the form of amorphous or liquid state, in the form of nano-crystalline or in general form where the local structure substantively different from the average structure determined from classical atomic diffraction.

The pair distribution function (PDF) analysis becomes necessary tool to predict the atomic structure of these low crystallinity materials by using data from the high energy X-ray scattering (HEXS). The PDF approach provides an important complement information by covering the full range of atom-atom distances, including first shell, outer shell, and long-range sphere. Experimentally, this function can be obtained in similar way to the powder diffraction experiment.[6] Indeed, this function corresponds to a histogram of interatomic distances. All interatomic distances are summed up and projected over the radius *r* and will give the scattered pattern which is then directly related to distribution of actual interatomic distances in spaces regardless of its crystalline or amorphous state[7]

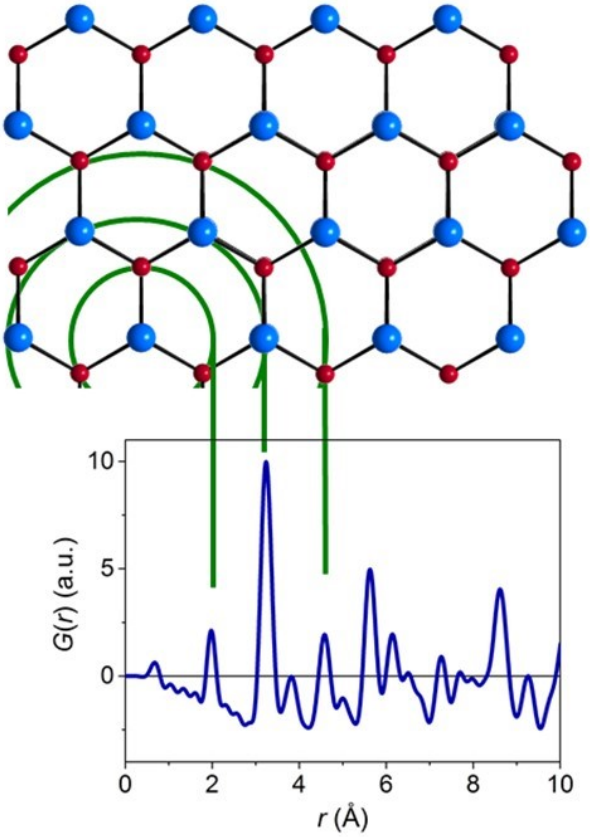

Figure 1. The principle of the pair distribution function (PDF) analysis. Consequently, as in a histogram, each peak corresponds to a distance, where neighbouring atoms are most likely found in the sample. The area under peaks corresponds to number of neighbours, scaled by scattering strength of respective atoms. The figure retrieves from the reference 7.

In this chapter, I report the real space atomic structure of the framework catalyst **FC-1** as shown in the Chapter 1 by using high energy X-ray scattering (HEXS) measurements and atomic pair distribution function (PDF) analysis. In our group, we have previously demonstrated pleasant stability and activities for the heterogeneous molecular-based photocatalytic H_2 evolution, Rh(II) dimer complex bearing 1,8-naphthalimide-based ligands (**FC-1** framework catalyst), described in the Chapter 1. Their high durability arose from the well-define structure has been clearly accomplished. Therefore, I would like to understand the structural-functional relationship of the framework catalyst **FC-1** by using these cutting edge X-ray techniques, as a guideline for future design of photocatalyst, and also partly due to the scientific interest in X-ray spectroscopy.

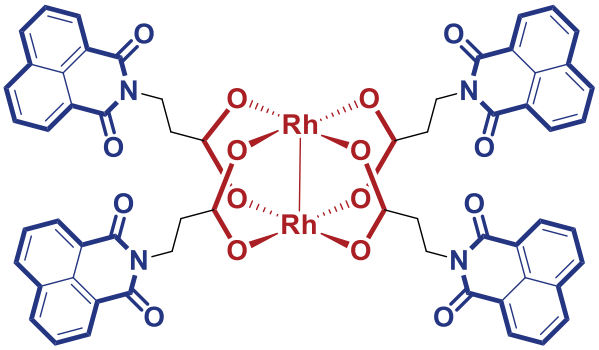

Figure 2. Chemical structure of **FC-1** (Rh_2(**NIP**)$_4$) from Chapter 1.

Structural investigation of the FC-1 framework catalyst by HEXS measurements and PDF analysis

The framework catalyst **FC-1** was synthesized as reported in chapter 1. Prior to the measurement, an obtained green powder of **FC-1** was sonicated in methanol for 15 min, then drop casted onto a glass slide. After air dried for several hours, the **FC-1** sample was loaded as powder into a 0.7 mm diameter thin-walled (10 μm) glass tube. Data suitable for PDF analysis were collected at the Advanced Photon Source (APS) of Argonne National Laboratory at the beamline 11-ID-B. High-energy X-ray of 58.96 keV (λ = 0.2113 Å) were used combination with an amorphous silicon-based flat panel detector.[8] Further details are provided in experimental section.

In this procedure, the experimental scattering patterns for **FC-1** catalyst powders, solvent trace, capillary container and instrument backgrounds were measured as a function of the scattered wave vector q, where $q = 4\pi\sin(\theta)/\lambda$ and 2θ is scattered angle in the range of $0.4 < q < 24$ Å^{-1}. Experimental HEXS patterns were used to generate the pair distribution function $G(r)$ using the program PDFgetX2.[9] The obtained scattering patterns were corrected for container and air to yield the total scattering for samples, $I(q)$ as shown in Fig. 3. Next, the reduced scattering structure function $F(q)$ was calculated from , $I(q)$ according to following equation, together with corrected for instrument background, multiple scattering, X-ray polarization, sample absorption and Compton scattering

$$F(\mathrm{q}) = q\left[\frac{I(q)}{f(q)^2} - 1\right]$$

where $f(q)$ is the sum of the composite atomic form factors, $f(q) = \sum_i^N f_i(q)$. The real space pair distribution function, *G(r)*, was obtained by direct Fourier transform of the oscillatory $F(q)$

$$G(\mathrm{r}) = \frac{2}{\pi}\int_0^{q_{max}} F(q)\sin(qr)\,dq$$

with $F(q)$ extrapolated to $F(0)$ below the experimental q range < 0.4 Å^{-1} and using q_{max} = 24 Å^{-1}. $G(r)$ is related to the real space electron density distribution function according to

$$G(\mathrm{r}) = 4\pi\mathrm{r}[\rho(r) - \rho_o]$$

where $\rho(r)$ is the spherical average of the real space electron density distribution function, and ρ_o is the average electron density of the sample. Thus, Fig. 4 shows the refined PDF data of **FC-1** in the real space arrangement.

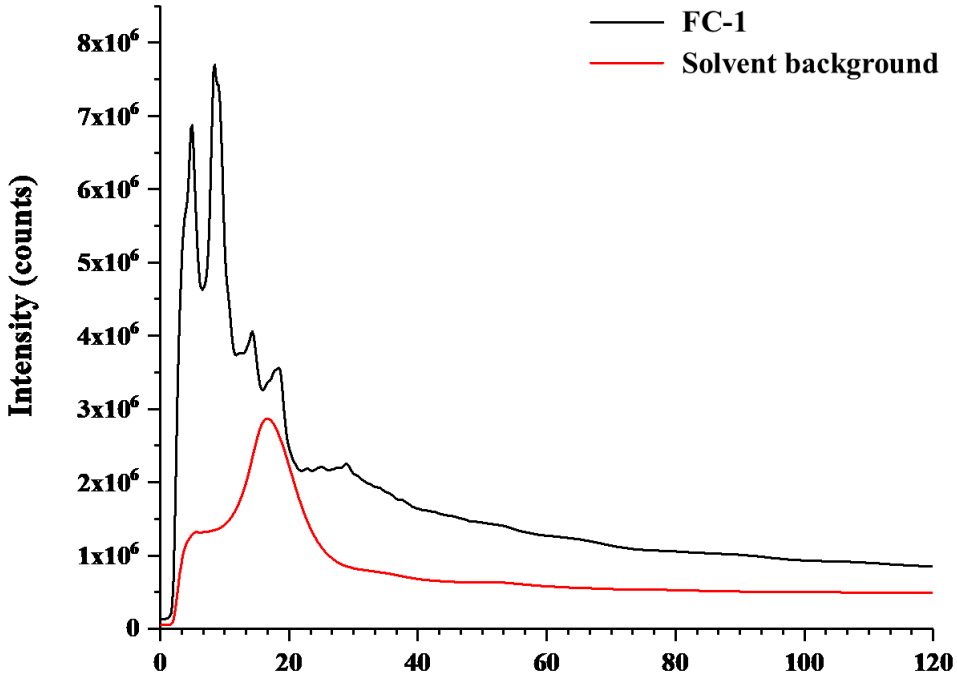

Figure 3. The measured X-ray scattering for solid phase **FC-1** (black line) and solvent background (red line) after corrected with scattering of container and air.

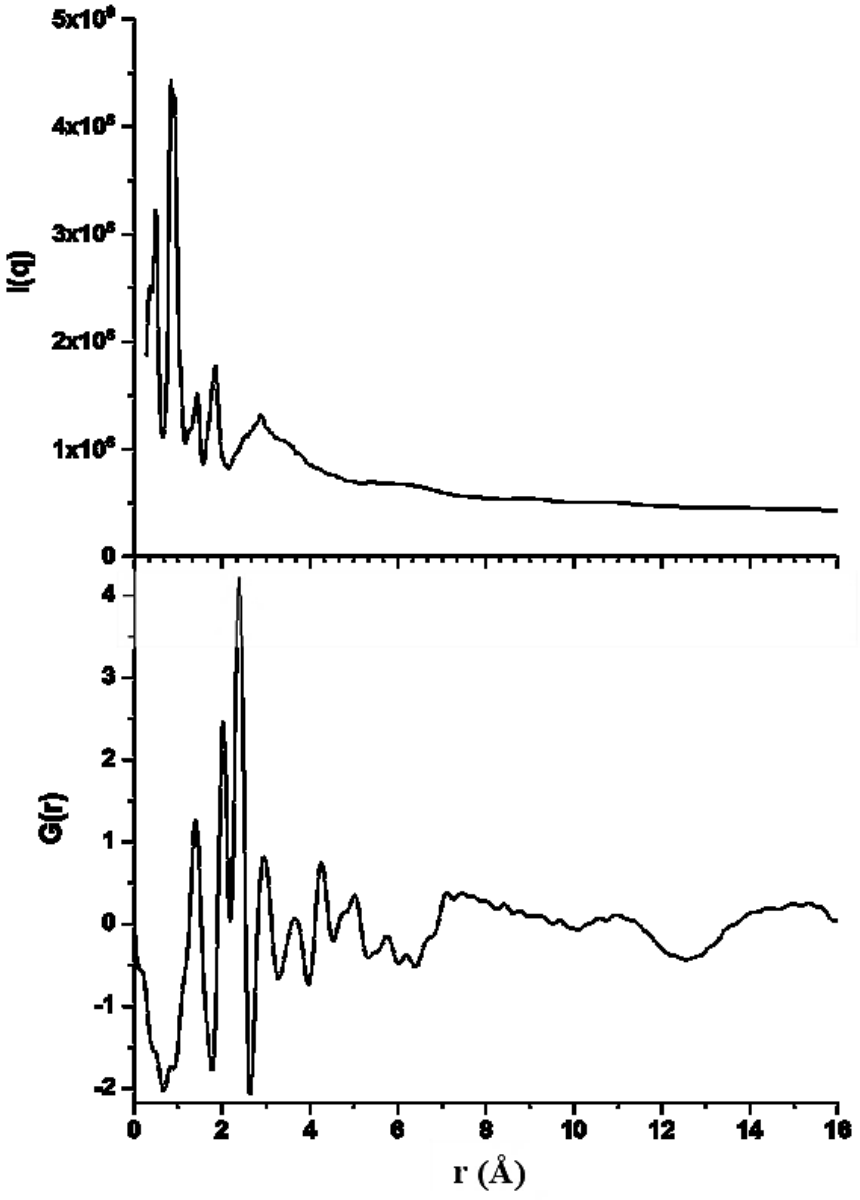

Figure 4. The corrected total scattering, $I(\mathrm{q})$ (top) and the pair distribution function, $G(\mathrm{r})$ (bottom) for **FC-1**.

Selected peaks of experimental $G(\mathrm{r})$ are labelled as a-g in Fig. 5. The peaks position of the PDF reflects the distribution of the distances between pair of atoms in **FC-1**. In principle, each peak in PDF is corresponding to a specific interatomic distance, and the relative intensity of the peak directly indicates to the number of these pairs of atoms. The width of the peak being related to the relative atomic displacement parameters of atoms forming the pairs, and its surface to produce their scattering power. Noticeably, $G(\mathrm{r})$ pattern was found few peaks (a-f) of **FC-1** at the low r region (r is about to 5 Å), which is the most important region to characterize inner shell structures of the materials. A broad feature at high r region (g) possibly arose from several degree of freedom of ligands, also the coordination of neighbouring molecules before damped away due to instrumental limitation. Therefore, the quantitative estimation of interatomic distances and the structural arrangement can be retrieved from the PDF analysis.

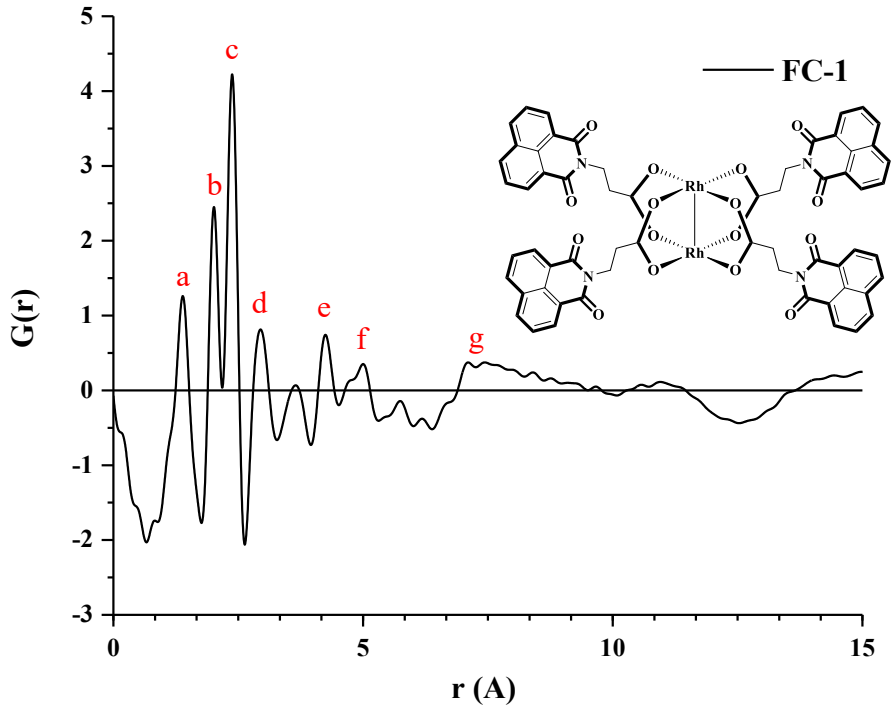

Figure 5. The experimental PDF, $G(\mathrm{r})$ for **FC-1** hydrogen-evolving framework catalyst powder.

Generally, the PDF analysis is being used as a comparative technique. Thus, the bulk structure of **FC-1** was subsequently verified by refining models against PDF data. Firstly, a single-crystal model of **FC-1** (here after, **SC-1**) with dimethylformamide (DMF) molecules at axial coordinated sites was used for evaluation as shown in Fig. 6. The normalized comparison revealed that overall peaks in low-r region are in good accordance (for example in the range 1.39 to 4.26 Å), suggesting that the inner shell structure of **FC-1** is resemble to the crystalline model **SC-1**. Further perceivable peaks beyond 5 Å for **SC-1** were observed progressively in the longer maximum atomic pair distances which correspond to highly ordered assembly of **NIP** moieties, while fairly broaden peaks were observed for **FC-1** in this same region due to more flexibility (indicated as pale blue in Fig. 6). These results suggest the similarity of inner shell structures between **FC-1** and **SC-1**, but they are different in term of molecular packing structure.

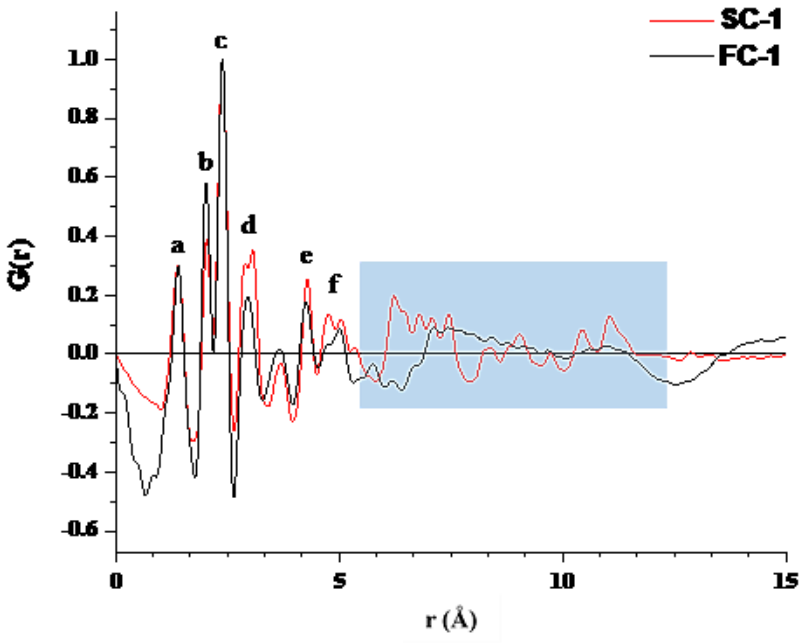

Figure 6. The comparative normalized $G(\mathrm{r})$ for experimental **FC-1** (black line) and calculated **SC-1** single-crystal model (red line). The differences of packing structure was indicated in pale blue.

The characteristics in experimental $G(\mathrm{r})$ of **FC-1** can be interpreted by comparison to $G(\mathrm{r})$ calculate from **SC-1** single-crystal model. Fig. 7 illustrated selected pair distribution features of **FC-1** in the real distances. In this sample, peak (a) at 1.39 Å is attributed to the bond distance of C(Ar)-N(Ar) of **NIP** moieties. The peak (b) at 2.01 Å is well matched with bond distance of Rh-O in the inner coordination shell of dirhodium centre. Following, peak (c) at 2.39 Å shown excellent fit with distance of Rh-Rh, which is in the range found for previously reported Rh(II) paddle-wheel dimers (2.316 to 2.486 Å).[10] Furthermore, peak (d) is corresponding to the Rh-C(AcO) in the outer sphere, while peak (e) can be assigned to distance of rhodium atom to alkyl chain linker (Rh-C(alkyl)). It is worth noting that the slight difference between the experimental **FC-1** and calculated **SC-1** model at higher interatomic distances may be causes from various factors, for example; instrumental resolution, counting statistics, particle size effect, measurement environment, thermal displacements and static disorder. Also, a small signal between peaks (d) and (e) is negligible in this investigation due to very weak intensity. These results suggest that the PDF analysis can provide the clear resolution of first shell Rh-ligand and Rh-Rh distances.

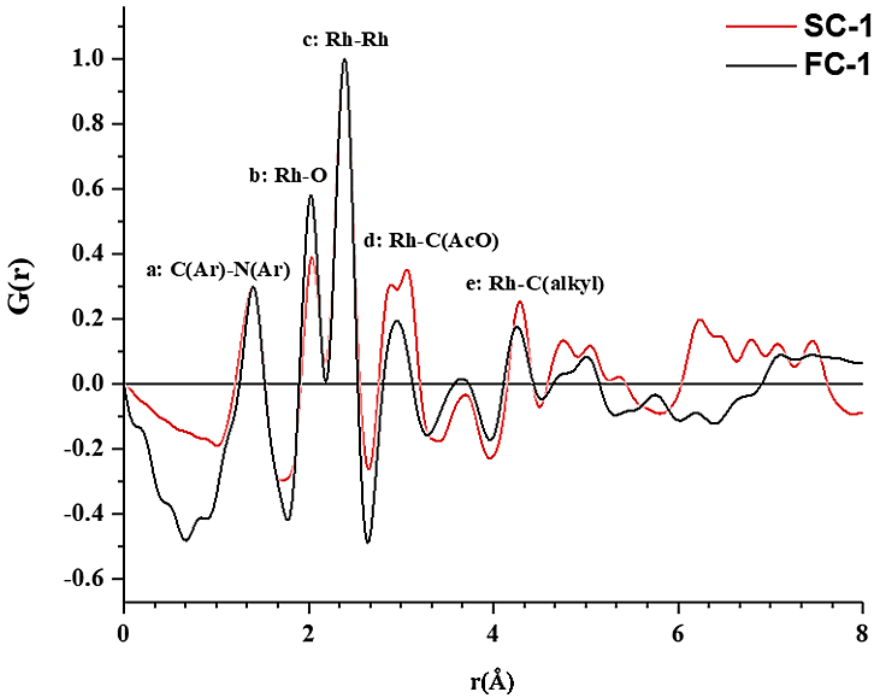

Figure 7. The pair distances assignment for PDF, $G(\mathrm{r})$ for experimental **FC-1** (black line) by compared with the model **SC-1** (red line).

Additionally, the confirmation of core shell structure of **FC-1** can be verified by comparing $G(\mathrm{r})$ calculated from a dirhodium tetraacetate ($Rh_2(OAc)_4$) which has an analogous core structure as shown in chart 1. The comparative results shown in Fig. 8, the peaks of modelling $Rh_2(OAc)_4$ are immediately damped away after 5 Å-region which is due to the absence of **NIP** moieties. This can be confirming that core shell structure are uniformed and peaks at high-r region might corresponded to pair distribution of Rh-ligand in outer shell.

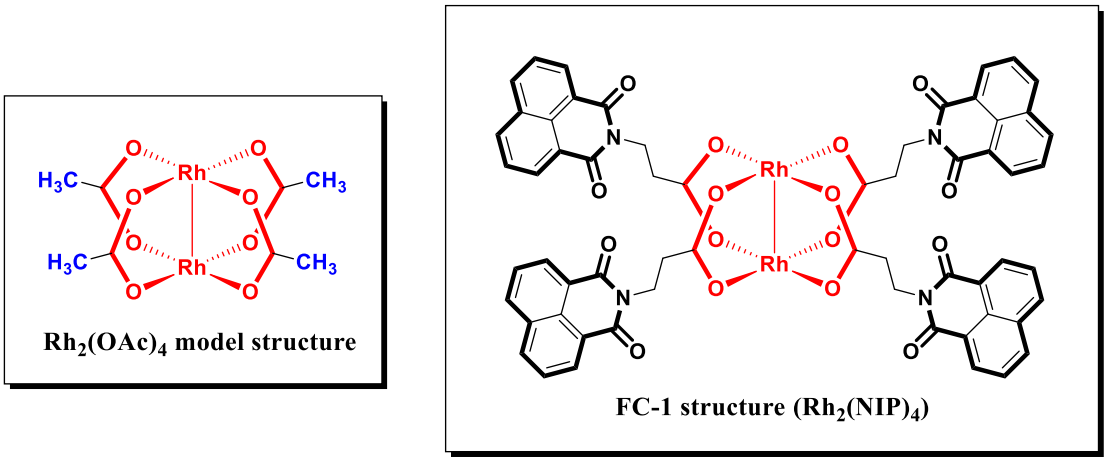

Chart 1. Chemical structure for $Rh_2(OAc)_4$ model and **FC-1** ($Rh_2(NIP)_4$) framework catalyst. An analogous core structure is shown in red.

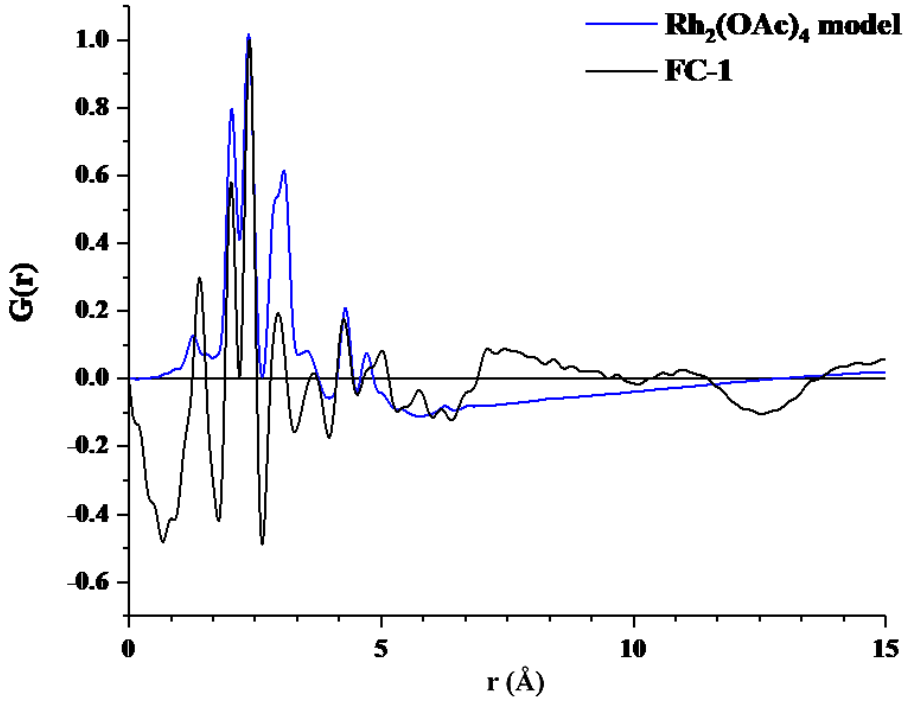

Figure 8. The normalized comparison of $G(\mathrm{r})$ calculated from the $Rh_2(OAc)_4$ model (blue line) and experimental **FC-1** framework catalyst (black line).

However, careful interpretation of the comparative PDF data revealed that there is a slight difference between $Rh_2(OAc)_4$ model and **FC-1** at around 3.63 Å (blue arrow, Fig. 9), which is related to the pair distance of Rh-CH_3(OAc). The characteristic feature appeared as broaden and low intensity due to the "wagging" vibration type of methyl groups in acetate core sphere.[11]

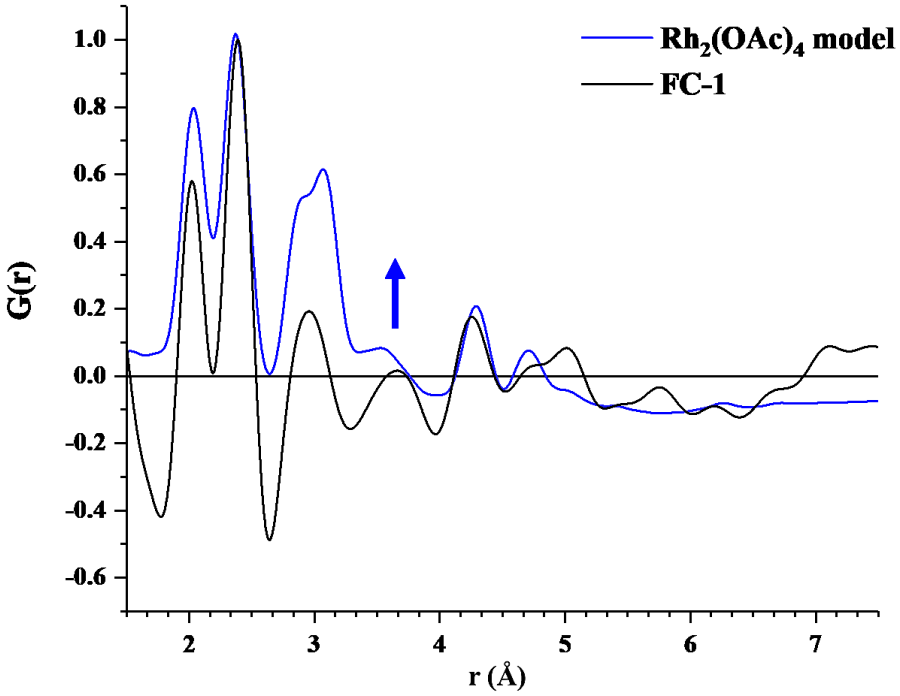

Figure 9. The normalized comparison in range 1.5–7.5 Å of $G(r)$ calculated from the $Rh_2(OAc)_4$ model (blue line) and experimental **FC-1** framework catalyst (black line). A growing peak at 3.63 Å is indicated with blue arrow.

In addition, more variation in the modelling study was performed to shed light on the effect of different coordination molecule at the axial sites of **FC-1**. Subsequently, the calculated PDF were obtained by modification of coordinated solvents of **SC-1** model to water, methanol and dimethylformamide, respectively (Fig. 10). The major changes were found at the peaks which were earlier assigned to Rh-O and Rh-C(AcO) pair distances (yellow stripes in Fig. 10). Even though the distribution difference is little, it is particularly useful for catalytic mechanistic study since it reflects the change in axial coordination sites of the dirhodium center, which is the active site for substrate binding. For this reason, the practise of techniques that possibly track the changes in solid-phase catalytic centre could provide insight into unravelling the source of enhanced catalysis as well as the catalytic key intermediate arrangements.

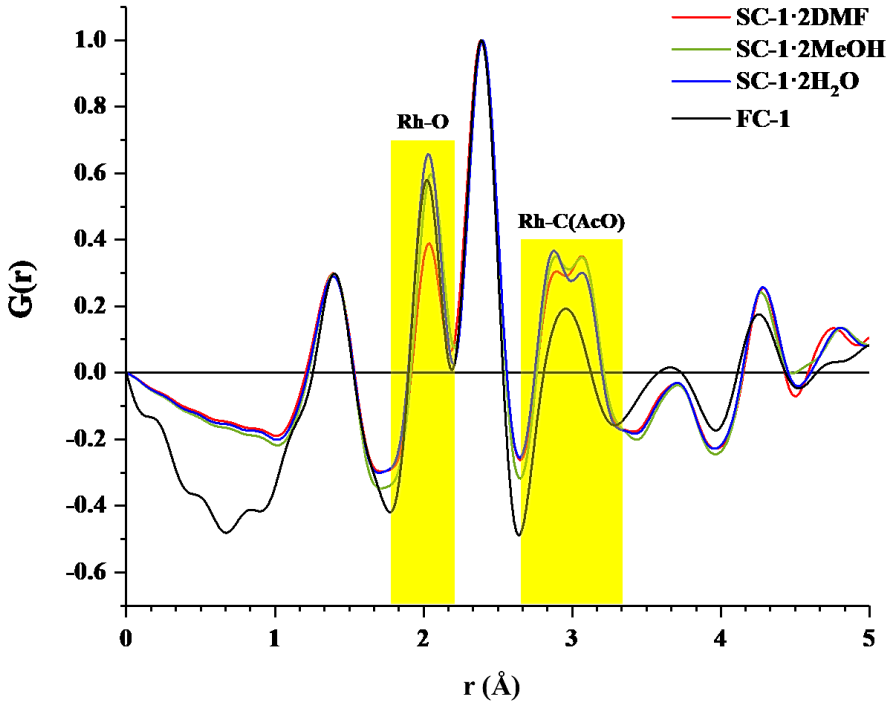

Figure 10. The normalized comparison of $G(\mathrm{r})$ calculated from various axial coordinated of **SC-1** models (dimethylformamide coordination = red line; methanol coordination = green line; water coordination = blue line) and experimental **FC-1** framework catalyst (black line). Alterations of progressive peaks are indicated with yellow stripes.

Conclusion

The solid-state phase X-ray scattering was used to characterise the real-space structures of framework catalyst **FC-1**. X-ray scattering results coupled with PDF analysis arise from interference from neighbouring atoms in the assembly structure and thus provide a rational distance of overall real space low-crystalline structures. By comparing the scattering patterns of experimental result obtained from framework catalyst **FC-1** with variation of calculated models, interatomic distances can be accurately assigned. The scattering pair distribution of **NIP** light-harvesting moiety and the rhodium dimer catalytic centre in the inner sphere assembly, approximately 0 – 5 Å, are successfully determined in experiment. Moreover, experimental investigation of analogous dirhodium fragment shown a clear evidence that the followed oscillation pattern at high-angle corresponded to interference risen from surrounded equatorial **NIP** ligand moieties at outer shell structure. The calculated from single-crystal models shown further oscillation peaks at higher angle. These occurrences reflect contributing of packing structure from naphthalimide rings in the **NIP** ligands from neighbouring molecules. This study demonstrated that it is possible to resolve the full inner and outer shell ligand structure for low-crystalline coordination complexes in solid state, which is important for further study on *in situ* mechanistic insight.

Experimental

Materials

3-Aminopropinoic acid, 1,8-naphthalic anhydride and benzoic acid were purchased from Tokyo Chemical Industry (TCI). Ethylenediaminetetraacetic disodium salt (EDTA-2Na, ≥99.0%) was purchased from Sigma-Aldrich. All solvents and reagents are of the highest quality available and used as received. H**NIP**, $Na_4[Rh_2(CO_3)_4]$, and **FC-1** were prepared by the literature methods.[12,13,14] All syntheses were performed under an atmosphere of dry argon at Masaoka group (Institute for Molecular Science, The Graduate University for Advanced Studies, Japan). The borosilicate glass capillary tubes (0.7 mm diameter thin-walled (10 μm)) used for X-ray measurement were purchased from Capillary Tube Supplies Ltd (CTS), United Kingdom.

Measurement apparatus

^{1}H NMR spectra were acquired on a JEOL JNM-LA400 spectrometer, where chemical shifts in DMF-d_7 or $CDCl_3$ were referenced to internal tetramethylsilane. Elemental analyses were carried out on a J-SCIENCE LAB MICRO CORDER JM10 elemental analyser. ESI-TOF-MS spectra were recorded on a JEOL JMS-T100LP mass spectrometer. Scanning electron microscopy (SEM) images were obtained on JEOL CarryScope JCM-5700. All the ESI-TOF mass spectrometric measurements were recorded in the positive ion mode at a cone voltage of 20 V. All spectroscopic measurements were investigated at Institute for Molecular Science, The Graduate University for Advanced Studies, Japan.

Synthesis of FC-1 hydrogen evolving framework catalyst

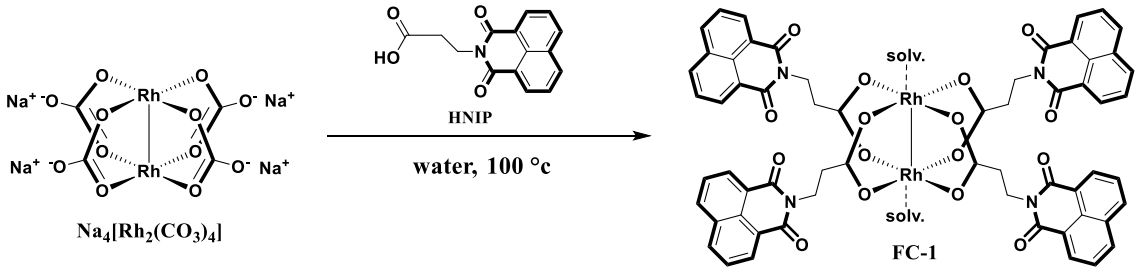

Scheme 1. Synthesis of **FC-1**

3-(1,8-Naphthalimido)propanoic acid (H**NIP**) was synthesized as previously reported.[12] Synthesis of **FC-1** was performed by following a published procedure.[14] A round bottom Schlenk flask was charged with $Na_4[Rh_2(CO_3)_4]$ (90 mg, 0.15 mmol), H**NIP** (323 mg, 1.20 mmol) and 30 mL of water. The mixture was refluxed for 2 h. The resulting green precipitate was obtained by filtration, washed with water and methanol. The green solid was stirred in the mixture of methanol (150 mL) and acetone (150 mL) to remove the unreacted ligand. The green solid was collected by filtration and washed by diethyl ether. After drying under air, **FC-1** was obtained as green powder. Yield: 76 mg (0.06 mmol), 40%. ^{1}H-NMR (400 MHz, DMF-d_7): 8.54 (d, J = 7.4 Hz, 2H, naphth) 8.39 (d, J = 8.2 Hz, 2H, naphth) 7.87 (t, J = 7.8 Hz, 2H, naphth) 4.18 (t, J = 7.6 Hz, 2H, N-CH_2) 2.48 (t, J = 7.6 Hz, 2H, CH_2-COO) ppm. ESI-TOF MS (DMF): *m/z* 1522.41 [1314.08 + 1-methyl-4,4'-bipyridinium + DMF − $2H_2O$] (Note that 1-methyl-4,4'-bipyridinium iodide was used as an additive for mass spectroscopy measurement). Elemental analysis for **FC-1**·$7.5H_2O$: Found: C, 49.3; H, 4.3; N 3.7. Calc. for $C_{60}H_{40}N_4O_{16}Rh_2$: C, 49.7; H, 4.1; N, 3.8%.

X-ray diffraction crystallographic data for SC-1[14]

Single crystal X-ray quality crystals of **SC-1** were grown by vapor diffusion technique from DMF/Et_2O solution. Crystals of **SC-1** were mounted in a loop. Diffraction data at 123 K were measured on a RAXIS-RAPID Imaging Plate diffractometer equipped with confocal monochromated Mo-Kα radiation and data was processed using RAPID-AUTO (Rigaku). The structure was solved by direct method using *SIR-92*[15] and refined by the full-matrix least squares techniques on F^2 (*SHELXL-97*).[16] All non-hydrogen atoms were refined anisotropically. The single-crystal X-ray diffraction measurements were performed at Institute for Molecular Science, The Graduate University for Advanced Studies, Japan.

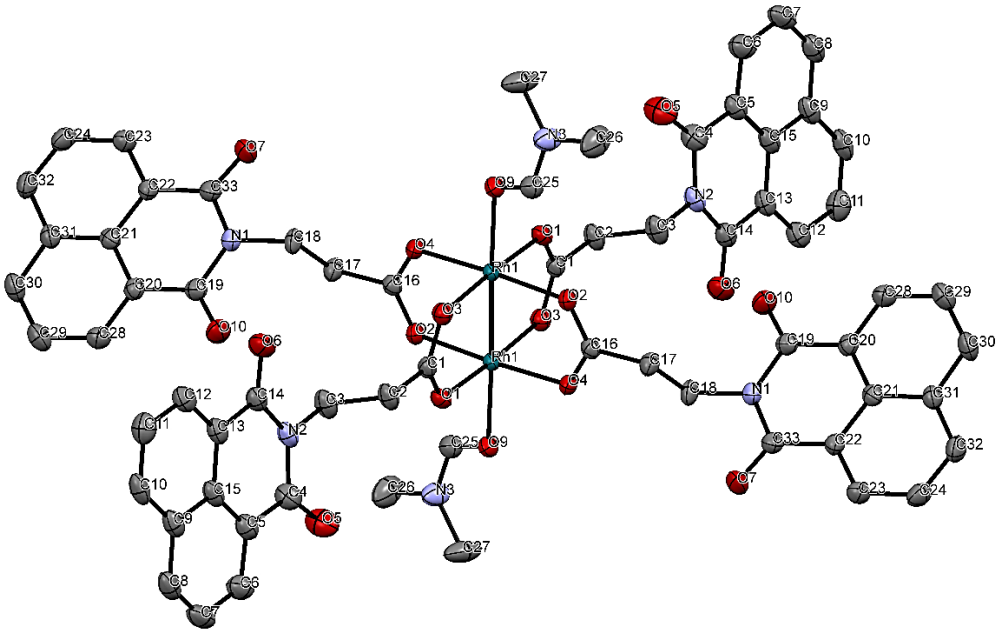

Figure 11. An ORTEP drawing for **SC-1** (50% probability ellipsoids). Hydrogen atoms and crystal solvent molecules are omitted for clarity.

Table 1. Summary of the crystallographic data for **SC-1.**

Formula	$C_{66}H_{54}N_6O_{18}Rh_2$
Fw	1424.99
crystal color, habit	emerald, needle
crystal size, mm^3	0.88 × 0.08 × 0.09
crystal system	*monoclinic*
space group	*P-1*
a, Å	10.0863(4)
b, Å	11.9840(5)
c, Å	14.7529(5)
β, deg	71.948(5)
V, $Å^3$	1694.81(11)
Z	2
F(000)	1730
d_{calc}, g/cm^3	1.619
μ(MoKα), mm^{-1}	0.711
T, K	123(2)
R_1	0.0755
wR_2	0.1863
GOF	1.737

High-energy X-ray scattering (HEXS) and Pair distribution (PDF) analysis.

Preparation of FC-1 for high-energy X-ray scattering measurement

The framework catalyst **FC-1** was synthesized as previously mentioned. Prior the measurement, 5 mg of an obtained green powder of **FC-1** was sonicated in 2 mL of methanol for 15 min, then 500 μL of methanol suspension was drop casted onto a glass slide. After several hours of air dried, the **FC-1** sample was loaded as powder into a 0.7 mm diameter thin-walled (10 μm) glass tube.

High-energy X-ray scattering (HEXS) measurement and PDF data processing

Data suitable for PDF analysis were collected at the Advanced Photon Source (APS) of Argonne National Laboratory at the beamline 11-ID-B.[6] High-energy X-ray of 58.96 keV (λ = 0.2113 Å) were used combination with an amorphous silicon-based flat panel detector mounted orthogonal to beampath. The sample to detector distance was approximately 190 mm across experiments and was calibrated using CeO_2 standard with program FIT2D.

In this measurement procedure, the experimental scattering patterns for **FC-1** catalyst powders, solvent trace, capillary container and instrument backgrounds were measured as a function of the scattered wave vector q, where $q = 4\pi\sin(\theta)/\lambda$ and 2θ is scattered angle in the range of $0.4 < q < 24$ Å^{-1}. Experimental HEXS patterns were used to generate the pair distribution function $G(\mathrm{r})$ using the program PDFgetX2.[7]

A single-crystal XRD crystallographic **SC-1** was used as comparative models to **FC-1** framework catalyst. All models were built by changing of axial coordinated solvents using program BIOVIA Discover Studio 2016. The scattering patterns, *S(q)* for the models were calculated from the atomic scattering parameters using the program SolX, [17] and the corresponding $G(\mathrm{r})$ patterns were calculated as described previously.[4,18]

References

[1] Selected examples: (a) A. S. Weingarten, R. V. Kazantsev, L. C. Palmer, M. McClendon, A. R. Koltonow, A. P. S. Samuel, D. J. Kiebala, M. R. Wasielewski and S. I. Stupp, *Nat. Chem.*, 2014, **6 (11)**, 964; (b) A. S. Weingarten, R. V. Kazantsev, L. C. Palmer, D. J. Fairfield, A. R. Koltonow, and S. I. Stupp, *J. Am. Chem. Soc.,* 2015, **137**, 15241; (c) N. Kaeffer, J. Massin, C. Lebrun, O. Renault, M. Chavarot-Kerlidou, and V. Artero, *J. Am. Chem. Soc*., 2016, **138**, 12308; (d) D. Kim, D. R. Whang, and S. Y. Park, *J. Am. Chem. Soc*. 2016, **138**, 8698; (e) W. Zhao, Y. Huang, Y. Liu, L. Cao, F. Zhang, Y. Guo and B. Zhang, *Chem. Eur. J.,* 2016, **22**, 15049; (f) J. Warnan, J. Willkomm, J. N. Ng, R. Godin, S. Prantl, J. R. Durrantb and E. Reisner, *Chem. Sci.*, 2017, **8**, 3070; (g) P. B. Pati, L. Zhang, B. Philippe, R. Fernández-Terán, S. Ahmadi, L. Tian, H. Rensmo, L. Hammarström, H. Tian *ChemSusChem,* 2017, **10**, 2480; (h) T. Banerjee, F. Haase, G. Savasci, K. Gottschling, C. Ochsenfeld, and B. V. Lotsch, *J. Am. Chem. Soc.*, in press DOI: 10.1021/jacs.7b07489.

[2] Selected examples: (a) A. Mukherjee, O. Kokhan, J. Huang, J. Niklas, L. X. Chen, D. M. Tiede, K. L. Mulfort; *Phys. Chem. Chem. Phys.*, 2013, 21070; (b) K. L. Mulfort, D. M. Tiede, *J. Phys. Chem. B*, 2010, **114**, 14572; (c) D. M. Tiede *et al*., *J. Am. Chem. Soc.*, 2012, **134**, 11096; (d) G. Kwon, O. Kokhan, A. Han, K. W. Chapman, P. J. Chupas, P. Du, D. M. Tiede, *Acta Cryst*. *B*, 2015, **71**, 713; (e) K. R. Yang, A. J. Matula, G. Kwon, J. Hong, S. W. Sheehan, J. M. Thomsen, G. W. Brudvig, R. H. Crabtree, D. M. Tiede, L. X. Chen, V. S. Batista, *J. Am. Chem. Soc.,* 2016, **138**, 5511.

[3] Selected examples: (a) F. M. Michel, L. Ehm, S. M. Antao, P. L. Lee, P. J. Chupas, G. Liu, D. R. Strongin, M.A. A. Schoonen, B. L. Phillips, J. B. Parise, *Science*, 2007, **316**, 1726; (b) C. Kumara, X. Zuo, D. A. Cullen, A. Dass, *ACS Nano*, 2014, **8**, 6431; (c) F. A. Rabuffetti , S. P. Culver , J. S. Lee and R. L. Brutchey, *Nanoscale*, 2014, **6**, 2909 (d) S. R. Bauers, S. R. Wood, K. M. Ø. Jensen, A. B. Blichfeld, B. B. Iversen, S. J. L. Billinge, D. C. Johnson, *J. Am. Chem. Soc.*, 2015, **137**, 9652; (e) X. Hua, Z. Liu, P. G. Bruce, C. P. Grey, *J. Am. Chem. Soc.*, 2015, **137**, 13612; (f) D. Hudry, D. Busko, R. Popescu, D. Gerthsen, A. M. M. Abeykoon, C. Kübel, T. Bergfeldt, B. S. Richards, *Chem. Mater*., 2017, **29**, 9238; (g) A. S. Batchellor, G. Kwon, F. A. L. Laskowski, D. M. Tiede, Sh.W. Boettcher, *J. Phys. Chem. C*, 2017, **121**, 25421.

[4] Selected examples: (a) J. Wang, X. Zuo, P. Yu, H. Xu, M. R. Starich, D. M.Tiede, B. A. Shapiro, C. D. Schwieters, Y.-X. Wang, *J. Mol. Biol.*, 2009, **393**, 717; (b) M. Hariharan, Y. Zheng, H. Long, T. A. Zeidan, G. C. Schatz, J. Vura-Weis, M. R. Wasielewski, X. Zuo, D. M. Tiede, F. D. Lewis, *J. Am. Chem. Soc.*, 2009, **131**, 5920; (c) R. Zhang, P. Thiyagarajan, .D. M. Tiede, *J. Appl. Cryst.*, 2000, **33**, 565; (d) D.I. Svergun, E.V. Shtykova, V.V. Volkov, L. A. Feigin, *Crystallogr. Rep*., 2011, **56**, 725; (e) M. Bacchi, G. Berggren, J. Niklas, E. Veinberg, M. W. Mara, M. L. Shelby, O. G. Poluektov, L. X. Chen, D. M. Tiede, C. Cavazza, M. J. Field, M. Fontecave, V. Artero, *Inorg. Chem.*, 2014, **53**, 8071; (f) Antoine E. Morandeau and Claire E. White, *J. Mater.*

Chem. A, 2015, **3**, 8597; (g) O. Kokhan, N. S. Ponomarenko, P. R. Pokkuluri, M Schiffer, K. L. Mulfort, D. M. Tiede, *J. Phys. Chem. B*, 2015, **119**, 7612; (h) K. Haldrup, A. O. Dohn, M. L. Shelby, M. W. Mara, A. B. Stickrath, M. R. Harpham, J. Huang, X. Zhang, K. B. Møller, A. Chakraborty, F. N. Castellano, D. M. Tiede, L. X. Chen, *J. Phys. Chem. A*, 2016, **120**, 7475; (i) M. Bacchi, E. Veinberg, M. J. Field, J. Niklas, T. Matsui, D. M. Tiede, O. G. Poluektov, M. Ikeda-Saito, M. Fontecave, V. Artero, *ChemPlusChem*, 2016, **81**, 1083; (j) N. Jürgensen, M. Ackermann, T. Marszalek, J. Zimmermann, A. J. Morfa, W. Pisula, U. H. F. Bunz, F. Hinkel, G. Hernandez-Sosa, *ACS Sustainable Chem. Eng.*, 2017, **5**, 5368.

[5] L.-L. Ooi, *Principles of X-ray crystallography*, Oxford University Press, United States, 2010.

[6] (a) K. L. Mulfort, A. Mukherjee, O. Kokhan, P. W. Du, D. M. Tiede, *Chem. Soc. Rev.*, 2013, **42**, 2215; (b) P. Bordet, *EPJ Web Conf.*, 2015, **104**, 01003-p.1.

[7] M. Zobel (25 November 2017), *the principle of the pair distribution function (PDF) analysis*. Retrieved from URL: http://www.mesostructures.uni-bayreuth.de/en/research/pair-distribution/index.html

[8] (a) P. J. Chupas, X. Qiu, J. C. Hanson, P. L. Lee, C. P. Grey, S. J. L. Billinge, J. *Appl. Cryst.*, 2003, **6**, 1342; (b) P. J. Chupas, K. W. Chapman, P. L. Lee, *J. Appl. Cryst.*, 2007, **40**, 463; (c) P. J. Chupas, K. W. Chapman, H. L. Chen, C. P. Grey, *Catal. Today*, 2009, **145**, 213.

[9] X. Qiu, J. W. Thompson, S. J. L. Billinge, *J. Appl. Cryst*., 2004, **37**, 678.

[10] (a) T. Itoh, M. Kondo, M. Kanaike and S. Masaoka, *CrystEngComm*, 2013, **15**, 6122; (b) T. Itoh, M. Kondo, H. Sakamoto, K. Wakabayashi, M. Kanaike, K. Itami and S. Masaoka, *Dalton Trans.*, 2015, **44**, 15334; (c) T. E. Cassandra, A.-T. Nkongho, K. K. Kenneth, J. Tana and F. Quarshiea, *Acta Cryst. E*, 2012, **69**, m639; (d) M. Ebihara, K. Yamada and T. Kawamura, *Acta Cryst. C,* 2006, **62**, m451; (e) N. N. Sveshnikov, M. H. Dickmana and M. T. Pope, *Acta Cryst. C,* 2000, **56**, m1193.

[11] D. M. Tiede et al., *Chem. Soc. Rev*., 2013, **42**, 2215.

[12] D. L. Reger, A. Debreczeni, B. Reinecke, V. Rasolov and M. D. Smith, *Inorg. Chem.*, 2009, **48**, 8911.

[13] L. Caulder and K. N. Raymond, *Acc. Chem. Res.* 1999, **32**, 975.

[14] R. Daneil L. *et al*., *Inorg. Chim. Acta*, 2011, **378**, 42.

[15] A. Altomare, G. Cascarano, C. Giacovazzo, A. Guagliardi. *J. Appl. Crystalogr.*, 1993, **26**, 343.

[16] G. M. Sheldrick, SHELXL-97, *Program for Crystal Structure Refinement*, University of Göttingen, Germany, 1997.

[17] (a) X. Zuo, G. Cui, K. M. Merz, L. Zhang, F. D. Lewis, D. M. Tiede, *Proc. Natl Acad. Sci. USA*, 2006, **103**, 3534; (b) J. L. O'Donnell, X. Zuo, A. J. Goshe, L. Sarkisov, R. Q. Snurr, J. T. Hupp, D. M. Tiede, *J. Am. Chem. Soc.*, 2007, **129**, 1578; (c) D. M Tiede, K. Mardis, X. Zuo, *Photosynth. Res.*, 2009, **102**, 267.

[18] (a) S. J. L. Billinge, M. G. Kanatzidis, *Chem. Comm.*, 2004, 749; (b) J. D. Blakemore, N. D. Schley, G. W. Olack, C. D. Incarvito, G. W. Brudvig, R. H. Crabtree, *Chem. Sci.*, 2011, **2**, 94; (c) P. Du, O. Kokhan, K. W. Chapman P. J. Chupas, D. M. Tiede, *J. Am. Chem. Soc.*, 2012, **134**, 11096.

Acknowledgements

It is my pleasure to acknowledge the role of several individuals who were accompanied me for completion of my doctoral study from October 2014 to March 2018 at the Department of Structural Molecular Science, School of Physical Sciences, the Graduate University for Advanced Studies (SOKENDAI) under direction of Dr. Shigeyuki Masaoka, Associate Professor of SOKENDAI and the researcher of Department of Life and Coordination-Complex Molecular Science, Functional Coordination Chemistry at Institute for Molecular Science (IMS).

I have particularly fortunate to work under the guidance of Associate Professor Shigeyuki Masaoka and Assistant Professor Mio Kondo since I were internship student of the EXODASS program (2013). It has been 6 months of a big turning point of my life to set direction to be a researcher. I would like to express my deepest gratitude to both of them. I truly enjoyed working in a research environment that stimulates original thinking and initiative, which they created. Assisted with Designed Assistant Professor Masaya Okamura (Nagoya University) who contributed numerous discussions that helped me to shape this project and giving comprehensive knowledge of chemistry. Their tenderhearted encourage and support students not only about study but also personal life made me always thankful for them. I have no any appropriate word to express how grateful I am to be their student.

I also deeply grateful for team of researchers at IMS, Professor Shigetoshi Aono, Assistant Professor Norifumi Muraki, Professor Yasuhiro Uozumi, Assistant Professor Takao Osako, Assistant Professor Go Hamasaka and Uozumi group members, Associate Professor Norie Momiyama, Assistant Professor Atsuto Izumiseki and Momiyama group members, Dr. Takuya Kurahashi, Professor Tesuro Murahashi and Assistant Professor Koji Yamamoto and their group members (Tokyo Institute of Technology) and further IMS members whose I am unable to mention all for greatly helpful advices and educative discussion through researches.

I am grateful for Professor Hidehiro Sakurai for provided me the great opportunity to join the internship program at IMS, his group members and Thai alumni (IMS and Osaka University), also Associate Professor Shuhei Higashibayashi (Keio University) and Dr. Koji Yamamoto and for indebt discussion through the joint seminar.

I would like to express my gratitude to Professor Hiroshi Yamamoto and Assistant Professor Masayuki Suda for the technical measurement of SEM images. I also would like to express my sincere appreciation to Mr. Seiji Makita, Ms. Michiko Nakano and Ms. Haruyo Nagao in IMS for technical measurements of elemental analysis and NMR spectroscopy.

I would also like to acknowledge the warmest friendship and the valuable input of Masaoka group members; Dr. Vijayendran K. K. Praneeth, Mr. Sze Koon Lee, Ms. Arisa Fukatsu, Mr. Hitoshi Izu, Mr. Takafumi Enomoto, Ms. Chihiro Matsui, Ms. Mami Kachi, Mr. Masahiro Tasaki. I would like recognize the important roles of our technician staff; Ms. Mari Kanaike, Ms. Akane Shibata, Ms. Miho Matsuda, Ms. Ms. Reiko Kuga and Kaori Wakabayashi for technical and laboratory routine support. I also grateful to Ms. Mayuko Taniwake and Ms. Kyoko Nogawa for their secretarial support. I am also thankful to Masaoka group alumni, Assistant Professor Masayuki Yoshida (Hokkaido University), Dr. Go Nakamura (NARD institute, Ltd.) and his kindhearted wife, Mr. Masakazu Murase (Toyota Central R&D Lab), Mr. Ke Liu, Ms. Yukino Fukahori and Mr. Riku Ushijima. Also the visiting researchers and students; Dr. Woi Pei Meng, Dr. Junjuda Unruangsri, Ms. Teh Swe Jyan, Ms. Marine Simöen (also her French gangster), Ms. Pennapa Tungjiratthitikan, Mr. Thitiwat Tanyalax and Ms. Jeevithra Subramanian.

I am greatly thankful to Dr. Takahiro Itoh, Dr. Yuki Okabe and Dr. Shun Hashiyada
Friends: *have less, but the best.*

I gratefully acknowledge Professor David M. Tiede and the Solar Energy Conversion group members of Argonne National Laboratory (ANL), and the beamline scientists at Advanced Photon Source (APS) for supported my visited, invaluable knowledge and opened up my new experiences through the internship program.

I would like to thanks the financial support from Course-by-course Education Program and Masaoka group for short-term stay abroad.

Finally, my deepest appreciation belongs to my parents, Mr. Sagnob Jinapang, Ms. Pitchakorn Makkhapan and my sister, Ms. Peeraya Jinapang for supporting my life, their warmhearted encouragement and respect my decision to live as a researcher. Also, special thanks to my significant other, Mr. Shun Ichii and his family for always kindly being beside and make things easier when my life get hard.

List of Publications

Chapter 1

"Development of a framework catalyst for photocatalytic hydrogen evolution"

Pondchanok Chinapang, Masaya Okamura, Takahiro Itoh, Mio Kondo and Shigeyuki Masaoka

Chem. Commun., **2018,** *54*, 1174.
Selected as the back cover picture
(Include in this thesis)

Chapter 2

Pondchanok Chinapang, Masaya Okamura, Takahiro Itoh, Akane Shibata, Mio Kondo and Shigeyuki Masaoka

Manuscript in preparation.
(Include in this thesis)

Chapter 3

Manuscript in preparation.
(Include in this thesis)

Other Publications

"Ferrocenyl derivative of 1,8-naphthalimide as a new turn-on fluorescent sensor for Au(III) ion"

Pondchanok Chinapang, Vithaya Ruangpornvisuti, Mongkol Sukwattanasinitt and Paitoon Rashatasakhon

Dyes Pigm, **2015**, *112*, 236–238.